Morphological studies of molecular recognition in calcite crystallization

Didymus, Jon M.

Award date:
1991

Awarding institution:
University of Bath

MORPHOLOGICAL STUDIES OF MOLECULAR RECOGNITION IN CALCITE ($CaCO_3$) CRYSTALLIZATION

submitted by **JON M. DIDYMUS**

for the degree of PhD

of the University of Bath

1991

COPYRIGHT

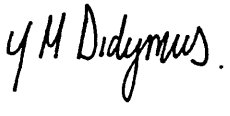

ProQuest LLC
789 East Eisenhower Parkway
P.O. Box 1346
Ann Arbor, MI 48106-1346

ABSTRACT

The concept of molecular recognition at inorganic-organic interfaces has been explored in biomineralization and related model systems. The influence of a range of synthetic and biological molecules on calcite ($CaCO_3$) crystals, grown from supersaturated bicarbonate solution, has been studied. Changes in crystal morphology, observed with optical and scanning electron microscopy, were used to evaluate the potency and selectivity of the molecules. Various α,ω-dicarboxylates, phosphates, phosphonates and sulphate caused distinct modifications in crystal habit. A common binding motif involving a stereochemical correspondence between the bidentate-bound additive molecules and carbonate anions in the $(1\bar{1}00)$ prismatic faces was identified. Selectivity for this face increased with more complementary binding configurations. Potency varied with the charge density on the oxygen atoms, ligand separation and molecular rigidity. X-ray diffraction, infra-red and Raman spectroscopy in addition to elemental microanalysis showed that the products were well-ordered, single crystals with the additives segregated at the mineral surface. A polysaccharide associated with coccoliths of the unicellular alga *Emiliania huxleyi* and alginic acid were also found to express prismatic faces whereas the bone protein, osteocalcin, had a non-specific morphological effect. A soluble, carboxylated, hyperbranched polymer promoted oriented nucleation on the $\{1\bar{1}00\}$ face due to partial segregation of the macromolecule at the air/water interface. Anti-freeze glycopeptides and polyvinyl alcohol induced the precipitation of vaterite. A proteoglycan and polygalacturonic acid had minimal morphological effect.

The early stages of biomineralization in *E. huxleyi* were studied by transmission electron microscopy, electron diffraction and energy dispersive X-ray analysis. Evidence for the nucleation of the main proto-coccolith crystals on the $\{11\bar{2}0\}$ face of calcite was obtained. The subsequent growth stages involved crystal interlocking

and fusion. A new crystal unit was discovered which has profound implications for the phylogenetic evolution of the genera and a folded macromolecular template was proposed to explain the conserved nucleation pattern. X-ray diffraction data indicated that nutrient-depleted culture conditions had no effect on biogenic calcite formation.

To my family

and Olga

Acknowledgements

As we know, no man is an island and it would be wrong to put my name to this thesis without mentioning the numerous people who have helped me during the course of my postgraduate studies. Those who gave so generously of their time in a busy and demanding working environment deserve just acknowledgement.

I am greatly indebted to my supervisor Professor Steve Mann for his enduring interest in the research right from the beginning and his enterprising and inventive spirit. I also owe a great deal to the energy, tireless help and enthusiasm of Dr Brigid Heywood who guided me through the greater part of the work in this thesis.

Thanks must also go to the enormous latent support of all my laboratory colleagues many who have come and gone over the three and a bit years. To Dr Sundara Rajam for her balance and wisdom. To Dr Vanessa Wade for thoughtfully weighed advice and encouragement. To Dr Nick Sparks for his patient education in electron microscopy. Justin Walker; the exemplary host and a valuable ally from the start, the vivacious lab presence of Fiona Meldrum, the juggling skills and genial enigmatic personalities of Nick Reeves and Chris Kemp (not forgetting Joe), Dr Danielle Hirsch and to those who appeared towards the end of my work: Jeremy Hopwood and his Kendalian anecdotes, Alex Lynch, Gaynor Price, Joanne Moore plus the valued help of Dr Kim Wong and Dr Doug Archibald.

I extend particular gratitude to Dr Eliseo Aso-Samper for a memorable collaboration at the end of my first year which manifested itself in part of chapter 4. The experience proved to be a lasting and much needed inspiration to my work. Also, to Pete Oliver for sharing the highly successful project on phosphorus-containing additives.

My appreciation goes to the invaluable "behind-the-scenes" and largely unsung work of the many technicians at Bath University: especially the unrelenting assistance of Robert Stevens and Sheila Osborne, Alan Carver for doing all the routine powder XRD and elemental microanalysis. In Electron Optics: Hugh Perrot, Kate Powell and Dr Glynn Love. Barry Chapman for HRXRD, and also to Joe Stainer, Reg Brown, Christine Triner, Birgit Bending, Pete Jewell, Simon Bowman, Liz Ringwald, Mike Lock for glassware and Betty at the servery.

I must also mention the many scientists that I learnt from or collaborated with especially Dr Jeremy Young for introducing me to the planetary relevance and beauty of coccoliths, for lending me his prized negatives and for his comments on chapter 6. Professor Westbroek for coccolith polysaccharide plus discussions, Dr T.E. Hardingham for proteoglycan, Professor A.L. DeVries for anti-freeze glycopeptide, Dr P. Hauschka for Gla protein and Dr Y.H. Kim for hyperbranched polymer. In addition, Professor Roger Davey and Gary Preece at ICI, Dr James Tililoye, Dr Denis Edwards, Dr Steve Parker, Dr Mary Mahon, Dr Brian Brisdon, Dr Tim St Pierre, Dr Juanma García-Ruiz, Professor Steve Weiner, Professor Lia Addadi and Dr Gordon Cressey.

I would also like to thank the Science and Engineering Research Council for funding this research and especially for giving me the opportunity to attend the Sixth International Symposium on Biomineralization in Japan.

Finally, this list of acknowledgements would not be complete without an expression of gratitude for the love and support from my Mum, Dad, Brother Tim and ..... Olga.

"Time's printless torrent grew ...

A scroll of crystal."

PB Shelley: Fragment on Keats

CONTENTS

CHAPTER 1 INTRODUCTION

Foreword

The central theme of this thesis concerns the morphology of the mineral calcite (calcium carbonate $CaCO_3$) and the ways in which it can be modified via specific molecular interactions. The work stems primarily from an interest in the field of *biomineralization* which investigates the formation of many minerals in living organisms. One of the most striking aspects of the biological deposition of calcite, such as in sea shells and in some planktonic marine algae, are the exotic shapes that are formed. In contrast, calcite precipitating in the absence of any biological influence, whether naturally in the geological environment or artificially in the laboratory, can be observed in much simpler forms. The more familiar characteristics of crystals such as geometric symmetries and plane faces are then evident.

At present, we are just beginning to understand how organisms control crystal shape in such a sophisticated manner. It appears that many aspects of mineralization, including morphology, are manipulated at the molecular level. Specialized proteins, closely associated with the mineral phase, appear to exert control via molecular interactions. However, the picture is not clear and so current approaches involve the use of model systems in order to rationalize some of the chemical processes taking place.

These studies in biomineralization are also relevant to the more general science of crystal growth in industry and technology. Calcium carbonate has found many industrial applications such as in paper coatings, fillers for plastics and rubbers, lime for deacidifying lakes and agricultural land (fertilizer), CO_2 release agent and as an optical material (eg nicol prisms). In these uses, there is often the commercial need to modify the morphology and other properties of the product. Mineral formation

can be a nuisance in industry eg scale deposits in boilers and pipes. The study of molecules effective at morphological control also enables the design of improved, and perhaps more environmentally-friendly, inhibitors of crystallization. Finally, these ideas may be equally applied to other crystalline substances of technological importance; particularly polar materials possessing properties such as piezoelectricity, pyroelectricity, second harmonic generation and frequency doubling.

The following introductory chapter begins by explaining a few pertinent terms and then goes on to outline current concepts in crystal growth which includes an in-depth review of morphology. A detailed description of the calcite structure is then given together with a brief look at other $CaCO_3$ mineral phases. The chapter finishes with a survey of the biomineralization of calcium carbonates.

1.1 *The Mineral Kingdom*

Crystals are objects of great mystery and beauty. One of their most attractive features has always been their outward symmetrical appearance. True crystal faces are solely due to the outcome of natural processes which indicate that there is an inherent order present within the substance. Cut gems are often confused with naturally-grown crystals but the shape of such manufactured specimens is purely due to the intervention of the craftsman.

A *mineral* is usually defined as being a homogeneous material of definite chemical composition, formed by the inorganic processes of nature (Dana 1932). It is normally a solid and will probably be crystalline. For the purposes of this thesis, an inorganically produced mineral is termed *geological.* A distinction is made here from a *synthetic* mineral made in the laboratory or a *biomineral* fashioned by a living organism.

The geometric external form of a naturally-created mineral is a reflection of its regular internal arrangement. This becomes more apparent at the microscopic level. A crystal is, in fact, any substance (usually a solid or liquid) with a periodic structure of atoms or molecules. In gases, atoms are separated by relatively large distances, interactions are minimal and complete disorder results. The atoms or molecules in liquids are more crowded which leads to some degree of order but in solids much stronger interactions lead to a rigid, fixed shape. Ordering results from the tendency for particles to maximize the attractive forces between themselves. The term *amorphous* solid or *glass*, relates to a substance that resembles a liquid in structure but has stronger bonds between its constituent molecules. It should be noted that a glass can be cut to have a external form which may appear crystalline but its shape bears no relation to its random molecular structure.

In recent years, solids with unusual properties of symmetry called *quasicrystals* have been discovered (Stephens and Goldman 1991). This new class of metal alloy materials exhibit five and ten-fold rotational symmetries in diffraction experiments which are normally excluded by conventional crystallography. Their atomic structure is not fully understood and are at present classified as neither wholely periodic crystals nor wholely amorphous materials. One theory describes the possible atomic arrangement in terms of two different unit cells that fit together according to specific rules.

A *single crystal* was a description that was originally applied to a separate, well-defined mineral exhibiting plane faces. Based on its appearance, it was thus thought to possess a high degree of purity and order. Modern usage relates to a material that is coherently ordered enough in three dimensions to give spots in a diffraction pattern. In practice, single crystals contain some impurities and defects. They can be shown to be composed of *mosaic blocks* having very slight

crystallographic misalignment relative to each other. This misorientation may only be as little as a tenth of a degree. If conditions are not favourable for single crystal formation multicrystalline materials result. These aggregates can be associated with some ordering in the case of *twins* whereby symmetry rules can be used to describe the relation of the components crystals. Aggregates with lesser degrees of order are normally termed *polycrystalline* and are structured out of misoriented *crystallites* or *grains* separated by grain boundaries.

1.2 *Basic Theories of Crystallization*

When a mineral comes into contact with solution, the type of phenomena observed may be described by a cycle of interconnecting events as shown in fig 1.1.

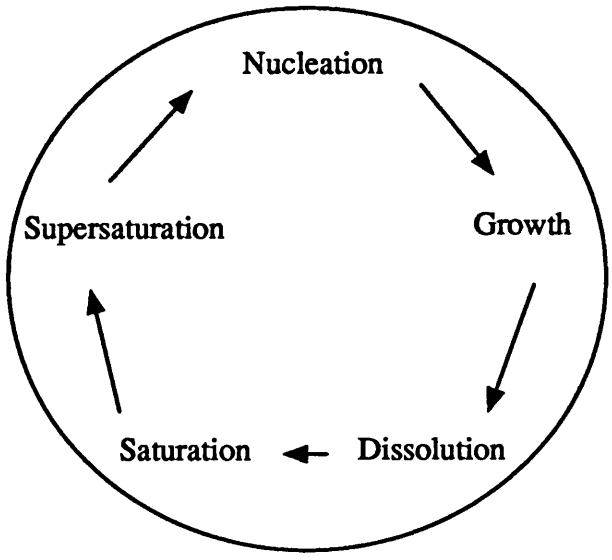

Fig. 1.1 *The mineral-solution cycle*

In this thesis, it is the phenomena of crystallization that is of interest and so the discussion begins with the spontaneous events occurring in a supersaturated solution, namely nucleation and growth.

Nucleation (Garside 1982)

The attainment of supersaturation, whereby the solute concentration is raised above that of a saturated solution, is necessary before any crystallization takes place. However, this state alone is not sufficient in itself. Prior to any growth, nuclei must be created in solution. The process of nucleation describes the formation of a new phase, in the midst of another, under conditions where a free energy barrier exists.

The classical description of nucleation refers to a process occurring in the complete absence of any apparent solid material and is termed *primary homogeneous*. In practice, particles of glass or dust are usually present in the bulk solution and so the concept of homogeneous nucleation is somewhat ideal. *Primary heterogeneous* processes are therefore more common. If nuclei form on a substrate of the same material, then the nucleation is termed *secondary*; the substrate can either be deliberately introduced into the crystallizing solution in the case of seed crystals or can be present as fragments of the primary nuclei.

Thermodynamics

A crystal nucleus or cluster is an extremely small particle and therefore has an enormous surface area relative to its volume. A significant proportion of the overall free energy of the nucleus (ΔG_N), which gives a measure of its tendency to grow or dissolve, thus comes from the surface term.

A solid surface in contact with solution, or any interface between two dissimilar phases, is inherently unstable. This is because atoms or molecules experience a deficit of bonding interactions at the interface compared to the bulk. The result is to produce an inward pressure or surface tension against which work must be done in the formation of the interface (ΔG_{surf} positive). This is counteracted by the energy released on the formation of bonds in the bulk phase (ΔG_{bulk} negative). The balance of these two opposing tendencies in an assumed spherical nucleus of radius r is

usually formulated as follows:

$$\Delta G_N = \Delta G_{surface} - \Delta G_{bulk}$$

The corollary to this is that homogeneous nucleation is similar to a chemical reaction in that it requires an activation energy before any change takes place. Using a mathematical relation between the solubility of a crystal and its size called the Gibbs-Thompson equation, ΔG_{bulk} can be substituted for kTlnS (k Boltzmann's constant, T absolute temperature, S supersaturation) and so the free energy of activation can be shown to be:

$$E_a = \frac{16\pi \Delta G^3_{surf}}{3(kTlnS)^2}$$

Consequently, most crystallizing solutions require a significant amount of supersaturation in order for nucleation to occur. In fact, the state of supersaturation is only possible under conditions of a free energy barrier otherwise crystals would drop out of solution the moment saturation was exceeded. The barrier to nucleation corresponds to a critical size for the cluster given by:

$$r^* = \frac{2\Delta G_{surf}}{kTlnS}$$

A nucleus will change its size so as to decrease its overall free energy. It will therefore spontaneously dissolve if its radius is less than critical or spontaneously grow if it is greater. Note that E_a is proportional to ΔG_{surf}^3 and lnS^{-2} which means that the activation energy is extremely sensitive to the nature of the interface and the degree of supersaturation. In the biological context, these factors can be adjusted via specific organic substrates and control of ion fluxes respectively.

Little is known at present as to the true nature of crystal nuclei but it remains an

active area of research. No empirical data exists for the critical radii of assumed spherical nuclei. However, experimental evidence has been obtained for very small particles (10-50 Å) in supersaturated solutions using techniques such as light scattering and crystalloluminescence. Recent work on very soluble inorganic materials, points to an extensive structuring in such solutions (Larson 1991). There is evidence for relatively large amorphous or partially solvated clusters having very high supersaturations in their interior thus resembling melts. Other workers studying polymorphic systems have employed chemical probes that interact with specific nuclei structures to test the assumption that nuclei of all possible phases are present. If recognition occurs between the probe and nucleus, growth inhibition can result. Selection of stable phases for inhibition will lead to the growth of less stable materials via kinetic control (Staab *et al* 1990).

Kinetics

The rate of formation of nuclei in solution J_N (analogous to the rate constant k for a chemical reaction) depends on this activation energy and can be formulated as follows:

$$J_N = Ae^{-Ea/kT}$$

Thus, the higher the activation energy barrier, the slower the nucleation rate of the particular phase from solution. For example, the number of nuclei, forming at any given time, will be small under conditions of a high interfacial energy ΔG_{surf} and/or low supersaturation. The influence of supersaturation on primary nucleation rate is shown in fig. 1.2. The *metastable* region describes conditions whereby crystallization is favoured but nucleation rate is negligible. The *labile* region relates to high supersaturations and high spontaneous rates of nucleation.

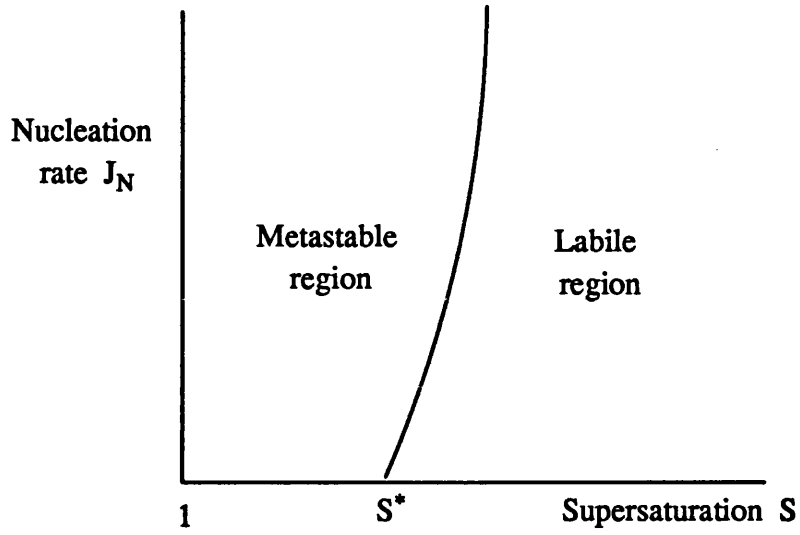

Fig. 1.2 *Primary nucleation rates over a range of supersaturation*

Ostwald Lussac Law of Stages (1897)

This important empirical rule is relevant to systems where more than one phase may potentially precipitate. For example, solutions containing mixed minerals or single mineral systems that show polymorphism such as $CaCO_3$ (section 1.3). It states that under low supersaturation conditions where precipitation is slow, the least soluble phase (eg calcite) will nucleate and grow as expected. But when crystallization is rapid (high supersaturation) more soluble, less stable phases will actually be formed preferentially (fig. 1.3). Thus, in the case of $CaCO_3$, amorphous or hydrated calcium carbonates may be favoured as initial products, followed by vaterite and aragonite before the most thermodynamically stable polymorph calcite.

Crystal Growth (Nielsen and Christoffersen 1982)

Thermodynamics

Growth of post-critical nuclei enables their free energy to decrease and is hence favoured in thermodynamic terms. Crystal growth can be considered as heterogeneous nucleation whereby material is deposited on the clusters.

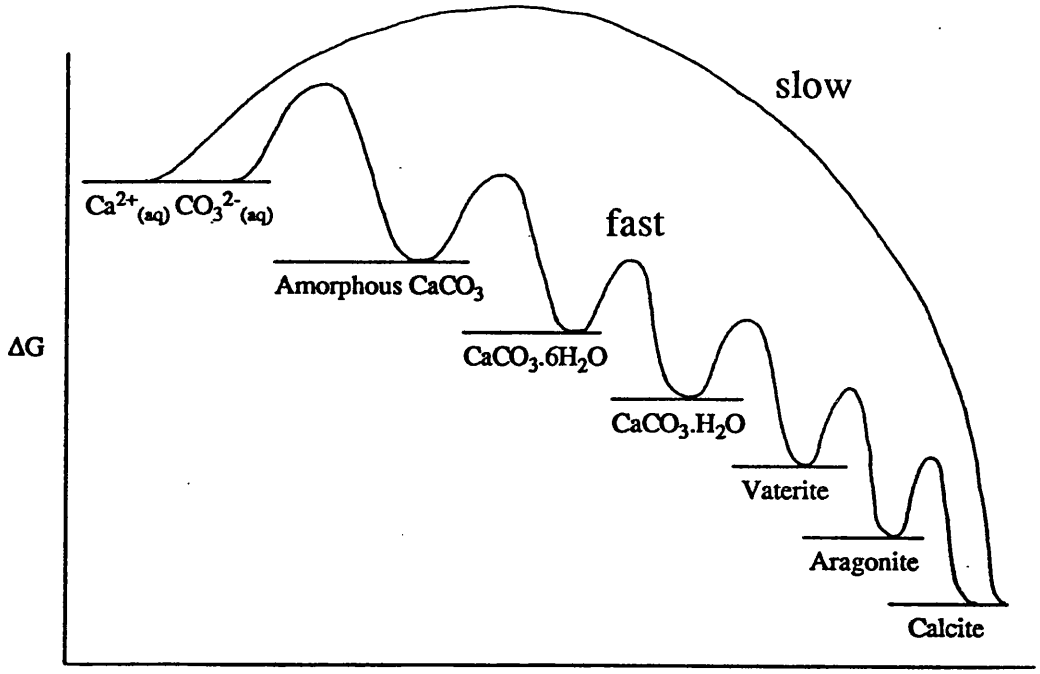

Fig. 1.3 *Two pathways to calcite in the polymorphic $CaCO_3$ system*

Because of uncertainties about the true nature of nuclei, it is unknown whether crystalline products grow from crystalline nuclei or instead from amorphous/hydrated precursors. Another question relates to the growth material arriving at the surface of the nucleus. Under conditions of low supersaturation and agitation, for example, hydrated ions or ion pairs will be present. Higher supersaturations and extensive stirring may favour growth via the aggregation of amorphous or solvated crystalline solute clusters.

Classical theory treats the seed clusters as crystalline and the growth material as simple geometric blocks to enable a quantitative treatment of the problem. Deposition onto the crystal surface and incorporation of material into lattice sites can, therefore, be thermodynamically correlated with bond formation between the blocks and hence energy change.

Even the most regular and flat crystal faces are usually highly imperfect at the sub-micron and nanometre level. Imperfections due to so-called steps, kinks and

dislocations which are observed to be geometric in form (fig. 1.4), provide various sites for adsorption. The most active sites for adsorption (highest binding energy) are the kinks because, nominally, three bonds can be formed as the block is incorporated. Steps sites are less active because two bonds are made and adsorption on terraces (flat surfaces) is least favourable because only one bond is possible.

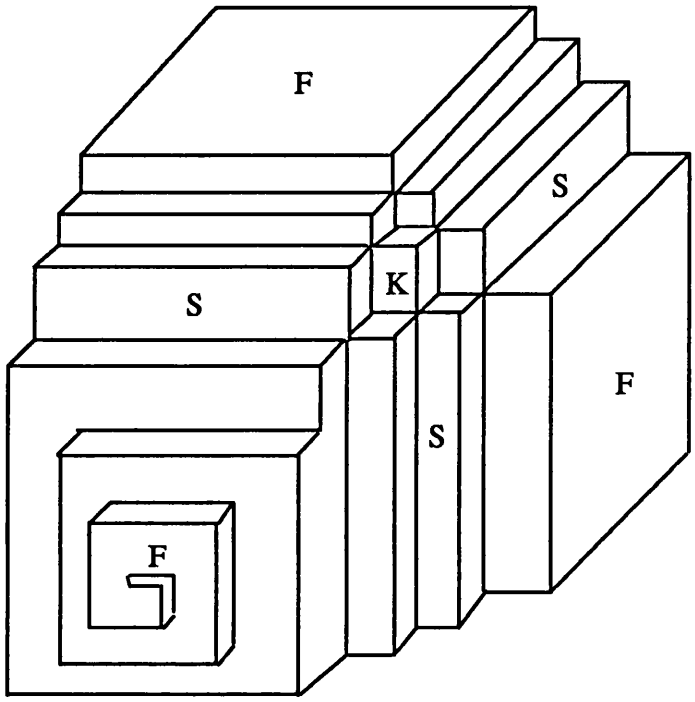

Fig. 1.4 *Geometrical representation of a calcite crystal showing flat (F) $(10\bar{1}4)$, step (S) $(10\bar{1}0)$ and kink (K) (0001) faces plus a growth spiral. Redrawn partly from Boistelle and Astier (1988).*

Growth, in the ideal case, can be imagined to proceed relatively easily as kinks sweep across steps which, in turn, themselves travel across the actual surface until it is completed. However, the formation of the next surface nucleus would be expected to form the greatest energy barrier to the overall process. The supersaturation required for growth to be spontaneous is related to this stage. In practice, it was found that crystals grew at much lower supersaturations than those calculated from this basic thermodynamic theory. This indicated that other sources of steps existed which were later identified as screw dislocations. The development of a growth

spiral emerging from one of these dislocations obviates the need for surface nucleation. The face therefore grows as if it were perpetually covered with steps.

Kinetics

The rate at which crystal growth takes place is usually dependent on the concentration or activity of lattice ions in solution. This driving force is conveniently expressed by the supersaturation.

$$S_R = \frac{\text{Activity of ions in solution}}{\text{Activity of ions in equilibrium with solid phase}} = \frac{(Ca^{2+})(CO_3^{2-})}{K_{sp}}$$

However, rate can be widely modified by the growth mechanism. For a crystal to increase in size, lattice ions must first be transported to the crystal surface (diffusion and/or convection). Ions in aqueous solution have coordination spheres of water molecules which must be released (dehydration step) before surface adsorption takes place. Finally, diffusion across the surface to find active sites occurs followed by integration into the crystal structure. Because these steps are consecutive, the slowest (highest energy barrier) will govern the overall rate depending on the prevailing conditions.

The rate of growth of a crystal face (hkl) is defined as the velocity along a vector normal to that face relative to a point inside the crystal (at its centre if it is centrosymmetric as in the case of calcite). It will normally have units in nms^{-1}, μms^{-1} or even mms^{-1}. It can be generally described in mathematical terms as follows:

$$J_G(hkl) = kS_A^x$$

The empirically-determined parameter x in the rate equation is equivalent to the order of the reaction (crystallization) and relates to the rate-determining step. The

mechanism may be *transport-controlled* meaning that diffusion and convection of ions from bulk solution to the crystal surface is the rate-limiting factor. In which case x takes the value of unity and the rate varies linearly with supersaturation.

$$J_G = kS_A$$

This mechanism can easily be identified because the rate is affected by agitation of the solution. Slow transport is favoured by conditions of high viscosity (which impedes ionic diffusion) and low mixing levels. Little can be inferred about the nature of the surface reactions except that they are very fast in comparison. An important point to note here is that chemical inhibitors are not likely to influence the rate under these circumstances. Alternatively, the rate can be *surface-controlled* whereby one of the interfacial reactions outlined above is relatively slow compared to the diffusion of ions to the growth sites ($\approx 10^{-9}$ m^2s^{-1}). The observed rate may then fit a power law:

$$J_G = kS_A^x$$

The parameter x can range anywhere from 2 to 4. For ionic crystals, the dehydration of small, highly charged cations, such as Ca^{2+}, is often significantly slow and can be rate-limiting. Activation energy barriers will vary for different reactions under different experimental conditions. Stirring will not affect rate in this case. Low supersaturations will normally be conducive to this type of kinetics.

The mechanism controlling the development of a particular face {hkl} is normally identified via empirical kinetic measurements and may change under different conditions. The overall rate of growth of the crystal is limited by the slowest growing faces only. More rapidly growing faces, with higher J_G values will tend to disappear from the crystal.

Morphology

As a crystal grows from a seed nucleus to maturity in a supersaturated solution, it will adopt a particular morphology or habit that is a reflection of the processes occurring at its surface. One of the first theoretical approaches to morphology was the thermodynamic treatment of Gibbs (1878) and Curie (1885) of a crystal in equilibrium with its surroundings. By analogy with a spherical drop of water, the equilibrium morphology of a crystal was also believed to have a minimum surface free energy for a given volume. Wulff (1901) showed that this shape was a closed convex polyhedron whereby the perpendicular distance from a central point to the faces was directly proportional to their free energy. Thus, a poorly ordered or amorphous material, with no definite surface structure and therefore overall isotropy, would tend to grow into a spherical particle in a supersaturated solution. However, strongly anisotropic substances like crystals would develop into polyhedra at equilibrium. The factors which give rise to a variation in surface free energies may either be structural features within the crystal or present in the surrounding medium.

Internal Factors Affecting Morphology

Classical crystallography in the eighteenth and nineteenth centuries was limited to the study of the external forms and symmetries of minerals. However, one the earliest attempts to account for the shapes of crystals by Haüy in 1784 focused on internal structure. Cleavage experiments showed that calcite crystals of any habit could be reduced to rhombohedral fragments. He also demonstrated that any face could be constructed by stacking rhombs in layers and omitting units at regular intervals. Although faces made in this way were highly stepped on the macroscopic level, they would become more planar as the size of cleavage unit decreased.

We now know that the morphology of a crystal is at base defined by the symmetry of its atomic structure. The complete set of symmetry operations possible in three

dimensional space are formally given by the space group which, in the case of calcite, is $R\bar{3}c$. Dana classified calcite according to its symmetry as belonging to the hexagonal system, trigonal division, rhombohedral class. The essential angular relationships between the different crystal faces are revealed by the stereographic projection.

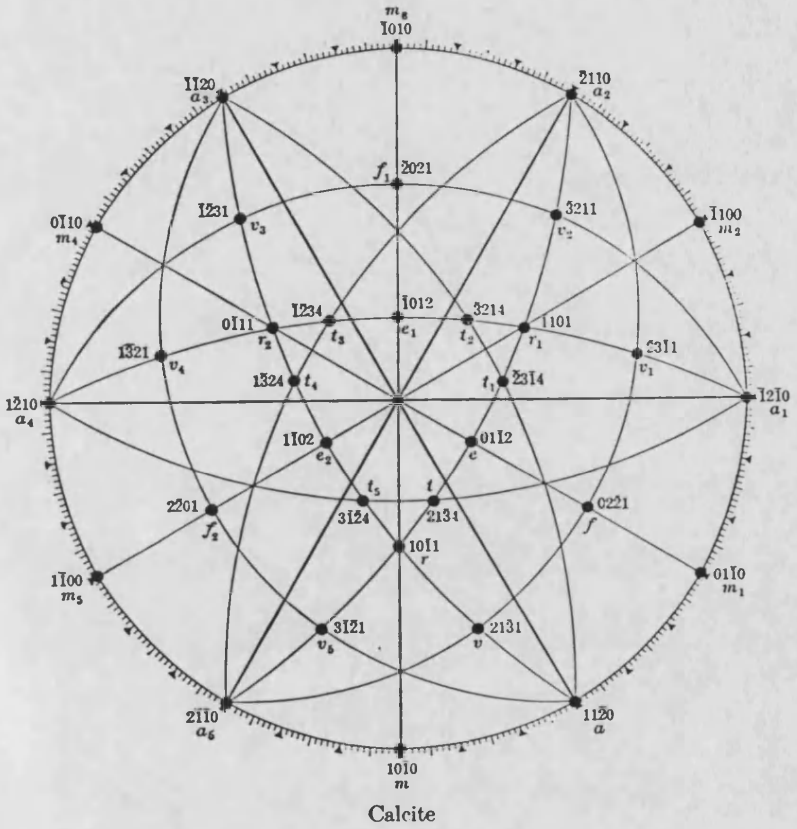

Fig. 1.5 *Stereographic projection of symmetry for calcite (Dana 1932)*

A crystal *form* encompasses all the faces required by each symmetry element eg the $\{1\bar{1}00\}$ forms of calcite include six faces related by a 6-fold rotation axis $(1\bar{1}00)$ $(\bar{1}100)$ $(10\bar{1}0)$ $(\bar{1}010)$ $(01\bar{1}0)$ $(0\bar{1}10)$. All the possible forms for calcite are given in fig. 1.6. The indices are stated in relation to the simplest X-ray hexagonal unit cell (a = 4.99 Å, c = 17.0 Å; c:a = 1.341) and have thus been converted from the indices used by Dana which were based on the morphological hexagonal cell (a = 9.98 Å, 8.52 Å; c:a = 0.854) in common with modern usage. For instance, the fundamental cleavage rhomb given by Dana as $\{10\bar{1}1\}$ becomes $\{10\bar{1}4\}$.

Basal Pinacoid 2 symmetry-related faces	{0001} c	(0001), (000$\bar{1}$)
Prism of the 1st Order 6 symmetry-related faces	{1$\bar{1}$00} m	(1$\bar{1}$00) ($\bar{1}$100) (10$\bar{1}$0) ($\bar{1}$010) (01$\bar{1}$0) (0$\bar{1}$10)
Prism of the 2nd Order 6 symmetry-related faces	{11$\bar{2}$0} a	(11$\bar{2}$0) ($\bar{1}\bar{1}$20) (1$\bar{2}$10) ($\bar{1}$2$\bar{1}$0) ($\bar{2}$110) (2$\bar{1}\bar{1}$0)
Pyramid of the 1st order Positive rhombohedra	{10$\bar{1}$4} r	(10$\bar{1}$4) ($\bar{1}$01$\bar{4}$) ($\bar{1}$104) (1$\bar{1}$0$\bar{4}$) (0$\bar{1}$14) (01$\bar{1}\bar{4}$)
	{10$\bar{1}$1} M	
	{40$\bar{4}$1} ρ	
	{10$\bar{1}$.16} z	
Negative rhombohedra	{01$\bar{1}$4} r	(01$\bar{1}$4) (0$\bar{1}$1$\bar{4}$) ($\bar{1}$014) (10$\bar{1}\bar{4}$) (1$\bar{1}$04) ($\bar{1}$10$\bar{4}$)
	{01$\bar{1}$2} f	
	{01$\bar{1}$8} e	
	{05$\bar{5}$.16} ϕ	
Pyramid of the 2nd Order 12 symmetry-related faces	{11$\bar{2}$8} o	
	{11$\bar{2}$4} s	
Pyramid of the 3rd Order 24 symmetry-related faces		
Positive scalenohedra	{21$\bar{3}$4} v	{21$\bar{3}$.16} t
Negative scalenohedra	{12$\bar{3}$4}	{13$\bar{4}$1} x

Fig. 1.6 *The possible forms for the hexagonal system, trigonal division, rhombohedral class (Dana 1932, pp121-125). Indices based on the hexagonal cell, (a = 4.99Å, c = 17.0 Å).*

The stereographic projection represents a definitive description of all the forms

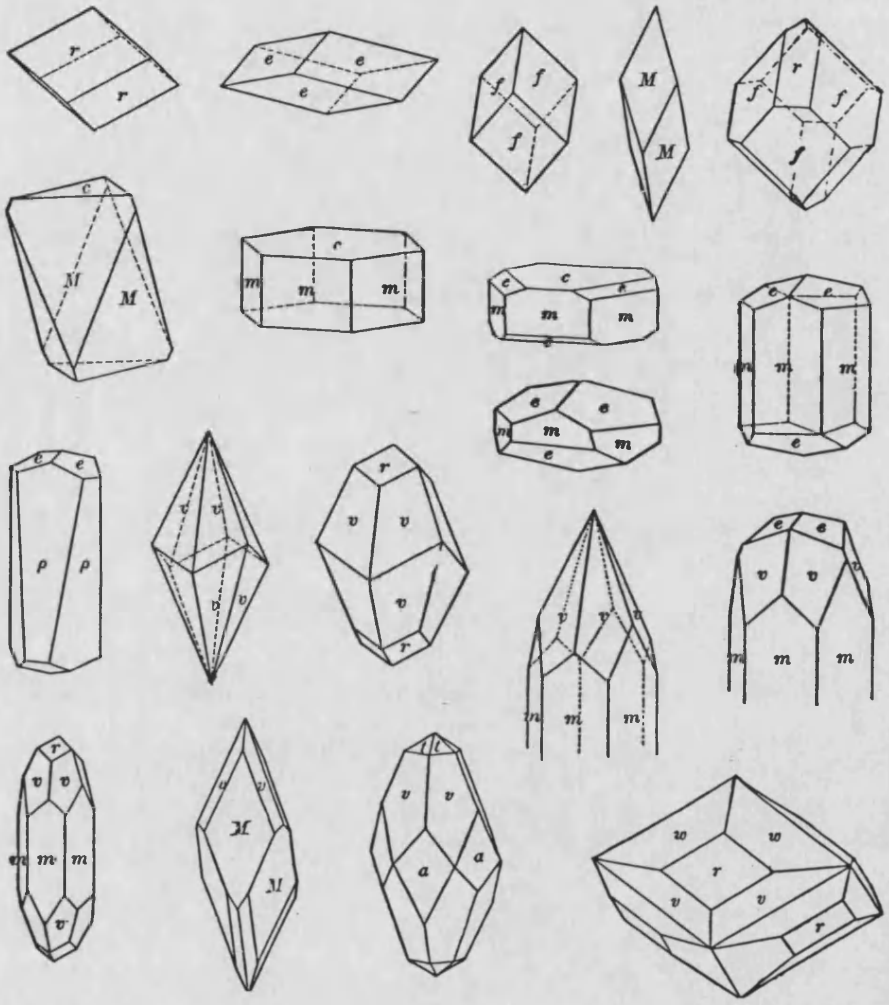

Fig. 1.7 *Some common geological habits of calcite (Dana 1932)*

possible for a mineral structure with that symmetry. The overall crystal habit is simply a combination of these various forms in order to totally enclose space. When the relative sizes and perfection of the faces also vary, it soon becomes apparent that an enormous range of morphologies are possible. In fact, calcite is renowned for being the mineral with the most varied number of habits (fig. 1.7); Palache (1943) documented 328 different calcites. However, the underlying symmetry is always constant and thus serves as a tremendously useful simplification which preserves all the essential angular relationships whilst disregarding the trivial variations. The law of constancy of interfacial angles, illustrated in fig. 1.8, is known as Steno's Law (1669).

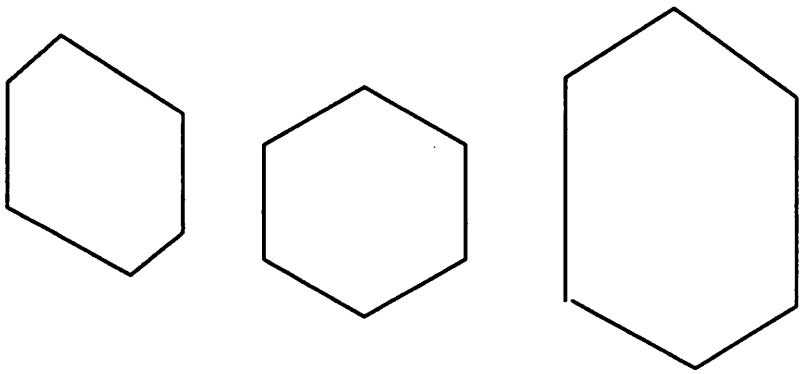

Fig. 1.8 *Constancy of interfacial habits despite differing habits*

The actual combination of forms observed is an expression of their relative growth rates during the transition between the nucleus and the final macroscopic form. The faces that bound a well-ordered single crystal are parallel to atomic planes which develop according to their individual surface free energies. This energy depends on the two-dimensional structure in the face and the interactions with the medium in which the crystal is growing. Those faces with high surface energy are fast growing and will become small or absent as the crystal matures. Stable, low energy faces grow slowly and usually dominate the final morphology. In the case of calcite, the $\{10\bar{1}4\}$ set are much more stable than any other forms and, because all six faces form a closed figure, they alone are usually characteristic of the mineral.

Prediction of Equilibrium Morphology from Crystal Structure

Because the interfacial free energy of a face is related to its structure, it should be possible to calculate such an energy and compare it to values for other surfaces on the crystal. This will enable a ranking system and a prediction of habit based on those forms with the lowest energy. However, it should be noted that the influence from the surrounding environment is not taken into account in this type of method.

The first theoretical attempts to relate habit to structure began with Bravais (1849) and later with Friedel (1904-1907) who related face development to the most closely packed planes. This made sense because, on crowded surfaces, atoms are closer and bonding interactions are generally stronger. A value for the highest reticular density (number of lattice points per unit area), which corresponded to the largest interplanar spacing d_{hkl}, could be assigned to each plane thus representing the most important forms (hkl). The Donnay-Harker (1937) extension then included space group symmetry elements (screw axes, glide planes, body centring) that provided a better measure of reticular density. However, despite some successes in prediction, it was soon realized that the theory had restricted validity. This has been attributed to problems defining the coplanar atoms in a face and hence the true reticular density. Furthermore, for ionic crystals the electrical neutrality of a face must also be taken into account (Wells 1946). Densely packed surfaces will only be stable if neighbouring atoms attract. However, if the plane is unicharged, ie contains only anions or cations, it will be highly unstable due to large coulombic repulsions. Nevertheless, despite the inherent difficulties, the method still remains a good first approximation.

The next main development in this area was the work of Hartman and Perdok (1955). Their analysis identified the direction of strong bond chains (periodic bond chains PBC's) in the structure. Surfaces bearing two PBC's (designated F faces) are the most stable whereas those with one or none are termed S (stepped) and K

(kinked) respectively. It provided the first quantitative measure of relative surface energies by calculating attachment energies E_{att} of a slice hkl to the bulk crystal. The morphologically important forms thus had the lowest values of E_{att}.

The current state-of-the-art are the atomistic calculations (Mackrodt *et al* 1987, Titiloye *et al* 1991). Lattice simulation techniques require accurate potentials and large amounts of computing power but are able to predict crystal habit with greater accuracy. Furthermore, they can be used to assess surface relaxation effects which can modify morphology significantly. In addition, the influence of solvent and impurities can also be simulated.

Prediction of Equilibrium Morphology for Calcite

Several workers have applied these theories to the calcite structure. Results are shown as follows:

hkil	Reticular Density
$10\bar{1}4$	12.00
$01\bar{1}2$	7.56
$21\bar{3}4$	6.00
0001	5.58
$11\bar{2}0$	4.92
$10\bar{1}0$	4.56
$10\bar{1}1$	4.14
$21\bar{3}\underline{1}\underline{6}$	3.48
$31\bar{4}\underline{2}\underline{0}$	2.60
$11\bar{2}3$	2.25
$01\bar{1}8$	1.00
$02\bar{2}1$	0.51

Table 1.1 *Bravais-Friedel Analysis of Calcite*

Morphological Importance excluding electroneutrality principle	Morphological Importance including electroneutrality principle
$01\bar{1}2$ (3.85 Å)	$10\bar{1}4$ (3.03 Å)
$10\bar{1}4$ (3.03 Å)	$11\bar{2}0$ (2.49 Å)
0001 (2.83 Å)	$01\bar{1}8$ (1.91 Å)
$11\bar{2}0$ (2.49 Å)	$21\bar{3}4$ (1.52 Å)
$11\bar{2}3$ (2.28 Å)	$10\bar{1}0$ (1.44 Å)
$20\bar{2}2$ (2.09 Å)	
$02\bar{2}4$ (1.93 Å)	
$01\bar{1}8$ (1.91 Å)	

Table 1.2 *Donnay-Harker method applied to calcite*

García-Ruiz and Hartman (1979)	Heijnen (1985)
$10\bar{1}4$ (F)	$10\bar{1}4$ (F_1)
$01\bar{1}2$ (S_1)	$01\bar{1}2$ (F_2)
$10\bar{1}0$ (S_2)	$11\bar{2}0$ (S_1)
$11\bar{2}0$ (S_3)	
$21\bar{3}4$ (K_1)	
0001 (K_2)	

Table 1.3 *The Hartman-Perdok Analysis of the Calcite Structure*

hkil	Unrelaxed surface energy γ (Jm^{-2})	hkil	Relaxed surface energy γ (Jm^{-2})
$10\bar{1}4$	2.098	$10\bar{1}4$	0.547
$11\bar{2}0$	2.769	$21\bar{3}1$	0.741
$1\bar{1}00$	3.511	$10\bar{1}2$	0.781
$20\bar{2}5$	3.906	$40\bar{4}1$	0.790
$40\bar{4}1$	4.208	$11\bar{2}0$	0.843
$01\bar{1}2$	4.338	0001	0.843
$10\bar{1}1$	4.396	$20\bar{2}5$	0.882
$10\bar{1}2$	4.818	$1\bar{1}00$	0.914
$21\bar{3}1$	4.034	$02\bar{2}1$	0.984
0001	4.995	$10\bar{1}1$	1.027
$02\bar{2}1$	5.847	$01\bar{1}2$	1.029

Table 1.4 *Results of atomistic calculations of surface energies in vacuo (Titiloye 1991; personal communication).*

From tables 1.1 to 1.4, it can be seen that there is overall agreement, amongst the different methods, on $(10\bar{1}4)$ being the most stable face. This bears out what is observed in experiments and in natural systems. However, there are some discrepancies in the stabilities of the subsequent forms. The negative rhomb $\{01\bar{1}2\}$ and first $\{1\bar{1}00\}$ and second order $\{11\bar{2}0\}$ prisms may all be quite close in energy. One important point which emerges from the atomistic calculations is that atoms or molecules are highly prone to relaxation (reconstruction) at the surface. Moreover, this effect contributes significantly to the stabilization of the face.

External Factors that Affect Morphology

Solvent

Extensive empirical studies (Wells 1946) showed that habit, especially for non-centrosymmetric crystals, could vary greatly with the choice of solvent indicating that the surface energies depended on the solid-solvent pair.

Rate of Growth and Diffusion

Wells (1946) was also aware that the rate of growth, as determined mainly by supersaturation but also temperature, pressure and agitation, was also important. Rapid growth will tend to exaggerate the habit where there is distinct anisotropy in growth along the different crystallographic directions ie at high supersaturations, needles become more elongated whilst tabular morphologies appear wider and thinner (Svanoe 1959, Boistelle and Astier 1988).

Lattice ion ratio, pH and control of diffusion have all been investigated in many experiments using gel media. McCauley and Roy (1974) first noticed the pH dependence of calcite morphology grown in silica gel. At pH 6, rhombohedra and spindle-shaped crystals were produced whereas at increasingly higher pH's, poisoning occurred leading to spherulitic, spicular and polycrystalline forms. García-Ruiz *et al* (1979) and Prieto *et al* (1981) synthesized the spindle morphologies at pH 8 and characterized the faces as a combination of flat $\{10\bar{1}4\}$ and curved $\{10\bar{1}0\}$. Diffusion control was invoked to explain the simultaneous formation of stable equilibrium forms $\{10\bar{1}4)$ together with less stable faces. Further work by García-Ruiz *et al* (1985, 1987, 1988) reported bizarre composites with non-crystallographic morphologies grown again in silica gel between pH 8.5 and 10. Stars with 5-fold rotational symmetry, spirals, twisted ribbons and "sheaf-of-wheat" morphologies were observed. The "induced morphology crystal aggregates", as they were called, were believed to develop in close association with a silicate matrix that was shown to surround all the calcite crystals.

Using counter-diffusion experiments in water, Kirov *et al* (1972) showed that the habit of calcite crystals could be readily changed from tabular to rhombohedral to prismatic simply by varying the ratio of lattice ions (Ca^{2+}/CO_3^{2-}). High $[Ca^{2+}]$ favoured elongated prisms whereas high $[CO_3^{2-}]$ produced tabular crystals dominated by (0001) faces. Rhombohedra precipitated at a ratio of 1:1.

Additives

Foreign substances (impurities, poisons, additives, inhibitors etc) of some sort in solution have probably received the greatest attention mainly from industrial experimentalists. A wide range of organic and inorganic crystals have been treated with a similarly extensive variety of cationic, anionic, inorganic and organic additives (Mullin 1961, Davey *et al* 1991). Calcite has not featured strongly in these studies and so the following account relates to other crystalline materials. Investigations involving calcite are reviewed instead in chapter 4 which deals with additives specifically.

The founding studies of Buckley (1949) and Whetstone (1955) used organic dyes to modify the habit of potassium salts and related efficacy to the matching of geometry and charge between dye and crystal face. This began the structural approach that has been pioneered recently by Israeli workers from the Weizmann Institute (Wiessbuch, Addadi, Lahav, Leiserowitz 1991). In modifying the habit of mainly molecular crystals (hosts), their approach has been to take a structurally similar additive (guest) that differs from the host molecules in a specific way. Because of the high degree of similarity between the two, the additives effectively impersonate the hosts and are incorporated into the lattice. However, once part of the crystal, the structural differences of the guests disrupt further growth in their local region which can result in morphological changes (fig. 1.9). In this way, it has been shown that additives can be "tailor-made" to carry out specific tasks in crystallization including habit modification.

Complementary studies on the kinetics of habit modification have elucidated some of the mechanisms involved. For example, Michaels and Colville (1960) measured the growth rates of different faces of adipic acid crystals. They were able to show that cationic amphiphilic molecules preferentially slowed the growth of the basal (001) forming plate-like crystals. Conversely, anionic amphiphiles affected

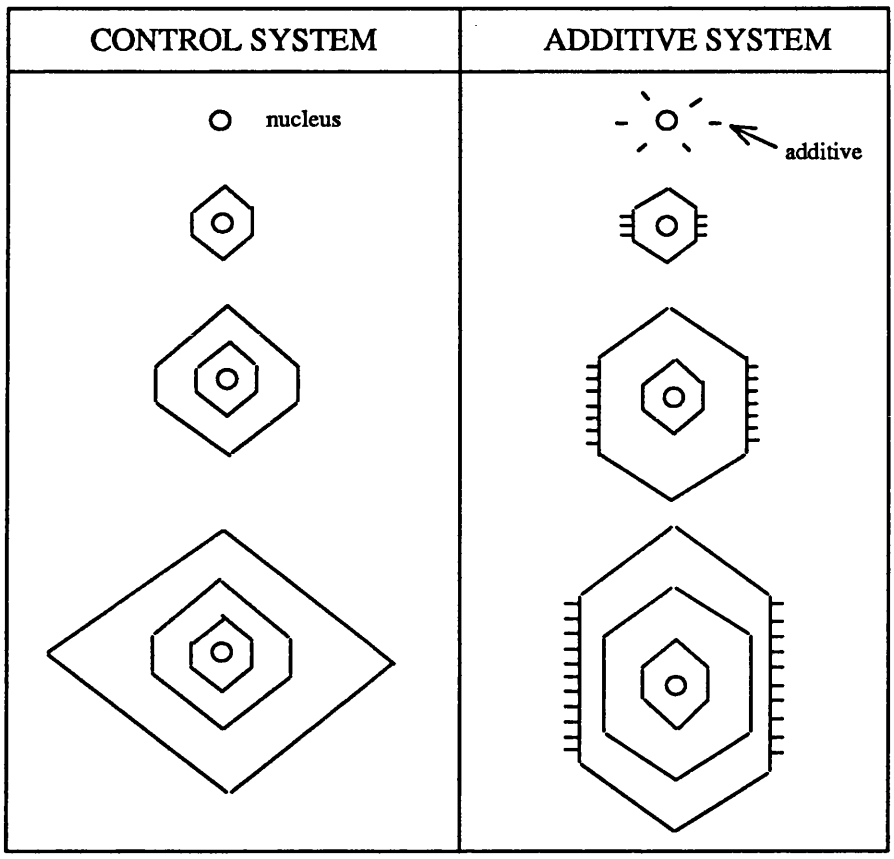

Fig. 1.9 *The morphological effect of an additive adsorbing on a specific set of symmetry-related faces*

prismatic faces and produced needle habits. Many others went on to develop kinetic models including additives for many ionic and molecular crystalline materials (see Davey *et al* 1991 for a review). The effect of additives has also been treated theoretically using Hartman-Perdok analysis to predict morphological changes (Berkovitch-Yellin 1985).

A further possibility for morphological modification, in which additives are indirectly involved, is the phenomenon of pseudomorphism. A novel habit of vaterite was synthesized via a phase transformation reaction that preserved the morphology of the precursor mineral ikaite (Shaikh 1990). Hexametaphosphate was used to inhibit the formation of calcite. It was suggested that geological calcite might also be modified in a similar way. In the natural environment (biological and geological), external conditions can be very varied. Iceland spar, calcite known for

its perfection, crystallizes under hydrothermal conditions of high temperature and pressure. It is also highly likely that a range of contaminating ions and organics are present. Given the variety of possible external conditions, perhaps it is not surprising that countless habits are observed (Sunagawa 1953, Folk *et al* 1985). However, the crystallographic symmetries, typical of inorganic processes, are maintained. Biological conditions are usually much milder than those encountered in geological environments. Nonetheless, organisms are able to finely control factors such as supersaturation, diffusion, pH and ionic strength. Moreover, various metabolites and specialized macromolecules may be deployed as "additives" (see section 1.4).

1.3 *Calcium Carbonate Minerals*

Pure calcium carbonate minerals are known to crystallize in a number of distinctly different phases or *polymorphs*. There are three recognised anhydrous forms plus some hydrated and amorphous phases. The most important of these and the focus for this thesis is calcite.

Calcite

This is the most stable form of crystalline calcium carbonate. In time, under ambient conditions, other polymorphs will transform spontaneously into the calcite structure whereupon no further change will be observed. Its structure has been known for a long time and was one of the first minerals to be studied by Bragg (1915) using X-rays.

Structure and Crystallography (Chessin and Hamilton 1965, Lippman 1973)

The structure is very similar to cubic close packed halite (NaCl) whereby calcium replaces sodium and carbonate substitutes for chloride. However, accommodation of the large planar carbonate ion causes a distortion of the face-centred unit cube of

halite to yield a face-centred rhombohedral cell instead. This distortion amounts to a compression along the triad axis of the cube which then becomes the unique 3-fold axis (*c* axis, [0001]) of the rhombohedron. It can easily be identified as the vertex where three obtuse angles of 101.9° meet; other vertices have two acute angles of 79.1° and one obtuse. This cell despite being useful in comparing the two mineral structures, is limited as a description because the motif of the carbonates is not taken into account. Historically, calcite has been discussed in relation to a host of different rhombohedral and hexagonal unit cells (table 1.5).

System	Cell Parameters	X-ray smallest cell	Cleavage Rhomb pseudo-cell	Cleavage Rhomb true cell
Rhombohedral axes	a_{rh} (Å)	6.37	6.42	12.85
	α	46.1°	101.9°	101.9°
	Z_{rh}	2	4	32
	Cleavage rhomb indices	{211}	{100}	{100}
Hexagonal axes	a_{hex} (Å)	4.99	9.98	19.96
	c_{hex} (Å)	17.06	8.5	17.06
	Z_{hex}	6	12	96
	Cleavage rhomb indices	{10$\bar{1}$4}	{10$\bar{1}$1}	{10$\bar{1}$1}

Table 1.5 *Various calcite unit cells (Deer et al 1962).*

Modern descriptions prefer the simplest hexagonal unit cell; the details of which are shown in table 1.6. Its main advantages are that easy identification of symmetry-related faces is possible and the unique three-fold axis in calcite [0001] corresponds to the vertical hexagonal *z* axis.

Lattice: Rhombohedrally-centred hexagonal: $a_h = 4.99$ Å, $c_h = 17.06$ Å

Number of formula units per cell (Z_h): 6

Space group: $R\bar{3}c$ (Number 167)

Atom type	Number of atoms	Wykoff notation	Point symmetry	Atomic Coordinates
calcium	6	b	3 (S_6)	0.00, 0.00, 0.00
carbon	6	a	32 (D_3)	0.00, 0.00, 0.25
oxygen	18	e	2 (C_2)	0.26, 0.00, 0.25

Table 1.6 *Lattice Parameters for Calcite*

Labelling planes in the hexagonal system utilizes Miller-Bravais four index notation (hkil). Since a_3 is redundant, i can be dropped and the plane labelled (hk.l) or simply (hkl) although the confusion with Miller indices is apparent here. Despite this, the Joint Committee on Powder Diffraction Standards (JCPDS) quote (hkl) indices for the simplest hexagonal cell. For quick reference, the indices of common planes of calcite in relation to the most popular cells in the literature are shown in table 1.7.

Hexagonal a_{hex} = 4.99 Å c_{hex} = 17.0 Å	Hexagonal JCPDS a_{hex} = 4.99 Å c_{hex} = 17.0 Å	Hexagonal a_{hex} = 9.98 Å c_{hex} = 8.52 Å	Rhombohedral α = 46.1° a_{rh} = 6.36 Å	Rhombohedral α = 101.9° a_{hx} = 6.36 Å
$10\bar{1}4$ r	104	$10\bar{1}1$ r	211	100
0001 c	006	0001 c	111	111
$10\bar{1}0$ m	300	$10\bar{1}0$ m	$2\bar{1}\bar{1}$	211
$11\bar{2}0$ a	110	$11\bar{2}0$ a	$10\bar{1}$	$10\bar{1}$
$01\bar{1}2$ f	012	$02\bar{2}1$ f	110	111
$01\bar{1}8$ e	018	$01\bar{1}2$ e	332	110
$21\bar{3}4$ v	214	$21\bar{3}1$ v	$31\bar{0}$	?
$10\bar{1}1$ M	202	$40\bar{4}1$ M	100	?
$02\bar{2}1$	021	$08\bar{8}1$	$11\bar{1}$	?
$40\bar{4}1$ ρ	401	$16.0.\bar{16}.1$ ρ	$3\bar{1}\bar{1}$	?

Table 1.7 *Interconversion of indices based on different calcite unit cells. Some of the more important morphological forms are shown.*

The Structure in Detail

This is easiest to visualize and relate to with the unique *c* axis in the conventional vertical position. The ionic arrangement can then be understood as being built up of planar layers of cations and anions stacking alternately along the *c* axis. This can be clearly seen when looking at the structure along one of the three *a* axes eg $[\bar{1}\bar{1}20]$ (fig. 1.10). These layers are the (0001) planes. Successive rows of anions or cations, corresponding to the (0006) d spacing, (0001) = 17.0 Å), are separated 2.84 Å apart. In the plane of the (0001) layer, anions or cations are arranged in a true hexagonal pattern of length 4.99 Å (the *a* axis dimension) (fig. 1.11). The whole structure can be approximated by a hexagonally close packed (hcp) arrangement of oxygens with calciums placed in octahedral sites such that each cation bonds to only one oxygen of each carbonate group. However, in an anionic layer planar carbonates are not quite hcp; O-O distance between different CO_3^{2-} groups in the plane = 3.26 Å, whereas twice the ionic radius for oxygen = 2.72 Å.

The carbonate CO_3^{2-} group is taken as a structural unit in all carbonate minerals.

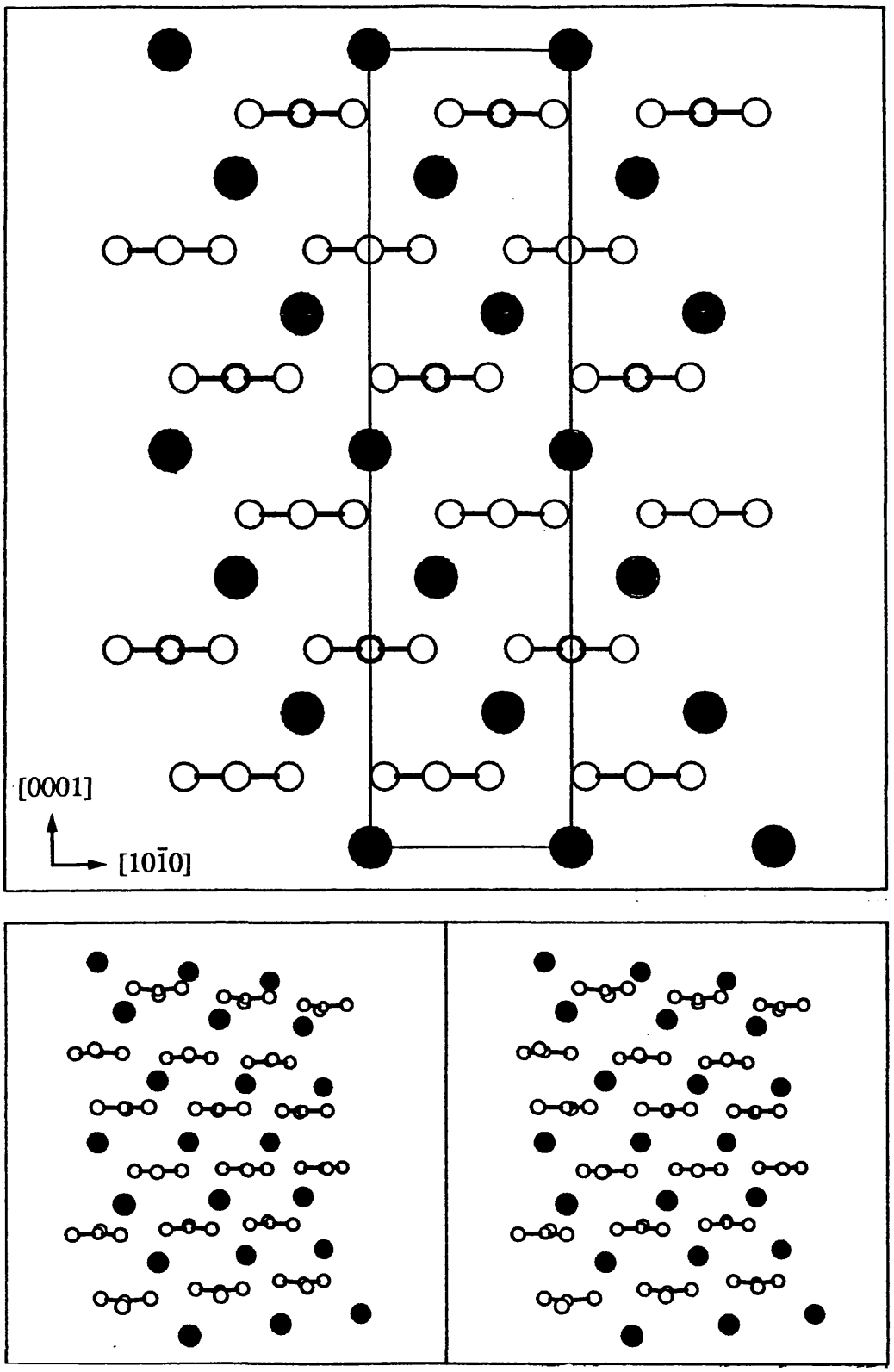

Fig. 1.10 *Unit cell projections along the a axis [$\bar{1}\bar{1}$20] of calcite. Black circles = Ca, open circles = C and O of carbonates.*

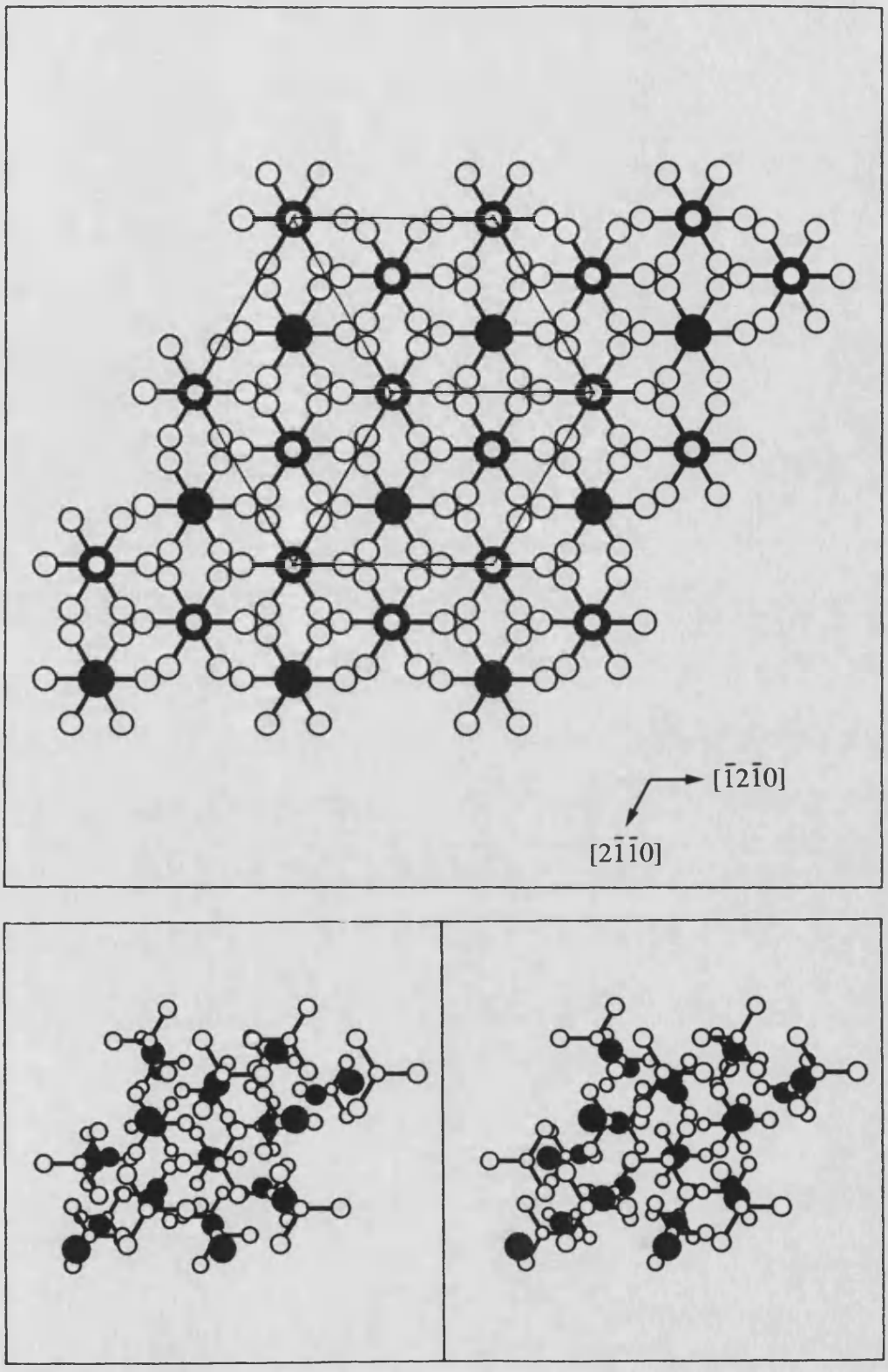

Fig. 1.11 *Unit cell projections along the c axis [0001] of calcite. Black circles = Ca, open circles = C and O of carbonates.*

Local point symmetry is D_3 (32) whereas it is D_{3h} (3/mm) for the free anion. The anion is essentially an equilateral triangle of side 2.2 Å with oxygens at the corners and carbon in the middle. Thus the O-C-O bond angle is 120°. The C-O bond is strongly covalent (78 % character based on Pauling electronegativities) and has been estimated to be four times as strong as any Ca-O bond. The coordination is the same as halite, Ca^{2+} has six oxygens as nearest neighbours all at distance of 2.38 Å (fig. 1.12). Pauling electronegativities show that the Ca-O bond is ionic in character (78 %) and the electrostatic bond strength = +0.33.

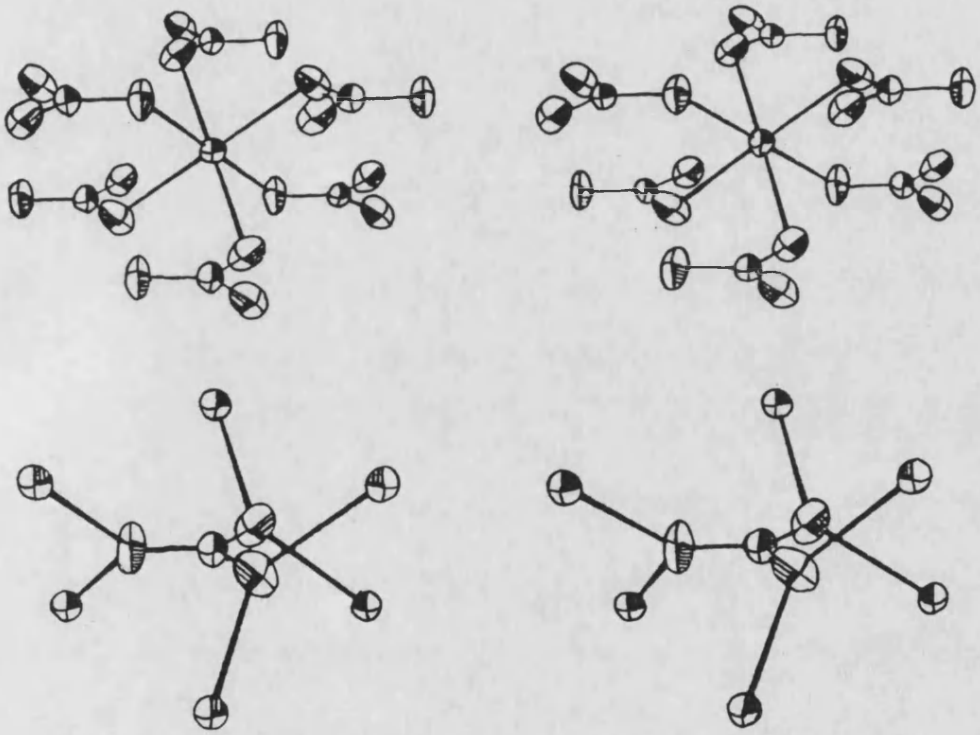

Fig 1.12 *Stereoscopic views of the local coordination geometry of calcite; (a) calcium, (b) carbonate {redrawn from Reeder (1983)}.*

Other Phases (Brooks *et al* 1950/51, Reeder 1983)

Aragonite is the second most thermodynamically stable anhydrous polymorph of calcium carbonate being slightly more soluble than calcite (pK_{sp} aragonite = 8.22; pK_{sp} calcite = 8.42). It is a well-defined mineral occurring naturally and crystallizing in the orthorhombic system (Pmcn). The structure can be approximated

as psuedo-hexagonal as it resembles hcp. As with calcite, rows of carbonates point in the same direction. Unlike calcite, Ca is coordinated by 9 oxygen nearest neighbours.

Vaterite is the least stable anhydrous phase ($pK_{sp} = 7.60$) with a primitive hexagonal lattice, space group $P6_3/mmc$ (no. 194). Dry crystals remain unchanged indefinitely but will transform to calcite when exposed to heat or moisture.

The existence of various hydrated phases of calcium carbonate has been reported although only two forms have been characterized; a monohydrate and a hexahydrate (Brooks *et al* 1950/51, Wells 1975). The hydrates are only generally stable in water at low temperature ie O°C. Additives are frequently required for their synthesis from solution in order to inhibit the formation of more stable phases. Crystallographic data has shown that $CaCO_3.6H_2O$ (ikaite) is constructed from $Ca^{2+}.CO_3^{2-}$ ion pairs isolated from each other by a complete sphere of water molecules. The calcium is 8-coordinate ($6H_2O$, 2O) sitting in the plane of the carbonate ion on a two-fold axis and these axes are arranged in a psuedo-hexagonal pattern. This structure may thus provide a good model for the ion pair in aqueous solution. The hexahydrate is normally observed in the form of long, transparent needles whereas the monohydrate is spherulitic in morphology.

Amorphous, hydrated and sometimes gel-like $CaCO_3$ materials are also known to precipitate under certain conditions but are poorly understood due to their variable composition. They are characterized as showing no X-ray diffraction pattern, broad IR bands and ill-defined morphologies under the electron microscope. Amorphous $CaCO_3$ materials are much more soluble than their crystalline counterparts and therefore are unstable with respect to phase transformation to calcite. However, Merten and Bachman (1980) reported the preparation of an amorphous precipitate that was stable in a sealed container for up to a month. Bills (1985) prepared a

similar material from metastable solution, by rapid filtering and drying, that could be heated to 200°C without giving an XRD pattern. Above this temperature, however, it spontaneously transformed to calcite.

There are a number of miscellaneous calcium carbonate phases known. Probably the most important is $CaMgCO_3$ (dolomite) which has the calcite structure but with alternating cationic layers of Ca^{2+} and Mg^{2+}. Other minor phases include, Kutnohorite $CaMn(CO_3)_2$, monoclinic calcium silicate carbonate $Ca_5(SiO_4)_2CO_3$, orthorhombic shortite $[Na_2Ca_2(CO_3)_3]$ and monoclinic gaylussite $[Na_2Ca_2(CO_3)_3.5H_2O]$.

Many divalent cations such as Cd, Mn, Fe, Mg, Co, Zn, Ba, Sr, Pb and Ni are known to replace Ca in calcite at ambient temperature and pressure. The lattice concentration of the impurity metal depends mainly on the similarity of the ionic radius to Ca (0.99 Å). In the case of Cd (0.95 Å) there is complete miscibility and a true solid solution results. Mn (0.80 Å) shows limited miscibility. Ions with more disparate sizes may only be present in trace concentrations. One of the most common natural substitutions is Mg (0.65 Å) present in high magnesian-calcites at a level of about 16 % (Deer *et al* 1962). Metals with dissimilar valencies such as Li^+, Na^+ and Al^{3+} are also found in calcite probably as interstitial impurities (Rajam and Mann 1990) or combined with other cations or anions.

There is evidence to show that anions are able to substitute for carbonate although it is unclear whether the impurities are surface-bound or actually incorporated into the structure. The species include sulphate, phosphate, silicate and nitrate (Ichikuni 1983). Circumstances are rather adverse for anionic substitution due to the unique combination of size, charge and shape of CO_3^{2-}.

1.4 *Biomineralization of Calcium Carbonates*

The deposition of calcium carbonate is widespread in biological systems occurring in all 5 kingdoms and no less than 28 phyla (table 1.8; Lowenstam and Weiner 1989). Calcification is a general term used to describe the precipitation of calcium not only as the carbonate but also as the phosphate, sulphate, oxalate and even fluorite. All three anhydrous carbonate phases plus the monohydrate and amorphous $CaCO_3$ have been observed in biology but calcite and aragonite are by far the most common.

Calcified tissues are hard and quite tough and can therefore provide support or protection for the organism. Occurrence in invertebrates is usually as a covering or encasement of the body (corals reefs, shells, molluscan and crustacean exoskeleton) or as structures which penetrate the body of the organism (spicules or ossicles). Several types of microstructure have been described in mainly calcitic shell material including prismatic, spherulitic, foliated and lamellar (Carter 1990).

There are several well-established non-skeletal functions. These include: the concentration of calcium as a detoxification mechanism (eels) or as an essential mineral store (plants); as an aid in tissue buffering (molluscs) and for gravity perception in balance organs (vertebrates). Given some of these diverse uses, it is clear that there exists the inherent biological capability to customize many crystallochemical properties. For example, the mineral phase, size, orientation, as well as the morphology, may all be tailored to suit the needs of the organism.

In some cases, however, although the mineral is associated with the organism, a definite function is not apparent. Mineralization can occur as a by-product of the normal metabolic activities of an organism. For example, photosynthetic activity lowers CO_2 levels which can cause supersaturation of surrounding waters with respect to $CaCO_3$ (see chapter 3).

Kingdom/Phylum	Organism/Biomineral/Function
Monera	
Cyanobacteria	Entophysalis: stromatolites
Pseudomonads	*Pseudomonas*: induced precipitate
Protoctista	
Dinoflagellata	Brown-green algae: *Scrippsiella*/cyst
Phaeophyta	Brown algae: *Padina*/surface deposit (?)
Rhodophyta	Red algae, coralline forms/exoskeleton
Chlorophyta	Green algae/exoskeleton
Charophyta	Stoneworts/induced precipitate (?)
Haptophyta	Coccolithophorids/exoskeleton (?)
Myxomycota	Slime moulds: *Didymium*/spore coat
Foraminifera	pore-studded shells (tests), spines
Ciliophora	*Spirostomum*/deposits in vacuoles (?)
Rhizopoda	*Paraquadrula*/exoskeleton
Zoomastigina	*Psuedokephyrion*/lorica (basket)
Fungi	
Mycophycophyta	Lichens/Ca store
Plantae	
Bryophyta	Liver worts, mosses/ Ca store (cystoliths)
Filicinophyta	Ferns/Ca store
Angiospermaphyta	Flowering seeded plants/ Ca store
Animalia	
Porifera	Sponges: Calcarea/exoskeleton, spicules
Coelenterata (Cnidaria)	Corals, sea pansies/exoskeleton
Platyhelminthes	Flatworms/spicules
Ectoprocta (Bryozoa)	Sea-mats/skeleton
Brachiopoda	Lamp shells/shell, endoskeleton, spicule
Annelida	Segmented worms: skeletal tubes
Sipuncula	Unsegmented worm: eg peanut worms/(?)
Mollusca	Gastropods: snails, limpets, whelks, mussels, clams, oysters (pearls)/shell Cephalopods: cuttlefish, nautilus/shell
Echinodermata	Starfish, sea-urchins, sea-lilies, sea-cucumbers/endoskeleton, spicules
Arthropoda	Crabs, barnacles/exoskeleton; crayfish, insects/Ca store; trilobites/eye lens
Chordata	Fish (otoliths), amphibians, reptiles, birds, mammals/gravity sensors (otoconia); reptiles, birds/eggshells; eels /Ca removal; sea-squirts/spicules

Table 1.8 *Calcium Carbonate Associated with Living Organisms*

Cell walls (polysaccharides) may then provide a convenient substrate for nucleation. This is probably the case with many bacteria and algae (soil bacteria, stromatolites, travertines, stoneworts, concretions) which can become encrusted and sometimes incarcerated by the mineral. The term *biologically-induced* mineralization describes processes where there is minimal or absent biological control.

Biomineral Morphology

The different crystalline morphologies produced by living organisms are very varied indeed. They range from the simple, inorganic habits, which are often associated with biologically-induced crystal formation, to the elaborate, micro-architectural structures of coccoliths and sea urchin spines illustrated in fig. 1.13.

The fact that some biomineral morphologies can be replicated generation after generation, and furthermore are often used to classify species, means that their manufacture is under genetic guidance. Quite how this is achieved is at present unclear. Detailed examinations of the composition of many biominerals has revealed the presence of organic molecules (matrix proteins) which seem to be intimately involved in the mineralization process. Thus, the current working hypothesis of many scientists in this area, is based upon control via matrix proteins and other macromolecules.

Macromolecules

The conventional technique for isolating macromolecules from biologically-calcified materials is the use of the chelating agent EDTA. As a result, an EDTA soluble and insoluble fraction is produced. Biominerals such as mollusc shells (Addadi and Weiner 1985, Weiner and Traub 1984, Wheeler *et al* 1988), coccoliths (de Jong *et al* 1979), sea urchin tests (Berman *et al* 1988) have all been subjected to this treatment.

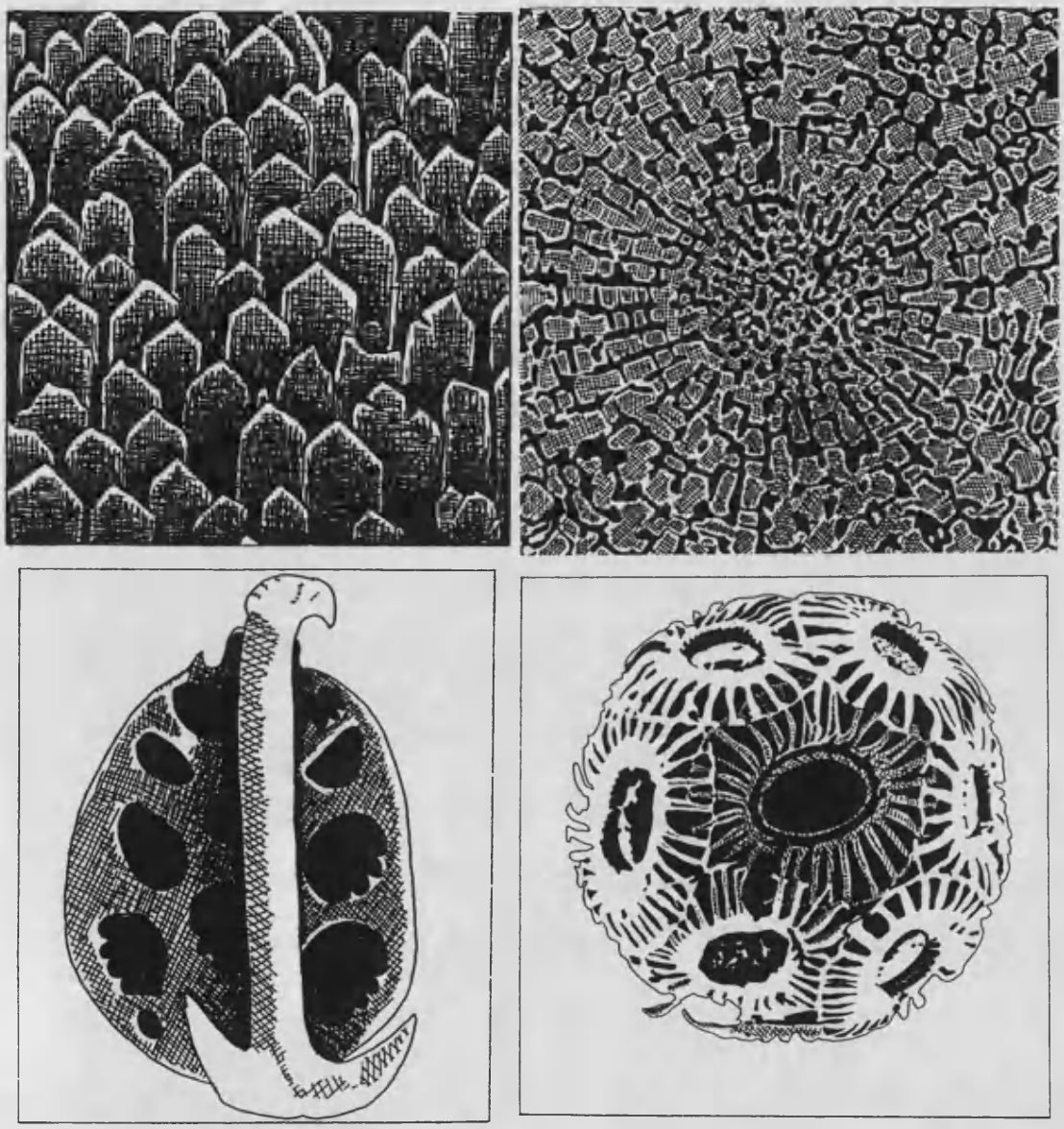

Fig. 1.13 Drawings of $CaCO_3$ biominerals, (a) shell of the bivalve Mytilus, (b) section through a sea urchin spine (c) sea cucumber ossicle, (d) coccoliths of E. huxleyi

Drawn from SEM's: (a) and (b) Carter (1990), (c) Stricker (1985), (d) Young , unpublished

Most research has focused on the soluble fraction. Analysis shows that it invariably contains macromolecules which are highly acidic. For example, proteins rich in aspartic and/or glutamic acids and occasionally phosphorylated serine and threonine residues form the basic structure. Carboxylated or sulphated polysaccharide side chains are also commonly found covalently bound to the peptide backbone (glycoproteins or proteoglycans). An exception is the macromolecule associated with coccoliths which is an acidic polysaccharide containing no protein content at all. The less studied, insoluble component is normally found to contain hydrophobic proteins (eg chitin) and are believed to have a structural or "framework" function.

Several functions for the macromolecules have been proposed and investigated mainly by examining their effect on crystal growth *in vitro* but the details of their actual operation *in vivo* still remain unknown. Their polyanionic nature and hence high charge density, strongly suggests that they are able to interact electrostatically with calcite. The macromolecules all bind calcium, although relatively weakly compared to the true Ca-binding proteins, and are observed to undergo changes in conformation. Many acidic glycoproteins, for example, adopt the β-sheet conformation *in vitro* in the presence of calcium.

Crystal Growth Inhibition Function

It has been postulated that acidic macromolecules act as powerful inhibitors of intracellular supersaturated solutions. A regulatory role in crystallization may thus be effected simply by their absence or presence or perhaps via more complex cellular signalling devices. This hypothesis has been supported by several *in vitro* experiments. Wheeler (1981) reported work with oyster matrix, Borman *et al* (1982) with coccolith polysaccharide, Wilbur and Bernhardt (1984) with extrapallial fluid and again Wheeler *et al* (1988) using phosphorylated and non-phosphorylated mollusc proteins. Marked inhibitory tendencies were reported in $CaCO_3$ crystal growth assays. Additional studies by Borman *et al* (1982) involving blockage or

removal of the anion moieties effectively deactivated the polysaccharide. In this way, the work was able to pinpoint binding sites with high (carboxylates) and low (sulphates) affinities for calcium.

Morphological Control Function

The work of Addadi and Weiner (1985) demonstrated the ability of dissolved matrix molecules in the β-sheet conformation to change the morphology of growing calcium dicarboxylate crystals. Certain faces sharing a common property of dicarboxylate stereochemistry were preferentially stabilized by the mollusc protein. Faces without the necessary stereochemical features, grew as normal indicating that little or no interaction had occurred. This study showed for the first time that an organic matrix was capable of altering crystal habit and that investigations of this kind were able to reveal some of the molecular mechanisms involved.

Berman, Addadi and Weiner (1988) then went on to compare the mollusc glycoprotein with a protein extracted from sea urchin tests. They conducted morphological studies on $CaCO_3$ growth and found that the mollusc protein did not adsorb on any specific face. However, the less acidic sea urchin protein expressed faces parallel to the $\{1\bar{1}00\}$. Evidence was also presented for occlusion of macromolecules in single crystals.

Some of the soluble additives employed in industry as inhibitors and habit modifiers are also present as metabolites in the intra- and extracellular fluids of most living systems. Metabolites such a phosphate, malonate, succinate, Mg^{2+}, $Fe^{2+/3+}$ etc, under biological control, may thus perform a similar function in the cell.

If the criterion for the specific adsorption of organic molecules is based on molecular features such as stereochemistry, all symmetry-related faces of the crystal would be stabilized. This is because surfaces related by symmetry elements have the

same structure. All {$1\bar{1}00$} faces of calcite, for example, ie ($1\bar{1}00$), ($01\bar{1}0$), ($10\bar{1}0$), ($\bar{1}100$), ($0\bar{1}10$), ($\bar{1}010$) are identical in atomic pattern, distances between ions and orientation of carbonates. However, some biominerals exhibit morphologies which appear to break the symmetry requirements of the space group. The single crystal segments of the coccolith of *E. huxleyi* show a ($10\bar{1}4$) face at the tip of the lower element. But the corresponding ($\bar{1}01\bar{4}$), related by a centre of symmetry, is absent on the crystal. This type of, apparently more sophisticated, control is not well understood. Intracellular biominerals are located within membranes or vesicles which are defined and organized by the cell. The membrane may impose a confined environment directing growth in patterns determined by the cellular morphology which overcome the inherent crystallographic tendencies of the mineral. There is evidence, however, that principle crystallographic directions of growth are selected in complex biominerals structures (eg *c* or *a* axes in calcite). Membrane assemblies may also be capable of regulating the injection of materials such as lattice ions and inhibitors into their interiors in a highly directional manner (Mann 1989a).

Nucleation Function

Glycoproteins known to inhibit crystal growth in solution, when immobilized on glass vials, have been shown to actually initiate nucleation (Addadi and Weiner 1985). Furthermore, the protein had the effect of statistically increasing the crystallographic orientation of the nuclei. These observations have underpinned the hypothesis that organized organic molecules can act as templates for nucleation. Unfortunately, *in vitro* studies may not accurately represent the conditions in vivo. Difficulties lie in the fact that biological molecules may have an entirely different mode of action in solution removed from their native environment. In the cell, their conformation is likely to be of paramount importance as is the case with other protein macromolecules such as enzymes. Very little is known about their secondary structures *in vivo*. However, it is hoped that the *in vitro* work is at least analogous to the processes occurring in the living systems.

Modelling Organic Matrices

A large number of diverse and complex organic molecules have been extracted from calcified tissues. Their detailed characterization thus poses considerable problems and assigning possible functions *in vivo* is particularly difficult. An alternative approach is to model the essential chemical features of the matrices using analogous molecules and determine their effect on *in vitro* crystal growth and nucleation.

Wheeler and Sikes have adopted a procedure that initially screens proteins (mainly from molluscs) for inhibitory activity and identifies the primary amino acid sequence. Structural features are then modelled using synthetic peptides and their effect on crystal growth compared with the biogenic material. The studies have evaluated the importance of polyanionic N terminal regions and hydrophobic C terminal domains in the molecules. Model peptides of polyaspartate and polyalanine compared well with the biogenic matrix (Wheeler *et al* 1988). This led to a hypothesis that inhibition occurs when the polyanionic portion of the molecule adsorbs onto a crystal face and the hydrophobic region left in solution interferes with the diffusion of lattice ions.

Addadi *et al* (1987) modelled the ability of acidic glycoproteins to promote oriented nucleation of calcite using sulphonated polystyrene films bearing adsorbed polyaspartate in the β-sheet conformation. In nucleation and calcium concentration assays, polyaspartate or sulphonated polystyrene on their own compared poorly to the combined sulphate and carboxylate system. The results suggested that sulphates in the natural protein may act as ion sinks whilst the apparently more organized carboxylates perform the function of oriented nucleation.

Langmuir monomolecular films have helped to explore the hypothesis that macromolecules can function as templates for crystal nucleation (Mann *et al* 1989b). Monolayers are easily manipulated assemblies of amphiphilic molecules organised

at the air-water interface. Their main advantage, as a model system, lies in the fact that they are well-characterized at the molecular level. Results have shown that stereochemical and geometrical matching can occur between the functional group of the organic molecule and a crystal surface. Thus, this kind of approach has shown quite clearly that organized macromolecules have the ability to act as templates.

Molecular Recognition

The study of biomineralization is now firmly established at the molecular level. The protein-mediated control exerted by some organisms in the interaction with minerals is in common with the specific nature of molecular biology. There are parallels between the function of matrix proteins and the function of enzymes or nucleotides. Crystal faces appear to be recognizable at the atomic level in the same way that substrates are recognized by enzymes or antigens by antibodies. Thus, the concept of *molecular recognition* is now being used (Mann 1988) to focus on the apparent complementarity at the interface between the organic (protein etc) and the inorganic (mineral). Probably the most basic interfacial feature is that of electrostatic charge correspondence. This can either take the form of a simple matching between a cationic face and anionic matrix surface or may involve more sophisticated recognition of geometrical charge patterns or motifs. Stereochemical complementarity of matrix functional groups and lattice molecular anions seems to be an additional factor in many cases. Also, hydrophobic and hydrogen-bond interactions may be important. Clearly, this is an exciting area of research and many questions remain unanswered. Thus, it was the aim of this thesis to further explore and elucidate these molecular recognition processes.

1.5 *Overview of the Thesis*

The main part of this work is devoted to simple chemical models of biomineralization. Specifically, the work enquires into the morphological effects of molecular additives on calcite crystallization. In chapter 3, the chosen method for preparing the crystals is described and investigated. Chapter 4 then goes on to assess a range of simple, low molecular weight, organic and inorganic additives and chapter 5 deals with the effects of some larger macromolecules. Also, complementary investigations of an $CaCO_3$ biomineral are presented. Chapter 6 describes further crystallographic studies on coccoliths from the marine alga *Emiliania huxleyi* focusing on the nucleation, growth and habit of the crystals at the early stages of formation. The thesis closes with general conclusions and recommendations for possible further work in chapter 7.

1.6 *References*

Addadi, L., Weiner, S. (1985), *Interactions Between Acidic Proteins and Crystals: Stereochemical Requirements in Biomineralization,* Proc. Natl. Acad. Sci. USA, **82**, 4110-4114.

Addadi, L., Weiner, S. (1986), *Interactions Between Acidic Macromolecules and Structured Crystal Surfaces. Stereochemistry and Biomineralization*, Mol. Cryst. Liq. Cryst., **134**, 305-322.

Addadi, L., Moradian, J., Shay, E., Maroudas, N.G., Weiner, S. (1987), *A Chemical Model for the Cooperation of Sulfates and Carboxylates in Calcite Crystal Nucleation. Relevance to Biomineralization*, Proc. Natl. Acad. Sci. USA, **84**, 2732-2736.

Berkovitch-Yellin, Z. (1985), *Toward an Ab Initio Derivation of Crystal Morphology*, J. Am. Chem. Soc., **107**, 8239-8253.

Berman, A., Addadi, L., Weiner, S. (1988), *Interactions of Sea Urchin Skeleton Macromolecules with Growing Calcite Crystals - A Study of Intracrystalline Proteins*, Nature, **331**, 546-548.

Bills, P.M. (1985), *The Precipitation of Calcium Carbonate Polymorphs In Vitro at 37°C*, Calcif. Tissue Int., **37**, 174-177.

Boistelle, R., Astier, J.P. (1988), *Crystallization Mechanisms in solution*, J. Cryst. Growth, **90**, 14-30.

Borman, A. de Jong, E.W., Huizinga, M., Kok, D.J., Westbroek, P., Bosch, L. (1982), *The Role in $CaCO_3$ Crystallization of an Acid Ca^{2+}-Binding Polysaccharide Associated with Coccoliths of Emiliania huxleyi*, Eur. J. Biochem., **129**, 179-183.

Bragg, W.L. (1915), *The Analysis of Crystals by the X-ray Spectrometer*, Proc. Roy. Soc. (London), **89A**, 468.

Bravais, A. (1849), *The Crystal Considered as a Simple Assemblage of Points,* Etudes cristallographiques (Paris), Part I, 101-194

Brooks, R., Clark, L.M., Thurston, E.F. (1950/51), *Calcium Carbonate and its Hydrates*, Phil. Trans. Roy. Soc. (London), **A243**, 145-167.

Buckley, H.E. (1933), *Systematic Habit-Variation in $KClO_3$ Crystals Produced by Dyes,* Z. Krist., **85**, 58.

Buckley, H.E. (1949), *Habit Modification in Crystals as a Result of the Introduction of Impurities During Growth*, Farad. Disc., **5**, 243-254.

Carter J.G. (Ed.), (1990), *Skeletal Biomineralization: Patterns, Processes and Evolutionary Trends (2 vols.)*, New York: Van Nostrand Reinhold.

Chessin, H., Hamilton, W.C. (1965), *Positions and Thermal Parameters of Oxygen Atoms in Calcite*, Acta Cryst. **18**, 689-693.

Curie, P. (1885), *On the Formation of Crystals and on Capillary Constants of their Different Faces*, Bull. Soc. Minéral., **8**, 145-150.

Dana, E.S. (1932), *A Textbook of Mineralogy*, 4th ed., Ford, W.E. (Ed.), New York: John Wiley and Sons.

Davey, R.J., Polywka, L.A., Maginn, S.J. (1991), *The Control of Crystal Morphology by Additives: Molecular Recognition, Kinetics and Technology*, in "Advances in Industrial Crystallization" Garside, J., Davey, R.J., Jones, A.G. (Eds.), pp 150-165, Oxford: Butterworth-Heinemann.

Deer, W.A., Howie, R.A., Zussman J. (1962), *Rock-Forming Minerals*, vol. **5**, pp 229-255, London: Longmans.

De Jong, E.W., Westbroek, P., Bosch, L., (1976), *Isolation and Characterization of a Ca^{2+}-Binding Polysaccharide Associated with Coccoliths of Emiliania huxleyi (Lohmann) Kamptner*, Eur. J. Biochem., **70**, 611-621.

Donnay, J.D.H., Harker, D. (1937), *A New Law of Crystal Morphology Extending the Law of Bravais*, Am. Mineralogist, **22**, 446-467.

Folk, R.L., Chafetz, H.S., Tiezzi, P.A. (1985), *Bizarre Forms of Depositional and Diagenetic Calcite in Hot Spring Travertines from Central Italy*, in Carbonate Cements, Schneidermann, N., Harris, P.M. (eds.), Spec. Pub., S.E.P.M., **36**, 349-369.

Friedel, G. (1907), *Studies on Bravais's Law*, Bull. Soc. Franc. Mineral., **20**, 326-455.

García-Ruiz, J.M., Prieto, M., Amorós, J.L. (1979), *On the Influence of Diffusion in the Formation of Curved Faces in Crystals. II Experimental*, Estudios geol., **35**, 449-457.

García-Ruiz, J.M. (1985), *On the Formation of Induced Morphology Crystal Aggregates*, J. Cryst. Growth, **73**, 251-262.

García-Ruiz, J.M., Dominguez Bella, S. (1987), *Banding Structures in Induced Morphology Crystal Aggregates of Calcium Carbonate*, J. Mat. Sci., **22**, 3095-3102.

García-Ruiz, J.M., Dominguez Bella, S., Gomez de Salazar, J.M. (1988), *Morphogenetical and Textural Characterization of Calcite IMCA grown in Silica Gel at pH 10*, J. Sed. Petrology.

Garside, J. (1982), *Nucleation*, in Biological Mineralization and Demineralization, Nancollas, G.H. (Ed.), pp 23-35, Berlin: Springer-Verlag.

Gibbs, J.W. (1878/1906), *On the Equilibrium of Heterogeneous Substances*, The Scientific Papers of J. Willard Gibbs, vol. 1, Thermodynamics, London: Longmans Green & Co.

Hartman, P. (1973), *Structure and Morphology*, in Crystal Growth: An Introduction, pp 367-402, Bardsley, W., et al (Eds.), North Holland/American Elsevier.

Hartman, P., Perdok, W.G. (1955), *On the Relation Between Structure and Morphology of Crystals*, Acta Cryst. **8**, I 49-52, II 521-525.

Haüy, R.J. (1860), *Elementary Treatise on Physics*, 2nd ed., pp 59-78.

Heijnen, W.M.M. (1985), *The Morphology of Gel Grown Calcite*, N. Jb. Miner. Mh., **8**, 357-371.

Ichikuni, M. (1983), *Anionic Substitution in Calcium Carbonate*, in Significance of Trace Elements in Solving Petrogenetic Problems and Controversies, Augustithis, S.S. (Ed.), pp 83-94.

Kirov, G.K., Vesselinov, I., Cherneva, Z. (1972), *Conditions for the Formation of Calcite Crystals of Tabular and Acute Rhombohedral Habits*, Krist. und Technik, **7**, 497-509.

Larson, M.A. (1991), *Solute Clustering and Secondary Nucleation,* in "Advances in Industrial Crystallization" Garside, J., Davey, R.J., Jones, A.G. (Eds.), pp 20-30, Oxford: Butterworth-Heinemann.

Lippman, F. (1973), *Crystal Chemistry of Sedimentary Carbonate Minerals*, in Sedimentary carbonate minerals, Minerals, Rocks and Inorganic materials Series, Berlin: Springer-Verlag.

Lowenstam, H.A., Weiner, S. (1989), *On Biomineralization*, Oxford: Oxford University Press.

Mackrodt, W.C., Davey, R.J., Black, S.N., Docherty, R. (1987), *The Morphology of* α-Al_2O_3 *and* α-Fe_2O_3*: The Importance of Surface Relaxation,* J. Cryst. Growth, **80**, 441-446.

Mann, S. (1988), *Molecular Recognition in Biomineralization, Nature*, **332**, 119-124.

Mann, S. (1989a), *Crystallochemical Strategies in Biomineralization*, in *Biomineralization: Chemical and Biochemical Perspectives*, Mann, S., Webb, J., Williams, R.J.P. (Eds.), pp 54-56, Weinheim: VCH.

Mann, S., Heywood, B.R., Rajam, S., Birchall, D. (1989b), *Interfacial Control of Nucleation of Calcium Carbonate Under Organized Stearic Acid Monolayers*, Proc. R. Soc. (London), **A 423**, 457-471.

McCauley, J.W., Roy , R. (1974), *Controlled Nucleation and Crystal Growth of Various $CaCO_3$ Phases by the Silica Gel Technique*, Am. Mineralogist, **59**, 947-963.

Merten, H.L., Bachman, G.L. (1980), Monsanto Company, St Louis, USA, *Stabilized Amorphous Calcium Carbonate*, US Patent no. 4,237,147.

Michaels, A.S., Colville, A.R. (1960), *The Effect of Surface Agents on Crystal Growth Rate and Crystal Habit*, J. Phys. Chem., **64**, 13.

Mullin, J.W. (1961), *Crystallization*, pp 128-135, London: Butterworths.

Nielsen, A.E., Christoffersen, J. (1982), *The Mechanisms of Crystal Growth and Dissolution*, in Biological Mineralization and Demineralization, Nancollas, G.H. (Ed.), pp 37-77, Berlin: Springer-Verlag.

Ostwald, W. (1897), Z. Physik. Chem., **22**, 289.

Palache, C. (1943), *Calcite: An Angle Table and Critical List*, Contr. 259, Dept. Mineralogy and Petrology, Harvard University, USA.

Rajam, S., Mann, S. (1990), *Selective Stabilization of the (001) Face of Calcite in the Presence of Lithium*, J. Chem. Soc. Chem. Commun., **24**, 1789-1791.

Reeder, R.J. (1983), *Crystal Chemistry of the Rhombohedral Carbonates*, Rev. Miner., **11**, 1-47.

Shaikh, A.M. (1990), *A New Crystal Growth Form of Vaterite, $CaCO_3$*, J. Appl. Cryst., **23**, 263-265.

Staab, E., Addadi, L., Leiserowitz, L., Lahav, M. (1990), *Control of Polymorphism by 'Tailor-Made' Polymeric Crystallization Auxiliaries. Preferential Precipitation of a Metastable Polar Form for Second Harmonic Generation*, Adv. mater. **2(1)**, 40-43.

Steno, N. (1669), *De Solido Intra Solidum Naturaliter Contento Dissertationis Prodromus*, Florence, Italy.

Stephens, P.W., Goldman, A.I. (1991), *The Structure of Quasicrystals*, Scientific American, April, 24-31.

Stricker, S.A. (1985), *The Ultrastructure and Formation of the Calcareous Ossicles in the body wall of the Sea Cucumber Leptosynapta clarki (Echinodermata, Holothuroida)*, Zoomorphology, **105**, 209-222.

Sunagawa, I. (1953), *Variation of Crystal Habit of Calcite*, Geol. Survey Japan Report no. 155, 1-66.

Svanoe, H. (1959), *Solids Recovery by Crystallization*, Chem. Eng. Progress, **55(5)**, 47-54.

Titiloye, J.O., Parker, S.C., Osguthorpe, D.J., Mann, S. (1991), *Predicting the Influence of Growth Additives on the Morphology of Ionic Crystals*, J. Chem. Soc., Chem. Commun., **20**, 1494-1496.

Weiner, S., Traub, W. (1984), *Macromolecules in Mollusc Shells and their Functions in Biomineralization*, Phil. Trans. R. Soc. Lond. **B304**, 425-434.

Weissbuch, I., Addadi, L., Lahav, M., Leiserowitz, L. (1991), *Molecular Recognition at Crystal Interfaces*, Science 9 Aug., **253**, 637-645.

Wells, A.F. (1946), *Crystal Habit and Internal Structure,* Phil. Mag. Ser. 7, **37**, 184-199 and 217-236.

Wells, A.F. (1975), *Structural Inorganic Chemistry,* 5th ed., p688, Oxford: OUP.

Wilbur, K.M., Bernhardt, A.M. (1984), *Effects of Amino Acids, Mg and Molluscan Extrapallial Fluid on Crystallization of Calcium Carbonate: In vitro Experiments,* Biol. Bull., **166**, 251-259.

Wheeler, A.P., George, J.W., Evans, C.A. (1981), *Control of $CaCO_3$ Nucleation and Crystal Growth by Soluble Matrix of Oyster Shell,* Science, **212,** 1397-1398.

Wheeler, A.P., Sikes, C.S. (1984), *Regulation of Carbonate Calcification by Organic Matrix,* Amer. Zool., **24**, 933-944.

Wheeler, A.P., Sikes, C.S. (1988), *Control of $CaCO_3$ Crystallization by Polyanionic-Hydrophobic Polypeptides,* in Chemical Aspects of Regulation of Mineralization, pp 15-20, Mobile, Alabama: University of South Alabama Publications.

Wheeler, A.P., Rusenko, K.W., Sikes, C.S. (1988), *Organic Matrix from Carbonate Biomineral as a Regulator of Mineralization,* ibid., pp 9-13.

Whetstone, J. (1955), *The Crystal Habit Modification of Inorganic Salts with Dyes,* Trans. Farad. Soc., **51**, 973-1142.

Wulff, G. (1901), *On the Question of the Rate of Growth and of the Dissolution of Crystals Faces,* Z. Krist., **34**, 449-530.

CHAPTER 2 INSTRUMENTAL AND EXPERIMENTAL METHODS

2.1 *Water Purification Procedure*

Local tapwater, of high hardness, was initially fed into an Aquatron A4D commercial still with dual boilers to produce double-distilled water. The output from the still was then further upgraded using a Purite Standard Stillplus^{TM} clean-up system incorporating a 0.2 μm bacterial filter, activated carbon cartridge and a mixed bed ion exchange column. The combination of these two procedures produced very high quality water (BS 3978 Grade 1) of typical conductivity better than 1 μScm^{-1} and pH 5-6.

2.2 *Preparation of Glassware*

All glassware was first soaked in hot detergent solution, then after rinsing with distilled water, re-soaked in dilute hydrochloric acid and finally rinsed with high quality water and dried in an oven.

2.3 *Preparation of Synthetic Calcium Carbonate* (fig. 2.1)

The supersaturated calcium bicarbonate solution was prepared according to the procedure adopted by Kitano (1962) with some modifications. BDH analar calcium carbonate, shown to be calcite by XRD analysis, was suspended (2.5 gl^{-1}) in Purite^{TM} distilled water. This suspension (pH 8.0-8.4) was then bubbled with carbon dioxide (3 $lmin^{-1}$) scrubbed through twin Hirsch bottles (250 ml) containing the same pure water for an initial period of one hour with mechanical stirring. The remaining calcium carbonate was then removed using Buchner filtration (Whatman filter paper no. 42). A further period of half an hour bubbling was then employed to dissolve any crystal nuclei that might be present. The resulting bicarbonate solution (pH 5.8-6.0) was then ready for crystal growth experiments and could be transferred to suitable crystallization dishes or bottles that were covered but left open to the atmosphere under ambient conditions or placed within a thermostatted bath.

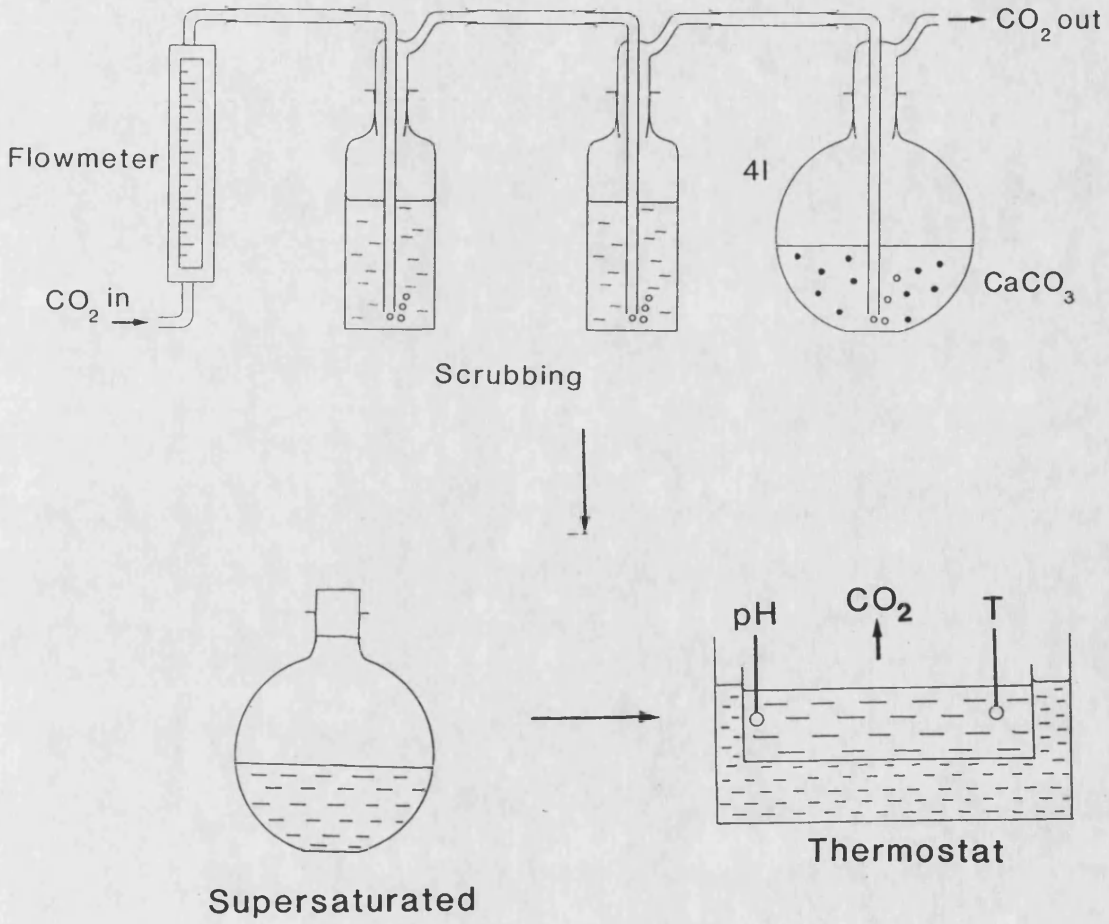

Fig. 2.1 Experimental apparatus for the preparation of $CaCO_3$

2.4 *EDTA Volumetric Analysis for Calcium* (Vogel 1978)

A value for the total dissolved calcium (Ca_T) in an aqueous system was determined by pipetting 25 ml of the solution to be analysed into a conical flask together with 2 ml of HCl (2 N) and 25 ml of distilled water. This solution was then boiled to completely remove carbonate and cooled. Then, 4 ml of NaOH (8 M) was added to adjust the pH to about 12-13. After allowing it to stand for a few minutes, six drops each of KCN (10 %) and hydroxylamine hydrochloride (10 %) plus approximately 0.05g of HHSNNA indicator 2-hydroxy-1-(2-hydroxy-4-sulpho-1-naphthylazo) -3-naphthoic acid were introduced. This was then titrated against standardized EDTA of concentration appropriate to the expected level of calcium in the solution. Colour change was from wine red (Ca-indicator complex) to dark blue (free indicator). All titrations were performed in duplicate.

2.5 *Measurement of pH*

Various instruments were used such as a Kent Industrial Instruments EIL 7045/46 digital pH meter plus Radiometer PHM84 research and standard meters and electrodes. Supplied standard buffer solutions, covering the pH range of interest were used to calibrate the electrode apparatus (Fisons phthalate pH 4; Fisons phosphate pH 7; BDH MgKI pH 9). Very pure water caused great instability in all electrode readings such that the measurement of pH was not accurate within at least 0.5 of a unit. The monitoring of pH changes was carried out with a JJ Instruments PL2500 chart recorder which was able to plot readings from two separate electrodes. Solutions were thermostatted with a TE-7 Tempette Tecam thermostat at 25 ± 1°C for this purpose.

2.6 *Optical Microscopy (OM)*

Two compound instruments were used; a Zeiss Axioskop and a Leitz Orthoplan capable of magnifications from x100 to x1000 at the eyepiece. Both were equipped for photomicrography producing 35 mm negatives with magnifications from x25 to

x250. The Zeiss was fitted with special objectives (x10, x20, x50, x100) that gave better than usual depth of field and obviated the need for cover glasses. Absolute limit of resolution was 0.25 μm. Polarised light was used in some cases to assess crystal orientation. Also, for *in situ* observations, a Meiji EMZ-TR-PB stereoscopic zoom instrument (x14 to x90 at the eyepiece) was used which could also be fitted with a camera (x3.5 to x22.5 on the negative).

Crystal samples were retrieved from the air/water interface so as not to disrupt surface structures and crystal orientations. This was achieved by carefully dipping glass slides or cover slips through the interface. Cover slips were placed on the bottom of each container in order to collect any bottom crystals that formed. These slips could then be mounted on slides with double-sided sticky tape. All specimens were viewed without covering.

Size measurements were made by one of two methods. It was possible to measure crystals directly during observation using eyepiece graticules. Data could also be taken from the 35 mm negative or print and the sizes calculated using the final magnification (calibrated against standard grids).

2.7 *Scanning Electron Microscopy (SEM)*

Because of limitations in resolution and depth of field with light microscopy, more detailed morphological examinations were carried out with scanning electron microscopy. A JEOL JSM T330 scanning electron microscope was used capable of usefully magnifying the crystals up to x20 000 when operating at 25 KeV. Absolute limit of resolution at 30 KeV is quoted as 7 nm for a gold specimen but in practice resolution is dependent on the sample and thus probably only 10-20 nm at best. Routine imaging up to x10 000 was carried out at 10-15 KeV.

Samples of crystals for SEM were prepared on cylindrical 10 mm diameter

aluminium stubs. Several loading techniques were employed. Crystals were either deposited directly onto the flat surface of the stub or onto a layer of double-sided sticky tape; the latter method ensured a more secure loading. Coverslips with attached crystals could also be mounted with double-sided tape. All stubs were then coated for 2-5 minutes with a thin layer of gold to prevent charging using an Edwards S150B sputter coater.

2.8 *Transmission Electron Microscopy (TEM)*

Samples were prepared for transmission electron microscopy on formvar-covered, carbon-coated, 3 mm copper grids. The main instrument used was the JEOL 2000FX capable of accelerating voltages up to 200 KeV having an absolute limit in point to point resolution of 2.8 Å and in lattice resolution of 1.4 Å. In addition, a JEOL 1200EX (120 KeV; resolution: point to point 4.5 Å; lattice 2.0 Å) was employed. Micrographic data was recorded on Agfa-Gevaert Scientia photographic plates (100 x 80 mm) located at the base of the instrument. The 2000FX instrument was fitted with 20, 40, 70, 120, 200 μm condenser apertures and 20, 50, 80 μm objective apertures. Operational procedures are described in
Appendix 1.

Selected area electron diffraction (SAED) could be carried out with three field limiting apertures of 300, 100 and 20 μm and camera lengths between 13-270 cm in 15 steps. Diffraction patterns were taken by first adjusting the magnification, aligning and focusing the TEM image and removing the objective aperture. On switching to Selected Area Mode, the field limiting aperture could be introduced, centred and focused. The pattern was then viewed by pressing Diffraction Mode and adjusted by tilting the goniometer (maximum X tilt = ± 30°) if necessary. Once a micrograph had been taken on manual exposure, the corresponding TEM image could then be recorded immediately afterwards. D spacings were calculated as follows:

$$d\text{Å} = \frac{\lambda\text{Å}\, L_{mm}}{r_{mm}}$$

λ Relativistic wavelength
@ 120 KeV = 0.0334 Å
@ 200 KeV = 0.0251 Å

L Camera length

r Distance from spot to origin

The pattern was indexed and checked for self-consistency via the vector addition and subtraction of surrounding spots forming parallelograms. The d spacing of planes, in addition to interplanar and interzonal angles, could be calculated using the equations in Appendix 2. The corresponding zone axis, a unique direction through the crystal lattice coplanar with all the diffracting planes, could then be worked out using simultaneous equations.

High resolution TEM (HRTEM) was carried out on the 2000FX. The instrument had to be carefully aligned and left to stabilize for some time before use. The technique required taking groups of micrographs of the same image at different conditions of defocus beginning at Gaussian (ideal focus) and ending at Schertzer (optimum under focus). Due to the relatively low decomposition temperature of $CaCO_3$ (*ca.* 900°C), calcite crystals were very sensitive to the electron beam and were easily damaged. Consequently, lattice imaging was performed under conditions of minimal beam exposure. This entailed the correction for objective astigmatism and focusing (Gaussian or defocus) on the carbon substrate at the required magnification (usually x400,000 or x500,000) whilst the crystal was out of the field of illumination. Once optimum conditions were set up, the crystal could be moved in and a micrograph quickly recorded. The crystal was always withdrawn from the beam in between exposures. Fringes were measured from large blow-up prints (x9) of the negatives. The error in magnification ($\approx$ 5%) was calculated by measuring (002) (3.36 Å)

fringes from a standard graphite specimen.

2.9 *Energy Dispersive X-ray Analysis (EDXA)*

Qualitative and semi-quantitative elemental analysis could be performed on the JEOL 35C SEM and both TEM microscopes with energy dispersive X-ray analysis (EDXA) technique. The detector used was a Link Li-drifted, silicon type and had a limit of detection, depending on the element, in the order of 0.5 % w/w. The SEM had a removal Be window on the SEM whereas the TEM instruments were windowless. A Link AN10000 X-ray microanalysis system accumulated and processed the spectra.

2.10 *X-ray Diffraction (XRD)*

Milligram samples were routinely assayed for the predominant crystalline phases using a Philips PW-1130 X-ray powder diffractometer fitted with a Debye-Scherrer camera (diameter = 11.4592 cm) employing the Straumanis method of mounting. The crystals were finely ground, placed in a Lindeman capillary tube (highly amorphous lithium glass) and exposed to Cu K_α radiation (α_1 = 1.54050 Å, α_2 = 1.54434 Å, weighted mean = 1.5418 Å) at 40 KV, 20 mA for 3-4 hours on average. In this arrangement, the distance between the entrance and exit holes represented 180° 2θ. The d-spacings were calculated from the Bragg equation: $n\lambda = 2d\sin\theta$ and compared to standard values obtained from the ASTM (JCPDS) cards.

Also a Philips PW 1730 diffractometer with a 4 KW X-ray generator and a long fine focus, 2 KW copper target tube was used. The diffractometer was fitted with a PW 1820/00 computer controlled vertical goniometer that was capable of scanning from 4-135° 2θ and a PW 1711/10 Xe proportional counter with graphite monochromator. Data was collected on a PM8203 chart recorder.

Miller-Bravais indices hkil or hk.l for planes/faces and Weber uvtw or uv.w indices

for directions based on the simplest, X-ray hexagonal unit cell for calcite (a = b = 4.99 Å, c = 17.00 Å; c/a = 3.41; $\alpha = 90°$, $\beta = 90°$, $\gamma = 120°$) were used throughout. Round brackets ie (hkil) signified a particular plane or face whereas curly brackets ie {hkil} represented a set of symmetry-equivalent planes or faces; similarly [uvtw] signified a single direction and <uvtw> symmetry-equivalent directions through the lattice. These had advantages over the Miller 3 index (hkl) or [uvw] notation, based on rhombohedral unit cells, in that symmetry-related indices could easily be recognised. Miller indices were therefore avoided in common with most modern descriptions of the calcite structure (see also chapter 1.3). However, the calculation of interplanar and interzonal angles required 3 index notation. Conversions between the two notations were as follows (McKie and McKie 1986, pp 69-75):-

(hkil) $\leftrightarrow$ (hkl) simply add/remove i as long as h+k+i=0

[uvw] $\rightarrow$ [UVTW]

$U = 1/3\ (2u - v)$

$V = 1/3\ (2v - u)$

$T = -1/3\ (u + v)$

$W = w$

[UVTW] $\rightarrow$ [uvw]

$u = U - T$

$v = V - T$

$w = W$

eg $[20\bar{2}1] \equiv [421]$

2.11 *Crystal Plotting Software*

Crystallographic data on calcite and other structures was obtained via national computer networks from the Cambridge Crystallographic Database at Daresbury, UK. Specifically, the Inorganic Crystal Structure Database (ICSD) was accessed and the files transferred back to the host computer (Gould mainframe, University of

Bath). A typical output dataset is shown in Appendix 3 and includes information such as the space group, unit cell parameters, atomic coordinates of the asymmetric unit and connectivity. The structure was viewed using the *PLUTO* program which additionally required, as input, the full set of symmetry operations pertaining to the space group; these were taken from the International Tables for Crystallography (1983). *PLUTO* was able to plot cell projections along directions specified either by a view line or view rotation matrix (see Appendix 3). The structure of planes/faces (hk.l) was visualized by specifying the rhombohedral vector [uvw] that is perpendicular to (hk.l) as the input view line. Matrix methods involving the reciprocal metric tensor for the hexagonal system were used to calculate this normal vector (McKie and McKie 1986, p151). Crystal morphology was plotted using the program *MORPH* developed by Dr Mark Davies and Dr Steve Parker of the Solid State Research Group, University of Bath. The space group, lattice vectors and relative surface energies of the chosen faces were required as input (see Appendix 3).

2.12 *Infra-red Spectroscopy (IR)*

Infra-red analysis of crystals was carried out on two instruments. A Perkin-Elmer 983 IR spectrophotometer complete with IR data station. Samples were prepared by suspending ground crystals in methanol and air-drying on to polished NaCl discs. Routine resolution was 3 cm^{-1} although individual peaks could be re-scanned at higher resolution eg 2 or 1 cm^{-1}. In addition, a Perkin-Elmer 1720X fourier transform infra-red (FTIR) spectrophotometer and data station were employed fitted with a diffuse reflectance unit. The samples were ground and mixed with KBr to make an approximately 1-10 % w/w solid solution. Routine resolution was 2 cm^{-1}.

2.13 *Elemental Microanalysis for C, H and N*

CHN analysis was conducted on a Carlo Erba model 1106 elemental analyser. The sample (usually about 5 mg) was burnt in a combustion tube at 1020°C in O_2

alongside a reference. The combustion products (CO_2, H_2O, N oxides etc) were then passed down a Cr_2O_3 column meeting Ag-coated mixed valence Co oxide to remove halogens and sulphur. In addition, heated Cu took out O_2 and reduced oxides of nitrogen to N_2. The outflow from this column containing only CO_2, H_2O and N_2 was then routed into a GC employing He as the carrier gas and a hot wire detector. Analyses were normally carried out in duplicate and results were found to have a reproducibility of better than 0.05 %.

2.14 *Raman Spectroscopy*

Approximately 50-100 mg of powdered sample were placed in a Lindeman capillary tube which was then sealed. Raman spectra were obtained with a SPEX model 1401 spectrophotometer. The source used was a 300 mW Lexer model 85 argon ion laser (λ = 5145 Å green or 4180 Å blue excitation lines). Light scattered was collected at 90° from the incident beam and routed through an entrance slit (200 μm), intermediate (250 μm) and exit slit (250 μm) before being detected by an EMI 9658A photomultiplier tube operating at 1.9 KV, -15°C.

2.15 *Surface Tension Measurements*

Isotherms were measured on a circular Nima Technology System 2000 Langmuir-Blodgett mini trough of 1 litre capacity, 995 cm^2 maximum and 25 cm^2 minimum area. Surface presure was measured with a Wilhelmy Plate balance. Operation was fully automated via an interface with a dedicated PC and software.

2.16 *References*

ASTM cards, *Annual Report to the Joint Committee on Powder Diffraction Standards.*

International Tables for Crystallography (1983), Vol. A, Space Group Symmetry, Hahn, T. (ed.), Dordrecht (Holland): D. Reidel Publishing Co.

Kitano, Y. (1962), *The Behaviour of Various Ions in the Separation of Calcium Carbonate from Bicarbonate Solution,* Bull. Chem. Soc. Jap., **35**, 1973-1980.

McKie, D., McKie, C. (1986), *Essentials of Crystallography*, Oxford: Blackwell Scientific Publications.

Vogel, A.I. (1978), *Textbook of Quantitative Inorganic Analysis*, 4th Ed., London: Longmans.

CHAPTER 3

STUDIES ON THE KITANO SYSTEM OF $CaCO_3$ CRYSTALLIZATION

3.1 INTRODUCTION

In order to study the influence of various molecules on calcite crystal growth, it was first necessary to consider suitable methods of crystallization. An ideal system would grow calcite reproducibly, in high yield with well-defined equilibrium morphologies and a homogeneous size distribution. There were also two additional requirements for work involving additives; firstly, the number of potentially interfering species in solution was best kept to a minimum and, secondly, the working pH range should be appropriate to the ionic species under study.

A number of preparations have been described. Perhaps most commonly used is the metastable $NaHCO_3/CaCl_2$ solution mixture adopted in many kinetic studies (Reddy and Nancollas 1971, 1973, 1976, Reddy 1977, 1986, Söhnel and Mullin 1982, Meyer 1984, Giannimaras and Koutsoukos 1986, House 1987, Walker *et al* 1991 etc). Janeković and Matijević (1985) reported the growth of monodisperse rhombohedral $CdCO_3$ by adding cadmium nitrate to a preheated 10 M urea solution. The procedure can be easily adapted for calcium carbonate. Another method is to bubble CO_2 through solutions of slaked lime [$Ca(OH)_2$]. However, it was decided that the system used extensively by Kitano, outlined first in 1962, was the most appropriate method. It involves bubbling carbon dioxide through a suspension of calcium carbonate which is then filtered to produce a clear, calcium bicarbonate solution. Supersaturation is then generated by the spontaneous evolution of dissolved carbon dioxide enabling precipitation to occur as follows:

$$Ca(HCO_3)_{2\,(aq)} \rightarrow CaCO_{3\,(s)}\downarrow + CO_{2\,(g)}\uparrow + H_2O_{(l)}$$

The method was chosen primarily because it is simple and involves few species in solution. Furthermore, in many cases, the natural formation of the mineral follows this route such as in marine environments, limestone terrains and hot springs.

Description of Solution Chemistry - Thermodynamics

At a given temperature, the solubility of $CaCO_3$ in pure water is highly dependent on the pH which is directly linked to the CO_2 content. Fig. 3.1 shows, for a system in equilibrium with calcite, how the pH and calcium concentration both vary with the partial pressure of carbon dioxide.

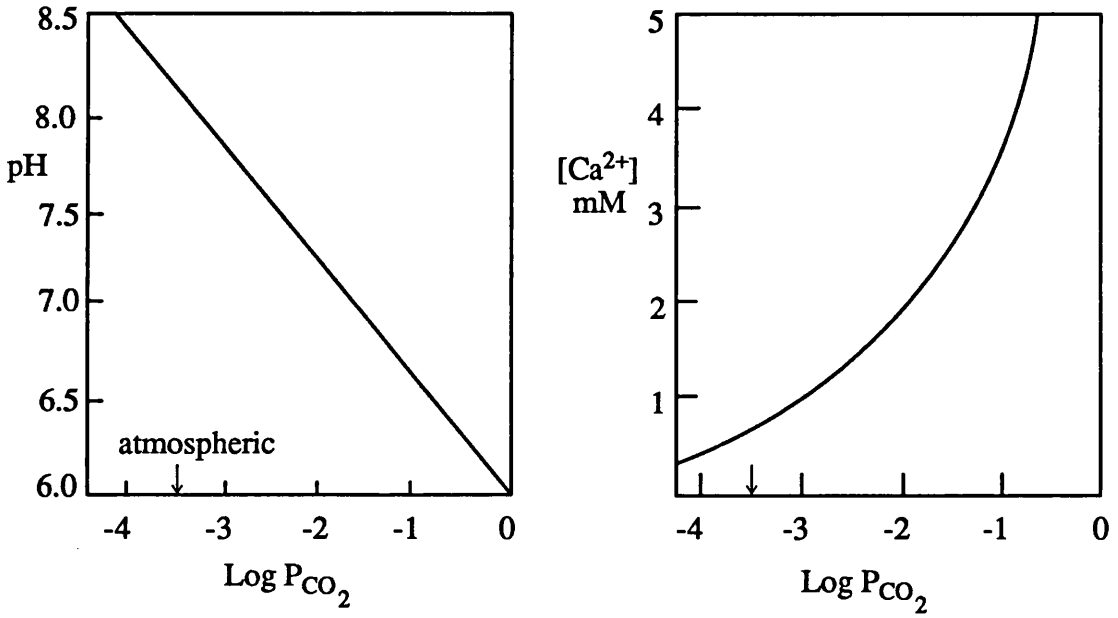

Fig. 3.1 *Relationship between pH-LogP_{CO_2} and [Ca^{2+}]-LogP_{CO_2} for pure water in equilibrium with calcite at 298K and one atmosphere total pressure. Redrawn from Drever (1982).*

Thus, at normal atmospheric pressure, P_{CO_2} = 0.0003 atm (log P_{CO_2} = -3.5), the pH is about 8.1 and the total calcium concentration approximately 0.5 mM. Whilst at 1 atm partial pressure (log P_{CO_2} = 0), pH ≈ 6 and $[Ca]_T$ ≈ 10 mM. The representative reaction equations for this system are shown in fig. 3.2.

At atmospheric pressure, the equilibrium is well over to the left and the forward

	pK
$CO_{2\,(aq)} + H_2O \rightleftharpoons H_2CO^*_{3\,(aq)}$	1.47
$H_2CO^*_{3\,(aq)} \rightleftharpoons H^+_{(aq)} + HCO^-_{3\,(aq)}$	6.35
$CO_3^{2-}{}_{(aq)} + H^+_{(aq)} \rightleftharpoons HCO^-_{3\,(aq)}$	-10.3
$CaCO_{3\,(s)} \rightleftharpoons Ca^{2+}{}_{(aq)} + CO_3^{2-}{}_{(aq)}$	8.42
$CaCO_{3(s)} + CO_{2(g)} + H_2O_{(l)} \rightleftharpoons Ca^{2+}{}_{(aq)} + 2HCO_3^-{}_{(aq)}$ (calcite)	5.92‡

$$K_{pso} = \frac{[Ca^{2+}][HCO_3^-]^2}{P_{CO_2}} \quad \text{mole}^3\ \text{litre}^{-3}\ \text{atm}^{-1}$$

$$\Delta G^o = +\ 33.7\ \text{KJmol}^{-1}$$

‡ Sillen (1971) 298 K, I→0, $P_{CO_2} = 0.0003$ atm

Fig. 3.2 *Carbonate equilibria and thermodynamic data*

process is thermodynamically unfavourable. Despite this, ΔG for the reaction can become negative if the P_{CO_2} increases above its standard state. Thus, bubbling CO_2 through a saturated solution will dissolve $CaCO_3$ until a new equilibrium is established. A subsequent lowering of P_{CO_2} in the water (eg due to outgassing) will lead to precipitation as the reaction shifts back to the left.

The CO_2 content and hence the solubility of calcite in natural waters can be quite variable. For example, rainwater often becomes enriched in calcium as it percolates through soil with a higher than atmospheric carbon dioxide content. $CaCO_3$ may then crystallize when these groundwaters are re-exposed to atmospheric conditions. Stalactites in subterranean caves are formed under these circumstances (Drever 1982, p 55). Hydrothermal waters, under great pressure in the earth's crust, carry significant quantities of dissolved calcium due to similar reasons. At hot springs, where the waters come to the surface, the sudden environmental change causes extensive precipitation (Press and Siever 1986). Another important phenomenon

involving this system are the biologically-induced deposits. Photosynthetic activity by aquatic organisms often results in localized regions of water being undersaturated with CO_2. Consequently, minerals accumulate at these specific sites which may be in the immediate vicinity of the organism or actually on the cell surface itself (Borowitzka 1989).

Aqueous CO_2 concentrations depend not only on the partial pressure of CO_2 in the gas phase but also on its solubility in water which varies markedly with temperature. Cold water is able to dissolve more CO_2 and can therefore contain more $CaCO_3$ than warm water. Accordingly, heating such solutions induces precipitation which is what happens when scale forms in boilers.

Kinetic Considerations (Stumm and Morgan 1981)

The available rate data for this system are shown in table 3.1. The rates of precipitation are governed by the gradual evolution of dissolved CO_2. The first order dehydration reaction takes approximately half a second to attain equilibrium whereas the ionic equilibria are extremely rapid. The time required to transfer CO_2 molecules from the aqueous to the gas phase depends chiefly on the thickness (δ) of a liquid boundary layer at the surface. This physical obstacle is affected only by the extent of mixing in the solution; δ is small for high agitation.

Reaction	Equation	Rate Constants @ 25°C
Carbonic acid formation	$HCO_3^-{}_{(aq)} + H^+{}_{(aq)} \rightleftharpoons H_2CO_3^*{}_{(aq)}$	$k = 4.7 \times 10^{10}\ M^{-1}sec^{-1}$
Dehydration	$H_2CO_3^*{}_{(aq)} \rightleftharpoons CO_2{}_{(aq)} + H_2O$	$k = 11.9\ sec^{-1}$
Gas Transfer	$CO_2{}_{(aq)} \rightleftharpoons CO_2{}_{(g)}$	? slow - depends on δ

Table 3.1 *Kinetic data for carbonate processes (Edsall 1969)*

3.2 EXPERIMENTAL

Pure, seedless, $Ca(HCO_3)_2$ solutions were prepared as described in Chapter 2.3. Volumes of 250 ml were poured into 1 litre capacity crystallization dishes and left to grow crystals open to the atmosphere. The dishes were loosely covered with filter paper to minimize contamination. Where measurements of pH and $[Ca]_T$ (EDTA titration) were taken over the course of the reaction, a thermostatic bath operating at 25°C was used.

Early crystallites were collected for transmission electron microscopy (TEM) and selected area electron diffraction (SAED) by sampling the supersaturated solution at 50, 60 and 120 minutes after crystallization had began. Grids were loaded by dipping through the surface followed by immediate blotting using filter paper and air drying. Mature crystals were retrieved as described in Chapter 2.6 and analysed by optical microscopy (OM), scanning electron microscopy (SEM), infra-red spectroscopy (IR) and powder X-ray diffraction (XRD). Size data was taken from OM micrographs by measuring the longest dimension of approximately 100 crystals. Computer calculations of initial solution speciation and degree of saturation with respect to solid phases were carried out using a program developed by Shellis (1988) called IONPRODUCT. The starting parameters of pH, $[Ca]_T$, P_{CO_2} and atmospheric pressure (mb) were used as input data. The program assumed a temperature of 25°C and required manual charge balance. Atmospheric pressure was not recorded in the experiments but was taken as 1.0 atmospheres (1013 mb).

Investigation of Factors Influencing System

A short study was undertaken to look at ways of improving the preparations of calcite. Optimization of the system required investigation of key factors such as initial supersaturation, temperature and CO_2 efflux rates. Supersaturation was varied by dilution of the fresh $Ca(HCO_3)_2$ solution whilst keeping the CO_2 flowrate (3

$lmin^{-1}$) and bubbling time (1 hr + 0.5 hr) constant. Dilutions from 2 times to 1000 times were evaluated. Crystallization at lower temperatures (0°C and 8°C) was investigated and compared to results obtained at ambient temperature (17-23°C). The outgassing rate of carbon dioxide was examined in two ways. Mechanical stirring of the crystallization solution was employed to speed up the release of CO_2 whereas placing an inert oil on the surface slowed it down. Pure vegetable oil and analar hexadecane were used as oil lids. In all experiments, a control was run in parallel for direct comparison. Crystal products were analysed by OM and XRD.

3.3 RESULTS

pH and $[Ca]_T$ changes

The pH variation with time for a typical run at 25°C is plotted in fig. 3.3a. The change is gradual over approximately 2 units of pH starting at 5.9 rising to about 7.8 after 20 hours and finally settling down at about 8.1 after a few days. The initial total calcium concentration in the bicarbonate solution was found to be on average around 8-9 mM corresponding to 0.36 gl^{-1} (360 ppm). This dropped to roughly 7 mM after 16-20 hours and about 0.5 mM after 45 days (fig. 3.3b).

Yields

The effect of bubbling the suspension with CO_2 for an hour resulted in about 1.0 gl^{-1} $CaCO_3$ or 0.4 gl^{-1} (400 ppm) Ca on average being dissolved. Thus, typical yields for 250 ml of crystallizing solution was approximately 0.25 g $CaCO_3$.

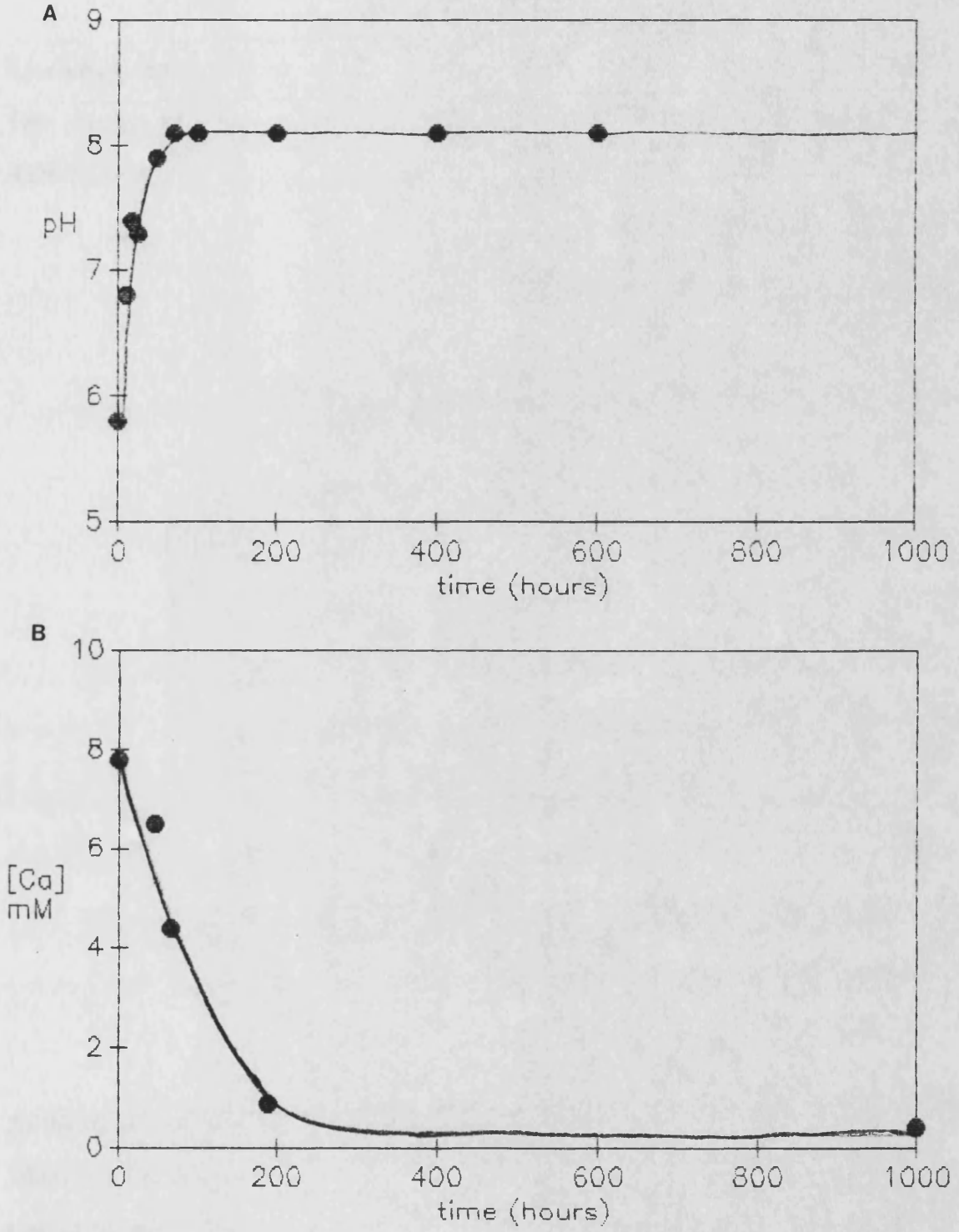

Fig. 3.3 *(a) Change of pH and total calcium concentration during crystallization.*

Speciation and State of Saturation

The results of thermodynamic calculations on the initial conditions using IONPRODUCT are illustrated in table 3.2.

P_{CO_2} = 1.0 atm $\quad$ $[Ca^{2+}]_T$ = 9.0 mM

T = 298 K $\quad$ pH = 5.98

Solid Phase	pIAP	pK_s	S
Calcite	8.52	8.48	0.95
Aragonite	8.52	8.35	0.80
Vaterite	8.52	7.91	0.49

I = 0.0251

Overall charge imbalance = -0.0101 mM

Table 3.2 *Results from IONPRODUCT program*

At the start of crystallization, the supersaturation ratio, as defined by $S = (IAP/K_s)^{1/n}$ where n is the number of ions in the mineral ($CaCO_3$ = 2), was effectively unity with respect to calcite taking into account variations in thermodynamic data and small charge imbalances. Consequently, the system was at equilibrium and supersaturation was zero.

Calculations made by Al-Khayat and Garside (1989) included a saturation state ratio based on the CO_2 content.

Input data: $P_{CO_2} = 0.316 \times 10^{-3}$ atm
$T = 290$ K
$[Ca] = 9$ mM
$pH = 6.00$

Results: $I = 0.0237$

Solubility of CO_2 at a particular ionic strength K_{CO_2} $= 0.0316$ mol l^{-1} atm^{-1}

Solubility of $CO_2 = K_{CO_2} P_{CO_2} = 0.1 \times 10^{-4}$ mol l^{-1}

Actual concentration of $CO_2 = [H_2CO_3^*] = 0.0367$ mol l^{-1}

$$S = \frac{[H_2CO_3^*]}{K_{CO_2} P_{CO_2}} = 3670$$

This parameter revealed the driving force for crystallization in the system. Once the bubbling stops, the calcium bicarbonate solution is supersaturated with respect to aqueous CO_2 and carbonic acid ($H_2CO_3^*$) but not with respect to the ion product. However, as the slow gas transfer process took place, the CO_3^{2-} activity and hence the supersaturation with respect to $CaCO_3$ increased. Actual levels were unknown because of the difficulty in conveniently measuring activity of CO_3^{2-}.

Observations on Mature Surface Crystals

Crystals, large enough to be seen with the naked eye, were first observed after about 2-4 hours located on the surface of the solution. Their numbers increased steadily attaining what appeared to be a steady state at about 16-20 hours. After this time, *in situ* optical microscopy revealed scattered aggregates and long disorganized chains of intergrown crystals growing in random directions on the surface (fig. 3.4). The chains were often branched and, in this way, loosely resembled dendrites.

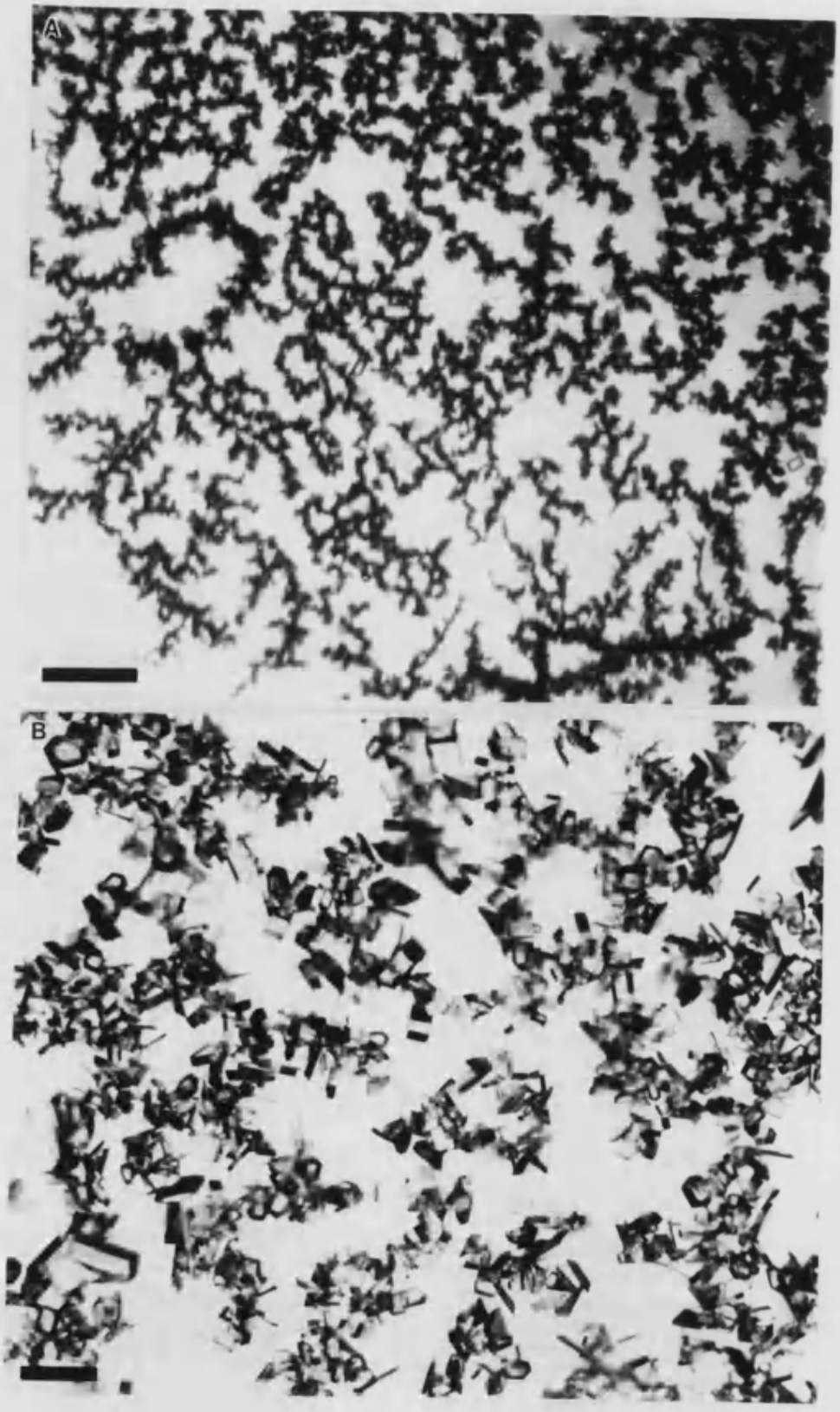

Fig. 3.4 *Optical micrographs of crystals grown at the surface of the crystallizing solution. Scale bars: (a) 0.5 mm, (b) 0.1 mm.*

Morphologically, three polymorphs could easily be distinguished. The main form present was calcite in the equilibrium rhombohedral habit despite being intergrown and frequently truncated. More regular calcite rhombohedra tended to grow separately from the chains. Sizes typically ranged from 10 to 80 μm indicating a spread of nucleation events (fig. 3.5a) and showed little change from 20 hours up to 100 hours. In addition, large mature vaterite "florets" (up to 150 μm) were evident at 16-20 hours often nucleated and growing off the strings of rhombs. Occasionally, "dumb-bell-shaped" bunches of acicular aragonite crystals were also observed at this time.

Most of the attention was focused on the calcite crystals which could be examined in finer morphological detail using the SEM. Regular rhombs were characterized by six smooth $\{10\bar{1}4\}$ faces. The edges of the faces varied from being similar in length (equant rhomb; top of fig. 3.6a) to highly disparate (cleavage rhomb; bottom of fig. 3.6a). Imperfections such as holes and pits were occasionally noticed (fig. 3.6d). A fairly frequent feature of all the surface calcite crystals was the truncation of $\{10\bar{1}4\}$ by one, or sometimes two, smooth faces (fig 3.6b, c, e). Indexing these truncations proved difficult although some were believed to be parallel to (0001) planes (fig. 3.6a; white arrow). Basal (0001) faces are identified by their three-fold or six-fold symmetry. Of the eight vertices of the rhomb, only two (the *c* vertices) are characterized by the meeting of three obtuse angles forming a triad axis. The other six have no rotational symmetry and can be distinguished because each vertex has one obtuse and two acute angles. In any case, these truncations were not governed by symmetry rules and were thus probably a simple result of the physical constraint of the air/water interface.

Sometimes a quite separate area of the surface, removed from the main sites of nucleation, displayed extraordinary arrays of triangular (fig. 3.7a) and pentagonal, "bottle-shaped" crystals (fig. 3.7b). In contrast to the chain aggregates, each crystal

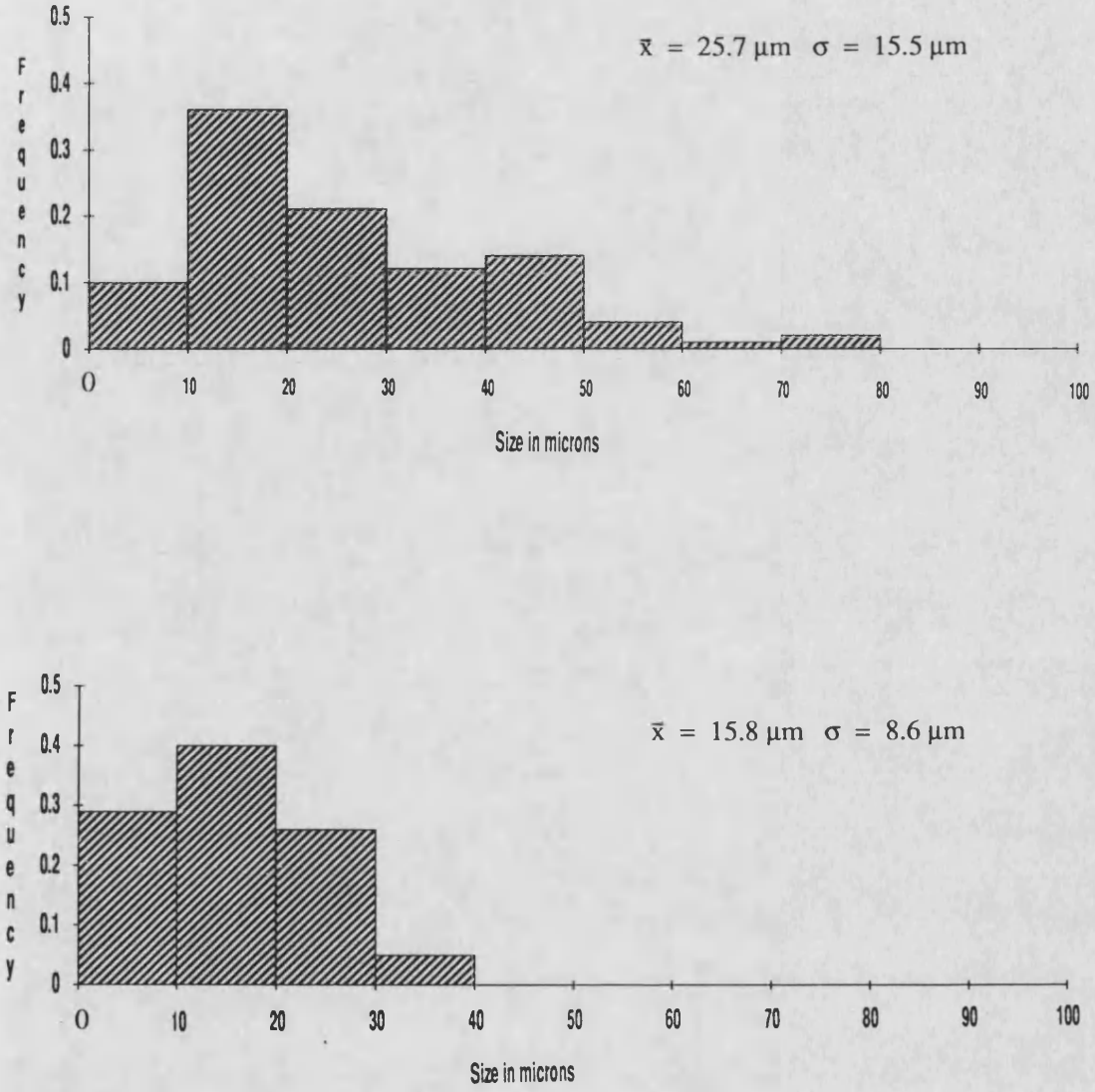

Fig. 3.5 *Size distributions for crystals grown at (a) the surface and (b) the bottom of the container.*

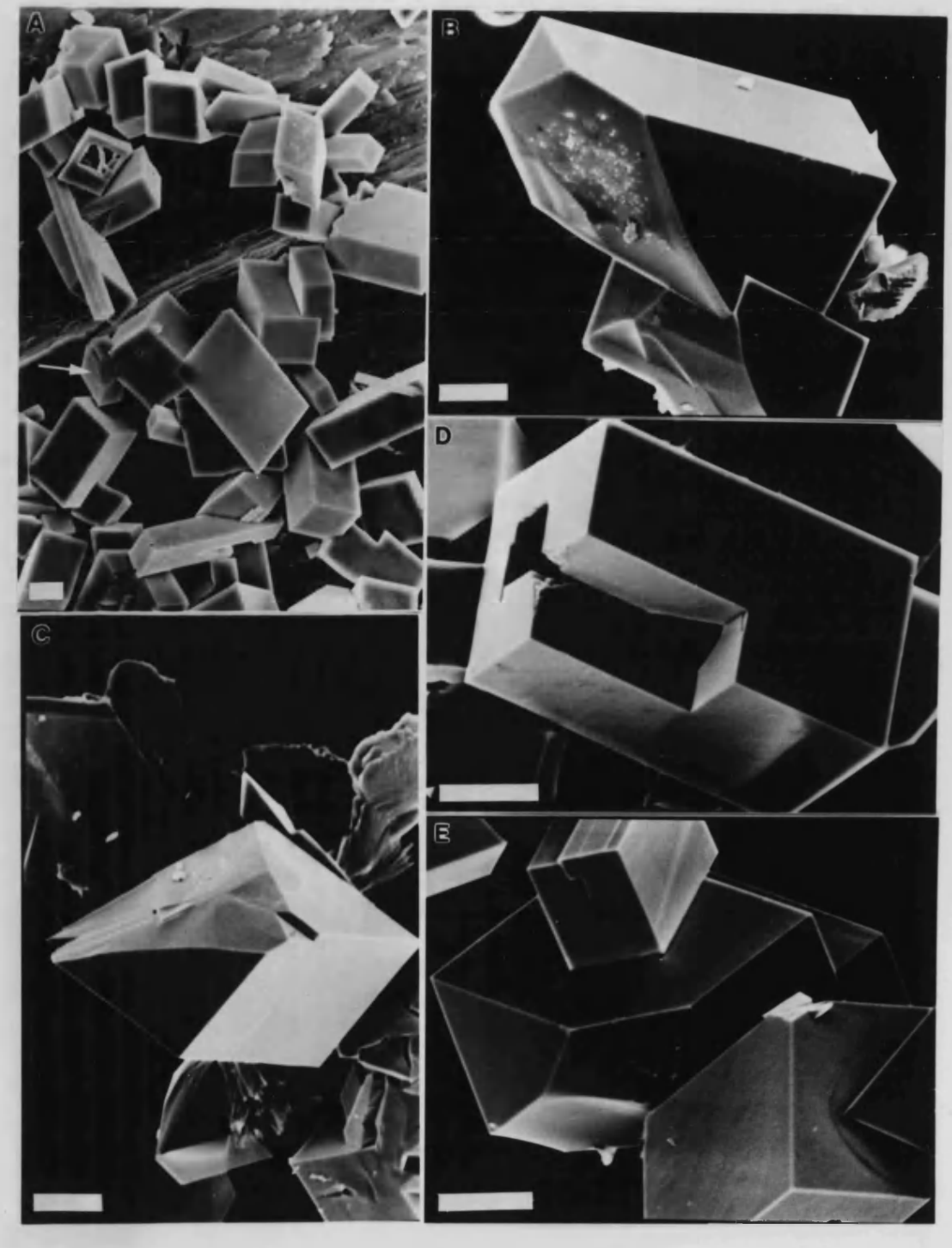

Fig. 3.6 *Scanning electron micrographs of surface calcite crystals. Scale bars = 10 μm.*

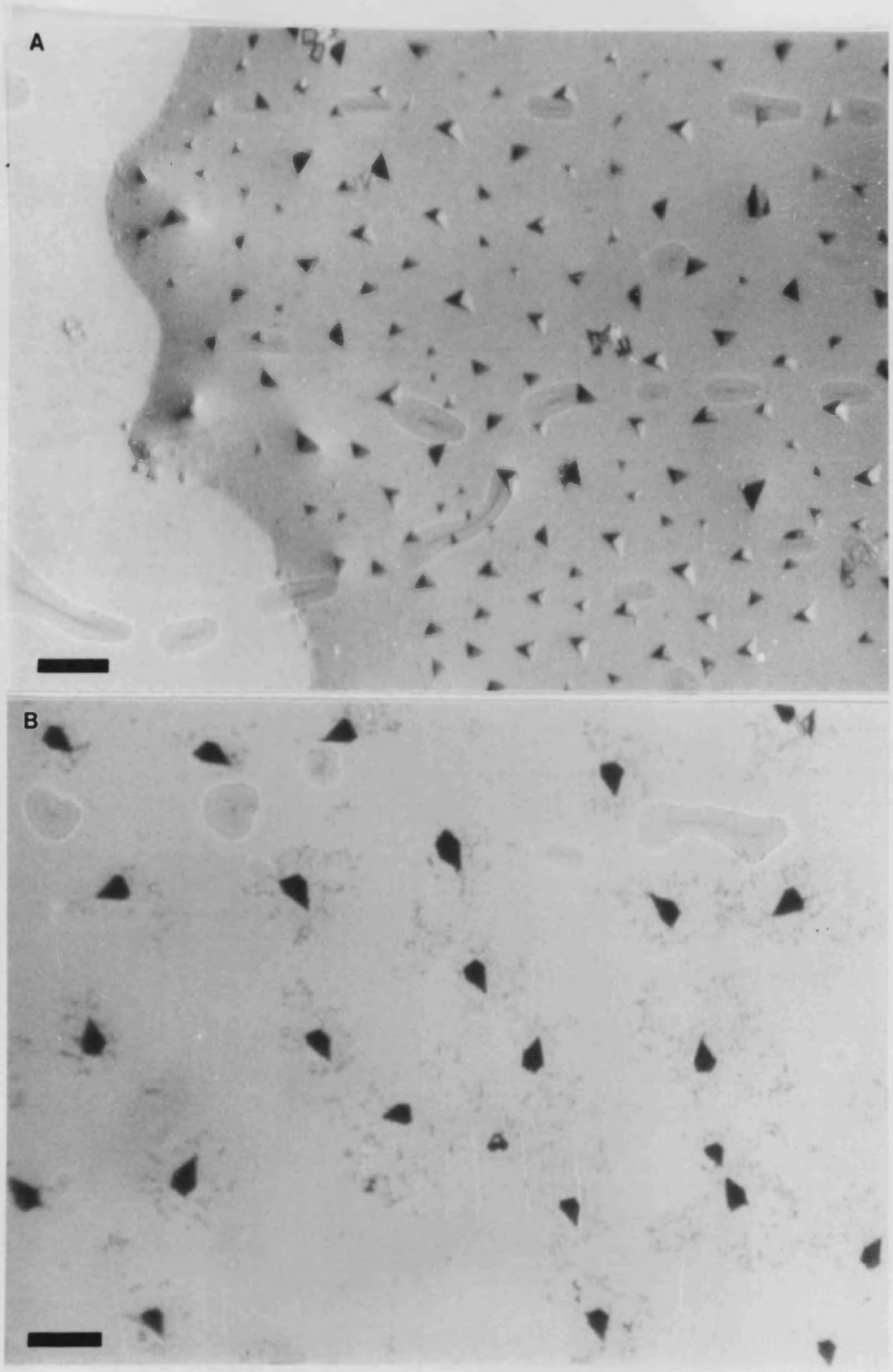

Fig. 3.7 *Optical micrographs of oriented surface crystals. Scale bars = 100 μm.*

had nucleated and grown in isolation from its neighbours resulting in a comparatively lower nucleation density. On closer inspection, the triangles can be seen to be *c* face or (0001) truncated equant rhombs aligned with their [0001] axes perpendicular to the air/water interface. The "bottle-shaped" morphologies in the SEM also appeared to be combinations of $\{10\bar{1}4\}$ and (0001) forms (fig. 3.6b, c, e. However, the $\{10\bar{1}4\}$ have grown unevenly to produce cleavage rhombs.

XRD and IR data on the recovered surface crystals identified calcite as the principal polymorph. Vaterite lines were usually present in the XRD at 16-20 hours (fig. 3.8) but were fairly weak by comparison. Aragonite lines were very rarely observed. Transmission IR detected fundamental bands at 710 cm^{-1} (ν_4), 880 cm^{-1} (ν_2), 1450 cm^{-1} (ν_3) and overtone at 1765 cm^{-1} ($2\nu_2$) (fig. 3.9). The ν_1 band (1090 cm^{-1}) present in vaterite and aragonite, but absent in calcite, was barely visible in the samples analysed.

Mature Bottom Crystals

Crystallites growing on the bottom and sides of the vessel were first noticed at about 10-20 hours. In contrast to those at the surface, they were more discretely nucleated (fig. 3.10). At similar ageing times, the crystals were comparatively smaller (5-40 μm at 93 hrs) and of a more homogeneous size distribution (fig. 3.5b). They were largely calcite rhombs, non-specifically oriented on the glass substrate. Their morphology tended to be more equant (fig. 3.11a, b, c) than the surface crystals. Large single steps (fig. 3.11c) were common on the faces which sometimes became rounded, roughened and foliated (fig. 3.11 b) probably due to dissolution processes. Fewer cleavage rhombs (fig. 3.11d) were present. Disc-like, immature vaterite crystals were also quite common appearing to be mostly oriented on the [0001] axis (fig. 3.10). Unfortunately, the yield, in comparison to the surface, was rather sparse. This, in conjunction with the fact that the crystals were firmly attached to the glass, made collection for analysis impractical.

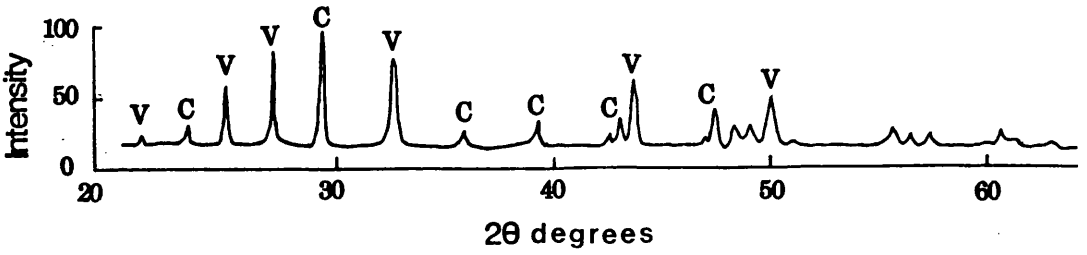

d (Å)	Observed I	Normalized I	Assignment
4.227	132	7	vaterite (002)
3.846	622	32	calcite (012)
3.573	513	26	vaterite (100)
3.293	790	41	vaterite (101)
3.034	1946	100	calcite (104)
2.841	79	4	calcite (006)
2.731	778	40	vaterite (102)
2.495	258	13	calcite (110)
2.284	542	28	calcite (113)
2.115	138	7	vaterite (004)
2.096	180	9	calcite (202)
2.064	494	25	vaterite (110)
1.927	200	10	calcite (024)
1.912	560	29	calcite (018)
1.876	330	17	calcite (116)
1.855	173	9	vaterite (112)
1.821	496	25	vaterite (104)
1.648	173	9	calcite (211)
1.606	303	16	calcite (122)
1.526	252	13	calcite (214)
1.510	132	7	calcite (119)
1.474	126	6	?
1.441	93	5	calcite (300)
1.423	75	4	calcite(00$\underline{12}$)

Fig. 3.8 *Results of X-ray diffraction on surface crystal products.*

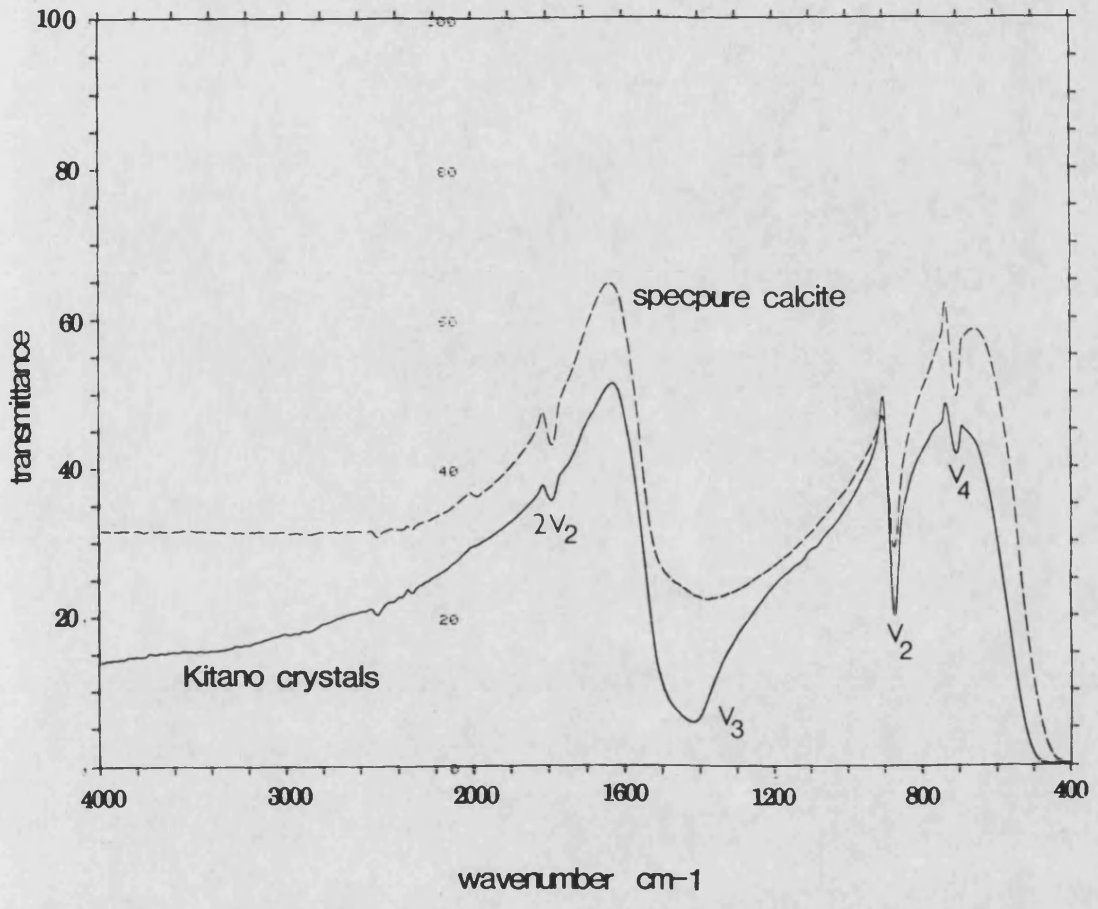

Fig. 3.9 *Transmission infra-red spectra of surface crystals shown in comparison to a pure calcite sample.*

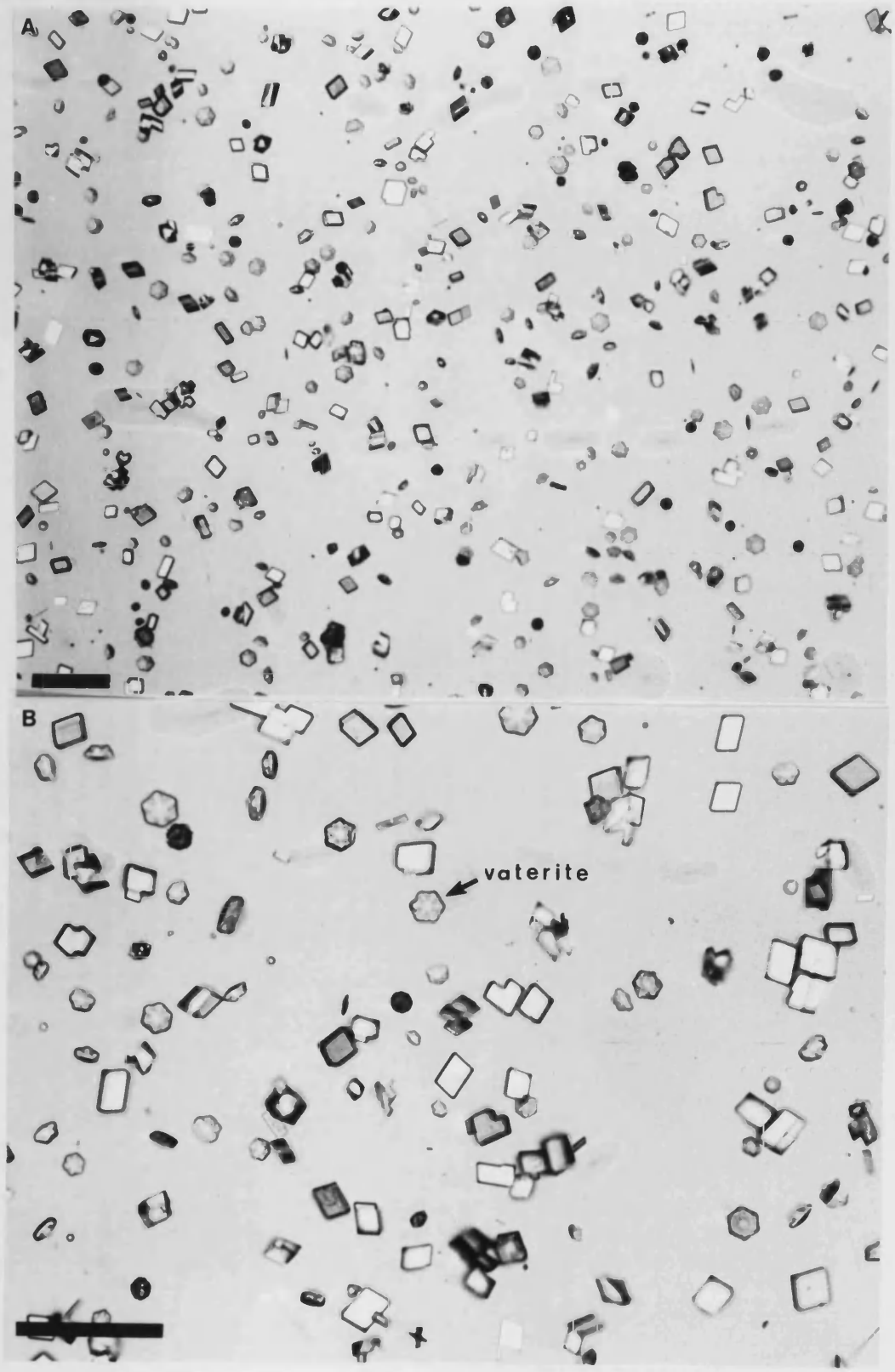

Fig. 3.10 *Optical micrographs of crystals grown at the bottom of the container. Scale bars = 100 μm.*

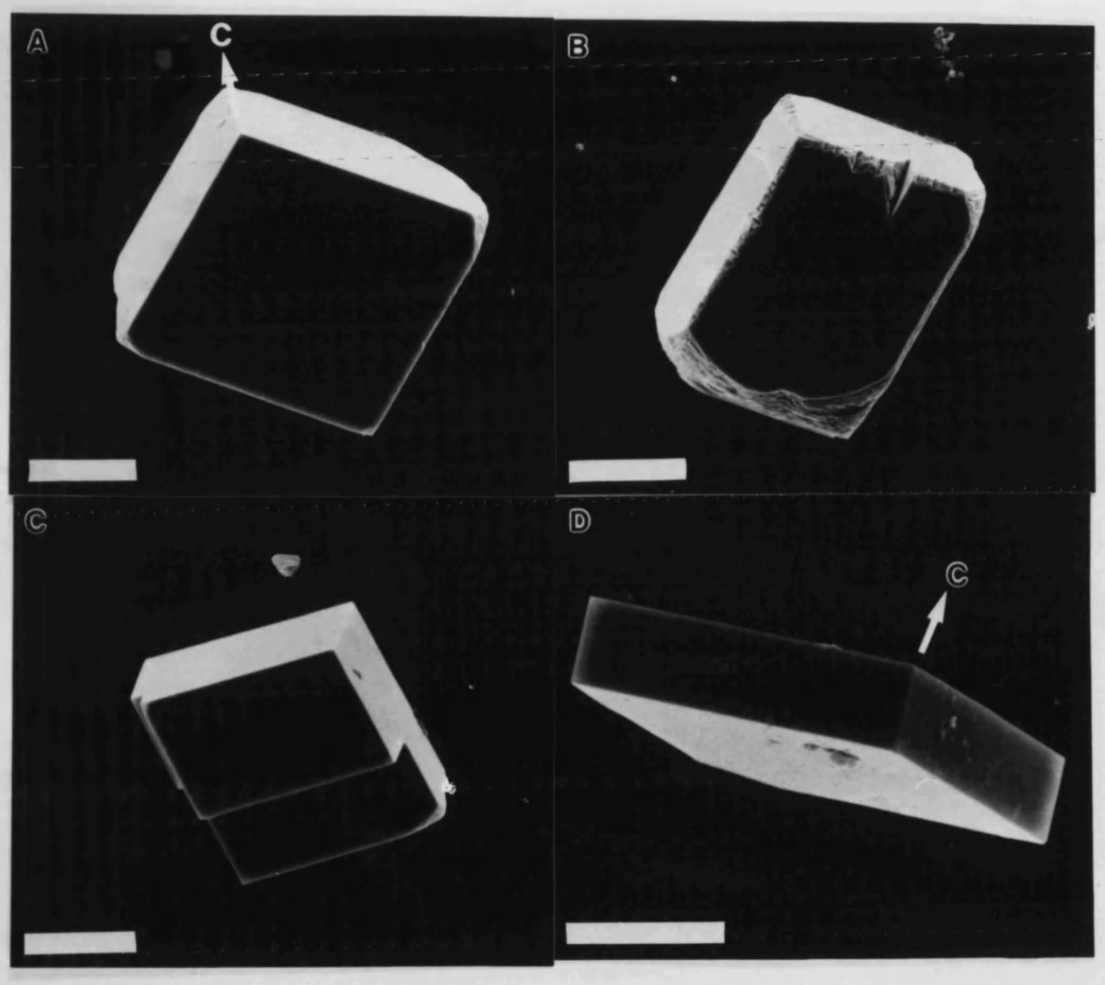

Fig. 3.11 *Scanning electron micrographs of bottom calcite crystals. Scale bars = 10 μm.*

Early Surface Crystals

TEM and SAED were used to investigate the nature of the crystals in the first few hours of crystallization. Difficulties with the grid loading technique meant that few surface crystals were available to study. At 50 minutes, calcite rhombs and vaterite discs between 4 and 6 μm (longest dimension) were observed (fig. 3.12). Diffraction patterns were taken off the edges of these crystals. The rhomb truncations appeared on some crystals but they were not readily indexable. In addition, some amorphous or poorly crystalline particles about 1 μm in diameter were present. There was no evidence for crystalline nuclei of rhombohedral morphology less than a few microns in solution.

Factors Affecting the System

Supersaturation

Based on OM observations, it was revealed that there was a direct correlation between the proportion of calcite obtained and the level of dilution. The upper limit was x10 (≈ 0.9 mM initial Ca) which arrested crystal formation completely even after 20 hours had elapsed. Obviously, the total yield was reduced according to the dilution used eg at x8: yield was, on average, 0.25/8 ≈ 0.03g per 250 ml dish whilst at x2 it was 0.25/2 ≈ 0.125 g.

Temperature

It was noticed that vaterite and aragonite were favoured by warm ambient temperatures. XRD data from low temperature preparations at 0°C and 8°C showed a significant reduction in the presence of these polymorphs at the surface. After several days of growth, the yield was similar to the control at room temperature but crystals were smaller (mean = 8 μm; σ = 6 μm) and more numerous (fig. 3.13a). Crystals could not be discerned at the bottom.

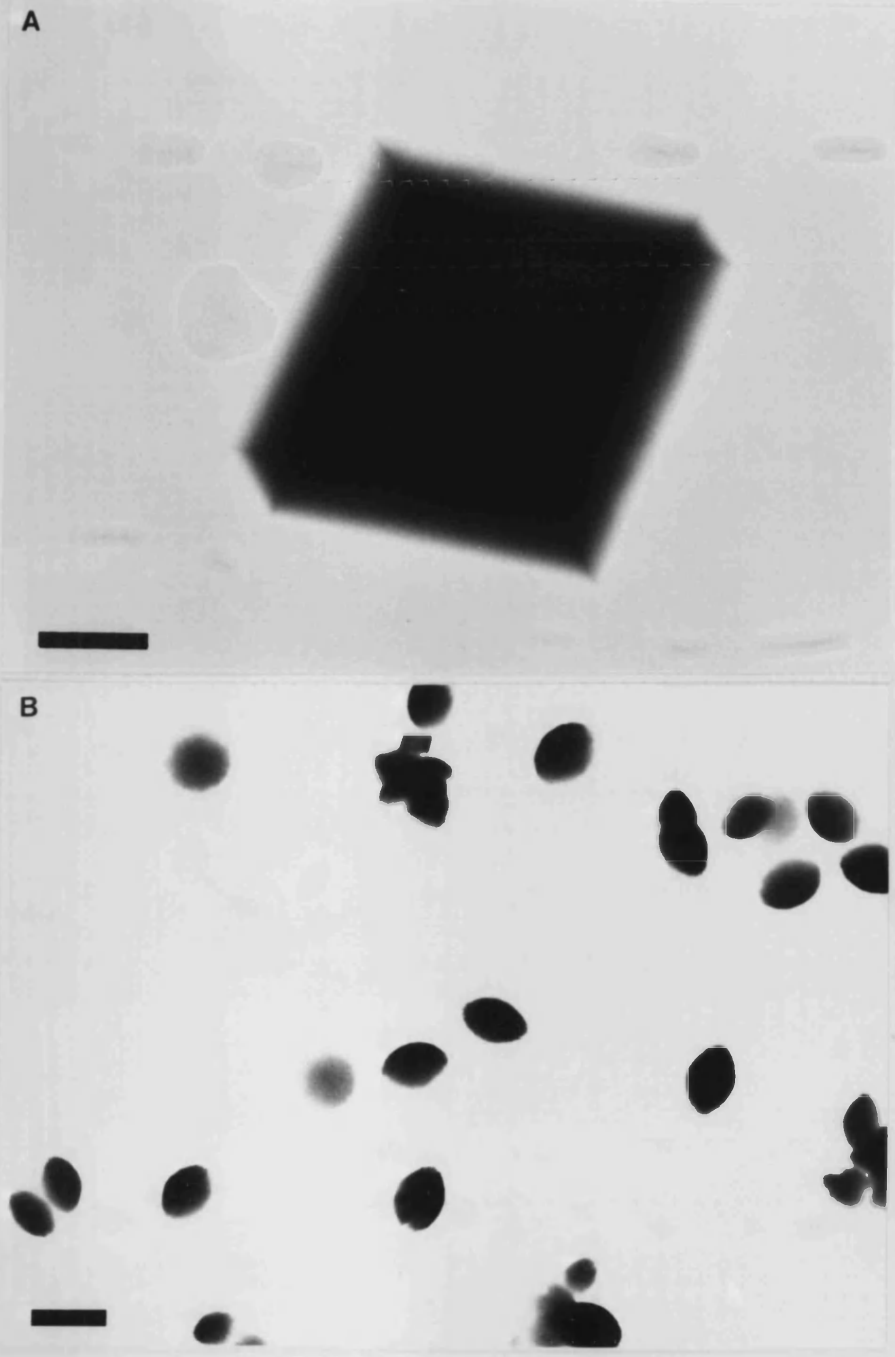

Fig. 3.12 *Transmission electron micrographs of immature surface crystals collected after 50 minutes. Scale bars (a) 1 μm, (b) 2 μm.*

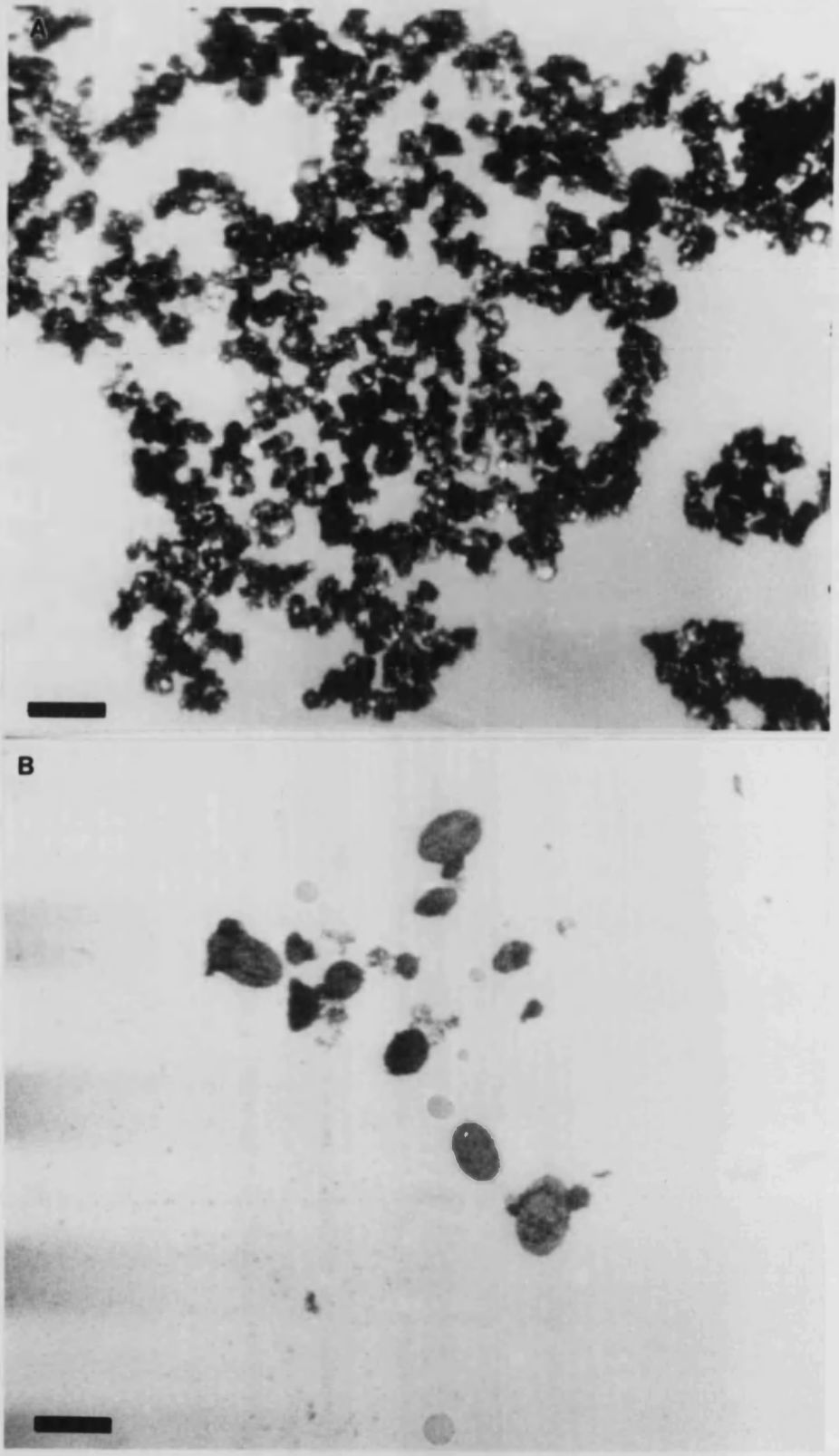

Fig. 3.13 *Optical micrographs of surface crystals grown at (a) low temperature: 0°C and (b) under conditions of high agitation. Scale bars = 100 μm.*

CO_2 Outgassing Rates

A dish, full to the brim of $Ca(HCO_3)_2$ solution, sealed with a glass plate to prevent the escape of CO_2, manifested no signs of precipitation after 20 hours. However, once the plate was removed, crystallization began as normal. The presence of an inhibitory oil lid on the surface resulted in a very pure preparation of calcite. The surface crystals were less intergrown and of a more uniform size. Moreover, a much higher nucleation density was observed on the bottom of the dish. The data is not presented due to problems associated with the recovery of the crystals and *in situ* microscopy.

Gentle agitation of the crystallization solution had the effect of increasing the vaterite population. High rates of stirring greatly accelerated the evolution of carbon dioxide producing spherulitic particles (25-150 μm; fig. 3.13b) after about 15-30 minutes indicating very rapid growth.

3.4 DISCUSSION

Growth appeared to be visually complete at about 16-20 hours although the pH was still rising slowly and the calcium concentration continued to fall after this time. A saturated solution of calcite, in contact with atmospheric CO_2 at 20°C, has a pH of 8.1 and contains about 0.5 mM Ca (Seidell 1965). Thus, according to the physical measurements, the attainment of equilibrium with calcite took approximately several weeks (> 200 hours). Whilst the depletion of carbonate ions appeared to coincide roughly with the end of growth, calcium was well above the saturated value at 16-20 hours. This was probably due to the significant quantities of vaterite present; a saturated solution of vaterite in equilibrium with atmospheric CO_2, will contain more Ca by virtue of its higher solubility. However, as time passed, the relatively unstable vaterite slowly redissolved and reprecipitated as calcite causing the calcium

concentration to drop to the saturated level of the more stable polymorph.

The intergrown, chains of surface crystals developed because material was preferentially deposited at the tips of the chains. This was typical of diffusion control and therefore indicative of rapid crystallization. The presence of unstable polymorphs also pointed to kinetic processes. On the other hand, the equilibrium morphologies suggested that actual crystal growth was quite slow and probably controlled by an interfacial mechanism such as the dehydration or adsorption of Ca^{2+} and CO_3^{2-} (Reddy 1981).

The calcite at the air/water interface was consistently truncated by what appeared to be (0001) forms. These planes are formally unicharged and so the faces will be either all cationic or anionic. The resulting net dipole that exists at the crystal surface causes a marked instability due to coulombic repulsions and consequently the faces are rarely observed in calcite morphologies. Therefore, quite why (0001) truncations were prevalent is difficult to explain. Somehow the physical or chemical features of the air/water interface are able to stabilize (0001). One possibility is that significant interfacial structuring of the water dipoles is present which is sufficient to offset this instability.

Another peculiarity was the high proportion of vaterite compared to aragonite the more stable, less soluble polymorph. One explanation of this fact might be the greater kinetic stability of vaterite. The ionic strength may also be implicated. Experiments with metastable solution mixtures of $NaHCO_3/CaCl_2$, nucleated significant quantities of vaterite at low ionic strength whereas the presence of a background electrolyte (NaCl) promoted calcite only (J.B.A. Walker, personal communication). Ostwald's Law might be invoked to explain the presence of vaterite, especially as nucleation appears to be rapid, although it is doubtful whether the supersaturation is very high.

The greater uniformity and consistency of the crystals that grew at the bottom of the containers was presumably a consequence of the lower levels of supersaturation. The main flux of CO_2 leaving the solution took place at the air/water interface which corresponded to the area of highest CO_3^{2-} concentration and hence supersaturation. The walls and base of the container provided alternative nucleation sites for gas bubbles but their rates of formation were probably relative lower resulting in reduced supersaturation and hence more calcite.

Investigation of System

The crystallization system was clearly sensitive in terms of its response to factors such as temperature, supersaturation, and carbon dioxide flux. Adjustment of these parameters yielded some control over polymorphism, crystal size and extent of surface disorder whilst having no effect on calcite morphology. The results of all the experiments were generally consistent with the driving force being the dissolved carbon dioxide and the rate of precipitation controlled by the gas transfer reaction. Low temperature crystallization tended to kinetically stabilize the system by delaying the loss of CO_2. Ambient temperature variations during normal runs were small (6°C maximum) and so not thought to be significant.

In the light of these results and conclusions, a fairly flexible procedure was adopted for use in calcite growth studies. The CO_2 flow rate and purging time were standardized (3 $lmin^{-1}$, 1 hr + 0.5 hr respectively). Bottom crystals were preferred for morphological analysis. Thermostatting the solutions was not considered vital. Oils were judged to be too inconvenient. Cool room temperatures were preferred.

Merits of system as a control

In terms of the general aims of the chapter, the Kitano system, although not ideal, was entirely adequate for use in crystal growth studies. Its main advantages were its simplicity and high yield yet low supersaturation. One problem was the widespread

aggregation of the bulk of the crystals (ie at the surface) which made morphological analysis troublesome. However, this difficulty could be avoided by concentrating on the bottom crystals. Also, kinetic studies of crystal growth, which might of been helpful, were not possible with this system due to the dominance of the gas exchange reaction.

Undoubtedly, the most surprising features of this system was the groups of oriented truncated rhombs at the air/water interface. The evenly spaced distribution might be attributable to the "Bénard Effect" (Tritton 1988). It is quite well known that, under certain conditions, shallow fluids, heated from below, form stable micro-convection cells in quiescent solution. In spermaceti oil, uniform, hexagonal cells can be observed in which the fluid rises in the centre and falls at the boundaries. Although no obvious heating was applied in the crystallization experiments, it might be possible that similar conditions are present in the Kitano system which feed only small areas of the surface with lattice ions. This would bring some order to the usual chaotic crystal growth and allow some nuclei to develop undisturbed. Furthermore, the high proportion of (0001) truncations is also consistent with extensive structuring of the interfacial water layer. These observations highlighted the heterogeneity of the surface growth processes where seemingly contrasting regimes existed side by side.

Having now evaluated this system of precipitation, it will be used to investigate the morphological effects of additives in the following chapters (4 and 5).

3.5 REFERENCES

Al-Khayat, A., Garside, J. (1989), *Reaction Crystallization of Calcium Carbonate,* Private communication, Chemical Engineering Dept., UMIST, Manchester, UK.

Borowitzka, M.A. (1989), *Carbonate Calcification in Algae - Initiation and Control,* in Biomineralization - Chemical and Biochemical Perspectives, Mann, S., Webb, J., Williams, R.J.P. (Eds.), pp 63-94, Weinheim: VCH.

Drever, J.I. (1982), *The Geochemistry of Natural Waters*, Englewood Cliffs, NJ, USA: Prentice-Hall.

Edsall, J.T. (1969), *CO_2: Chemical, Biochemical and Physiological Effects,* Foster, R.E. *et al* (Eds.), Washington DC: NASA SP-188.

Giannimaras, E.K., Koutsoukos, P.G. (1987), *The Crystallization of Calcite in the Presence of Orthophosphate*, J. Coll. Int. Sci., **116(2)**, 423-430.

House, W.A. (1981), *Kinetics of Crystallization of Calcite from Calcium Bicarbonate Solutions*, J. Chem. Soc. Faraday Trans., 1, *77*, 341-359.

House, W.A. (1987), *Inhibition of Calcite Crystal Growth by Inorganic Phosphate*, J. Coll. Int. Sci., **119(2)**, 505-511.

Janeković, A., Matijević, E. (1985) *Preparation of Monodispersed Colloidal Cadmium Compounds*, J. Coll. Int. Sci., **103(2)**, 436-447.

Kitano, Y. (1962), *The Behaviour of Various Ions in the Separation of Calcium Carbonate from Bicarbonate Solution*, Bull. Chem. Soc. Jap., **35**, 1973-1980.

Meyer, H.J. (1984), *The Influence of Impurities on the Growth Rate of Calcite*, J. Cryst. Growth, **66**, 639-646.

Press, F., Siever, R. (1986), *Earth*, 4th ed., pp 173-174, New York: W.H. Freeman & Co.

Reddy, M.M., Nancollas, G.H. (1971), *The Crystallization of Calcium Carbonate I*, J. Coll. Int. Sci., **36(2)**, 166-172.

Nancollas, G.H., Reddy, M.M. (1971), *The Crystallization of Calcium Carbonate II*, J. Coll. Int. Sci., **37(4)**, 824-830.

Reddy, M.M., Nancollas, G.H. (1973), *Calcite Crystal Growth Inhibition by Phosphonates*, Desalination, **12**, 61-73.

Reddy, M.M., Nancollas, G.H. (1976), *The Crystallization of $CaCO_3$ - IV Effect of Mg, Strontium and Sulfate Ions*, J. Cryst. Growth, **35**, 33-38.

Reddy, M.M. (1977), *Crystallization of $CaCO_3$ in the Presence of Trace Amounts of Phosphorus-Containing Anions*, J. Cryst. Growth, **41**, 287-295.

Reddy, M.M. (1981), *Crystal Growth of Calcite from Calcium Bicarbonate Solutions at Constant P_{CO_2} and 25°C: a Test of a Calcite Dissolution Model*, Geochim. Cosmochim. Acta, **45**, 1281-1289.

Reddy, M.M. (1986), *Effect of Mg ions on Calcium Carbonate Nucleation and Crystal Growth in Dilute Aqueous Solutions at 25°C*, from Studies in Diagenesis, Mumpton, F.A. (Ed.), US Geological Survey Bulletin, **1578**, 169-182.

Seidell, A. (1965), *Solubilities of Inorganic and Metal-Organic Compounds*, Vol. 2, 4th ed. by Linke, W.F., p 536, Washington DC: American Chemical Society.

Shellis, R.P. (1988), *A Microcomputer Program to Evaluate the Saturation of Complex Solutions with Respect to Biominerals*, Cambios, **4(3)**, 373-379, Oxford: IRL Press.

Sillen, L.G. (1971), *Stability Constants of Metal-Ion Complexes, Part 1: Inorganic Ligands*, London: The Chemical Society.

Stumm, W., Morgan, J.J. (1981), *Aquatic Chemistry*, 2nd ed., New York: John Wiley-Interscience.

Söhnel, O., Mullin, J.W. (1982), *Precipitation of Calcium Carbonate*, J. Cryst. Growth, **60**, 239-250.

Tritton, D.J. (1988), *Physical Fluid Dynamics*, 2nd ed., pp 35-47, Oxford: Clarendon Press.

Walker, J.B.A., Heywood, B.R., Mann, S. (1991), *Oriented Nucleation of $CaCO_3$ from Metastable Solutions under Langmuir Monolayers*, J. Mater. Chem. **1(5)**, 889-890.

CHAPTER 4

Morphological Effects of Some Simple Organic and Inorganic Anionic Molecules on Calcite Crystallization

4.1 INTRODUCTION

A general review concerning the effects of additives on crystallization was given in chapter 1.4. This introduction now summarizes studies undertaken on calcite. Despite numerous investigations, the additives employed have been restricted to a few types of oxyanions and cations. Most popular have been phosphorus-containing anions (phosphates and phosphonates) and Mg^{2+} as well as some carboxylates, amino acids and other cations.

The majority of these substances have been investigated for their inhibitory effects on crystallization and dissolution. Early research was prompted by their industrial applications such as in scale prevention whereas later workers were interested in the role of natural inhibitors in sedimentology and oceanography. Hatch and Rice (1939) were one of the first to look at the adsorption and inhibitory action of hexametaphosphate. Raistrick (1949) later suggested that this adsorption might occur on (0001) planes and Brooks *et al* (1950/51) demonstrated its use for the preparation of metastable phases by blocking the more stable ones. Some of the possible mechanisms of inhibition were elucidated by the kinetic measurements of Reddy and Nancollas (1973), Reddy (1977), House (1987), Meyer (1984), Giannimaras and Koutsoukos (1987). They have all concluded that adsorption at active sites (kinks) on the calcite surface takes place, blocking further growth. Ishikawa and Ichikuni (1981) and Ichikuni (1983) showed that the additives are also homogeneously incorporated into the lattice. Many others have demonstrated the inhibitory effects of Mg^{2+} ions (Simkiss 1964, Pytkowicz 1965, Biscoff 1968,

Berner 1975, Reddy and Nancollas 1976, Meyer 1984, Wilbur and Bernhadt 1984, Reddy 1986). The mechanisms involved are very similar to that of phosphorus-containing compounds. Less studied experimentally, but important for sedimentologists looking at calcium carbonate precipitation in seawater, have been amino acids (Suess 1970, Berner *et al* 1978, Carter 1978, Mitterer and Cunningham 1985), fatty acids (Berner *et al* 1978) and sulphate (Reddy and Nancollas 1976). In addition, dicarboxylates have been shown to be influential in inhibiting the dissolution of cleaved calcite surfaces (Compton *et al* 1990).

Additives have also been implicated in the crystallization of metastable polymorphs of $CaCO_3$. Brooks *et al* (1950/51) used Calgon (polymetaphosphates and polyphosphates) and magnesium ions in the preparation of metastable anhydrous and hydrated phases. Kitano examined the influence of a large range of inorganic (1962) and organic material (Kitano and Hood 1965) and was able to show that calcite, aragonite and vaterite can be selectively precipitated by the use of foreign cations. More recently, Merten and Bachman (1980) have used a variety of so-called "hydrogen-bonding materials" such as sucrose, methanol and glycine to stabilize amorphous calcium carbonate.

However, of greatest relevance to this thesis are the papers that have documented additives capable of inducing morphological changes to calcite. Amongst the earliest references were Buehrer and Reitemeier (1940) who noticed ill-defined crystals growing in the presence of sodium hexametaphosphate. Much more recently, Vanderheiden (1987) reported a patent for the synthesis of spherical calcite crystals using polyphosphate. McCauley and Roy (1974) presented data showing that Mg and Ni could causes distortion in calcite rhombs as did Reddy and Nancollas (1976) with Mg. More specific alterations in habit have also been described. Perhaps the most common morphology effected has been the prismatic or *c* axis spindle. Folk (1974, 1978), Lahann (1978) and Cailleau *et al* (1980) all

described possible mechanisms for such modifications due to Mg^{2+}. By counter diffusing Ca^{2+} and CO_3^{2-} through silica gels, García-Ruiz and co-workers (1979, 1985, 1987, 1988) and Prieto *et al* (1981) were able to grow these habits and many other more complex aggregates with non-crystallographic morphologies. Although no formal additive was present in these systems, silicate membranes were shown to exist around the crystals and were thus intimately involved in the growth process. By the same technique, Heijnen (1985) grew spindle-shaped calcite, indexed the faces and rationalized some of the results in terms of Hartman-Perdok theory. The appearance of additive-induced, basal (0001) faces has also been published. Hirano and Kikuta (1986) used a combination of a hydrothermal environment and 3 M $NaNO_3$ solution whereas Rajam and Mann (1990) showed that Li^+, under much milder conditions, had a marked stabilizing effect on these otherwise highly unstable faces.

The first known work examining the influence of carboxylates on calcite morphology was conducted by Sanderson and Mann (1988). Preliminary results found that malonic acid in solution could also produce spindle-shaped crystals. The results were explained in terms of preferential adsorption of the additive on the stereochemically similar prismatic faces. In this way, growth was inhibited in directions perpendicular to the *c* axis. By using a range of related carboxylic acids, the study identified molecular properties of the additives affecting the morphological interaction. These included: *Number of functional groups*; dicarboxylates were much more effective at habit modifications than mono-functional acids due to the chelate-type binding of both carboxyl groups. *Chain length*; in a homologous series of linear, aliphatic dicarboxylic acids up to the fourth member (glutaric), the morphological effects were found to tail off with increasing chain length. Thus, malonic acid (C_3) had a greater consequence than succinic (C_4) which, in turn, had a greater effect than glutaric (C_5). This effect was ascribed to the greater flexibility of the molecules. *Chain rigidity*: it was also noted

that the unsaturated and hence more rigid C_4 acid, *cis*-butenedioic (maleic), was more potent than its saturated counterpart, succinic acid. In contrast, the *trans* isomer (fumaric) had a minimal effect probably because both its carboxylates were fixed in a conformation which prevented binding in a chelate fashion. This was evidence that rigidity in the molecule could enhance the interaction provided the conformation disposed the functional groups in the correct position.

Objective and Overview

The general aim of this work was to further explore interactions at the molecular level occurring between additives in solution and growing crystalline phases. By using systematic crystal growth studies, it was hoped that certain key molecular properties of the additive could be correlated with their effect on growth and morphology. Such groundwork would then establish principles which might be applied towards the more complex mineral-macromolecule interactions in biomineralization and other fields of study.

All experiments were conducted on the basis of a direct comparison between growth under the influence of the additive and growth in its absence (control system). Resulting changes in morphology were used in order to probe the nature and extent of these interactions. For this purpose, the mineral calcite was eminently suited because its structure and properties are well understood. Likewise, structurally simple and well-characterized additives were used. The molecules investigated were all organic and inorganic anions. They included a variety of α,ω-dicarboxylates, phosphates and phosphonates plus sulphate and nitrate.

The investigations fell into three main areas. Firstly, the preliminary experiments of Sanderson and Mann on carboxylates were repeated and then extended using higher saturated homologues and various derivatives. Secondly, various other oxyanions were tried; in particular, the phosphorus-containing compounds. Thirdly, physical

and chemical characterization of some of the modified morphologies was carried out. Some important unresolved questions remained: Were the additives associated with the crystals ? If so, were they occluded or surface-bound and, if only present at the surface, were they preferentially adsorbed on the effected faces ?

4.2 EXPERIMENTAL MATERIALS AND PROCEDURES

Additive Materials

Succinic, adipic, azelaic, maleic, glutamic and aspartic acids were purchased from BDH Ltd. Malonic, glutaric, pimelic, suberic and fumaric were obtained from Aldrich Ltd. γ-Carboxyglutamic acid was from Sigma Ltd. Table 4.1 summarizes the available general information on most of the organic acid additives used. The molecules had the basic structure illustrated in fig. 4.1 where n = 1-8 and included the *cis* and *trans* isomers of the unsaturated n = 2 homologue, the α-amino derivatives of the n = 3 and 4, and the α-amino, ω(γ)-carboxylate derivative of n = 3. Actual molecular structures are shown in fig. 4.2.

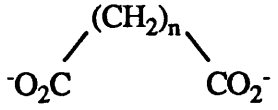

Fig. 4.1 *Generic structure of α,ω-dicarboxylates*

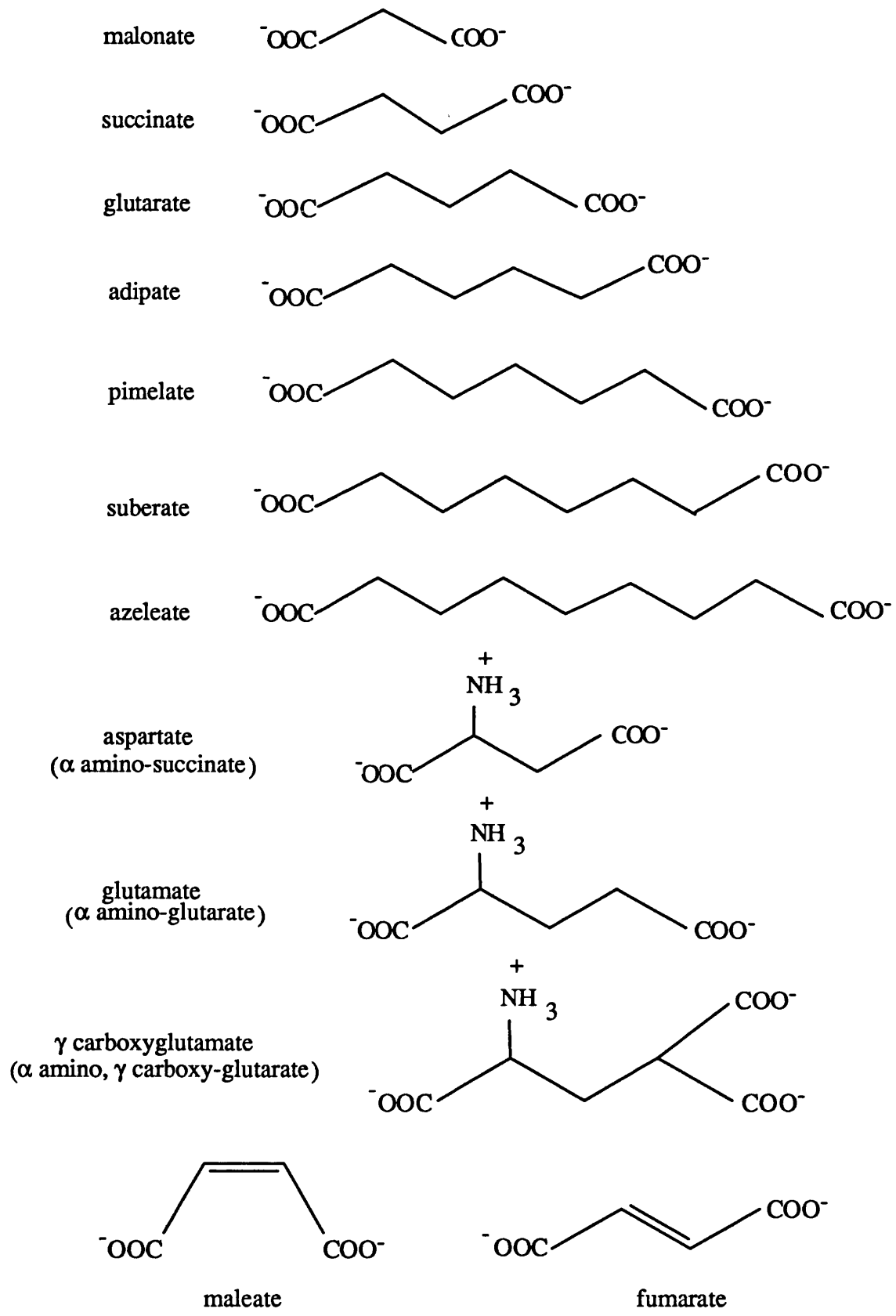

Fig. 4.2 *Structures of α,ω-dicarboxylates studied*

Acid	Formula	pK_{a1}	pK_{a2}	K_{stab}
malonic	$CH_2(COOH)_2$	2.83	5.69	1.51
succinic	$C_2H_4(COOH)_2$	4.16	5.61	1.20
glutaric	$C_3H_6(COOH)_2$	4.31	5.42	1.08
adipic	$C_4H_8(COOH)_2$	4.43	5.41	2.19
pimelic	$C_5H_{10}(COOH)_2$	4.48	5.42	-
suberic	$C_6H_{12}(COOH)_2$	4.52	5.40	-
azelaic	$C_7H_{14}(COOH)_2$	4.55	5.41	-
maleic	*cis*-$C_2H_2(COOH)_2$	1.83	6.07	1.10
fumaric	*trans*-$C_2H_2(COOH)_2$	3.03	4.44	0.48
aspartic	$C_2H_4(COOH)_2NH_2$	1.88	3.65	1.60
glutamic	$C_3H_6(COOH)_2NH_2$	2.19	4.25	2.05

Table 4.1 *Acid dissociation constants and calcium stability constants for α,ω-dicarboxylic additives. NB/ no available data for γ-carboxyglutamic or sebacic (C_{10}) acids.*

Analar sodium nitrate, 1-naphthyl disodium orthophosphate and phenyl phosphate were purchased from BDH Ltd. Phenyl phosphonic acid was from Aldrich Ltd. Methane phosphonic, methylene diphosphonic, 1,2-ethylene diphosphonic acids and n-butyl dihydrogen phosphate were all obtained from Lancaster Synthesis Ltd. Trisodium orthophosphate and AR sodium sulphate was from FSA chemicals. All reagents used were of the highest available purity. Molecular structures are shown in fig. 4.3.

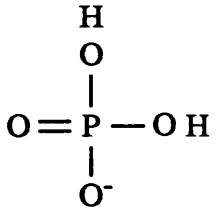

phosphate

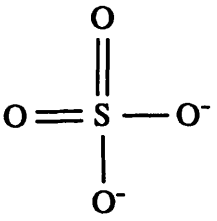

sulphate

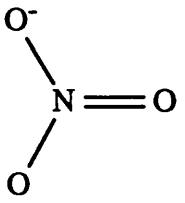

nitrate

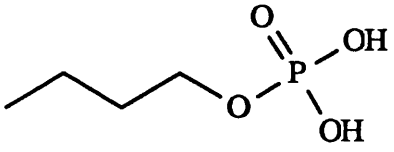

butylphosphate

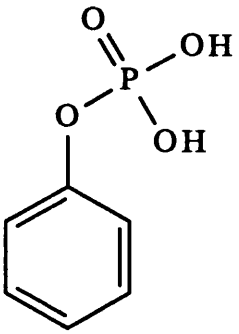

phenylphosphate

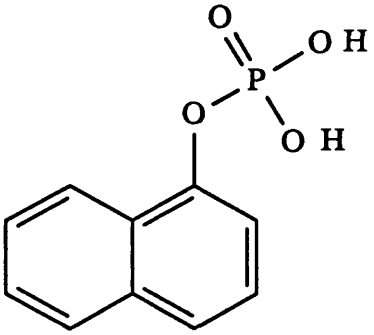

napthylphosphate

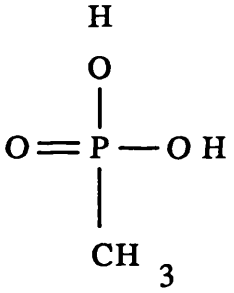

methyl phosphonate

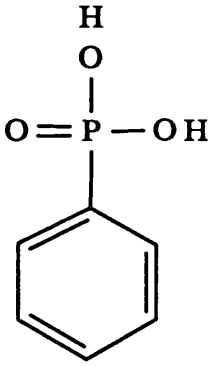

phenylphosphonate

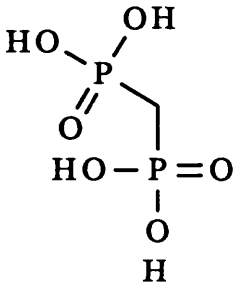

methylene diphosphonate

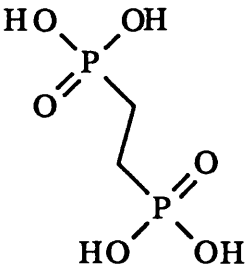

ethylene diphosphonate

Fig. 4.3 *Structures of oxyanions studied*

Additive	pK_{a1}	pK_{a2}	pK_{a3}	pK_{a4}	Speciation at pH = 6	K_{stab}
orthophosphate	2.1	7.2	12.7	-	94% $H_2PO_4^-$ 6% HPO_4^{2-}	1.1 2.7
sulphate	-3	1.9	-	-	100% SO_4^{2-}	2.3
nitrate	-1	-	-	-	100% NO_3^-	0.7
butyl dihydrogen phosphate	1.9	6.8	-	-	87% $butOPO_3H^-$ 13% $butOPO_3^{2-}$	- -
methyl phosphonic acid	2.4	7.3	-	-	96% $MePO_3H^-$ 4% $MePO_3^{2-}$	- -
methylene diphosphonic acid	?	1.5	6.8	10.1	86% $[Mediphos]^{2-}$ 14% $[Mediphos]^{3-}$	3.3 2.8
ethylene diphosphonic acid	1.5	2.7	7.4	9.0	96% $[Etdiphos]^{2-}$ 4% $[Etdiphos]^{3-}$	- -

Table 4.2 *Acid dissociation constants and calcium stability constants for various oxyanions studied. NB/ no available data for 1-napthyl-orthophosphate, phenyl orthophosphate or phenyl phosphonic acid. Data from Sillen (1965), Hogfeldt (1982), Perrin (1979).*

Procedures

Supersaturated calcium bicarbonate solutions were prepared as described in chapter 2.3.

Introduction of Additives into Solution

Experiments consisted of the various additives added individually to separate, equal portions of the freshly made calcium bicarbonate solution. Generally, the containers used were loosely-covered, round pyrex crystallizing dishes (ID 135 mm; 1 litre capacity). Initially, the x2 dilution, low temperature (8°C) and oil lid systems (as described in chapter 3) were employed for pure preparations of calcite crystals. However, preliminary experiments showed that most additives acted as effective overall inhibitors of crystallization and when combined with the above retarded systems, almost all precipitation stopped. For this reason, the standard control

conditions (dishes left on the bench at ambient temperature; 18-23°) were implemented. Most substances were dissolved-up in a small amount of supersaturated solution before being added to the dish. Those that were only partially soluble were added as the solid directly to the dish and stirred in. The total dissolved calcium (Ca_T) in the system was determined by EDTA titration. Additive concentration was expressed as a Ca_T/additive molar ratio. Care was taken to ensure that the final volumes and calcium concentrations remained constant in all systems. In each group experiment, a control was employed where no additive was present allowing direct comparisons to be made.

α,ω-Dicarboxylates

All acids were compared at a fixed ratio of 3:1 ie [Ca_T] ≈ 9 mM and [acid] ≈ 3 mM. This enabled assessment of their relative potencies. Some of the more effective ones such as malonic, γ-carboxyglutamic and aspartic acids, were selected for concentration studies. For malonate, a variation of between 0.4 mM to 10 mM was set up corresponding to Ca_T/malonate ratios of about 25:1 down to 1:1. Aspartate was studied over a range of 440:1 down to 1:1. Due to its great expense, γ-carboxyglutamic experiments were scaled down to 10 ml dishes whilst keeping the surface area/volume ratio constant. Ratios were varied from 435:1-3:1.

Oxy-phosphorus and other oxy-anionic additives

These substances were investigated at ratios of 1:1, 10:1, 100:1, 1000:1 and 10,000:1 depending on their potency. More potent compounds were studied at 50,000:1 and 100,000:1 and less potent ones at 0.1:1 (1:10) and 0.01:1 (1:100).

Routine Analysis of Crystal Products

Samples of crystals were collected after about 75-100 hours ageing depending on the extent of overall inhibition. Both surface and bottom samples were routinely retrieved on glass cover slips either dipped through the surface or placed on the

bottom of each dish. These were then mounted on glass slides for OM or on aluminium stubs for examination by SEM. All remaining surface material was isolated from the solution by Büchner filtration, air-dried and stored in a desiccator. Routine structural analysis was carried out on all samples by powder XRD. Miller-Bravais and Weber indices based on the simplest hexagonal cell (a = 4.99 Å, c = 17.06 Å) were used throughout.

Further Characterization of Additive-modified Crystals

More detailed analyses were carried out on samples of habit-modified calcite either grown in the presence of aspartate or malonate at Ca/additive ratios = 3:1 or orthophosphate at 10:1. Bulk quantities were prepared involving several 6 litre batches of $Ca(HCO_3)_2$ solution, split into 2 litre lots and grown in 3 litre crystallization dishes. Additives were introduced to two lots and the remaining left as a control. Harvesting was generally at 40-60 hours ageing although early crystals were collected for TEM at 0.3, 0.6, 1, 2 and 3 hours after crystallization had begun by dipping copper grids through the surface of the solution. Approximately 80-100 mg of surface crystals were recovered from each dish. The bottom material was discarded. In addition, controls, aged for 27.5 hours, were incubated with the same quantity of additive for a further 40 hours. The calcite morphologies from each system were checked briefly by optical microscopy and all precipitates were thoroughly washed with Purite distilled water and desiccated prior to further examination.

Quantitative elemental microanalysis for C, H and N was used to determine whether malonate or aspartate was associated with the habit-modified and incubated crystals. Four samples each of the aspartate-modified and aspartate-incubated material were also subjected to 30, 60, 90 and 120 seconds etching in 0.5 % HCl. This was followed immediately by washing in Purite distilled water, Büchner filtration and drying in a cool oven (< 100°C).

Infra-red spectroscopy was employed as an analytical technique and also to probe the binding modes of the additives present in the samples. Conventional transmission and diffuse reflectance FTIR was conducted on ground and unground phosphate-modified, aspartate-modified and aspartate-incubated samples.

Lattice parameters for aspartate and phosphate-modified crystals were accurately measured using the Philips PW 1710 diffractometer calibrated against specpure BDH analar calcium carbonate. The vertical goniometer was generally programmed to scan 20-90° 2θ which took about an hour. This assembly was able to measure 2θ to within 0.001°. Approximately 100-150 mg of sample powder were placed in a 3 cm^2 shallow holder, smoothed off and a diffractogram recorded. Scans were performed in triplicate; the samples being removed and re-mounted after each scan. An average value of 2θ was then taken and d spacings calculated for the $\{10\bar{1}4\}$, $\{0006\}$, $\{11\bar{2}0\}$ and $\{30\bar{3}0\}$ reflections.

Structural integrity was also examined via a Raman spectroscopic study of the lattice vibrational modes of unground aspartate-modified calcite. The SPEX spectrophotometer was scanned from 1200 → 50 cm^{-1} from the exciting line at a rate of 50 $cm^{-1}min^{-1}$.

In order to test the hypothesis that adsorption occurred preferentially on particular faces, spatially resolved, windowless EDXA was carried out on sodium orthophosphate-modified crystals. Samples were carbon-coated as gold was found to obscure the phosphorus peak in the spectrum. The JEOL 35C SEM enabled beam focusing to ≈ 1-5 μm^2, allowing comparative, semi-quantitative measurements to be made on both the rhombohedral $\{10\bar{1}4\}$ and effected $\{44\bar{0}1\}$ faces.

4.3 RESULTS

4.3.1 *The Influence of Functionalized and Non-functionalized α,ω-Dicarboxylates*

General Results

Physical data for all the systems at a Ca/additive ratio of 3:1 is presented in table 4.2. In the presence of additives, total yields (surface + bottom crystals) were reduced by about 40-70% which appeared to reflect the trend in calcium stability constants (table 4.1). Powder XRD showed that the majority of the precipitates were pure calcite although the control, aspartate and glutamate produced small quantities of vaterite.

Acid	Total Yield (g)	Mean size (μm)	σ (μm)	XRD
control	0.16	25.1	10.1	C, V
malonic	0.08	20.6	9.7	C + ?
succinic	0.07	29.5	12.7	C
glutaric	0.08	30.0	12.0	C + ?
adipic	0.07	33.1	13.2	C
pimelic	0.07	25.3	11.6	C
suberic	-	28.1	11.4	-
azelaic	-	24.7	11.6	-
maleic	0.10	20.2	8.1	C
fumaric	0.11	30.1	9.8	C
aspartic	0.08	18.8	9.1	C, V
glutamic	0.08	30.0	10.0	C, V
γ-gla*	-	10.0	4.6	V, C

Table 4.2 *Experimental data on surface $CaCO_3$ crystals obtained with each additive at Ca/α,ω-dicarboxylate = 3:1 and ageing time = 85-135 hours; $[Ca]_T$ = 8.7 mM (0.867 gl^{-1} $CaCO_3$). All volumes 250 ml.*
** γ-carboxyglutamic acid*

The main exception was γ-carboxyglutamate which generated large amounts of vaterite. Mean sizes and standard deviations for calcite crystals were fairly uniform for each additive and were not very different from the control population. Again, γ-carboxyglutamate was anomalous causing a marked reduction in the average size.

Malonate

In the presence of the C_3, saturated homologue, calcite crystals grew at the surface, bottom and sides of the dishes. Surface yields were reduced by increasing acid concentration such that an upper threshold of 10 mM, corresponding to Ca/malonate = 1:1, inhibited nucleation entirely. Despite this, calcite crystal sizes showed little variation over the range. The unknown lines in the XRD for malonic were weak and thus may have been due to small amounts of calcium malonate salts.

At low calcium to malonate ratios (ie 3:1, 5:1,), spindle-shaped habits were precipitated at the surface and bottom of the dish. These morphologies were elongated along the *c* axis, had smooth {10 $\bar{1}$4} end faces and a rounded central body of roughened, curved faces (fig. 4.4). These new surfaces were approximately parallel to the *c* axis and were always striated and textured due to extensive micro-stepping by {10$\bar{1}$4}. No single set of plane, symmetry-related faces were expressed which was indicative of a pseudo-specific interaction between the additive and the crystals. A calcite crystal with a similar habit was composed using the crystal morphology plotting program *MORPH* by specifying {hkl}'s and adjusting the relative surface energies (fig. 4.5). In this way, the curved faces were shown to be combinations of first {1$\bar{1}$00} and second order {11$\bar{2}$0} prisms and possibly steep rhombohedra.

Mature crystals were too thick for electron diffraction. Nevertheless, SAED was possible off the edges or, in the case of fig. 4.6, on the *c* vertex tip. Strong patterns were recorded that corresponded to the <$\bar{5}$501> zone axis of calcite which subtends

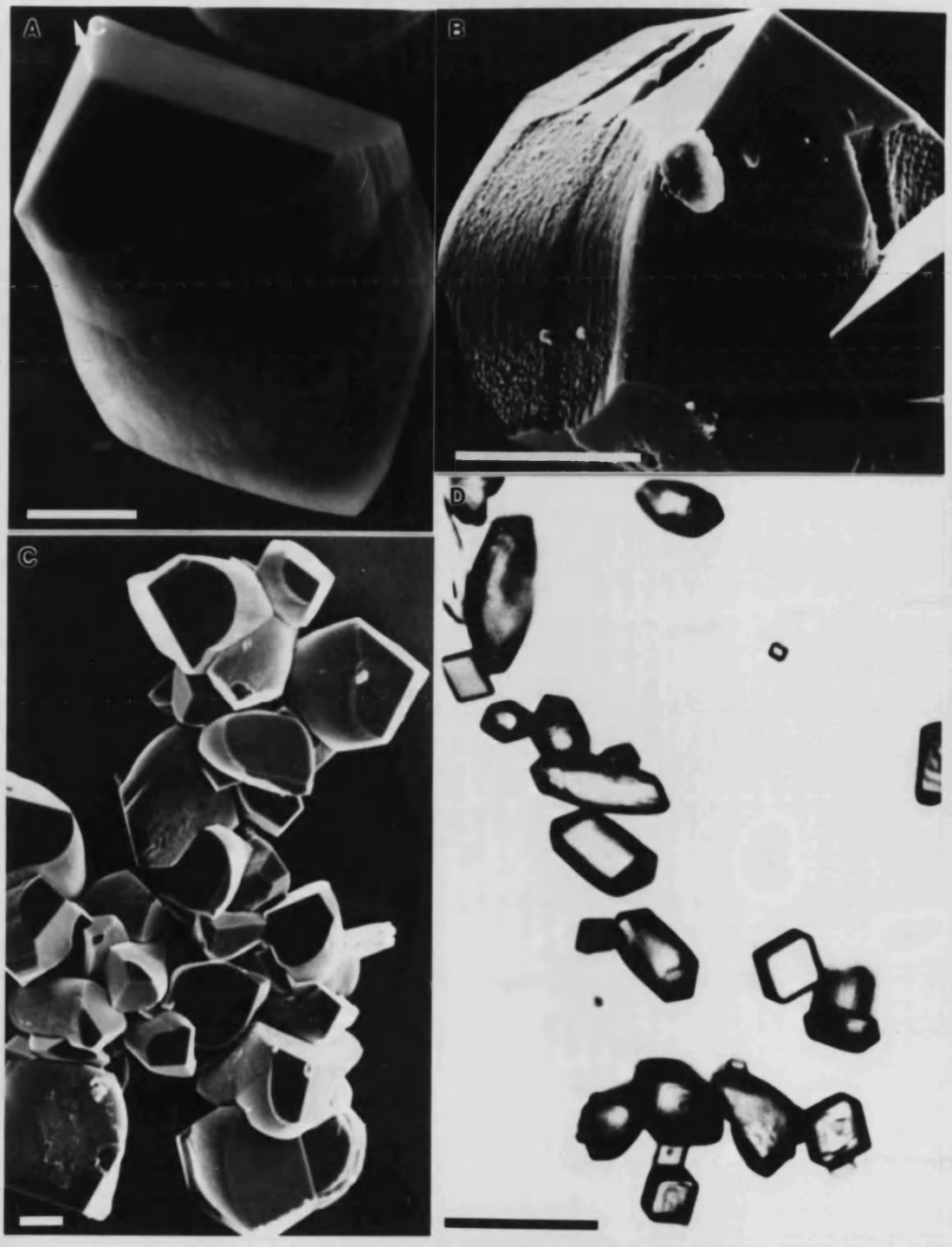

Fig. 4.4 *Micrographs of crystals grown in the presence of a high concentration of malonic acid, calcium/additive ratios = 3:1-5:1, at the surface of the crystallizing solution (a, b, c) and at the bottom of the container (d). Scale bars 10 μm.*

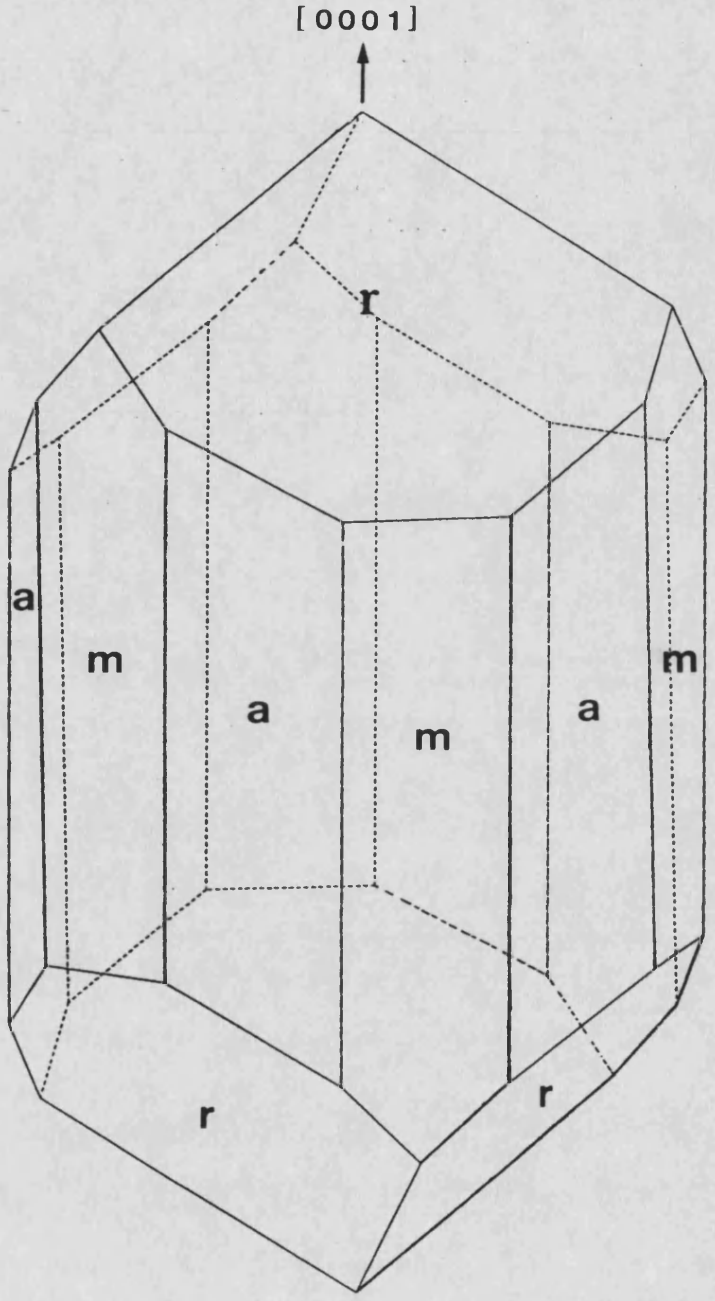

Fig. 4.5 *Spindle-shaped morphology generated by the program MORPH exhibiting r* $\{10\bar{1}4\}$, *a* $\{11\bar{2}0\}$ *and m* $\{1\bar{1}00\}$ *faces.*

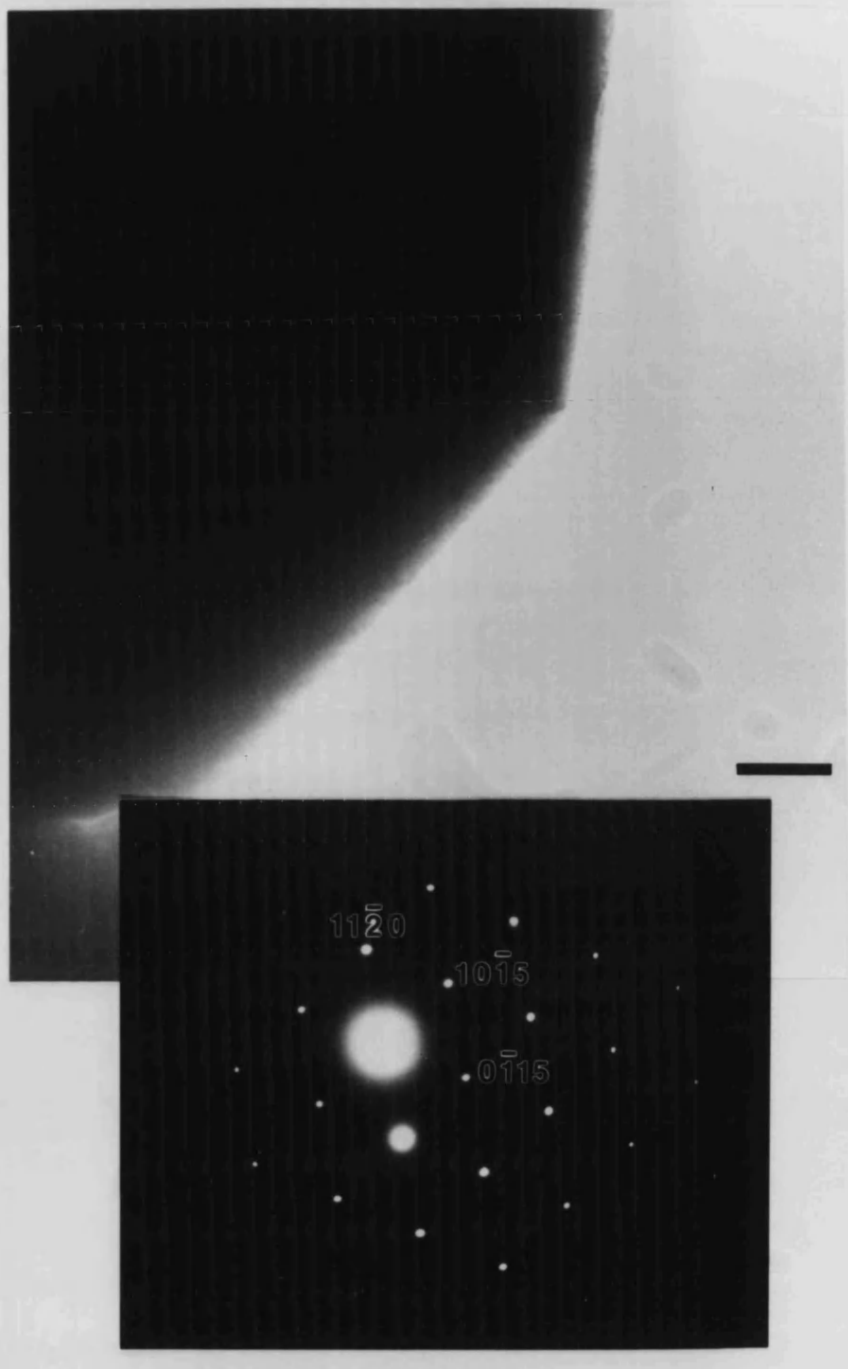

Fig. 4.6 *Transmission electron micrograph and associated selected area electron diffraction pattern, corresponding to the <$\bar{5}501$> zone, of the c vertex tip of a malonate-effected surface crystal grown at a calcium/additive ratio = 3:1. Scale bar 1 μm. (Courtesy of Dr Brigid R. Heywood).*

an angle of 1.1° to [1$\bar{1}$00]. This was indication that the spindles were well-ordered single crystals. It also provided some evidence that first order, prismatic faces were in contact with the TEM grid surface although insufficient data was recorded to confirm this observation.

At intermediate Ca/malonate ratios (ie 8:1 and 12:1), many rhombs, both truncated and regular, exhibited the same curved faces but they were generally less developed (fig. 4.7a, b). Spindle morphologies were present but in lower numbers compared to the systems with higher acid levels. Minimal morphological change was observed at high Ca/malonate ratios (ie 23:1) (fig. 4.7c, d). The majority of crystals resembled those in the control ie regular and truncated rhombs with smooth {10$\bar{1}$4} faces. However, there was a small but significant proportion with pitted and etched faces that did not appear in the control and occasionally a spindle morphology.

Effect of Chain Length (fig. 4.8)

Succinic and, to a lesser extent glutaric acid, had a very similar mode of interaction to malonate. Crystals with {10$\bar{1}$4} end faces and curved prisms or steep rhombs were observed. However, the numbers of crystals affected by these additives was much less. Fig. 4.9 shows the proportion of crystals that have undergone similar morphological change for all of the n = 1-7 saturated homologues studied. Thus, higher homologues after glutaric had minimal effect. The slight rise in effect for pimelic was not significant.

Suberic, azelaic and sebacic acids were only partially soluble in the crystallizing solution. Undissolved suberic and azelaic remained on the bottom of the dish so it was possible to sample the surface calcite crystals for analysis. However, yields were not recorded for these acids because the calcite became mixed with the undissolved acids during filtration. Sebacic contaminated the surface crystals preventing any kind of analysis. Calcium glutarate salts may have been responsible

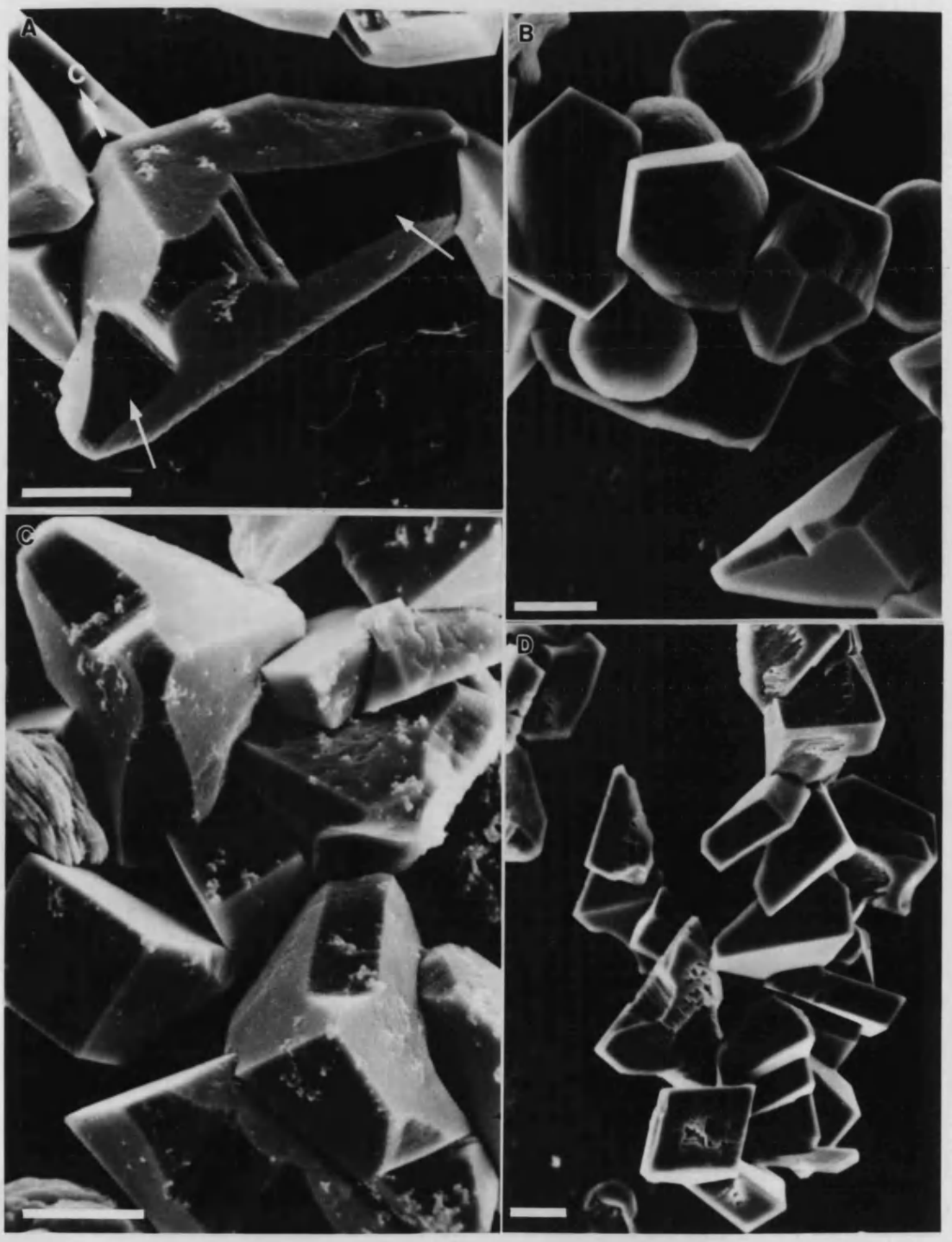

Fig. 4.7 *Scanning electron micrographs showing the influence of malonic acid on surface crystals at lower concentrations (a, b) calcium/additive ratios = 8:1-12:1 and (c, d) at 23:1. Scale bars 10 μm.*

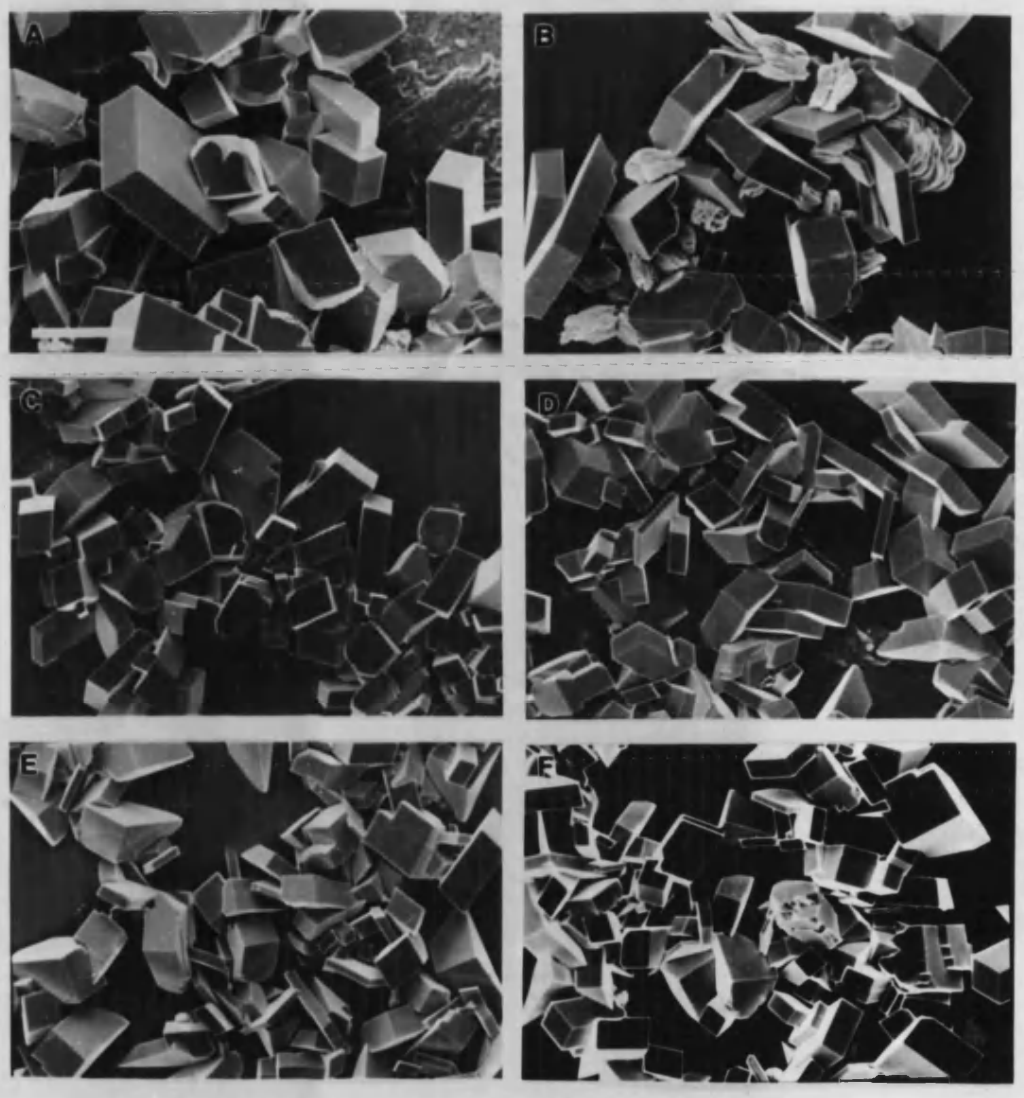

Fig. 4.8 *Scanning electron micrographs illustrating the effect of the longer chain saturated dicarboxylates on surface crystals at a calcium/additive ratio = 3:1 (a) succinate (b) glutarate (c) adipate (d) pimelate (e) suberate (f) azeleate. Scale bars 50 μm.*

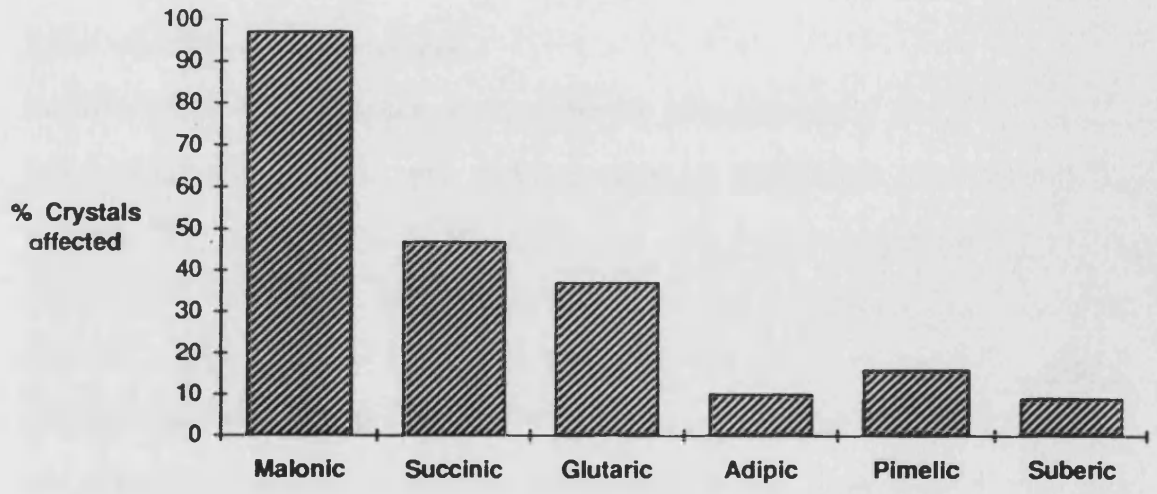

Fig. 4.9 *Bar chart showing the statistical proportion of crystals affected for each of the saturated dicarboxylates studied at 3:1.*

for the unknown lines in the XRD.

Effect of Unsaturation

Maleic acid also produced spindles (fig. 4.10a). These were similar to malonate although the *c* axis elongation was less marked and on some crystals the $\{10\bar{1}4\}$ ridges were partially missing. Instead roughened, steep rhombohedral type faces were present (fig. 4.10b). In stark contrast, there was no noticeable effect at all with fumaric acid (fig. 4.10c, d). The yield data was also consistent with this observation.

Effect of α-Amino Functionalization

Substitution of an α-hydrogen of succinate for an amino group to give aspartate (amino-succinate; DL only was tried), resulted in appreciable enhancement of potency. Whereas a Ca/succinate ratio = 3:1 had only a minor influence on morphology, Ca/aspartate ratios as high as 17:1 were enough to induce distinct changes. Again, prismatic-type faces were observed but these appeared to be smoother and better defined than those for succinate or malonate (fig. 4.11a). Also, *c* axis elongation was more marked. Complete inhibition of crystallization occurred at 0.4:1 whereas no morphological effect was noticed above 90:1. The immature, early crystallites were smaller (4-6 μm) and thin enough for electron diffraction data to be taken through their central area (fig. 4.12). Several single crystal patterns were observed corresponding to $<5\bar{5}01>$ and $<3\bar{4}11>$. The latter zone is actually closer to $[1\bar{2}10]$ (23.6°) than $[1\bar{1}00]$ (36.6°) suggesting a more rounded morphology including first and second order prisms. An α-amino functionalization of the weakly interacting glutarate, to give glutamate, also improved the potency but not to the same extent as aspartate (fig. 4.13). Glutamate, at a ratio of 3:1, was similar in its potency to succinate.

Effect of α-Amino, ω-Carboxylate Functionalization: γ-Carboxyglutamate (Gla)

The lowest concentration studied was Ca/gla = 435:1. Here, the main change in

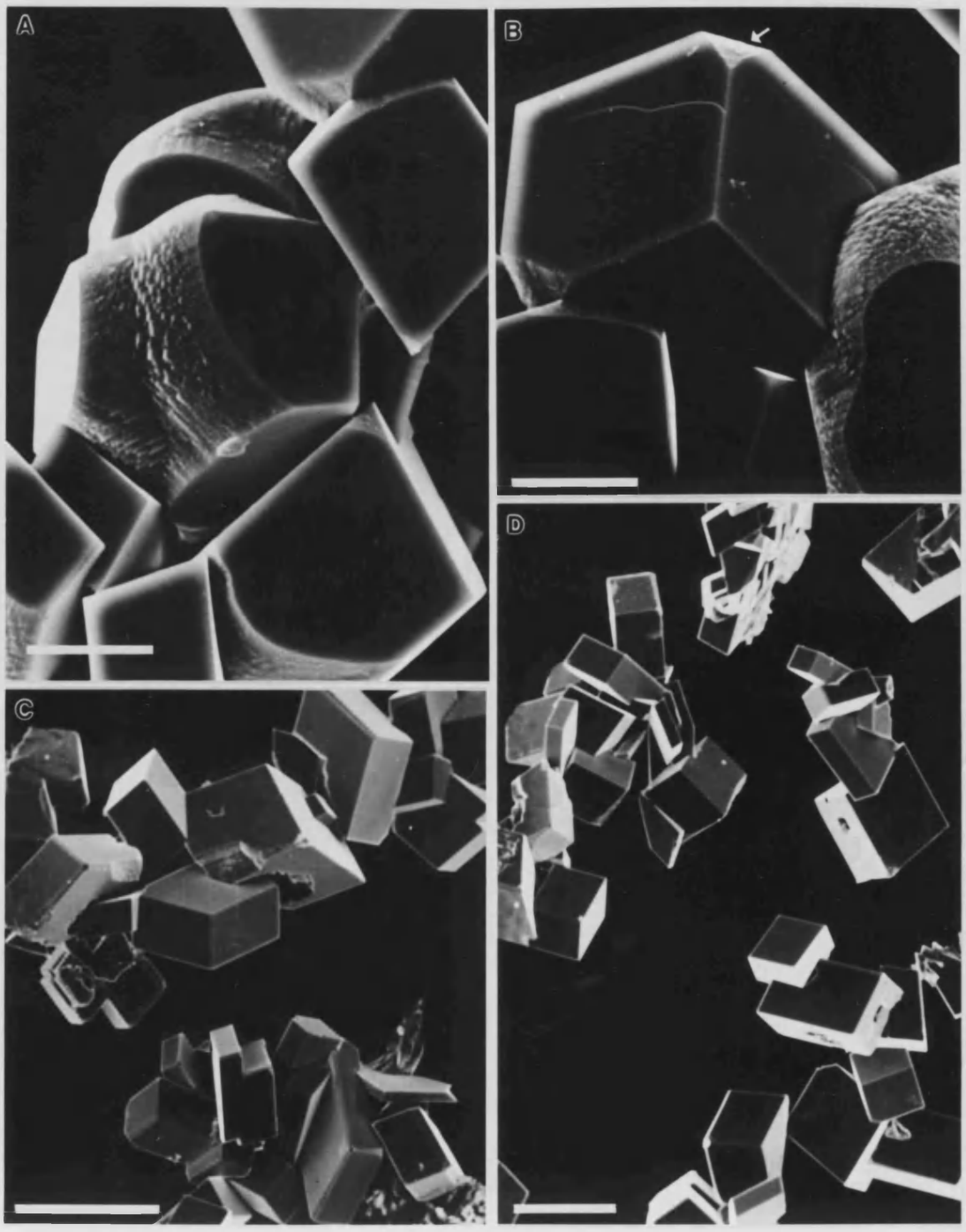

Fig. 4.10 *Scanning electron micrographs of surface crystals grown in the presence of unsaturated aliphatic dicarboxylates at calcium/additive ratios = 3:1 (a, b) maleic acid, scale bars 10 μm (c, d) fumaric acid, scale bars 50 μm.*

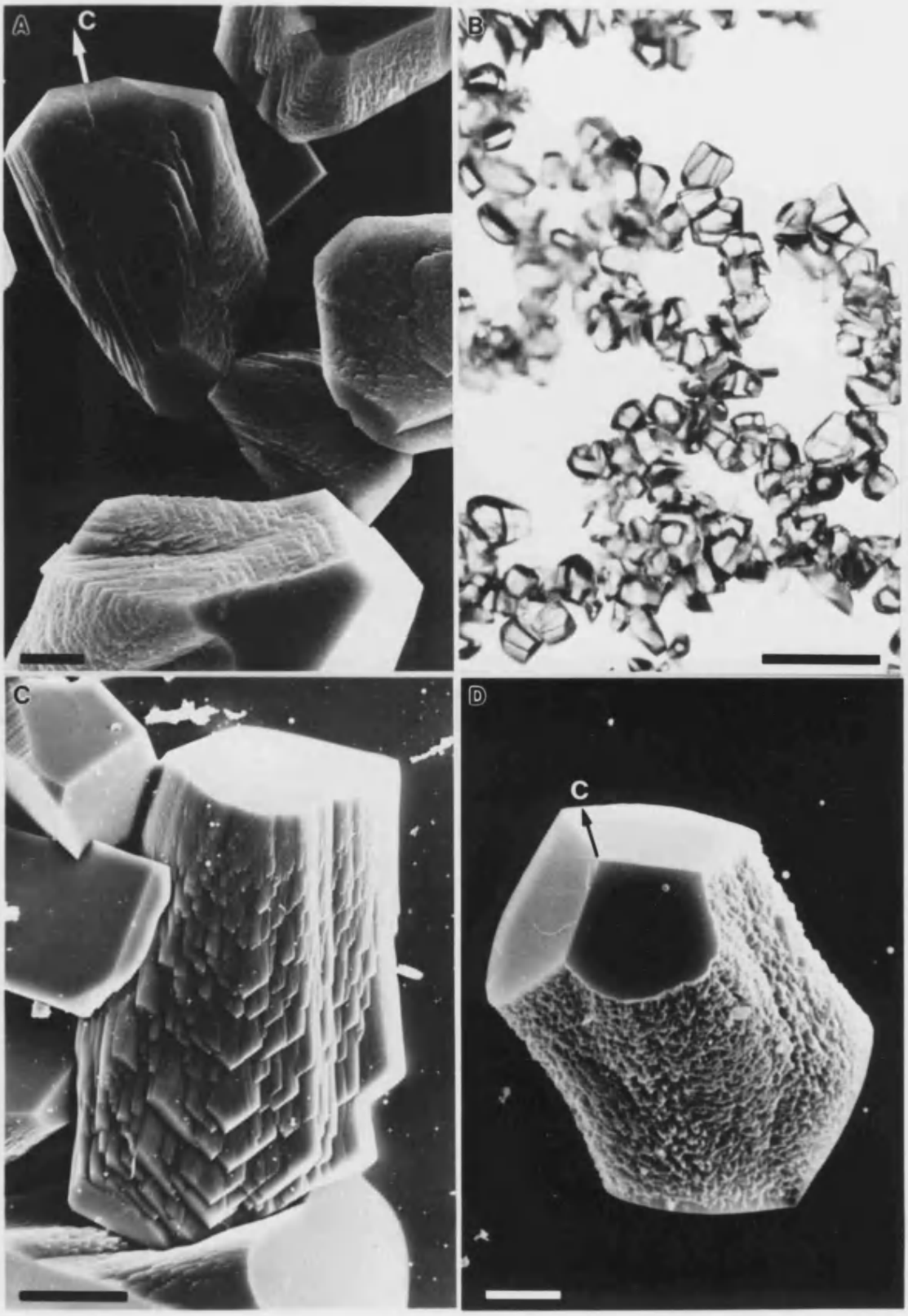

Fig. 4.11 *Micrographs depicting the morphological influence of aspartic acid (a) surface crystals at a calcium/additive ratio = 17:1, scale bar 10 μm (b, c) surface crystals at a ratio = 3:1, scale bars (b) 100 μm (c) 10 μm and (d) bottom crystals at 3:1, scale bar 2 μm.*

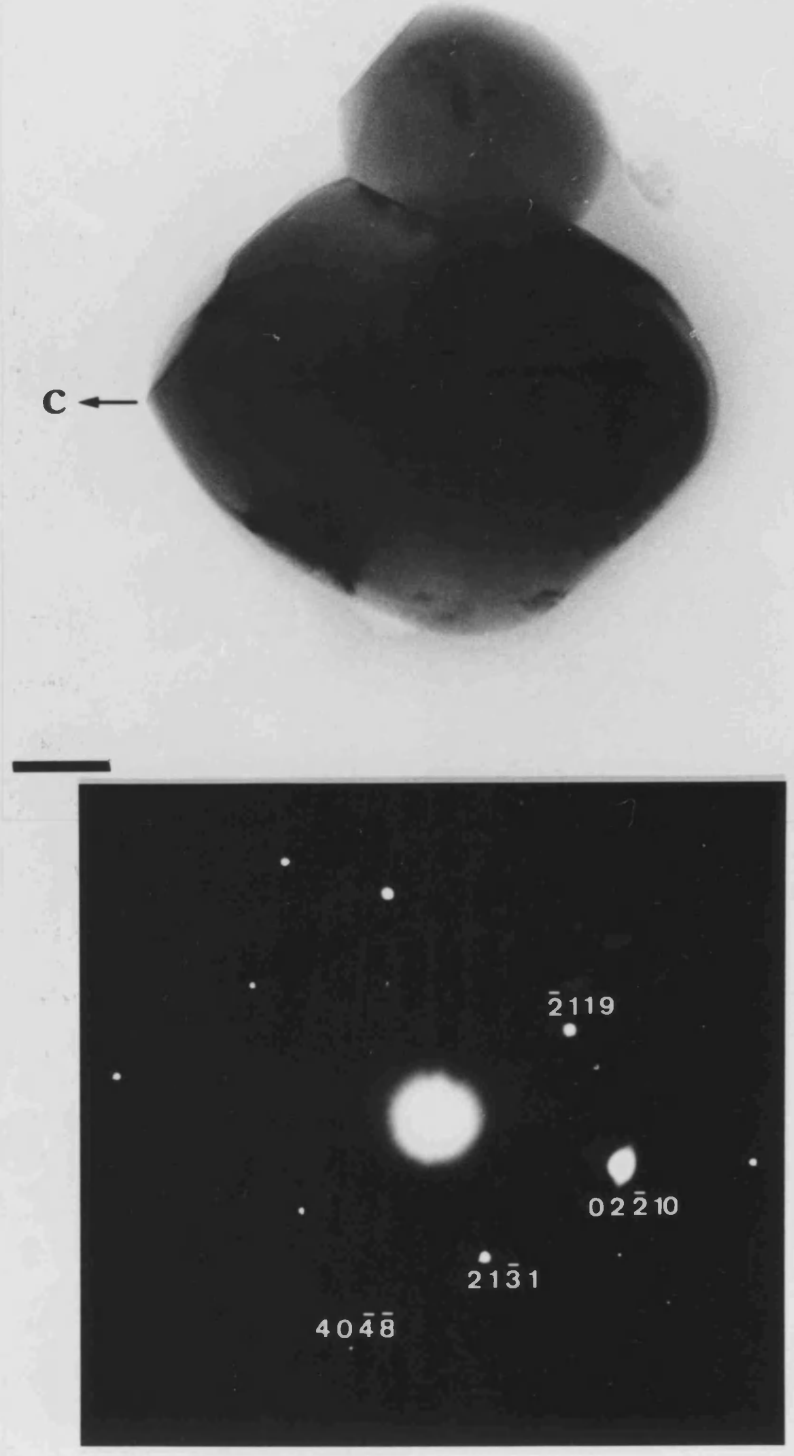

Fig. 4.12 *Transmission electron micrograph and associated selected area electron diffraction pattern, corresponding to the <3$\bar{4}$11> zone, of an aspartate-modified surface crystal, collected at 1 hour, grown at calcium/additive = 3:1. Scale bar 50 nm.*

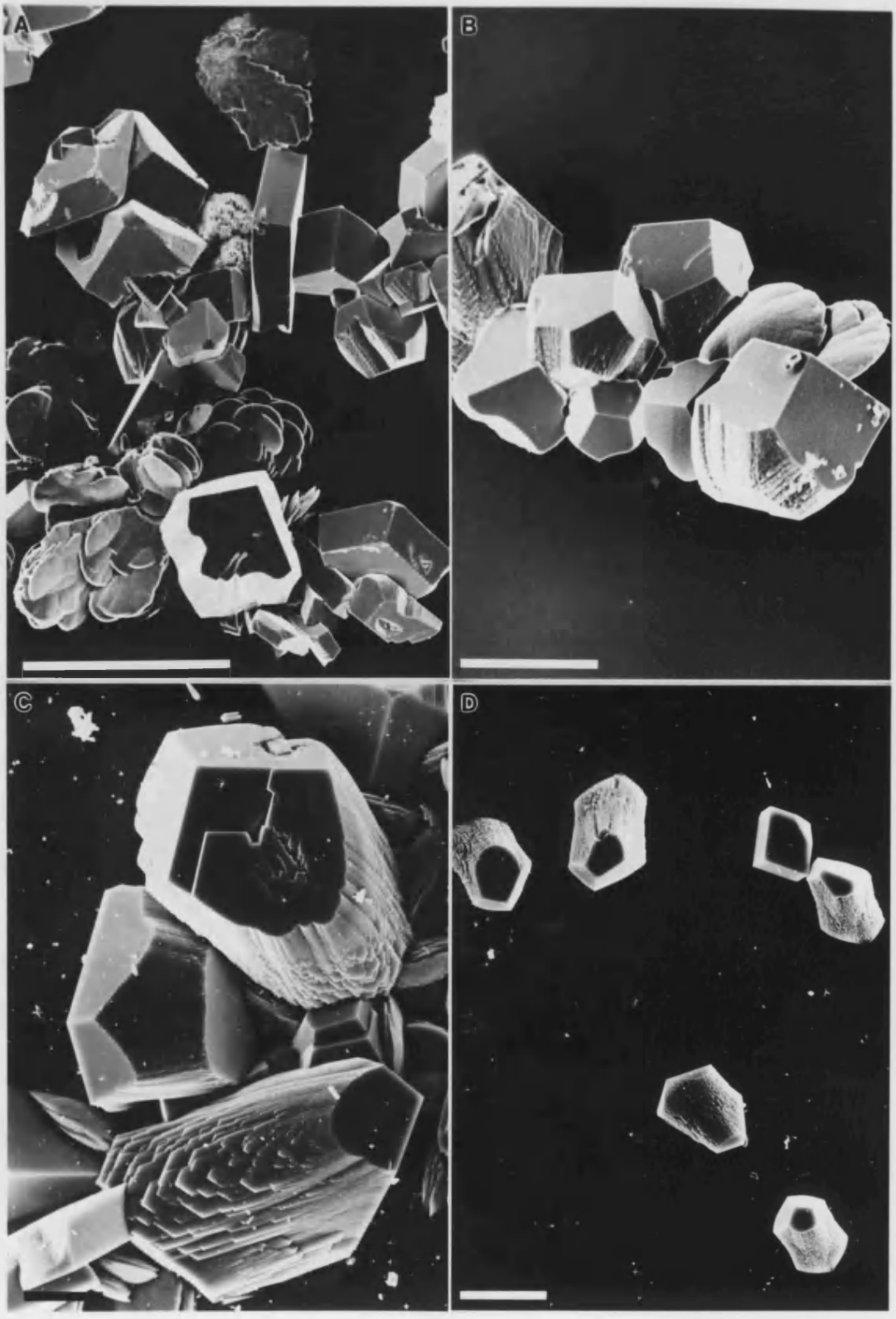

Fig. 4.13 *Scanning electron micrographs comparing the effect of glutamic acid at calcium/additive ratios = 3:1 (a) surface and (b) bottom crystals with aspartic acid at 3:1 (c) surface and (d) bottom crystals. Scale bars (a, b) 50 μm (c, d) 10 μm.*

morphology was the appearance of striated and stepped faces along the edge of the rhombs (fig. 4.14a). At a ratio of 85:1, calcite spindles showed well-developed, euhedral prisms (fig. 4.14b, c). The faces were fairly roughened and extensively stepped exhibiting beautiful "gothic" arching (fig. 4.14d). The apex of each arch pointed along the crystallographic *c* axis which was considerably elongated in the crystal. These forms could be indexed morphologically as a first order $\{1\bar{1}00\}$ set. This was because they cut across the $\{10\bar{1}4\}$ ridges and were thus distinct from the second order prisms $\{11\bar{2}0\}$ which were rotated about the *c* axis by 30° and cut from vertex to vertex (fig. 4.15).

At Ca/gla = 27:1, here the spindle-shaped habits (fig. 4.16a) and truncated rhombs with straight prismatic sides were in greater abundance but the arching described above was absent. At the low ratios (eg 3:1), entirely different crystal morphologies were predominant. Calcite had crystallized in very small (mean 10 μm; σ 4.6 μm), curious ovaloid "pine cone" shapes (fig. 4.16b closed arrow, c and d) with small $\{10\bar{1}4\}$ faces could be seen. Also present were a population of larger (mean 29.9 μm; σ 10.8 μm) spherical, glassy deposits (fig. 4.16b open arrow).

Because of the miniature scale of the experiments using γ-carboxyglutamate, yield data, as weights in grams, was not recorded. However, based on visual assessments of the surface crystals, it was clear that the system at Ca/additive ratio = 3:1 had a substantially reduced yield compared to the control (approximately half). Chirally-resolved material (D and L), as well as the racemic (DL), was tried although no significant difference in morphological effect or potency were noticed.

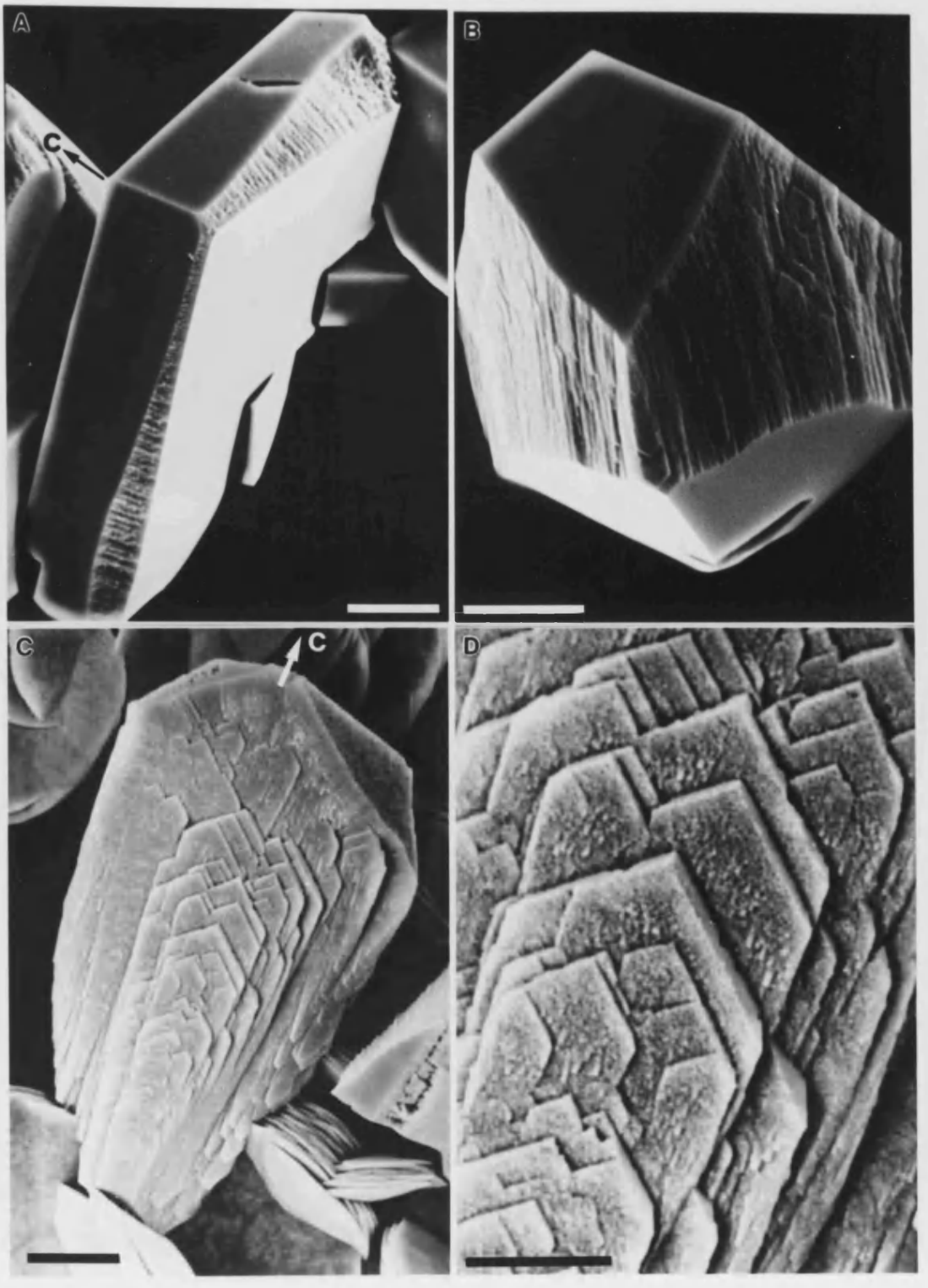

Fig. 4.14 *Scanning electron micrographs of surface crystals grown in the presence of γ-carboxyglutamic acid (a) calcium/additive = 435:1 (b, c, d) 85:1. Scale bars (a, b, c) 10 μm (d) 5 μm.*

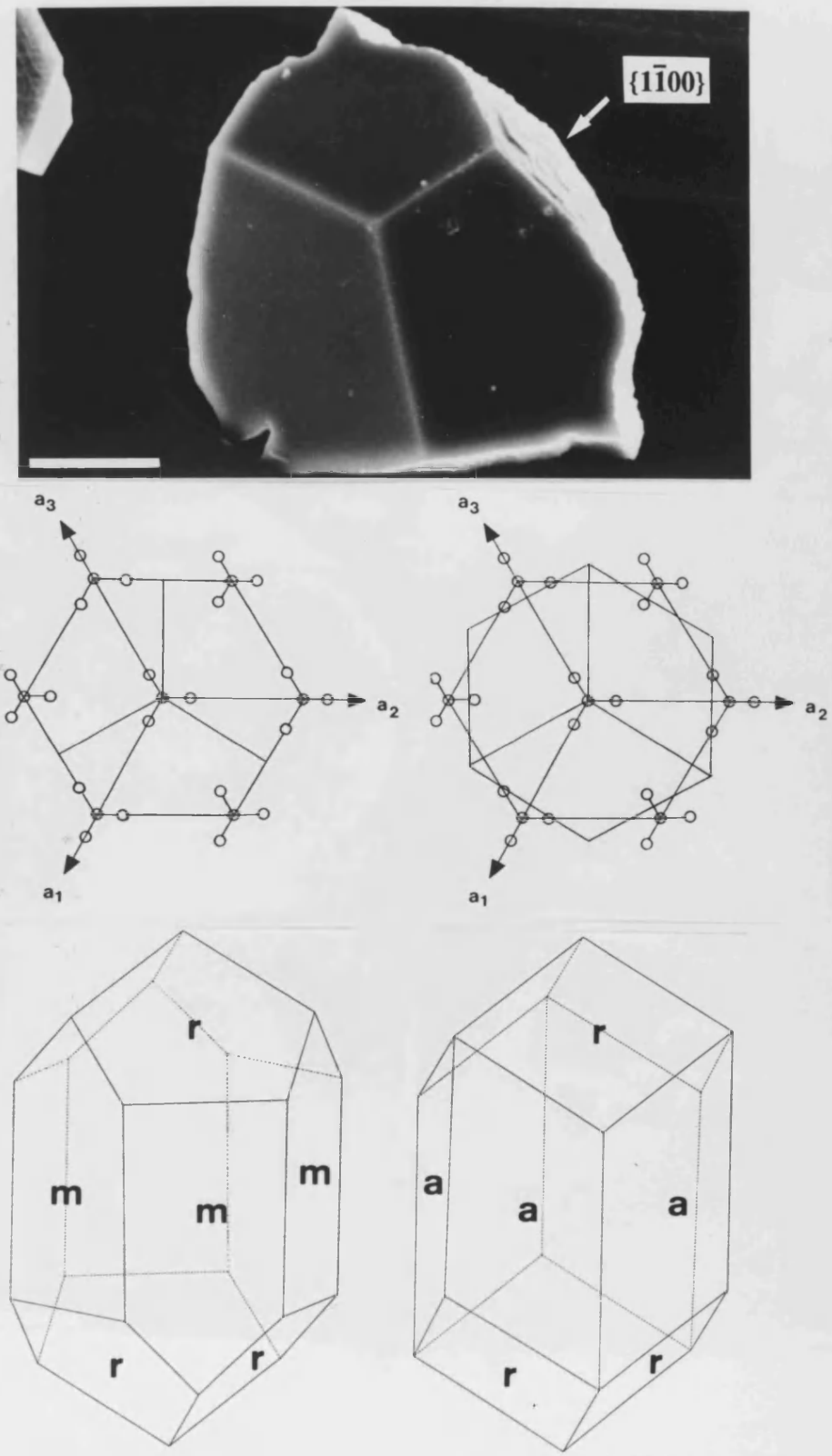

Fig. 4.15 *Scanning electron micrograph taken above the c vertex of a crystal grown at calcium/γ-carboxyglutamate = 85:1. The effected face was indexed as (1$\bar{1}$00). Scale bar 10 μm. The relationship between first m {1$\bar{1}$00} and second order a {11$\bar{2}$0} prisms and rhombohedral r {10$\bar{1}$4} is illustrated in the drawings below.*

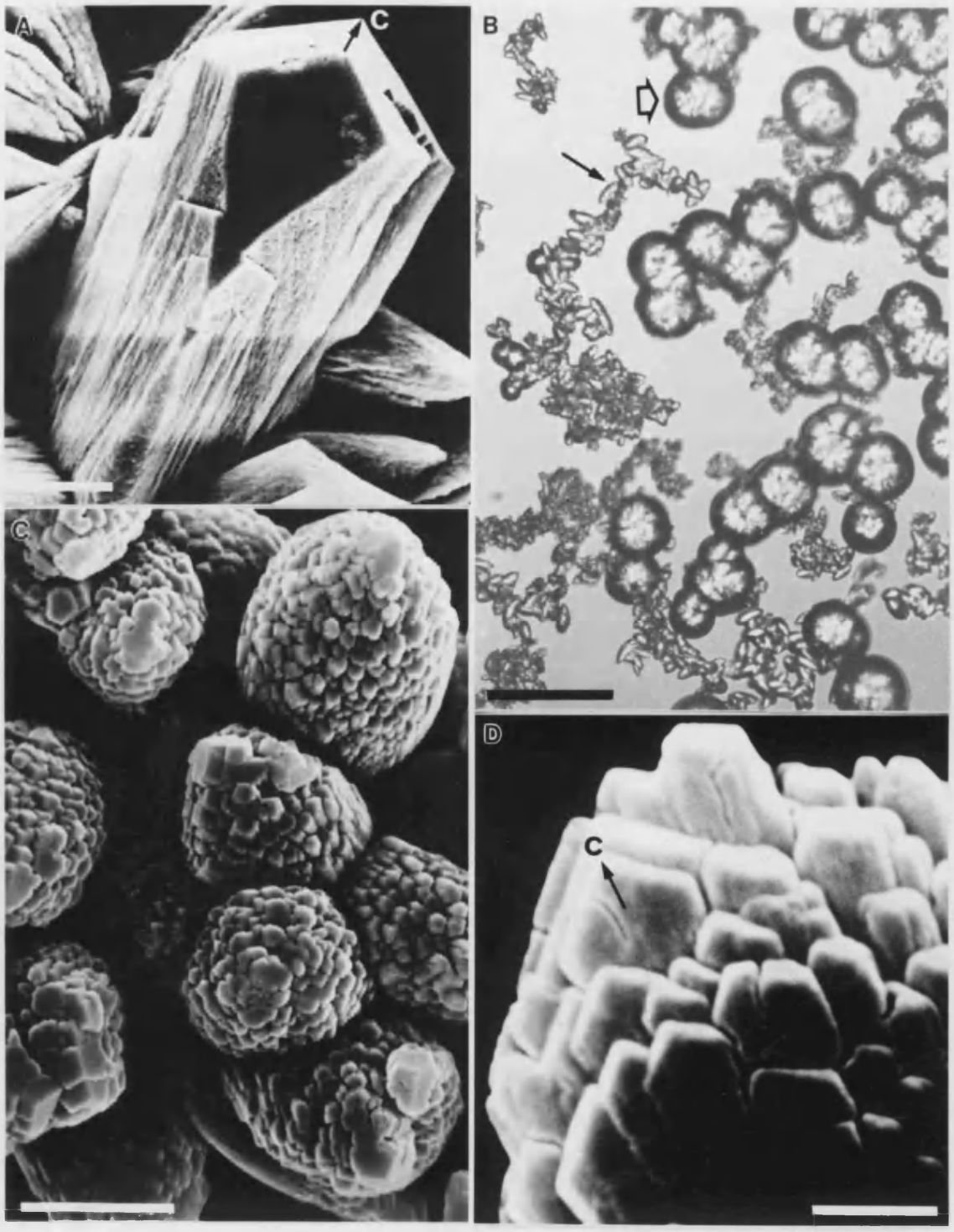

Fig. 4.16 *Micrographs demonstrating the effect of higher concentrations of γ-carboxyglutamic acid at the surface (a) calcium/additive = 27:1 (b, c, d) 3:1. Scale bars (a, c) 5 μm (b) 50 μm (d) 1 μm.*

4.3.2 Influence of Organic/Inorganic Oxyphosphorus and other Oxyanions

General results

A summary of the experimental data obtained is given in table 4.4.

Phosphate

Orthophosphate, predominant as $H_2PO_4^-$ at pH 6, was a very potent additive being effective at ratios as high as 10,000:1. Unlike the dicarboxylate additives, phosphate tended to aggregate the calcite crystals; an effect which seemed to be dose dependent. The morphological interaction, however, appeared similar to that of the carboxylate anions. At the lower ratios (10:1, 100:1), the crystals were distinctly elongated along the *c* axis (fig. 4.17a, b) and smooth, stepped faces were evident. Their distinct tapering suggested that they had a slight inclination to the *c* axis (fig. 4.17c). $\{40\bar{4}1\}$ ρ faces like these are known for calcite (Dana 1932). A morphology combining these forms with $\{10\bar{1}4\}$ was drawn using *MORPH* (fig. 4.17d). The resulting habit was similar although the steep rhombohedra proved to be the symmetry related $\{4\bar{4}01\}$ instead; $\{40\bar{4}1\}$ point in the opposite direction when combined with $\{10\bar{1}4\}$. Some crystals displayed several rhombohedral ends that were slightly misoriented with respect to each other (fig. 4.18a, b). This was probably due to heterogeneous nucleation and growth on the $\{4\bar{4}01\}$ faces induced by the presence of adsorbed phosphate. A significant elongation of the *c* axis also occurred to crystals grown at 1000:1 (fig. 4.18c) although this effect diminished at 10,000:1 (fig. 4.18d) and was absent at 50:000:1 and 100,000:1.

Effect of hydrophobic substituents

Ester derivatives of orthophosphate ($ROPO_3H^-$) showed a marked reduction in morphological effect as the R group increased in size and hydrophobicity (H > butyl > phenyl > naphthyl) (cf. fig. 4.17a, b with fig. 4.19). ^{n}Butyl-dihydrogen-phosphate was effective at 10:1 (fig. 4.19a) but only weakly interacted with the crystals at

Additive	Ca/additive ratios studied	XRD	Yield (g)
control	-	C, V	0.05
orthophosphate	1:1	amorphous	0.29
	10:1	C, A	0.04
	100:1	C	0.03
	1000:1	-	-
	10,000:1	C, V	0.03
	50:000:1	C, V	-
	100,000:1	C, V	0.05
n-butyldihyrogen-phosphate	1:1	-	0.00
	10:1	C	0.06
	100:1	C	0.04
	1000:1	C, V	0.04
phenyl orthophosphate	1:1	C, V	0.02
	10:1	C, V	0.01
	100:1	C, V	0.04
	1000:1	C, V, A	0.04
napthyl orthophosphate	1:1	C, V	0.11
	10:1	C, V	0.04
	100:1	C, V, A	0.05
	1000:1	C, V	0.05
methyl phosphonate	10:1	-	0.00
	100:1	C, V	0.03
	1000:1	C, V	0.04
	10,000:1	C, V, A	0.04
phenyl phosphonate	1:1	amorphous	0.10
	10:1	C	0.04
	100:1	C, V	0.06
	500:1	C, V	
	1000:1	C, V, A	0.07
methylenediphosphonate	10:1	-	0.00
	100:1	-	0.00
	1000:1	C	0.04
	2500:1	C	0.03
	3500:1	C	0.03
	5000:1	C, V	0.04
	7500:1	C, V	0.04
	10,000:1	C, V	0.03
ethylenediphosphonate	10:1	amorphous	0.28
	100:1	C	0.06
	1000:1	C	0.04
	10,000:1	C, V	0.04

Table 4.4 *Experimental results for oxyanions studied.*

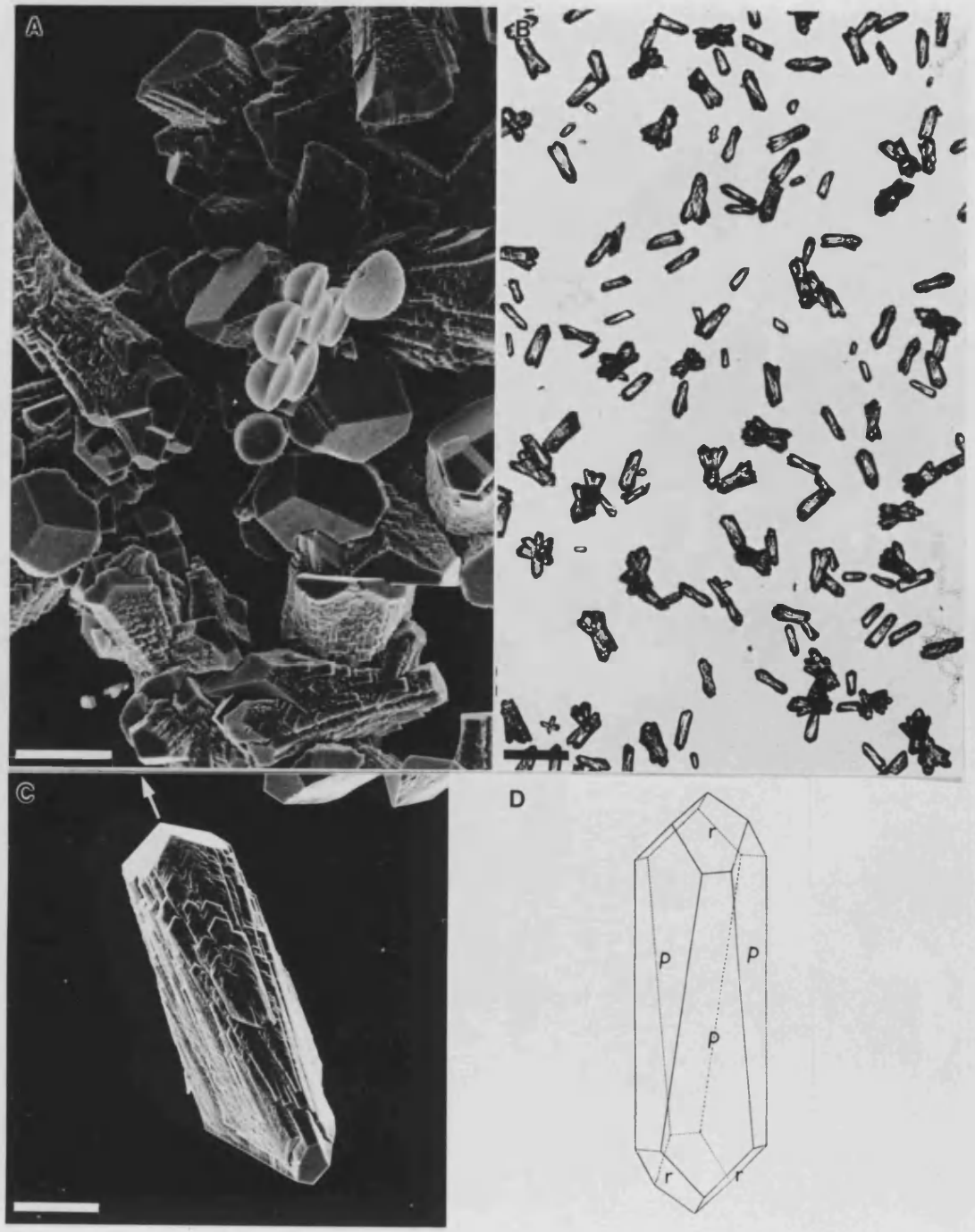

Fig. 4.17 *(a, b, c) Micrographs of crystals grown under the influence of orthophosphate at calcium/additive ratios = 10:1-100:1. Scale bars (a, c) 10 μm (b) 100 μm (d) MORPH plot of a similar habit exhibiting r {10$\bar{1}$4} and p {4$\bar{4}$01}.*

Micrographs taken by P. Oliver.

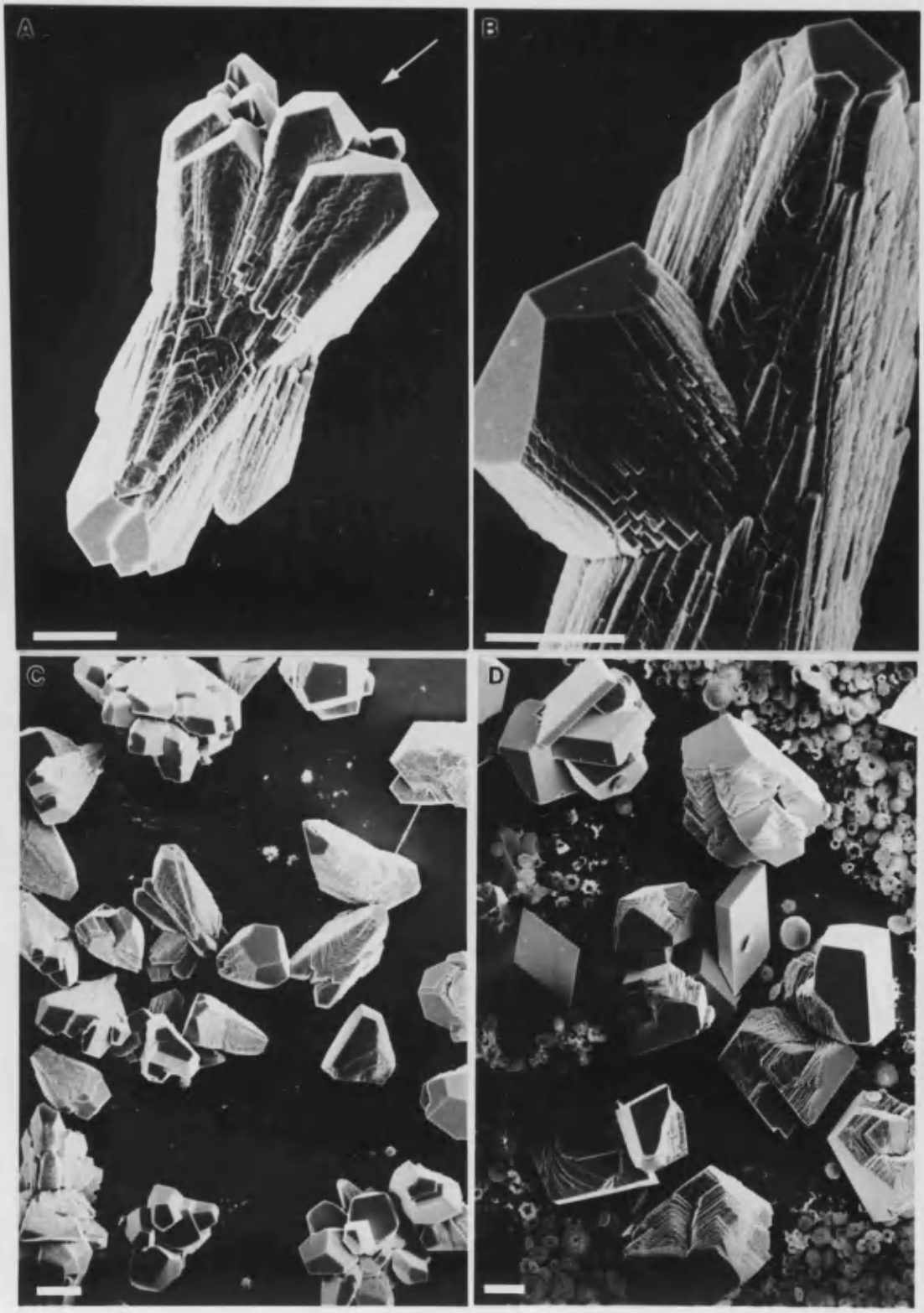

Fig. 4.18 *Scanning electron micrographs of orthophosphate-modified crystals (a, b) calcium/additive = 100:1 (c) 1000:1 (d) 10,000:1. Scale bars 10 μm.*

Micrographs taken by P. Oliver.

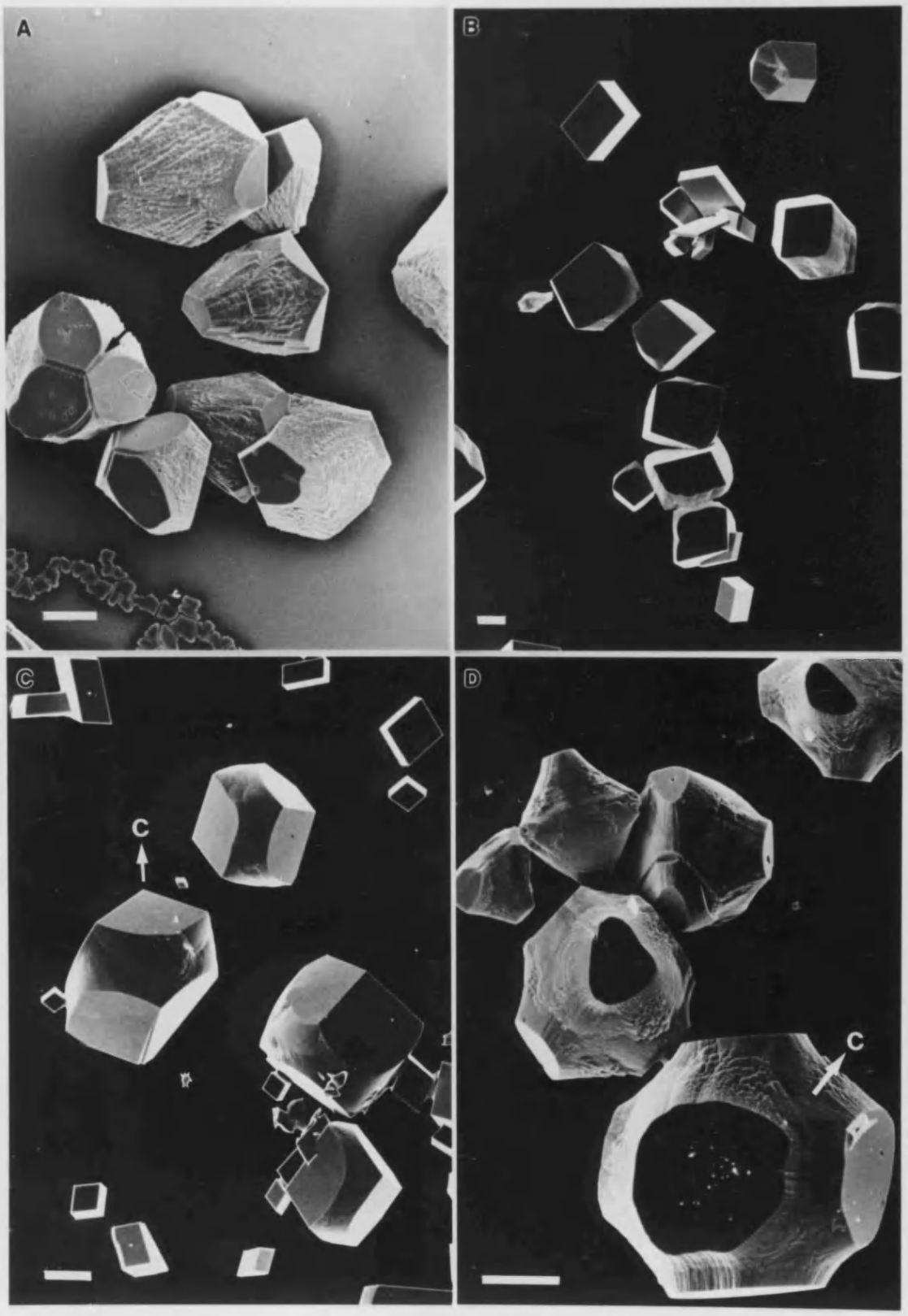

Fig. 4.19 *Scanning electron micrographs illustrating the effect of increasingly hydrophobic substituents on bottom crystals (a) ⁿbutyl dihydrogen phosphate 10:1 (b) phenyl phosphate 10:1 (c) phenyl phosphate 1:1 (d) napthyl phosphate 1:1. Scale bars 10 μm. Micrographs taken by P. Oliver.*

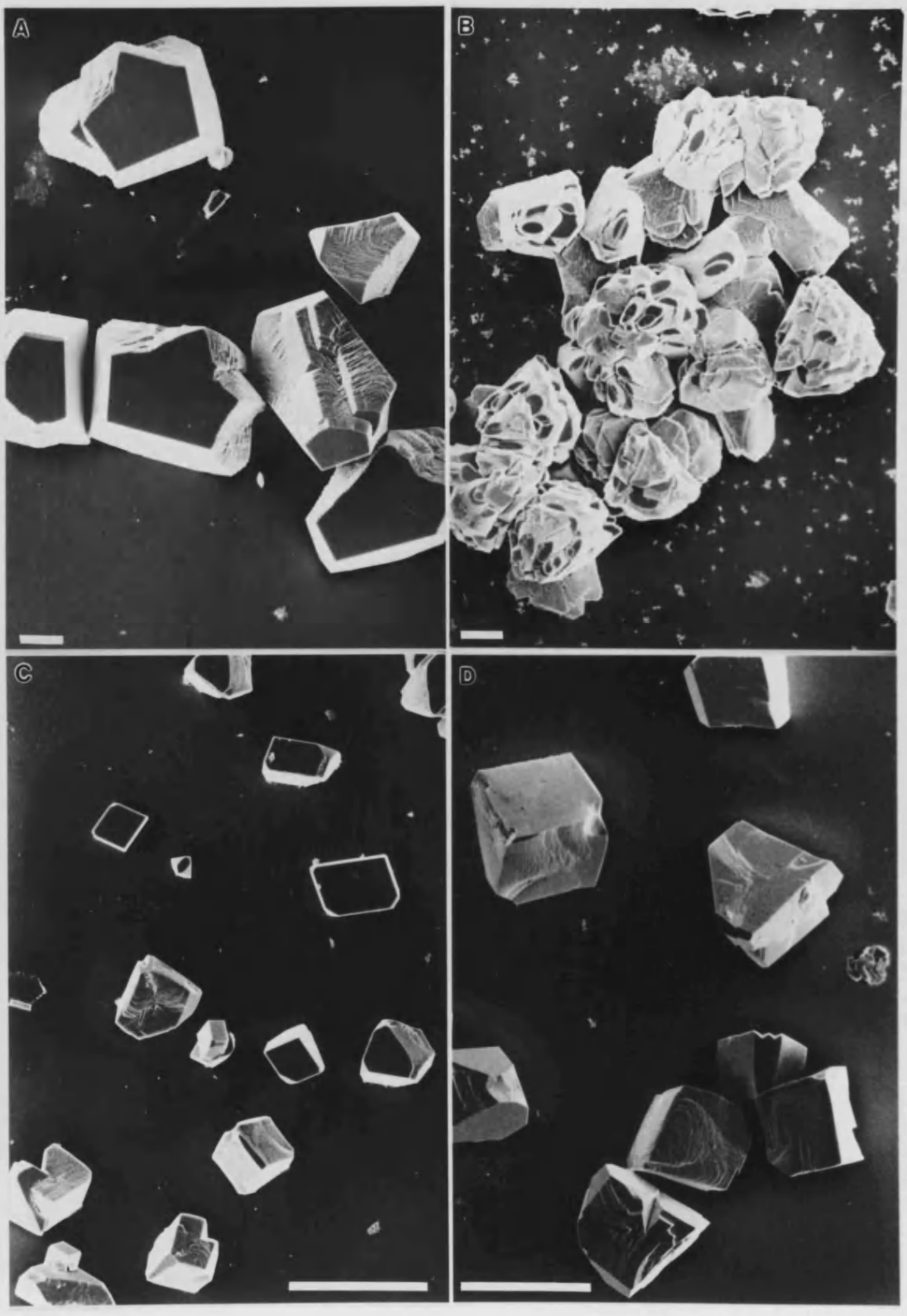

Fig. 4.20 *Scanning electron micrographs showing the effect of (a) methyl phosphonate 100:1 and (b) 10:1 plus (c) phenyl phosphonate 10:1 and (d) 1:1. Scale bars (a, b) 10 μm (c, d) 50 μm. Micrographs taken by P. Oliver.*

100:1 and higher. Morphologies were prismatic, occasionally with small $\{01\bar{1}8\}$ forms present (arrow). The phenyl phosphoester had some effect at 10:1 (fig. 4.19b) although at 1:1 produced habits with a well-defined, curved cross section but little elongation along the *c* axis (fig. 4.19c). These curved faces were surprisingly smooth compared to surfaces effected by other additives. 1-Naphthyl-orthophosphate had no effect at 10:1 but at 1:1 produced bizarre crystals possessing trenches where $\{10\bar{1}4\}$ ridges used to be thus corresponding roughly to negative rhombohedral $\{01\bar{1}8\}$ forms (fig. 4.19d). The three-fold axis could only just be discerned.

The same hydrophobic substituent effect was noticed for the two mono-functional phosphonates (methyl > phenyl) (fig. 4.20). At 100:1, methyl phosphonate gave prismatic/steep rhombohedral faces whereas at 10:1, it caused substantial intergrowth and aggregation with a similar morphological interaction. The phenyl phosphonate was slightly less potent than its phosphate counterpart but the former produced quite a different morphology. At 10:1, phenyl phosphonate appeared to produce several morphologies although after closer examination a common mechanism could be seen at work. The additive was able to express what looked like negative rhombohedral faces to varying extents on different crystals. They were only recognised because some crystals exhibited both the familiar smooth positive rhombs in combination with these new roughly textured faces. Thus, it was possible to ascertain the relationship between the complementary sets of rhombs. However, with many crystals, the rough faces predominated; a small, smooth, remnant face being all that was left of the positive form. In order to index these forms, it was necessary to measure the angle subtended between the face and the *c* axis which is the common reference point for calcite. Unfortunately, as the crystals were very small, no direct measurements could be taken. It was also very difficult to obtain this kind of data from micrographs. However, it was assumed that the positive forms were $\{10\bar{1}4\}$. According to Dana (1932), the faces which truncate the ridge

separating adjacent {10$\bar{1}$4}, are the {01$\bar{1}$8}. These forms have the same position relative to the horizontal axes as the first order prism {01$\bar{1}$0} but the angle between the plane and the vertical *c* axis is 63.8° unlike {10$\bar{1}$4} where it is 45.4°. Note that other rhombs could have been chosen such as {10$\bar{1}$1}, {10$\bar{1}$2}, {02$\bar{2}$1} etc which are truncated by {01$\bar{1}$2}, {01$\bar{1}$4}, {4$\bar{4}$01} etc respectively. On the other hand, *MORPH* showed the forms to be {01$\bar{1}$2} and not {01$\bar{1}$8} (fig. 4.21). Another feature of the crystals displaying both negative and positive rhombs, was the appearance of trenches along the positive {10$\bar{1}$4} ridges. These hollows were connected to the encroaching negative {01$\bar{1}$8} and probably represented an intermediate morphology.

Effect of a ω-Phosphonate Functionalization

A further $-PO_3H^-$ functionalization of the methyl and ethyl phosphonates to give the corresponding diphosphonates resulted in a substantial enhancement of potency comparable to orthophosphate and with a similar mechanism of interaction. The diphosphonates (methylene diphosphonate and ethylene diphosphonate) affected the morphology of calcite at ratios of 10,000:1. The methylene additive at 1000:1 to 3500:1 (fig. 4.22a), induced the precipitation of aggregated, ill-defined crystals identified, by XRD, as calcite. At 5000:1 and above, it had no effect. Ethylene diphosphonate was slightly less potent producing strange triradiate crystals with, what looked like, roughened {4$\bar{4}$01} faces at 1000:1 (fig. 4.22b). Both the compounds caused extensive aggregation and disruption of crystallization at the lower ratios especially methylene diphosphonate.

Other Inorganic Oxyanions

Oxyanions of stronger acids were less effective in modifying crystal growth. Sulphate ions in solution at a ratio of 10:1 had a similar to phenyl phosphate in that rounded prismatic faces were expressed and minimal elongation of the *c* axis took place (fig. 4.23a). On the other hand, nitrate ions had no effect on morphology even when present in very high concentration (ratios of 0.01:1) (fig. 4.23b). Instead, the

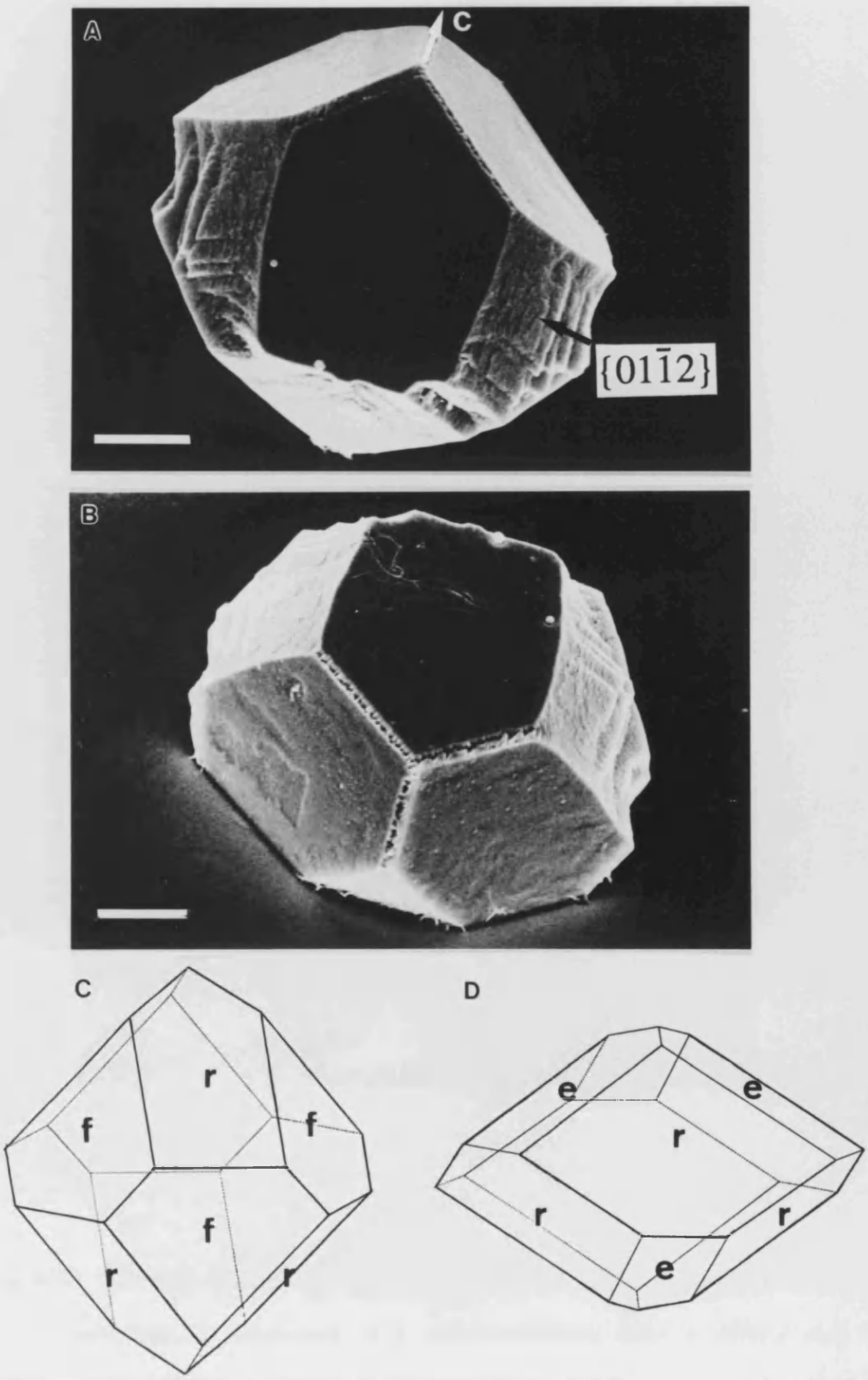

Fig. 4.21 *(a, b) Scanning electron micrographs of phenyl phosphonate-modified bottom crystals (scale bars 5 μm) compared to MORPH plots showing morphologies exhibiting combinations of positive and negative rhombohedral faces: (c) +r {10$\bar{1}$4} and -f {01$\bar{1}$2} (d) +r {10$\bar{1}$4} and -e {01$\bar{1}$8}.*

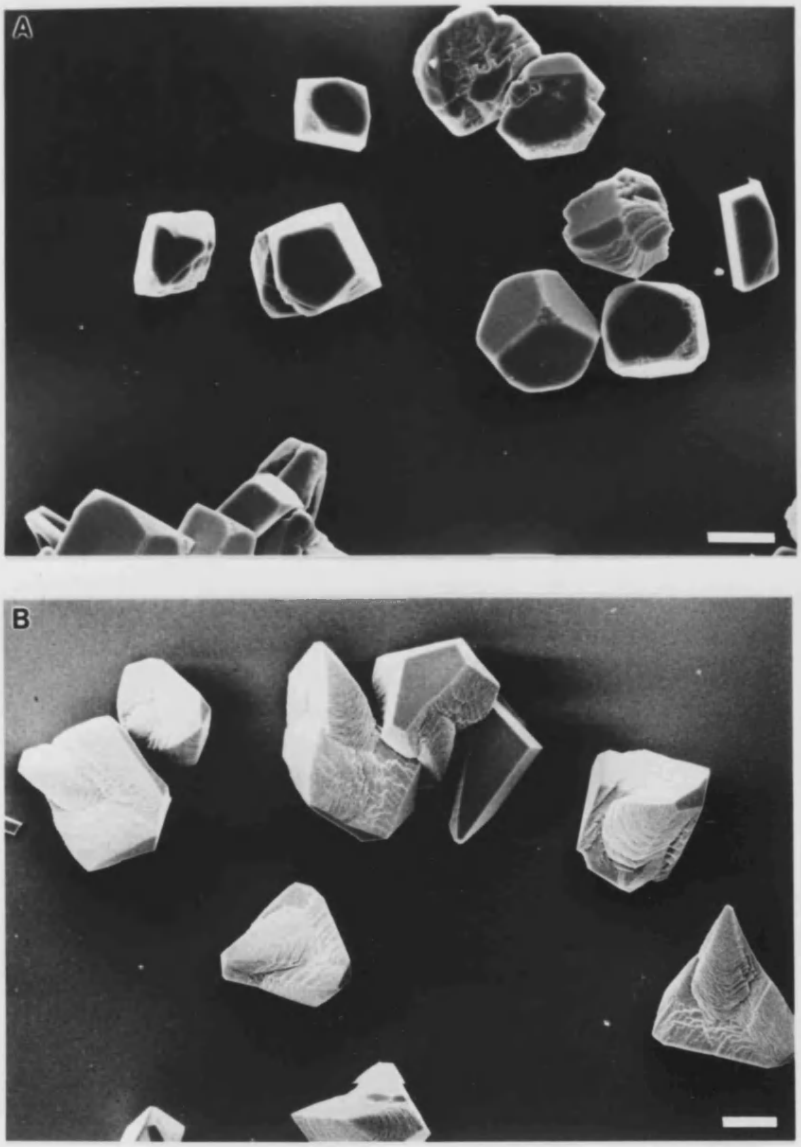

Fig. 4.22 *Scanning electron micrographs of surface crystals grown in the presence of (a) methylene diphosphonate at a calcium/additive ratio = 3500:1 and (b) ethylene diphosphonate at 1000:1. Scale bars 10 μm.*

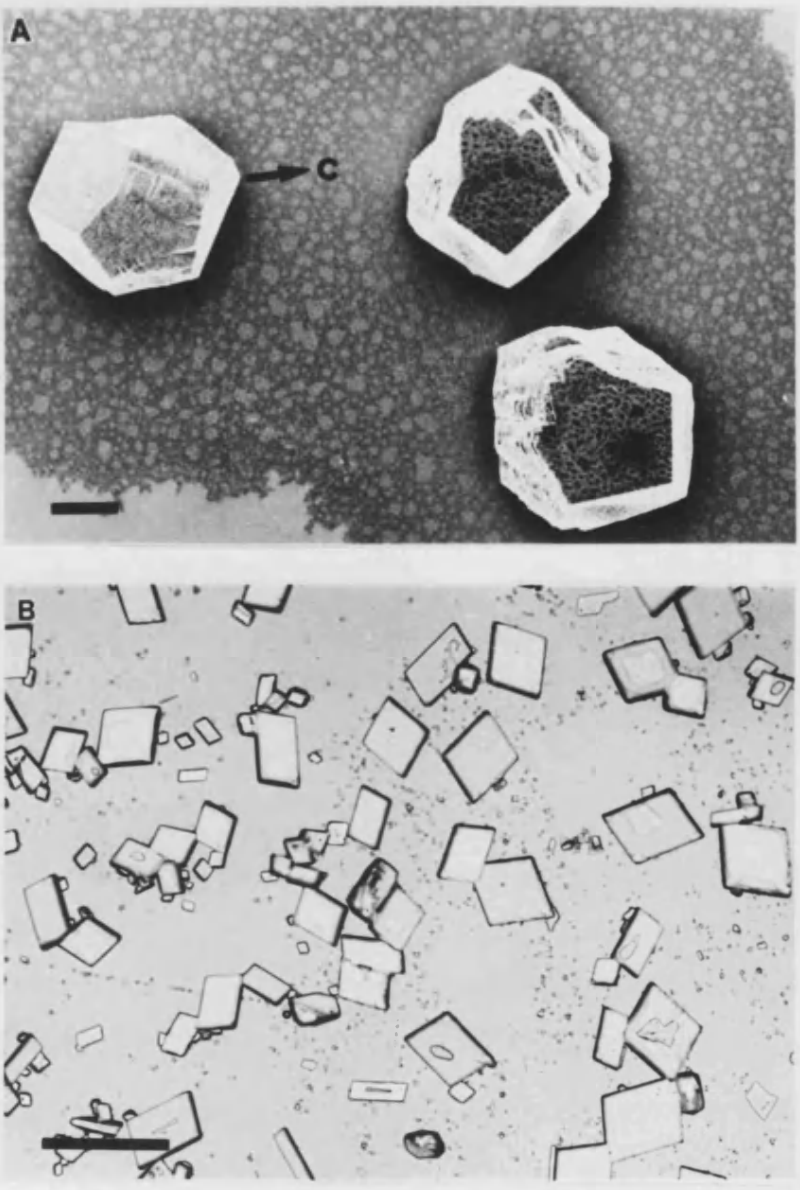

Fig. 4.23 *Micrographs showing the effect of (a) 10:1 sulphate, scale bar 10 μm and (b) 0.01:1 nitrate, scale bar 100 μm. Micrographs taken by P. Oliver.*

increased ionic strength of the solution inhibited all growth of metastable phases. XRD data showed very pure precipitates of calcite.

4.3.3 *Further Characterization of Habit-Modified Crystals*

Elemental Microanalysis

The results are shown in table 4.5.

Sample	%C	%H	%N
control	11.98	0.00	0.01
malonate-modified	12.10	0.23	0.01
malonate-incubated	11.98	0.10	0.00
aspartate-modified	12.10	0.23	0.27
aspartate-incubated	12.05	0.15	0.08

Table 4.5 *Results of elemental analysis for C, H and N*

It can be seen that, compared to the control, a significant increase in %C and %H is observed for malonate-modified crystals and %C, %H and %N for aspartate. This is corresponds to a take-up of *ca.* 2.5% aspartate based on the nitrogen content or *ca.* 5% based on hydrogen. The higher hydrogen-based value was probably due to some small amount of residual water and was therefore less accurate. The malonate content (based on hydrogen) was substantially greater at approximately 12%. Similarly, the incubated samples (surface adsorbed only) showed increases although not to the same extent as the modified materials. This was not conclusive evidence for incorporation, however, as the surface areas of each powder may have varied significantly.

Infra-red Spectroscopy

Transmission IR detected a weak, unsymmetrical extra band at around 1030 cm^{-1}, characteristic of P-O stretching, in precipitates grown in the presence of at 100:1 Na_3PO_4. A higher resolution (1 cm^{-1}) scan of the peak revealed a doublet or possibly a triplet indicating a symmetry lowering of the the phosphate group from T_d to C_{2v} or C_{3v} (fig 4.24a). Similar results have been observed for adsorbed phosphate and sulphate at the surface of the iron oxide, goethite (Anthony 1990). However at 10:1, a more symmetrical band was observed (fig. 4.24b) typical of tetrahedral phosphate perhaps present as coprecipitated calcium phosphate phase although no XRD data was recorded that supported this speculation. This evidence suggested that the molecule was segregated to the surface and was bound in either a bidentate or tridentate manner. In the case of aspartate-modified crystals, no extra bands were observed. The more sensitive FTIR, on the other hand, showed the appearance of N-H stretching and deformation vibrations not present in the control (fig. 4.25a, b cf. fig. 4.26a). These peaks were indistinguishable from data on control crystals incubated in aspartate solutions of identical concentration for the same length of time (fig. 4.26b). An attempt was made to remove the surface adsorbed material from the incubated and modified samples by etching with 0.2% HCl solution. Unfortunately, it proved very difficult to remove the organic material even from the incubated sample without dissolving a large proportion of the crystals.

High Resolution X-ray Diffraction

The routine XRD and electron diffraction confirmed that the aspartate, malonate and phosphate-modified crystals were well-ordered calcite showing all the symmetry-related planes for the space group. Additional analysis by higher resolution XRD on aspartate and phosphate-modified (10:1) crystals consistently detected a 0.1-0.3 % increase on all planes but this was not taken as a significant change in lattice parameters (fig. 4.27, table 4.6).

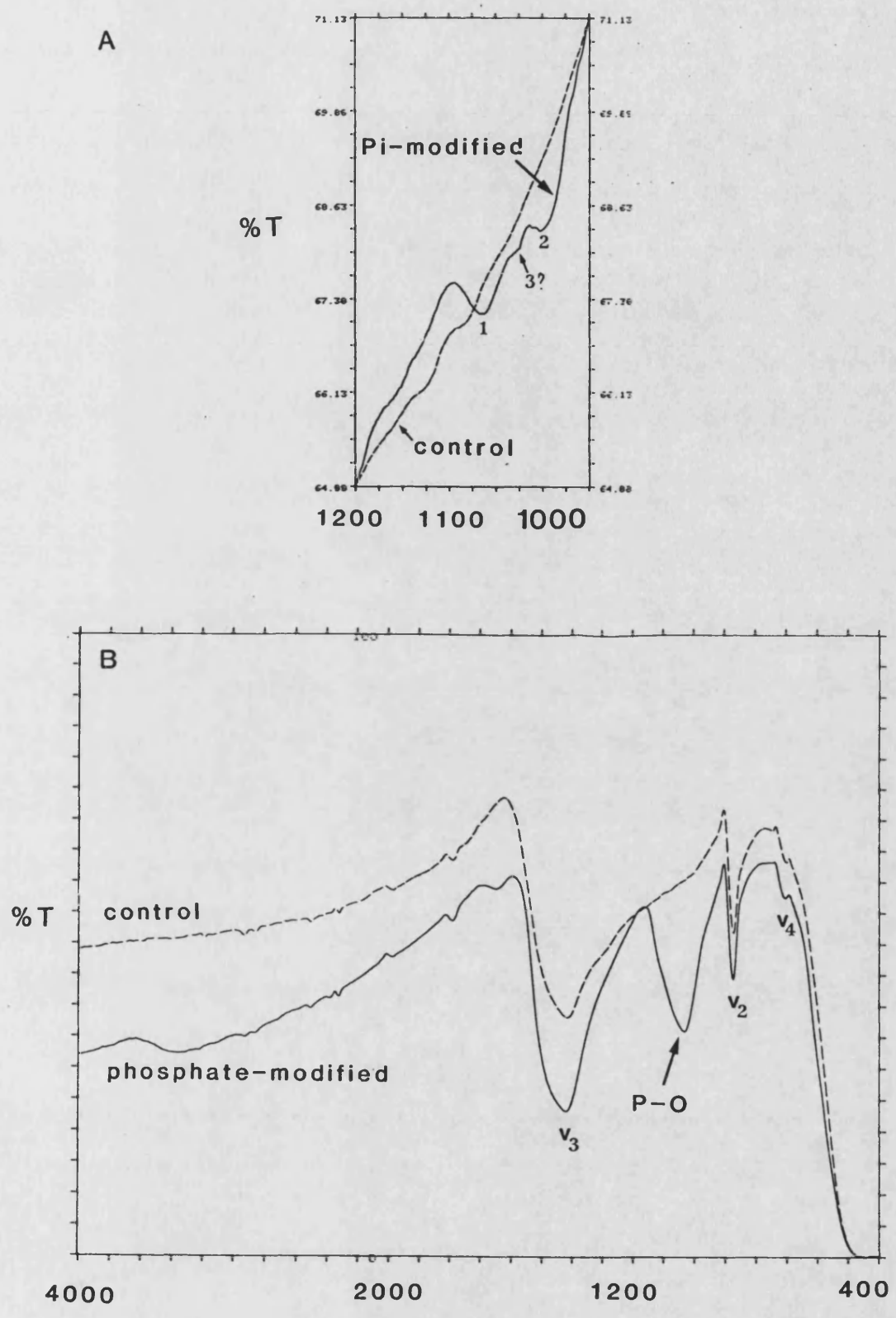

Fig. 4.24 *Transmission infra-red spectra of surface crystals grown in the absence and presence of orthophosphate (a) calcium/additive ratio = 100:1, 1 cm^{-1} resolution and (b) 10:1, 3 cm^{-1} resolution.*

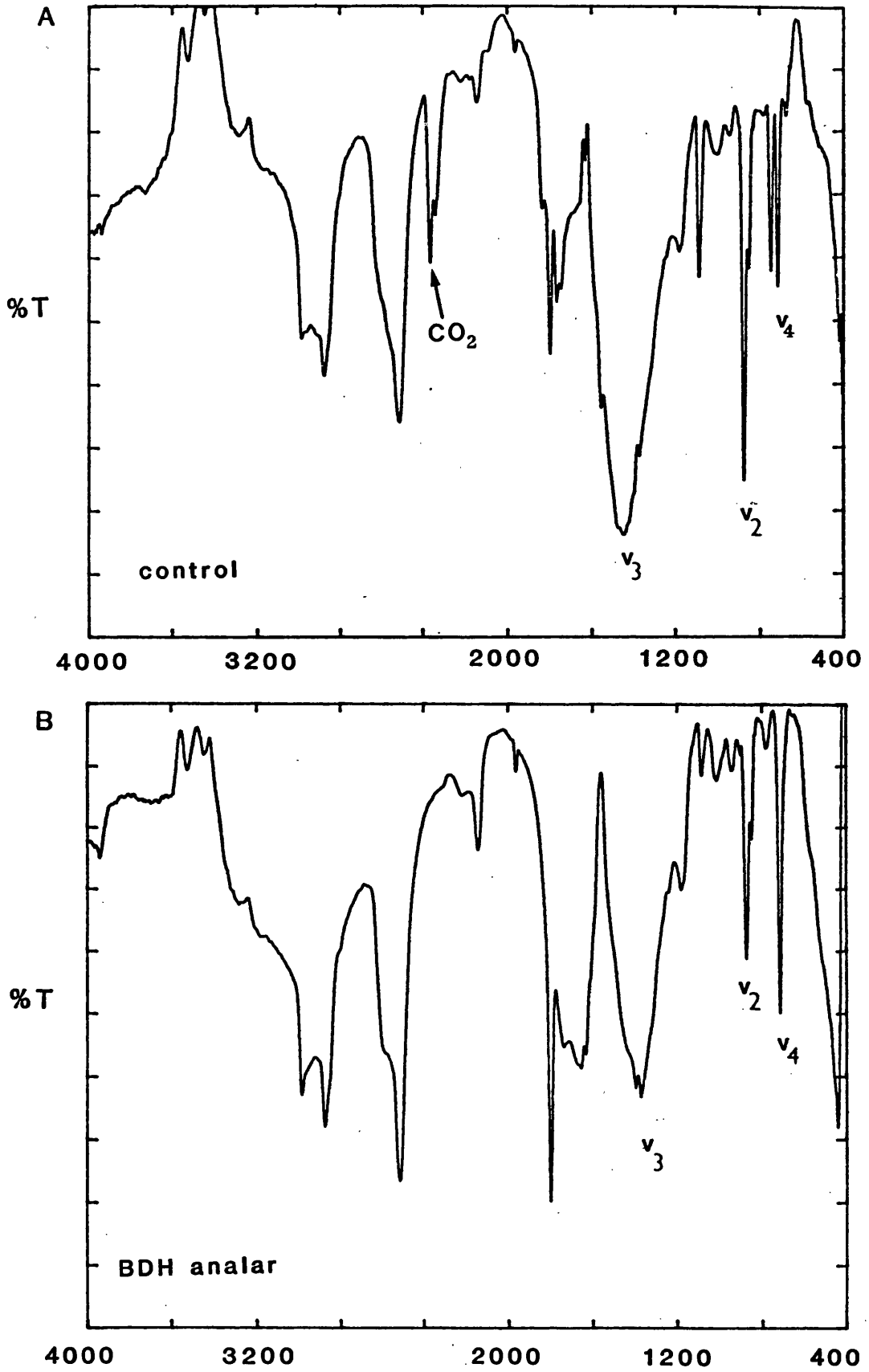

Fig. 4.25 *Diffuse reflectance Fourier transform infra-red spectra at 2 cm^{-1} resolution of (a) surface control crystals and (b) specpure calcite. Both 10% w/w in KBr.*

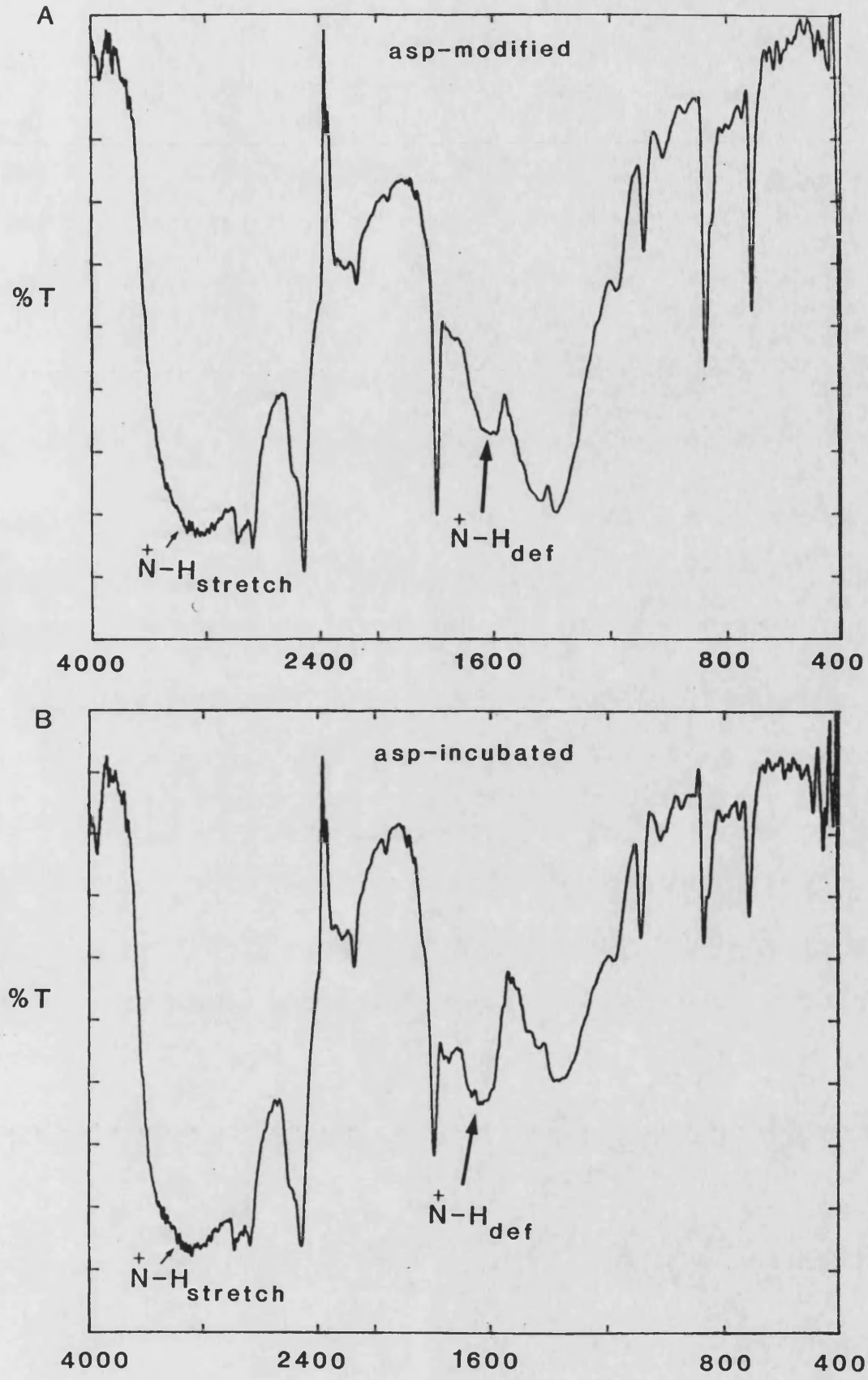

Fig. 4.26 *Diffuse reflectance FTIR spectra (2 cm^{-1}) of surface crystals (a) grown and (b) incubated in the presence of aspartate at 3:1.*

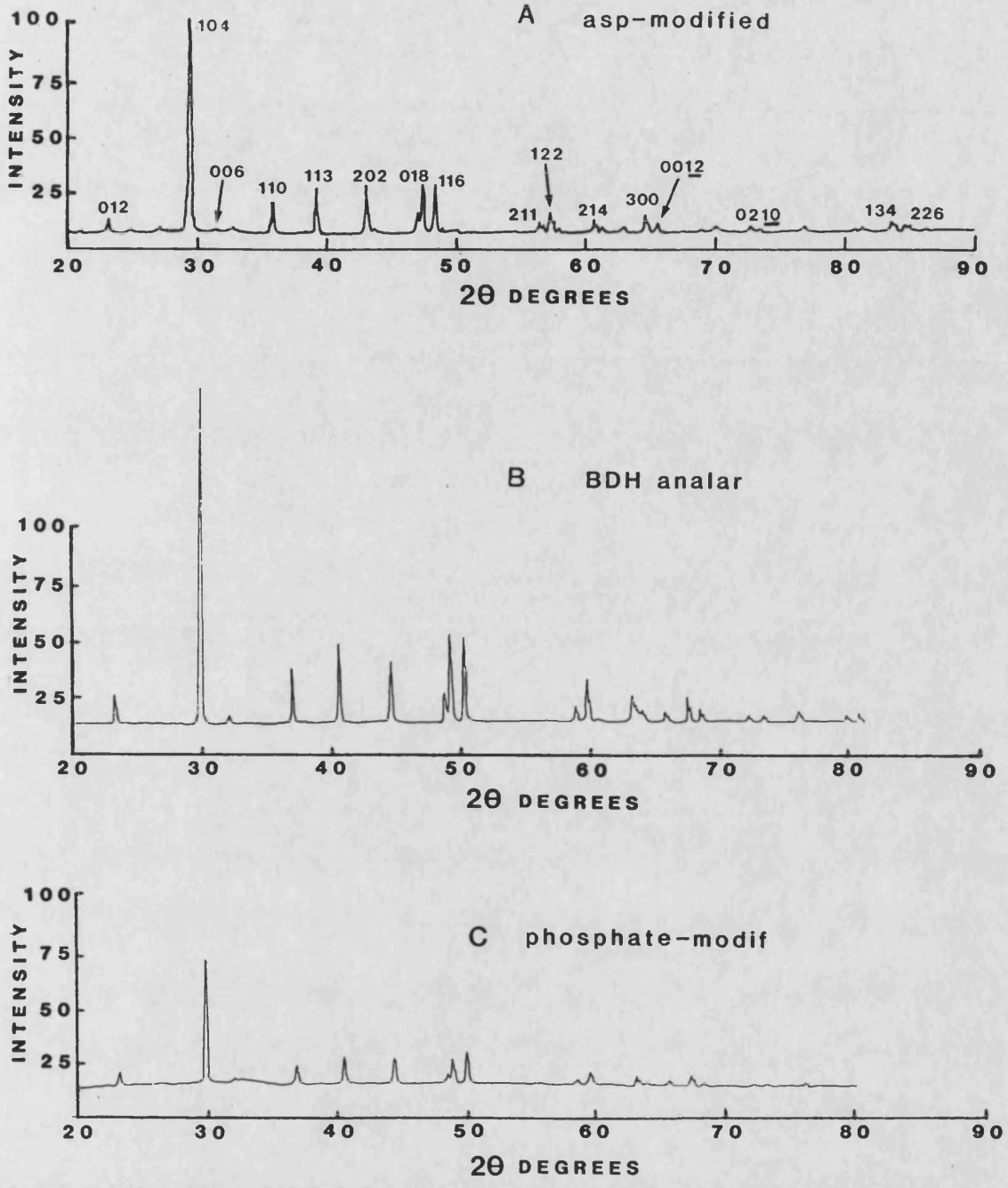

Fig. 4.27 *High resolution X-ray diffractograms of surface crystals grown in the presence of aspartate at 3:1 and phosphate at 10:1 compared to data for pure calcite.*

JCPDS hkl	D spacings (Å)			
	BDH analar	Control	Aspartate-modified	Phosphate-modified
(104)	3.0361	3.0343	3.0426	3.0417
(006)	2.8445	2.8420	2.8519	2.8483
(110)	2.4953	2.4949	2.4992	2.4986
(300)	1.4416	1.4413	1.4430	1.4421

Table 4.6 *High resolution XRD results; d spacings calculated for selected planes using λ=1.5418 Å.*

Raman Spectroscopy

A standard calcite Raman spectrum (5 peaks predicted by Group theory for carbonate with point symmetry D_{3d}) was observed for the aspartate-modified crystals. Peaks were recorded at 1085 (ν_1) and 710 (ν_4) due to internal vibrations of the carbonates, and at 278, 150, 90 cm^{-1} assigned to external (lattice) vibrations (fig. 4.28c cf. a, b). No perceptible shift or disturbance in the lattice vibrational modes of calcite was detected implying a complete retention of structural integrity.

Spatially-Resolved Elemental Analysis

Spectra for the analysis of phosphate-modified crystals at 10:1 are shown in fig. 4.29. Ca, C, O, and P was detected indicating the adsorption of phosphate on all faces analysed. Peaks for the counter ion, Na, were not present ruling out the possibility of phosphate present as a drying artefact. However, no significant increase in the P signal was observed on the $\{4\bar{4}01\}$ which may have been due to the lack of sensitivity in the instrument.

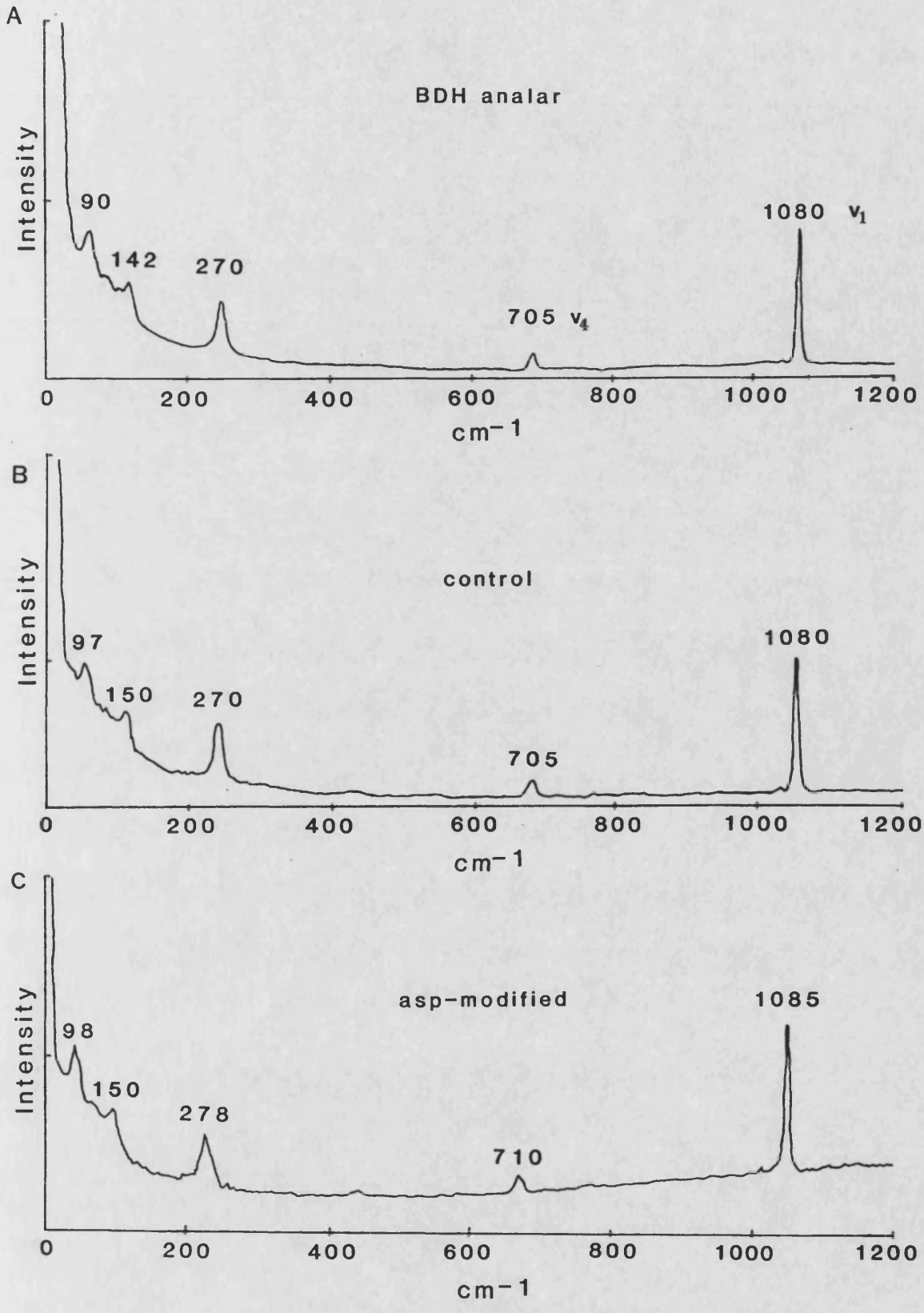

Fig. 4.28 *Raman spectra of aspartate-modified surface crystals compared to those from the control and a pure calcite sample.*

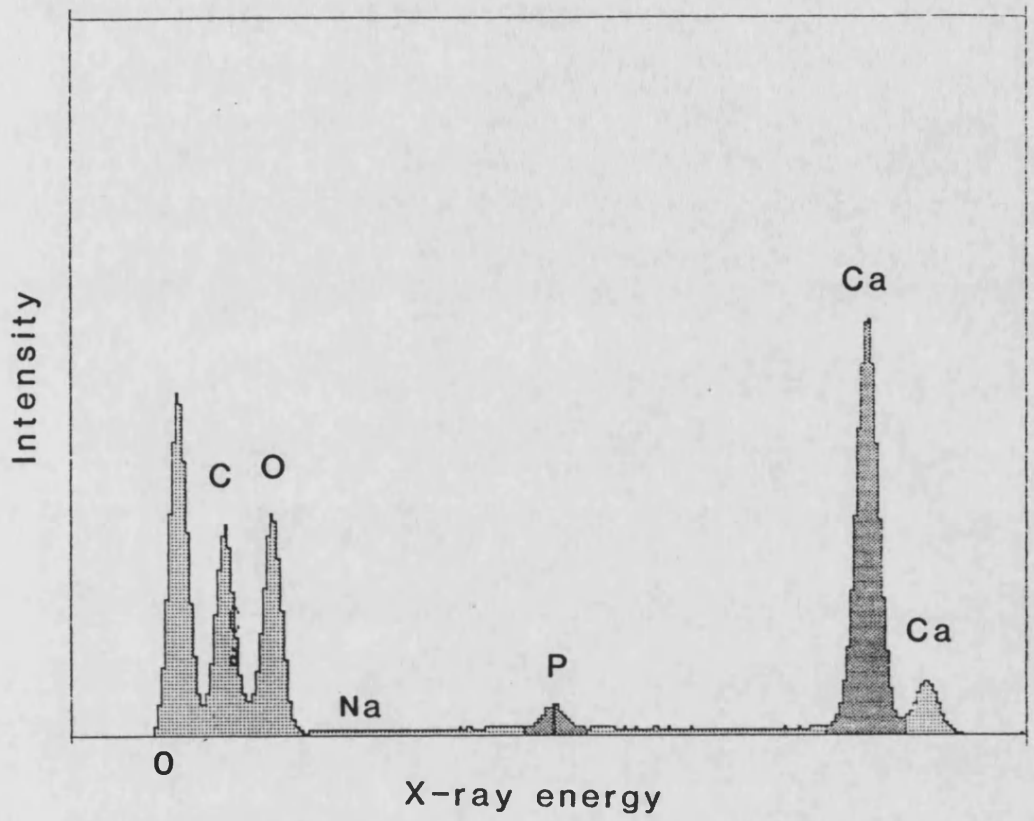

Fig. 4.29 *EDXA spectra taken from a broad area of orthophosphate-modified crystals grown at a calcium/additive ratio of 10:1.*

4.4 DISCUSSION

Crystal-Additive Interactions

The pK_a values of the additives used indicated that some were partially and many fully ionized under the experimental conditions studied (pH 6). The surface charge of calcite has been the subject of many investigations. Previous estimates of the isoelectric point have varied widely from 5.4-10.8. However, recent studies have determined IEP = 10.4 (Giannimaras and Koutsoukos 1987) and identified Ca^{2+} and CO_3^{2-} only as the major ions responsible for the electrical state on the $\{10\bar{1}4\}$ crystal face over the pH range 7-12 (Thompson and Pownall 1989). Thus, at pH 6, surface CO_3^{2-} ions would be protonated to HCO_3^- and H_2CO_3 thus leading to an overall positive charge on formally neutral faces. This agrees with reports that calcite preferentially adsorbs anionic organic acids such as aspartic and stearic from sea water (pH 8) (Suess 1970, Carter 1978, Mitterer and Cunningham 1985). It was therefore concluded that the additive anions would be readily attracted to surface Ca^{2+}. Also, it could be assumed that the bonds formed between Ca^{2+} and ligand oxygens were highly electrostatic with essentially no covalent character.

Malonate

Malonic acid was typical of most additives in that, as the concentration was varied, it showed a definite window in which morphological effects were noticed. An upper limit was reached when complete inhibition of crystallization occurred (with other substances, this was mitigated by their solubility). The lower end of the window was defined when just enough molecules were present in order to discern a morphological effect. These limits are defined by the power of the anion to complex free calcium and its ability to compete with carbonate ions for surface sites. Although these effects were found to be dose-dependent, a single mechanism of interaction was evident occurring at definite sites ie faces parallel to the *c* axis. At high Ca/malonate ratios, there were few sites covered and hence little expression of

the interacting faces. However, at low ratios sufficient molecules were present to compete with carbonate ions and well-developed faces were produced.

The results with malonic acid reproduced those of Sanderson (1988). Though calcium to additive ratios were not used in his work, at concentrations similar to his (assuming comparable dissolved calcium), spindle-shaped calcite were synthesized. The optimum conditions for their formation was when calcium was in slight excess compared with malonate ie Ca/malonate ratios = 2:1-5:1. Thus, a fairly high concentration of additive was required.

With regard to the mechanism of habit modification, malonate was clearly very effective at inhibiting growth perpendicular to the *c* axis particularly at low Ca/additive ratios. Thus, there was a selective interaction with faces in the [0001] zone which was pseudo-specific as no single set of symmetry-related forms were expressed ie $\{1\bar{1}00\}$ or $\{11\bar{2}0\}$ prisms. A consideration of the structures of such faces and the coordination chemistry of malonate is therefore appropriate to the understanding of this interaction. Computer-generated cell projections drawn by *PLUTO* enable the surface structure and stereochemistry to be clearly visualized (figs. 4.30 and 4.31). It can thus be seen that all prismatic faces of calcite have a common stereochemical property concerning the planar carbonate anions which protrude at 90° to the surface. This is also essentially the case with some steep rhombohedra such as $\{44\bar{0}1\}$ (protruding at 86.4°) whereas carbonates on other important forms extend outwards at more acute angles $\{01\bar{1}2\}$ (63.8°) $\{10\bar{1}4\}$ (45.4°). The growth of prisms and steep rhombs will thus require the insertion of carbonate ions perpendicular to the face in a planar, bidentate fashion. This may be contrasted against adsorption on the (0001) which will proceed via tridentate binding of the anion parallel to the face (fig. 4.32).

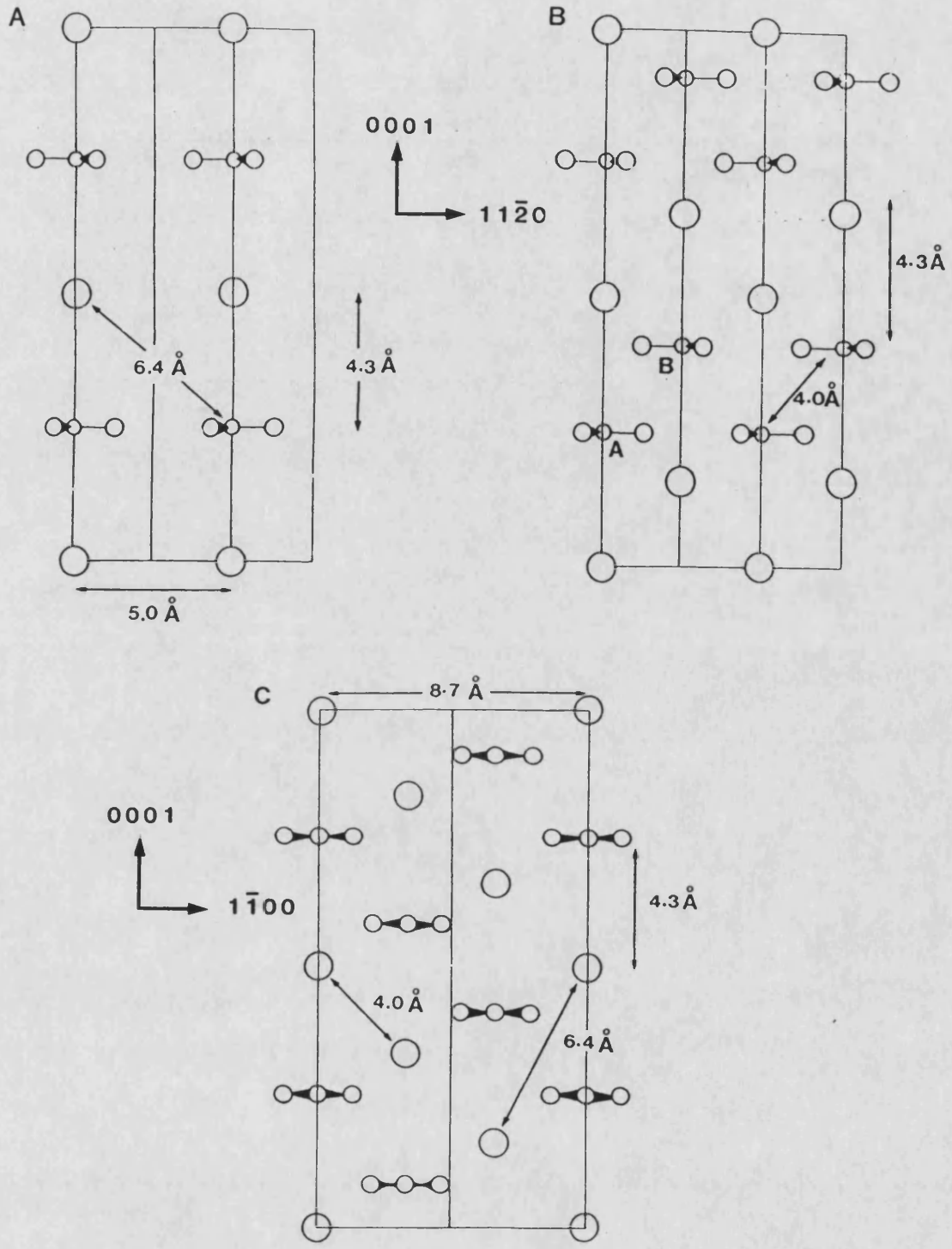

Fig. 4.30 *Unit cell projections for calcite: (a) prismatic 1st order m {1$\bar{1}$00} and steep rhombohedron ρ {40$\bar{4}$1}, coplanar atoms only (b) the same faces but with additional non-coplanar atoms from plane above (c) prismatic 2nd order a {11$\bar{2}$0}. All surfaces are neutral.*

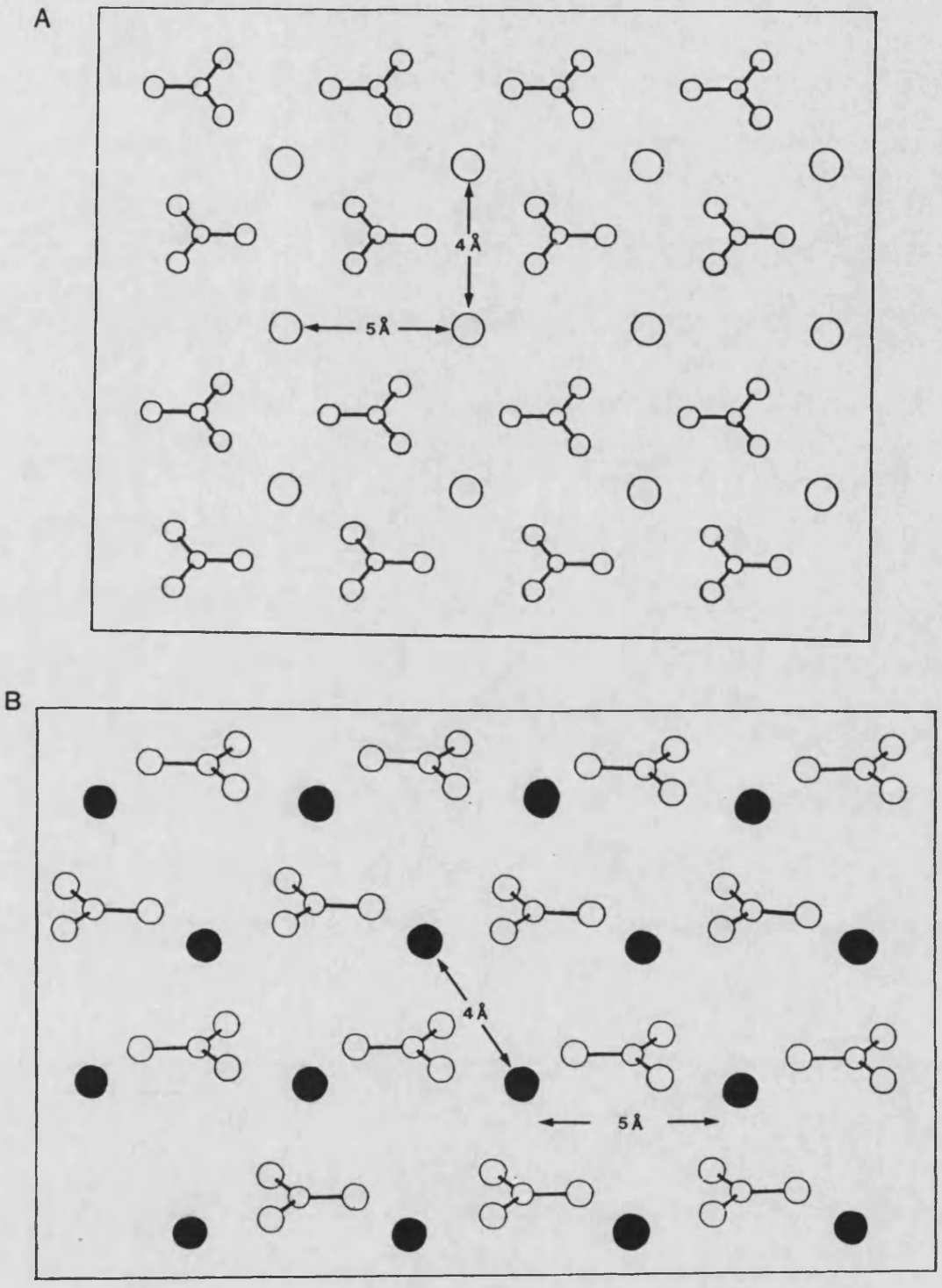

Fig. 4.31 *Unrelaxed surface structures of two calcite rhombohedra: (a) the r {10$\bar{1}$4}; coplanar atoms only and (b) the f {01$\bar{1}$2}; the black circles (Ca) are below the carbonates and not strictly coplanar.*

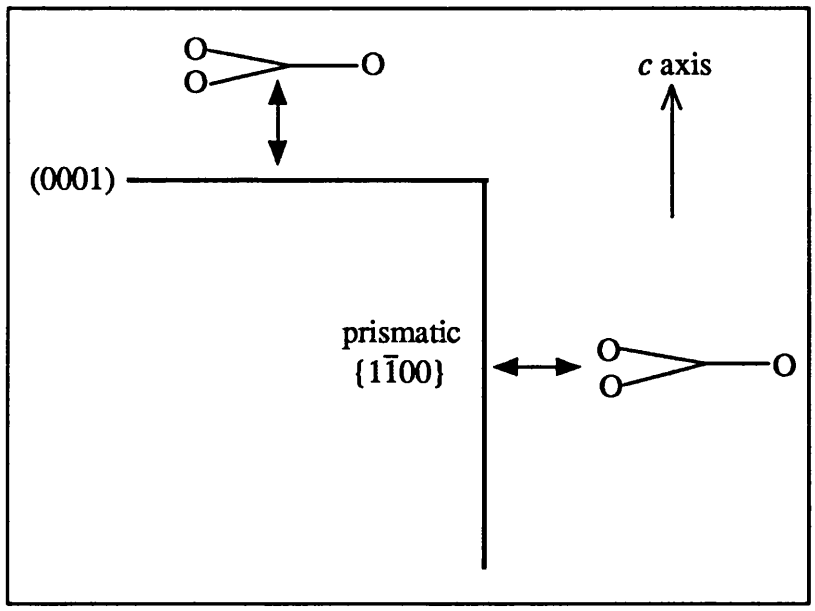

Fig. 4.32 *Comparison of binding modes for carbonate anions on the basal (tridentate) and prismatic (bidentate) faces.*

The primary binding modes of calcium to carboxylate groups have been studied in detail (Einspahr and Bugg 1981). For a single functional group, both unidentate and bidentate interactions are possible (fig. 4.33a). Curry *et al* (1985) further identified the "malonate" mode in the crystal structure of the calcium complex of methylmalonic acid. This involves the chelation of calcium by oxygens from both carboxylate moieties. Albertsson *et al* (1978) have also reported such a binding mode for calcium malonate dihydrate (fig. 4.33b).

The distance between carboxylate groups in malonate is ca. 4 Å which happens to be close to that for adjacent coplanar layers of carbonate sites in the {11$\bar{2}$0} and adjacent, non-coplanar sites on the {1$\bar{1}$00}. It is therefore plausible that this molecule can chelate surface calciums roughly mimicking the insertion of lattice anions. The results with monofunctional carboxylates (acetate; Sanderson) and those in which chelation is not possible (fumarate), also suggest that dual binding is important for the interaction to affect bulk morphology. However, as it is pseudo-specific, there probably exists some degree of mismatch between acid and

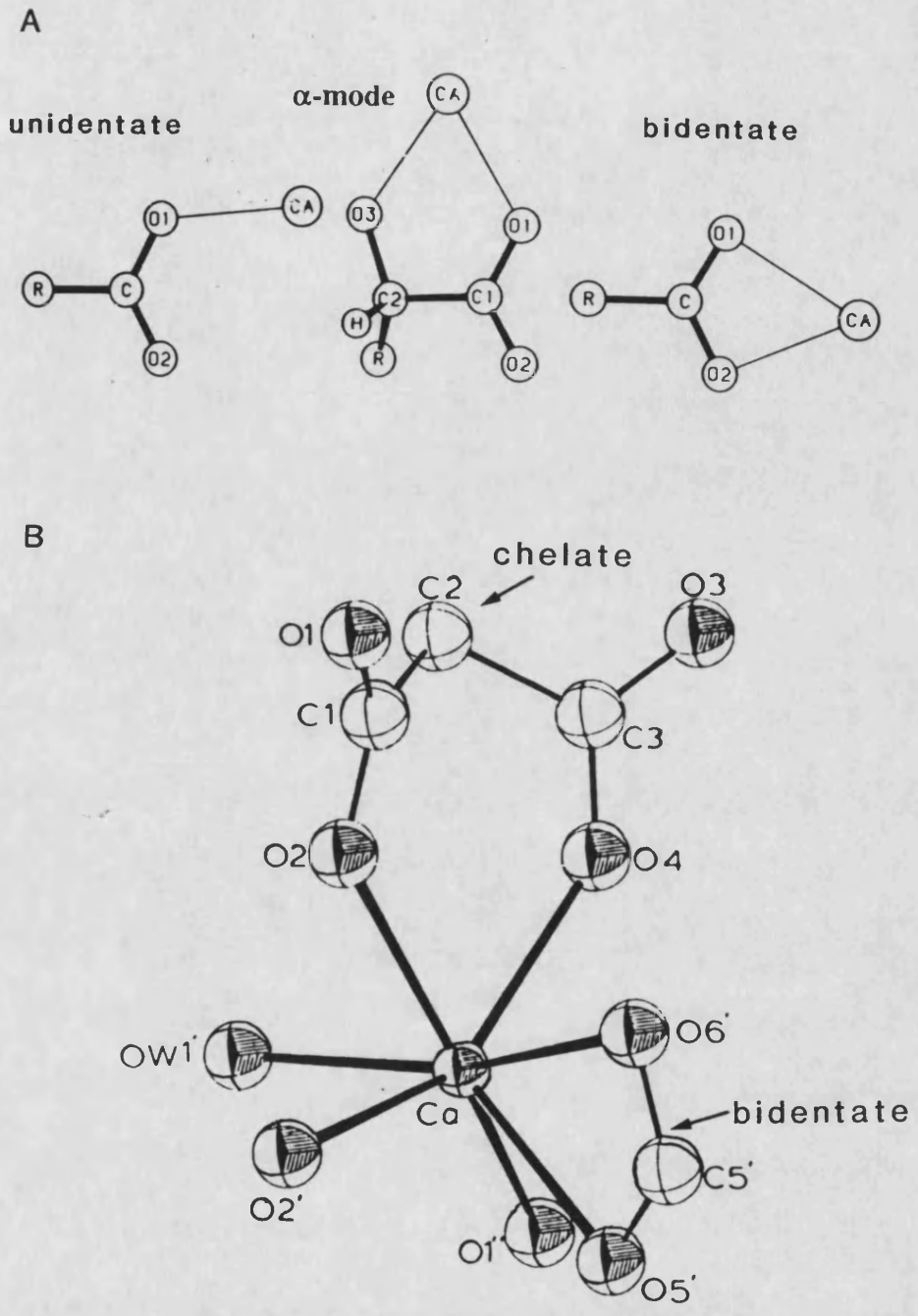

Fig. 4.33 *(a) Primary binding modes of single carboxylate anions to calcium (redrawn from Einspahr and Bugg 1981) and (b) chelate mode of interaction as illustrated in the crystal structure of the hydrated calcium complex of α-methylmalonate (redrawn from Curry et al 1985).*

lattice. Interestingly, malonate and other dibasic acids with a similar spacing between their anionic groups, all inhibit the enzyme succinate dehydrogenase which catalyses the removal of methylene hydrogens from succinate without themselves being affected. It has therefore been postulated that the catalytic site of the enzyme has two suitably spaced cationic regions to attract the substrate (Lehninger 1970). This is further evidence that such dicarboxylates interact without difficulty using both functional groups in a fully outstretched conformation of a very definite spacing.

Adsorption on to other surfaces, such as the $\{10\bar{1}4\}$, was demonstrably less favourable probably because the face is essentially tridentate and so the molecule fails to satisfy its full bonding requirements (fig. 4.31a). Similarly, the already unstable, dipolar basal planes (0001), require tridentate ligands for significant stabilization (figs. 4.15 and 1.11 in chapter 1).

The projecting hydrophobic, carbon backbone of a dicarboxylate held in a bridging conformation on the surface would tend to interfere with the adsorption, surface diffusion or integration of lattice ions and thus impede further growth. This is a kinetic effect because the activation energy barriers for these steps would then be significantly raised. The rate determining step in calcite growth is usually considered to be the dehydration of the lattice ions or their incorporation into active sites (Reddy 1981). Thus, the growth rate of prismatic-type faces was reduced compared to the relatively unhindered $\{10\bar{1}4\}$ and $\{0001\}$ resulting in the elongation along the *c* axis. One explanation of this fact maybe that the surface coverage on the prisms is greater providing a more effective screen to lattice ions. Another possibility is that the additive molecules are simply held less firmly on $\{10\bar{1}4\}$ (because the full bonding requirements are not met) and therefore are displaced more easily by incoming lattice ions.

Adsorbed molecules will also change the surface free energy σ_{hkl} of the faces on which they become attached. In this way, the appearance of new prisms might be explained by a lowering of $\sigma_{1\bar{1}00}$ with respect to $\sigma_{10\bar{1}4}$. However, even if the additive were to sit precisely in lattice sites then, at best, the surface free energy would remain unchanged. Any small strain or mismatch though, would probably increase coulombic repulsions and so raise rather than lower σ. The effects of adsorbed additives on crystal habit are therefore better explained by kinetic processes.

An alternative explanation of the morphological effects of malonate may be ascribed to changes in the Ca^{2+}/CO_3^{2-} ratio brought on by appreciable complexation of calcium by the additive. At low Ca/malonate ratios, the acid is present in significant quantities and will inevitably remove free calcium from solution. Kirov *et al* (1972) reported very similar morphological changes of calcite by varying the Ca^{2+}/CO_3^{2-} ratio in aqueous counter-diffusion experiments. Although, prismatic type habits were produced under conditions of excess rather than insufficient calcium. Heijnen (1985) also synthesized spindle morphologies at high Ca^{2+}/CO_3^{2-} using silica gel. The curved faces were more well-defined being $\{01\bar{1}2\}$ and $\{11\bar{2}0\}$. Prieto *et al* (1981) grew the same crystals in gels concluding that diffusion conditions were responsible for the simultaneous appearance of both flat and curved faces $\{1\bar{1}00\}$ and $\{11\bar{2}.12\}$. However, the later work of García-Ruiz *et al* (1985) highlighted the importance of a silicate membrane which forms around spindle-shaped crystals in silica gel. At pH 9-10, the membrane contains sufficient amounts of $HSiO_3^-$ and SiO_3^{2-} which could interact with the calcite surfaces in a similar way to the carboxylate additives.

Chain length

Morphological changes for the saturated acids indeed became less marked as the separation of the carboxylate groups increased. The higher homologues, looked at for the first time in this thesis, reflected this trend. There was no evidence for any

double binding of the longer chain molecules over several carbonate layers. For a molecule to bridge two layers, it must have its carboxylate groups spaced at least 5.7 Å apart. Glutarate and the higher homologues have spacings fulfilling this requirement but empirically no interaction of this sort was identified. Calcium has a more or less constant affinity for the acids shown when in a complex (table 4.1) and so this was not a factor. Increasing the carbon chain caused two properties to change in magnitude: (a) the double negative charge was increasingly spread over the molecule and so the spatial charge density was dramatically reduced; (b) the flexibility or conformational entropy in the chain was increased which also serves to dissipate the charge. Thus, malonate with the highest spatial charge density and least flexibilty had the most powerful electrostatic interaction with the crystal lattice. Conversely, glutarate and longer chain acids had more dispersed charge densities and greater numbers of possible conformations; these two factors combined to make binding with both carboxylates less favourable.

Chain Rigidity (Unsaturation)

The results with maleate and fumarate suggest that cooperative binding of both carboxylates is necessary for significant change in crystal habit. This is because the C=C double bond confers rigidity on the molecule and, whereas the *cis* isomer (maleate) can still bind with both carboxylates, the *trans* isomer (fumarate) can only interact with one (see fig. 4.35).

The maleate dianion is similar to malonate in that it has approximately the same spacing between its carboxylate groups (4 Å). The main difference is the rigidity of the molecular backbone which is greater for maleate. As was previously mentioned, the results with the long chain aliphatic dicarboxylates pointed to molecular flexibility as a source of loss of morphological interaction. However, elongation, which is taken as a measure of this interaction, was more marked for malonate than for maleate. It thus appears that a high spatial charge density is not the only factor

and that a small amount of flexibility is advantageous. On answer maybe that stereochemical interactions are enhanced. For example, by rotation about the middle carbon centre, malonate can subtly adapt its stereochemistry in order to strengthen the electrostatic interaction between its negative charge and surface calcium ions. This option is ostensibly not open to the maleate molecule.

α-Amino Functionalization

Results showed that an α-amino functionalization of succinate, to give aspartate, led to improvements in potency and selectivity. It is geometrically possible for aspartate to span three layers of carbonate sites on the $\{1\bar{1}00\}$ face in a chelate conformation. It is also stereochemically feasible for the cationic amino group (fully ionized at pH 6) to replace a Ca^{2+} site in the surface. Thus, one simple explanation of the observed specificity of this additive might be due this extra binding site on the molecule. This would then allow greater contact between the adsorbate and the crystal face and perhaps assist an improved electrostatic attraction.

Interestingly, the corresponding functionalization of glutarate, to give glutamate, did not show comparable effects. Thus, the increased charge separation tended to offset the amino binding effect which suggested that the dominant binding sites on amino acid molecules were the carboxylate anionic groups. The cationic site was then available to reinforce this principal mode of interaction.

α-Amino, ω-Carboxylate Functionalization

However, a γ-COO^- functionalization of glutamate, to give γ-carboxyglutamate conferred a greater spatial charge density and number of molecular binding sites. As the results demonstrate, this led to an even more potent and specific additive capable of expressing well-defined $\{1\bar{1}00\}$ or $\{4\bar{4}01\}$ faces. Fig. 4.34 illustrates a proposed binding mode on the first order prismatic face. NB/ the $\{1\bar{1}00\}$ is essentially structurally identical to the $\{4\bar{4}01\}$.

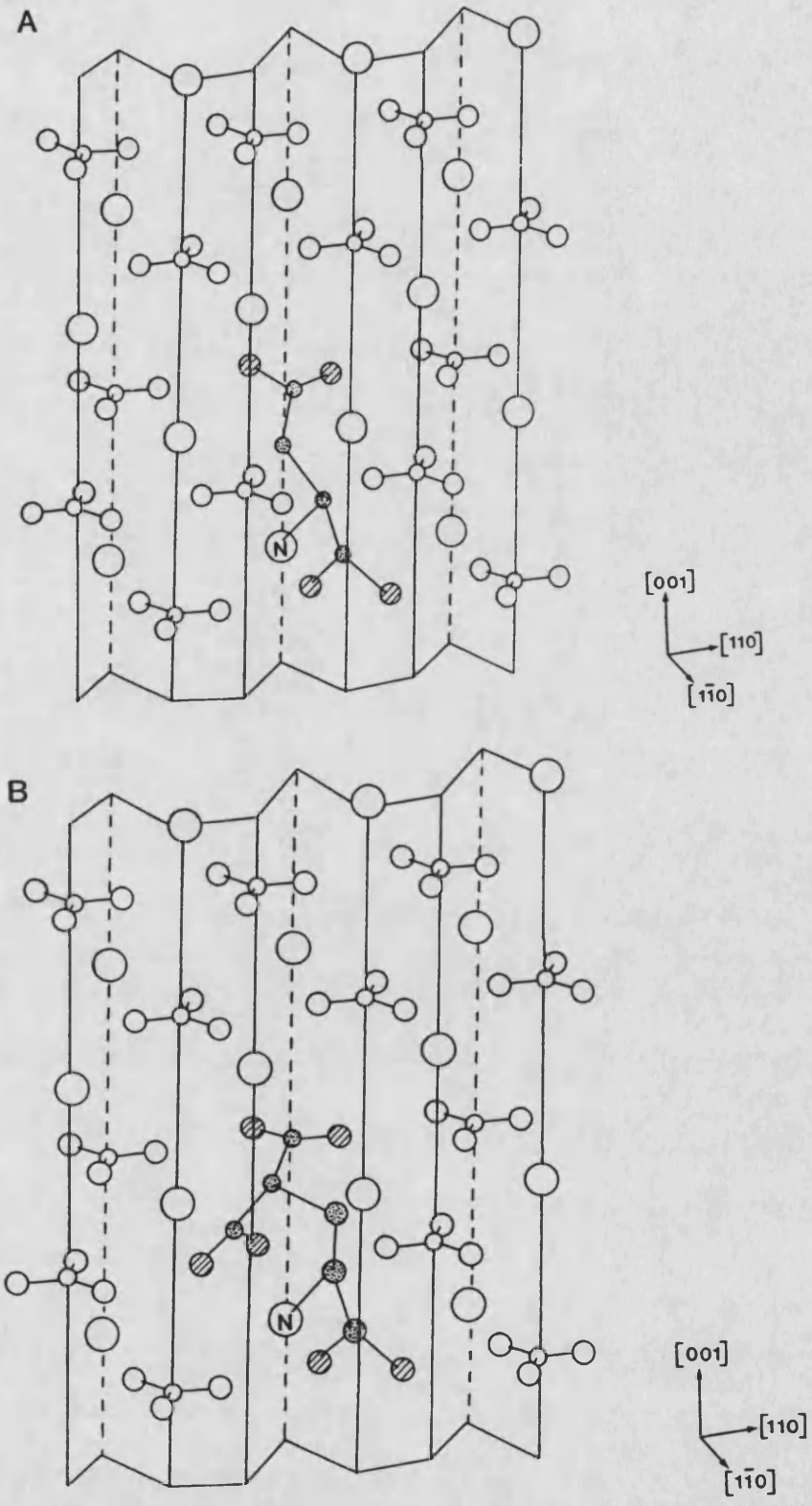

Fig. 4.34 *Perspective drawings of possible binding modes of aspartate and γ-carboxyglutamate molecules on the (1$\bar{1}$00) face of calcite. Large open circles = Ca, hatched small circles = carboxylate oxygens, small black circles = carbon atoms of additive molecules. Hydrogens not shown for clarity.*

The question remains as to why the set of first order prisms {1$\bar{1}$00} are selected over the similar second order set {11$\bar{2}$0}. Structures of both faces, drawn by *PLUTO*, are shown in fig. 4.30. For non-coplanar {1$\bar{1}$00}, calciums run in rows parallel to, and at right angles to, the *c* axis. The carbonate oxygens project at 60° to the face. In contrast, coplanar, second order surfaces are more densely packed. Calciums are arranged parallel and at 45° to the *c* axis. The carbonates, equivalent in each row, now point directly out from the face, alternating single and double oxygens as the layers are crossed. The reason why {1$\bar{1}$00} faces are favoured over {11$\bar{2}$0} is due to this difference in stereochemistry. Because of the arrangement of all anionic sites in all layers on the {1$\bar{1}$00}, carboxylates can bind with both oxygens thus closely mimicking carbonates themselves. On the other hand, successive anionic sites on the {11$\bar{2}$0} are not equivalent meaning that, for dicarboxylate binding, one COO^- group will only bind with a single oxygen. This will be electrostatically less favourable. Sites in every second layer, however, are equivalent but the cationic sites are not positioned within reach of the amino group. An alternative, simpler explanation maybe that the first order is intrinsically more stable than the second order and so are more predisposed to stabilization by additives. This is, in fact, borne out by recent atomistic calculations (Titiloye 1991, personal communications; see also table 1.4 in chapter 1).

Phosphate

Phosphate is a tetrahedral molecule and therefore has the option of binding calcium in either a bidentate (point symmetry then lowered to C_{2v}) or a tridentate (lowered to C_{3v}) fashion. The morphological results strongly implied that the bidentate mode of interaction was favoured. As already mentioned, the {44$\bar{1}$0} faces are effectively identical in their surface characteristics to {1$\bar{1}$00}. The vibrational spectra of the adsorbed additives were less convincing indicating that bi- or tridentate interactions could be occurring. The experiments also demonstrated the phenomenal potency of

the molecule, compared even to γ-carboxyglutamate. The speciation at pH 6 is $H_2PO_4^-$ (95%) and HPO_4^{2-} (5%) which is surprising as the predominant monoanion has a low affinity for calcium (log K_{stab} = 1.1) and would thus be expected to interact weakly with calcite. Perhaps, this points to chemical processes such as ligand (proton) exchange occurring at the crystal/solution interface raising the concentration of the dianion in this vicinity. A lack of hydrophobic moiety may explain the aggregating effect that phosphate had on calcite $CaCO_3$ crystals. A bidentate-bound molecule will direct P-OH bonds out into solution thereby potentially attracting further crystal nuclei.

The same trend of decreasing potency with increasingly hydrophobic moiety was noticed for the phosphoesters (butyl-phosphate, phenyl-phosphate and napthyl-phosphate) and the phosphonates (methyl-phosphonate and phenyl phosphonate) as was for the dicarboxylates. This was also a consequence of the diminishing spatial charge density on these molecules. The more active phosphate group allowed more sterically bulky substituents to be used which had the effect of dramatically reducing the crystal aggregation.

ω-Phosphonate Functionalization

The huge gain in potency observed for the diphosphonates re-emphasized that the primary mode of interaction for these additives was via the highly active, anionic functional group. Their strong aggregating power was presumably due to the second phosphonate moiety which, on adsorption of one end of the molecule, would protrude into solution. This would especially be the case if a large degree of mismatch occurred between phosphonate and carbonate sites on the surface.

Phenyl Phosphonate

All the additives studied in this chapter expressed prismatic or steep rhombohedral faces to varying extents. The one striking exception was phenyl phosphonic acid at

10:1 and 1:1 which was able to stabilize the negative rhombohedral $\{01\bar{1}2\}$ face. The unrelaxed surface structure is shown in fig. 4.31b. According to the way, in which the plane is defined, $\{01\bar{1}2\}$ may be classed as neutral or unicharged (dipolar). In any case, cations or anions in each plane are arranged in a pseudo-hexagonal pattern and carbonates are oriented at 26.2° and 63.8° to the face. The phenyl phosphonate molecule consists of a planar, aromatic ring directly attached to an "tripod" of oxygens forming the active phosphonate group. Tridentate binding would therefore be expected to take place because this allows the bulky ring to be at a maximum distance from the face. Conversely, bidentate interactions will force the hydrophobic moiety close to the surface. Thus, the ring places steric constraints on the electrostatic interaction between phosphonate and surface calciums. In the case of phenyl phosphate, however, rotation about the C-O-P linkage enables the aromatic ring to be at a maximum distance from the face for a bidentate mode of interaction. A tridentate additive might be predicted to express the (0001) or even $\{01\bar{1}8\}$ but it appears that these faces are too unstable. $\{01\bar{1}2\}$ are intermediate in character between bi- and tridentate and are exhibited probably because they are intrinsically much more stable.

Sulphate and Nitrate

Nitrate anions have the same stereochemistry as carbonate and so their presence in the crystallizing solution sets up a competition process for lattice sites. The results demonstrated the importance of the magnitude of the electrostatic charge in this competition as nitrate, with its single charge, was ineffective when compared to the doubly charged carbonate. The tetrahedral SO_4^{2-} has a similar spatial charge density as phosphate but was much less potent. This is because the sulphate anion is a weaker base and so the partial negative charge on oxygens in S-O is less that for P-O (sulphur has the same electronegativity as carbon). Thus, potency is determined not by the overall charge density but, more specifically, by the density on the ligand oxygens. The different affinities for Ca^{2+} is reflected in the log stability constants

for these species: ($CaCO_3^o$) = 3.2; ($CaHPO_4^o$) = 2.7; ($CaSO_4^o$) = 2.3; ($CaNO_3^+$) = 0.68). The very pure preparation of calcite in the presence of high concentrations of nitrate was almost certainly due to the significantly increased ionic strength of the crystallizing solution. This has the effect of enlarging the ionic atmosphere of lattice ions which screens their charges more effectively and so slows their aggregation during nucleation. In this way, the most thermodynamically stable phase is favoured.

Crystal-Additive Association

Results from the analysis of aspartate, malonate and phosphate-modified crystals confirmed that the additive was associated with the inorganic phase even after thorough washing in dilute acids. The evidence pointed to the molecules being segregated at the surface rather than incorporated in the structure. Some workers, studying metastable $CaCl_2/NaHCO_3$ solution mixtures, have concluded that metaphosphate is adsorbed (Buehrer and Reitemeier 1940) whereas others (Brooks *et al* 1950/51, Ishikawa and Ichikuni 1981) have provided evidence for phosphate or metaphosphate occlusion. Brooks *et al* published XRD data showing that the unit cell had contracted by *ca.* 1%. Leaching experiments by Ishikawa and Ichikuni pointed to a homogeneous distribution of PO_4^{3-} in the calcite lattice. In the case of malonate and aspartate, it is very unlikely that such molecules could occupy lattice sites without severe disruption of the calcite structure. There is also the possibility that acids may be adsorbed onto perfect crystal domains (at mosaic boundaries) and thus incorporated, in a similar way to the postulated intracrystalline proteins in sea urchin biominerals (Berman *et al* 1990). However, no evidence was found to support this possibility.

General Conclusions

The work in this chapter demonstrated that specific morphological changes can be produced by low molecular weight anionic species in solution. It has also shown that the structural approach involving the concept of molecular recognition can be used

to adequately explain these changes. The study focused on some of the crucial molecular properties of the additives that appeared to be responsible for particular effects on bulk morphology.

Effects such as the potency or activity of the additive were dependent primarily on the electrostatic charge density present on the ligand atoms (oxygens); small, highly charged, strongly basic molecules being the most effective. This seemed to be enhanced by a balance of rigidity in the molecular backbone, so as not to dissipate the charge density, and enough conformational freedom to enable improved stereochemical interactions. An additional factor was hydrophobicity which, on the whole, tended to decrease the habit-modifying effect due to the dissipation of charge density. Finally, chemical processes such as ligand (proton) exchange reactions were also implicated in reinforcing the potency.

Another important effect was the specificity or selectivity of the interaction. Empirically, this was mainly governed by the stereochemistry of the additive active group. Bidentate ligands preferentially bound to bidentate faces although, as the tridentate ligand-surface pairs showed, this was probably also dependent on the inherent stability of the effected face. The prime stereochemical interaction then appeared to be augmented by molecules having higher numbers of commensurate binding sites (charge centres) with which to stabilize the face. The term commensurate is important as these sites must be complementary in their geometries, electrostatic charge and stereochemical requirements (fig. 4.35).

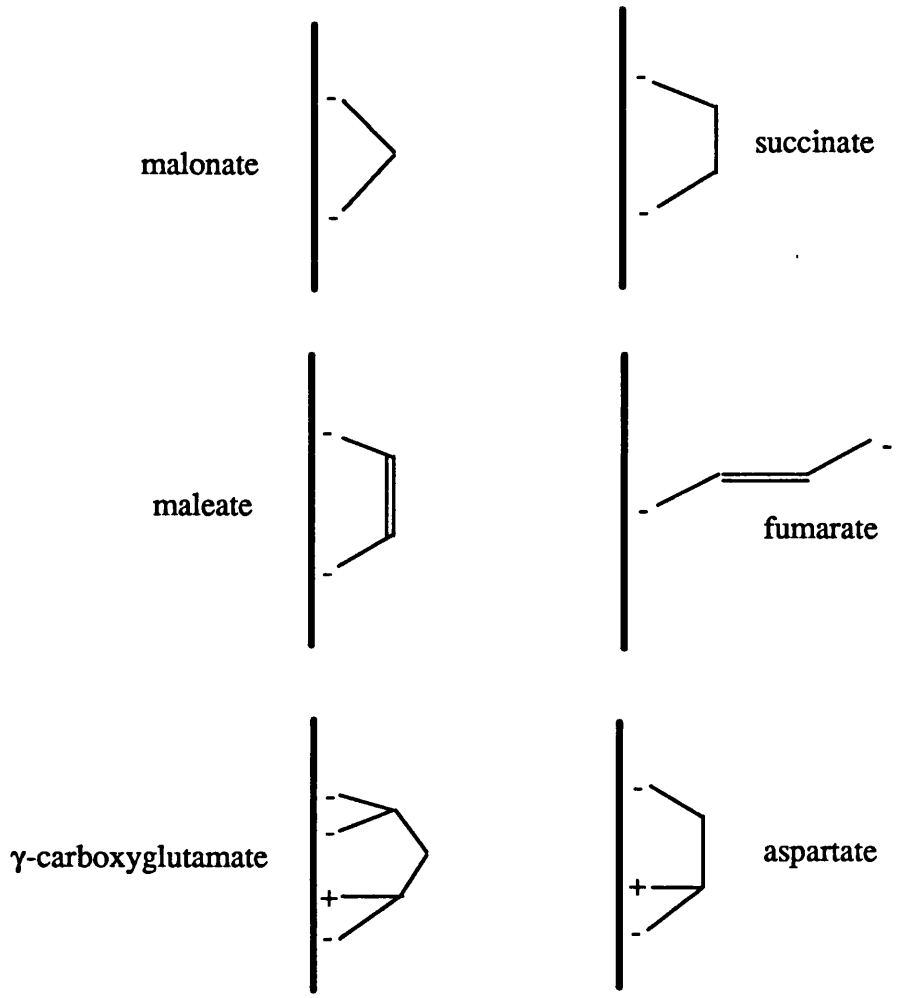

Fig. 4.35 *Schematic illustration of envisaged binding modes of some dicarboxylates*

Relevance to Biomineralization

The findings in this chapter also has implications for the understanding of biomineralization. It can be concluded that carboxylate, phosphoester and ester sulphate groups on macromolecules could be responsible for controlling the morphology of biogenic calcite. As there are substantial differences in the potency of these species, the spacing of such functional groups on proteins may be critical ie for carboxylates, cooperative interactions between neighbouring anions is required for the effect to be significant.

Spindle-shaped calcite crystals, very similar to those precipitated in the presence of malonate, have been observed in the inner-ears of mammals and reptiles (Ross and Pote 1984). These minute biominerals, known as otoconia, are linked by membranes and add mass to sensory hairs which act as gravity receptors. The otoconia are closely associated with proteins containing high levels of acidic amino acids. Interestingly, preliminary studies have detected γ-carboxyglutamic acid in this organic material. When linked to other residues in the protein, γ-carboxyglutamate will have a malonate moiety as a side chain disposed away from the peptide backbone. Hence, the specific morphology of otoconia crystals could be attributed to interactions between such carboxyl-functionalized macromolecules and prismatic or steep rhombohedral faces of calcite.

Acknowledgements

All the work on phosphorus-containing compounds was carried out in association with Peter Oliver (BSc Project Report, 1990, School of Chemistry, University of Bath). The study of aspartic acid was also part of a collaboration with Eliseo J. Aso-Samper (PhD thesis 1991, chapter 2, Department of Geology, University of Zaragoza, Spain).

4.5 REFERENCES

Albertsson, J., Oskarsson, Å., Svensson, C. (1978), *An X-ray and Neutron Study of a Gel-Grown Phase of Calcium Malonate Dihydrate*, Acta Cryst., **B34**, 2737-2743.

Anthony, G.M. (1990), *In Situ Investigations of Adsorption on Iron Oxide in Aqueous Solution*, NACE (Houston, USA) Proceedings, "Corrosion 90", April 23-27, paper 97.

Berman, A., Addadi, L., Kvick, Å., Leiserowitz, L., Nelson, M., Weiner, S. (1990), *Intercalation of Sea Urchin Proteins in Calcite: Study of a Crystalline Composite Material*, Science, 2 November, **250**, 664-667.

Berner, R.A. (1975), *The Role of Mg in the Crystal Growth of Calcite and Aragonite from Seawater*, Geochim. Cosmochim. Acta, **39**, 489-504.

Berner, R.A., Westrich, J.T., Graber, R., Smith, J., Marttens, C.S. (1978), *Inhibition of Aragonite Precipitation from Supersaturated Seawater. A Laboratory and Field Study*, Am. J. Sci., **276**, 713-730.

Biscoff, J.L. (1968), *Kinetics of Calcite Nucleation: Magnesium Ion Inhibition and Ionic Strength Catalysis*, J. Geophys. Res., **73**, 3315-3322.

Brooks, R., Clark, L.M., Thurston, E.F. (1950/51), *Calcium Carbonate and its Hydrates*, Phil. Trans. Roy. Soc. (London), **A243**, 145-167.

Buehrer, T.F., Reitemeier, R.F. (1940), *The Inhibiting Action of Minute Amounts of Sodium Hexametaphosphate on the Precipitation of Calcium Carbonate from Ammoniacal Solution II*, J. Chem. Phys. **44**, 552-574.

Cailleau, P., Dragone. D., Esclamadon, J., Girou, A., Humbert, L., Roques, H., Sellier, E. (1980), *Cristallisation en Milieu Libre et en milieu Poreux, Dissolution et Pression-Dissolution: Principaux Resultats Experimentaux,* in Cristallisation, Deformation, Dissolution des Carbonates, pp 81-109, Bordeaux: Institut de Géodynamique de l'Université de Bordeaux III.

Carter, P.W. (1978), *Adsorption of Amino Acid-Containing Organic Matter by Calcite and Quartz*, Geochim. Cosmochim. Acta, **42**, 1239-1242.

Compton, R.G., Pritchard, K.L., Unwin, P.R., Grigg, G., Silvester, P., Lees, M., House, W.A. (1989), *The Effect of Carboxylic Acids on the Dissolution of Calcite in Aqueous Solution*, J. Chem. Soc. Faraday Trans. 1, **85(12)**, 4335-4366

Curry, M.A., Eggleston, D.S., Hodgson, D.J. (1985), *Calcium and Magnesium Binding to γ-Carboxyglutamate and β-Carboxyaspartate Residues: Structures of Calcium and Magnesium Complexes of Methylmalonic acid*, J. Am. Chem. Soc., **107(26)**, 8234-8238.

Dana, E.S. (1932), *A Textbook of Mineralogy*, 4th ed., Ford, W.E. (Ed.), New York: John Wiley and Sons.

Einspahr, H., Bugg, C.E. (1981), *The Geometry of Calcium-Carboxylate Interactions in Crystalline Complexes*, Acta Cryst., **B37**, 1044-1052.

Folk, R.L. (1974), *The Natural History of Crystalline Calcium Carbonate: Effect of Magnesium Content and Salinity*, J. Sed. Petrology, **44**(1), 40-53

Folk, R.L. (1978), *A Chemical Model for Calcite Crystal Growth and Morphology Control, J. Sed. Petrology*, **48(1)**, 345-347.

Giannamaras, E.K., Koutsoukos, P.G. (1987), *The Crystallization of Calcite in the Presence of Orthophosphate*, J. Coll. Int. Sci., **116(2)**, 423-430.

García-Ruiz, J.M., Prieto, M., Amorós, J.L. (1979), *On the Influence of Diffusion in the Formation of Curved Faces in Crystals. II Experimental*, Estudios geol., **35**, 449-457.

García-Ruiz, J.M. (1985), *On the Formation of Induced Morphology Crystal Aggregates*, J. Cryst. Growth, **73**, 251-262.

García-Ruiz, J.M., Dominguez Bella, S. (1987), *Banding Structures in Induced Morphology Crystal Aggregates of Calcium Carbonate*, J. Mat. Sci., **22**, 3095-3102.

García-Ruiz, J.M., Dominguez Bella, S., Gomez de Salazar, J.M. (1988), *Morphogenetical and Textural Characterization of Calcite IMCA grown in Silica Gel at pH 10*, J. Sed. Petrology, ????

Hatch, G.B., Rice, O. (1939), *Surface Active Properties of Hexametaphosphate*, Ind. Eng. Chem., **31**, 51-57.

Heijnen, W.M.M. (1985), *The Morphology of Gel Grown Calcite*, N. Jb. Miner. Mh., **8**, 357-371.

Hirano, S., Kikuta, K. (1986), *Solubility and Hydrothermal Growth of Calcite Single Crystals in Nitrate Solution*, J. Cryst. Growth, **79**, 223-226.

Högfeldt, E. (1982), *Stability Constants of Metal-Ion Complexes, Part A: Inorganic Ligands*, London: Pergamon.

House, W.A. (1987), *Inhibition of Calcite Crystal Growth by Inorganic Phosphate*, J. Coll. Int. Sci., **119(2)**, 505-511.

Ishikawa, M., Ichikuni, M. (1981), *Coprecipitation of Phosphate with Calcite*, Geochem. Journal, **15**, 283-288.

Ichikuni, M. (1983), *Anionic Substitution in Calcium Carbonate*, Signf. Trace Elem. Solving Petrog. Probl. Controversies, Augustithis, S.S. (Ed.), 83-94.

Lahann, R.W. (1978), *A Chemical Model for Calcite Crystal Growth and Morphology Control*, J. Sed. Petrology, **48(1)**, 337-344.

Lehninger, A.L. (1970), *Biochemistry*, pp 160-161, New York: Worth Publishers Inc.

Kitano, Y. (1962), *The Behaviour of Various Ions in the Separation of Calcium Carbonate from Bicarbonate Solution*, Bull. Chem. Soc. Jap., **35**, 12.

Kitano, Y. Hood, D.W. (1965), *The Influence of Organic Material on the Polymorphic Crystallization of Calcium Carbonate*, Geochim. Cosmochim. Acta, **29**, 29-41.

Kirov, G.K., Vesselinov, I., Cherneva, Z. (1972), *Conditions for the Formation of Calcite Crystals of Tabular and Acute Rhombohedral Habit*, Kristal. u. Technik., **7**, 497-509.

McCauley, J.W., Roy, R. (1974), *Controlled Nucleation and Crystal Growth of Various $CaCO_3$ Phases by the Silica Gel Technique*, Am. Mineralogist, **59**, 947-963.

Meyer, H.J. (1984), *The Influence of Impurities on the Growth of Calcite,* **66**, 639-646.

Mitterer, R.M., Cunningham, J.R. (1985), *The Interaction of Natural Organic Matter with Grain Surfaces: Implications for Calcium Carbonate Precipitation,* in Carbonate Sediments, pp 17-31, The Society of Economic Palaeontologists and Mineralogists.

Oliver, P. (1990), *A Morphological Study of Calcite Crystal Growth in the Presence of Oxy-Phosphorus Compounds,* BSc thesis, University of Bath.

Perrin, D.D. (1979), *Stability Constants of Metal-Ion Complexes, Part B: Organic Ligands,* London: Pergamon.

Prieto, M., Garcia-Ruiz, J.M., Amoros, J.L. (1981), *Growth of Calcite Crystals with Non-Singular Faces,* J. Cryst. Growth, **52**, 864-867.

Pytkowicz, R.M. (1965), *Rates of Inorganic $CaCO_3$ Nucleation,* J. Geol., **73**, 196-199.

Raistrick, B. (1949), *The Stabilization of the Supersaturation of Calcium Carbonate Solutions by Anions Possessing O-P-O-P-O Chains,* Faraday Disc., **5**, 234-237.

Rajam, S., Mann, S. (1990), *Selective Stabilization of the (001) Face of Calcite in the Presence of Lithium,* J. Chem. Soc. Chem. Communications, **24**, 1789-1791.

Reddy, M.M., Nancollas, G.H. (1973), *Calcite Crystal Growth Inhibition by Phosphonates,* Desalination, **12**, 61-73.

Reddy, M.M., Nancollas, G.H. (1976), *The Crystallization of $CaCO_3$ - IV Effect of Mg, Strontium and Sulfate Ions,* J. Cryst. Growth, **35**, 33-38.

Reddy, M.M. (1977), *Crystallization of $CaCO_3$ in the Presence of Trace Amounts of Phosphorus-Containing Anions*, J. Cryst. Growth, **41**, 287-295.

Reddy, M.M. (1981), *Crystal Growth of Calcite from Calcium Bicarbonate Solutions at constant PCO_2 and 25°C: a test of a calcite dissolution model,* Geochim. Cosmochim. Acta, **45**, 1281-1289.

Reddy, M.M. (1986), *Effect of Mg ions on Calcium Carbonate Nucleation and Crystal Growth in Dilute Aqueous Solutions at 25°C*, from Studies in Diagenesis, Mumpton, F.A. (Ed.), US Geological Survey Bulletin, **1578**, 169-182.

Sanderson, N.P. (1988), *A Study of the Morphological Effects of Organic Dicarboxylates on Calcium Carbonate*, BSc Thesis, University of Bath.

Simkiss, K. (1964), *The Inhibitory Effects of Some Metabolites on the Precipitation of $CaCO_3$ from Artificial and Natural Seawater*, J. Consol. Internat. l'Explor. Mer., **29**, 6-18.

Sillen, L.G. (1965), *Stability Constants of Metal-Ion Complexes, Part 1: Inorganic Ligands*, London: The Chemical Society.

Ross, M.D., Pote, K.G. (1984), *Some Properties of Otoconia*, Phil. Trans. R. Soc. Lond. **B304**, 445-452.

Suess, E. (1970), *Interaction of Organic Compounds with $CaCO_3$ - Associated Phenomena and Geochemical Implications*, Geochim. Cosmochim. Acta, **34**, 157-168.

Thompson, D.W., Pownall, P.G. (1989), *Surface Electrical Properties of Calcite*, J. Coll. Int. Sci. **131(1)**, 74-82.

Vanderheiden, D.B. (1987), Pfizer Inc., New York, *Spherically-Shaped Precipitated Calcium Carbonate, its Preparation and Use,* US Patent no. 4,714,603.

Wilbur, K.M., Bernhardt, A.M. (1984), *Effects of Amino Acids, Mg and Molluscan Extrapallial Fluid on Crystallization of Calcium Carbonate: In Vitro Experiments*, Biol. Bull., **166**, 251-259.

CHAPTER 5

The Influence of some Macromolecular Additives on the Crystallization of Synthetic Calcium Carbonate

5.1 INTRODUCTION

The previous chapter dealt with the habit changes of calcite crystals induced by certain simple, low molecular weight organic and inorganic additives. Attention now turns to the larger, more complex macromolecules involved in $CaCO_3$ biomineralization processes.

As was mentioned in chapter 1, the current paradigm in this area of research is the use of *in vitro* experiments to study the effects of extracted biogenic macromolecules on their corresponding inorganic phase. The most common approach involves a kinetic assessment of their relative ability to inhibit nucleation and growth in supersaturated solutions (Wheeler *et al* 1981, Borman *et al* 1982 etc). Comparisons can then be made after structural modifications such as the removal of carboxylates or ester sulphates. In addition, synthetic analogues can be tested (Wheeler and Sikes 1988, Sikes *et al* 1990).

To date, changes in the habit of the crystals produced in the presence of these macromolecules have not been widely studied. The morphological approach was first adopted by Addadi and Weiner (1985, 1986) and has been used to make the important distinction between specific and non-specific inhibitors. For example, solubilized glycoproteins, extracted from sea urchins, are very selective in their interaction with calcite such that $\{1\bar{1}00\}$ faces are preferentially expressed (Berman *et al* 1988). A stereochemical complementarity is found to exist between the anions in the face and the active functional groups of the protein. In contrast, glycoproteins from certain molluscs are non-specific inhibitors of calcite and affect the

morphology of the crystals such that they become ill-defined and deformed. In this case, it is thought that interactions are dominated by electrostatic factors rather than stereochemistry.

In an attempt to further investigate the nature of the specific inhibitors, studies using model polymers have been undertaken (Addadi *et al* 1987, 1990). The work has revealed some important points. Firstly, selectivity appears to be highly dependent on the secondary structure of the macromolecule. In order that the stereochemical information of the functional groups is recognized, the polymer must have an ordered conformation such as an anti-parallel β-pleated sheet. Secondary structure is affected not only by the environment eg pH or the presence of Ca^{2+} but also by the size of the molecule. Secondly, electrostatic interactions, which are the main driving force for adsorption, can overcome the stereochemical factors and lead to loss of selectivity. Thus, a heavily charged macromolecule may be non-specific even if it has the appropriate functional groups and conformation.

This approach has been very productive in elucidating some of the fundamental mechanisms of molecular recognition in biomineralization. However, at present, only the sea urchin and mollusc glycoproteins have been studied in this way.

Objective

It was therefore the purpose of this chapter to extend the work of Addadi *et al* and additionally to build on the model studies presented in chapter 4. It was intended to make use of the present well-characterized crystallization system and an assortment of biogenic macromolecules and synthetic polymers that were available.

Background to Some of the Macromolecules Studied

Coccolith Polysaccharide

One very important molecule, especially in the context of this thesis, was the acidic

polysaccharide associated with coccoliths of *E. huxleyi* (chapter 1.4 and chapter 6). The inhibitory effects on calcite crystallization have been demonstrated (Borman *et al* 1982) but many questions remain as to its function and operation *in vivo*. The molecule has a mannose backbone with side chains of rhamnose, xylose and mannose. It has anionic (galacturonic acid) and hydrophobic regions (methylated sugars) and is thought to have a sulphate ester core (de Jong *et al* 1976). Studies indicate that the inhibitory tendency is due to the carboxylate groups only which are located on the outer surface of the molecule. Its weight average molecular weight $M_w = 88.6 \pm 3.2$ kDa, and number average molecular weight $M_n = 49.1 \pm 1.5$ kDa giving a polydispersity $\gamma = M_w/M_n = 1.8$ (Borman 1986).

Model Polysaccharides

Polygalacturonic acid and alginic acid were chosen as two model acidic polysaccharides in common with Borman *et al* (1982) who carried out kinetic studies of $CaCO_3$ inhibition. Polygalacturonate, also known as pectate, is a straight chain homopolysaccharide of (1→4)-linked α-galacturonate. Alginate is a natural product extracted from brown algae (Kelp) and is a straight chain, heteropolysaccharide of mainly β-D-mannuronate-(1→4)-α-L-guluronate. According to Borman *et al*, both molecules contain about 2.5 times more carboxylate groups than the coccolith polysaccharide. Their results showed that alginic acid was comparable in its inhibitory tendencies to the coccolith macromolecule but that polygalacturonic acid was about 20 times less effective.

Bone Gla Protein

Osteocalcin is a prominent non-collagenous protein found in bones and teeth and is thought to be closely involved with calcification. It is of interest mainly because it has been well-characterized. Primary sequence data is known (eg Poser *et al* 1980, Carr *et al* 1981) and, in this respect, it is unusual because it contains three γ-carboxyglutamic acid residues hence its alternative name, Gla protein. This small

macromolecule (47-50 residues) binds calcium undergoing a change in conformation from random coil to α-helix at pH 7.4 (Hauschka 1981). It has an isoelectric point of about 3.7 and been observed to inhibit the precipitation of hydroxyapatite (Price *et al* 1976). Proteins containing γ-carboxyglutamic acid have also been reported in $CaCO_3$ corals (Hamilton *et al* 1982) and so are not restricted to vertebrate biomineralization.

Proteoglycans

These are a more complex class of non-collagenous macromolecules present in vertebrate mineralizing tissues and thought to regulate the formation of hydroxyapatite crystals (Chen *et al* 1984). Monomer units consist of a protein core to which are attached many polysaccharide chains functionalized by carboxylate and sulphate. These monomers are strongly anionic and can be very large indeed (4000 kDa). In their native environment, they form even bigger complexes with hyaluronic acids.

Anti-Freeze Glycoprotein

Polar fishes survive the freezing of their body fluids by producing a range of glycopeptides of varying sizes that efficiently inhibit the propagation of ice crystals. Studies have shown that these anti-freeze molecules adsorb on ice nuclei and slow the growth in the direction of the *a* axes (Raymond *et al* 1989). The peptide is very simple consisting of only two amino acids, alanine (hydrophobic R group: $-CH_3$) and threonine (uncharged polar R group: $-CH(OH)CH_3$) in the repeating sequence Ala-Ala-Thr. Each threonine is attached, via a glycosidic linkage, to the disaccharide, β-D-galactopyranosyl-(1→3)-2-acetamido-2-deoxy-α-D-galact o-pyranose (DeVries 1988). Circular dichroism studies have indicated that the molecule is in an extended coil or three-fold helix conformation in water.

Hyperbranched Polyphenylene

In addition to the biological biopolymers, a synthetic polymer with unusual properties was investigated. A carboxylate derivative of a fully aromatic, water-soluble, hyperbranched polyphenylene has been claimed to act as a "unimolecular micelle" due to its ability to complex and solubilize non-polar guest molecules such as *p*-toluidine in water (Kim and Webster 1990). The polymer consists of between 40-60 phenyl units that branch outward from a central point forming a roughly spherical molecule with carboxylates on the outer surface.

5.2 EXPERIMENTAL MATERIALS AND PROCEDURES

Procedures

Supersaturated calcium bicarbonate solutions were prepared as described in chapter 2.3. 10 ml of this freshly prepared solution was placed in 20 ml capacity (25 mm diameter) glass vials, covered but left open to the atmosphere. The additives were introduced immediately as aliquots (no greater than 500 µl) taken from stock solutions. The final concentrations studied are shown in table 5.1. Vials were then aged on the bench at ambient temperature (16-18°C). In this way, the final volumes and calcium concentrations were kept constant in all systems. As before, the initial total dissolved calcium (Ca_T) was determined by EDTA titration. Pure calcium bicarbonate solutions, as well as solutions containing buffer chemicals at the maximum concentration used in the additive systems, were employed as controls. All experiments were performed in duplicate or triplicate depending mainly on the amount of macromolecular material available.

Additive	Concentration Studied ($\mu g ml^{-1}$)	Ca/additive molar ratio
Coccolith Polysaccharide (PSL)	0.03 0.3 3.0 30	15,000,000:1 # 1,500,000:1 150,000:1 15,000:1
Alginic acid (ALG)	0.03 0.3 3.0 30	- - - -
Polygalacturonic acid (PGU)	0.03 0.3 3.0 30	150,000:1 ~ 15,000:1 1500:1 150:1
Osteocalcin (Gla)	0.18 0.54 0.96 1.9 3.0	300,000:1 100,000:1 56,000:1 28,000:1 20,000:1
Proteoglycan monomer (PG)	18 180 1800	1,000,000:1 * 100,000:1 10,000:1
Anti-freeze Glycopeptide (AFGP)	16 160 330 1600	12,000:1 $ 1,200:1 580:1 120:1
Polyvinyl Alcohol (PVA)	12.5 25 50 250	2000:1 ∞ 1000:1 500:1 100:1
Hyperbranched Polyphenylene (HBP)	3.2 32 320	10,000:1 + 1000:1 100:1

Table 5.1 *Range of macromolecule concentrations studied assuming average molecular weights: # 49.1 kDa, ~ 5 kDa, * 2000 kDa, $ 21.5 kDa, ∞ 3 kDa, + 3.8 kDa*

Materials

Polysaccharide (PSL) extracted from isolated coccoliths of *Emiliania huxleyi* (strain L) was kindly supplied by Professor P. Westbroek (University of Leiden, Netherlands). Stock solutions were made up from lyophilized PSL dissolved in 0.01M NH_4HCO_3 (BDH).

Osteocalcin, from monkey (MGla; mw 5889 Da) and bovine (BGla; mw 5200-5900 Da) sources was obtained from Dr P. Hauschka (Harvard School of Dental Medicine, Boston, USA). Both proteins were reported to have a high sequence homology. Stocks were prepared in Purite^{TM} distilled water with no buffer.

Proteoglycan (PG) monomer (mw 1000-4000 kDa) from pig laryngeal cartilage was kindly supplied by Dr T. Hardingham (Kennedy Institute of Rheumatology, London). The protein core was attached to about 100 chondroitin sulphate chains (*ca.* 20 kDa each) and perhaps 40 keratan sulphate chains (*ca.* 7 kDa each). Chondroitin sulphate was 75% 4-sulphate on N-acetyl-D-galactosamine, 20% 6-sulphate and 5% pure sugar residues. Stocks were prepared from lyophilized PG dissolved in 0.01M MOPS (4-morpholine-propane-sulphonic acid; Aldrich; pK_a = 7.2) buffer solution.

An unknown mixture of five anti-freeze glycopeptides (AFGP) (mw 10.5, 17.0, 21.5, 28.8, 33.7 kDa) from the blood of the Antarctic fish *Dissostichus mawsoni* was obtained from Professor A.L. DeVries (University of Illinois at Urbana-Champaign, USA). A stock was made up in Purite^{TM} distilled water only.

The carboxylic acid derivative of hyperbranched polyphenylene (HBP) polymer was synthesized and supplied by Dr Y.H. Kim (Central R&D Department, EI du Pont de Nemours & Co., Wilmington, USA). M_w = 5.750-7.077 kDa, M_n = 3.810-3.910 kDa, γ = 1.5, pK_a = 3.0-5.0. Some of the free acid (0.32 g; a brown powder) was

suspended in about 40 ml distilled water and dissolved by adding a minimum quantity of 8M NaOH after which the clear brown solution (pH 12) was adjusted carefully to pH 6.2 with 2N HCl without precipitating polymer. Finally, the volume was made up to 50 ml (stock = 1.0 mM). It was used unpurified in crystallization experiments. Surface tension measurements, using a NIMA mini-trough, were taken to assess the surface activity of HBP. The polymer was not added to the surface of pure water as in conventional procedures. Instead, 1 litre of HBP solution (320 μgml^{-1}; pH 6.2) was introduced to completely fill the trough, surface cleaned by a vacuum suction pasteur pipette, and then the isotherm recorded. Compression rate was 100 cm^2min^{-1}.

A 75% hydrolysed sample of polyvinyl alcohol (PVA) was obtained from Aldrich Ltd. The repeat unit is -{$CH_2CH(OH)$}-. It had a molecular weight of about 3 kDa and thus an average of about 50 hydroxyls per molecule.

The sodium salt of polygalacturonic (PGU) was purchased from Sigma Ltd. It had a reported molecular weight of 4-6 kDa and thus consisted of approximately 20-30 sugar residues. Alginic acid (ALG) was from BDH Ltd. No molecular weight information was available.

Analysis of Crystal Products

Due to the small scale of the experiments, the amount of crystals produced were insufficient for characterization by many techniques. All crystals were collected after about 75-130 hours ageing being either retrieved on glass cover slips dipped through the surface or placed on the bottom of each vial. The slips were then mounted on glass slides for optical microscopy (OM) or on aluminium stubs for examination by scanning electron microscopy (SEM). In the case of AFGP, enough crystals were grown to enable powder X-ray diffraction (XRD) analysis (3 mg) and quantitative elemental microanalysis for C, H and N (2.8 mg). The latter technique

was used to determine whether anti-freeze glycopeptide was associated with the crystals. Samples were thoroughly washed in Purite^{TM} water and then dried in a cool oven prior to analysis.

5.3 RESULTS

Based on visual observations, the additives had a minimal effect on crystal sizes and surface yields with some exceptions. Control crystals grown in these vials, which held a considerably smaller volume than the dishes used in chapter 3, were no different in any respect (fig. 5.1a, b). Buffer chemicals had no discernable effect at the levels studied (fig. 5.1c, d). The bottom and sides of the vials were also generally free of crystals.

Coccolith Polysaccharide and Model Macromolecules

At concentrations of 0.03 and 0.3 μgml^{-1}, the polysaccharide had little effect on crystallization apart from reducing the amount of vaterite present (fig. 5.2a). Above these levels, surface yields were actually increased over those of the controls; the crystals spreading to cover the full surface area of the vial (fig. 5.2b). This also coincided with a general disappearance of crystals at the bottom of the container. Concentrations of 3 μgml^{-1} was sufficient to cause detectable rounding of calcite rhombs as shown in fig. 5.2c and fig. 5.3a. A level of 30 μgml^{-1} induced quite extensive aggregation forming fused chains over much of the surface (fig. 5.2d and fig. 5.3b). Calcite morphologies were dramatically altered to rather ill-defined, curved and often *c* axis elongated prisms (fig. 5.2d and fig. 5.3c, d). Thus, the macromolecule did not appear to be highly specific in its interaction although there was, arguably, some form of generalized recognition taking place with the prismatic faces.

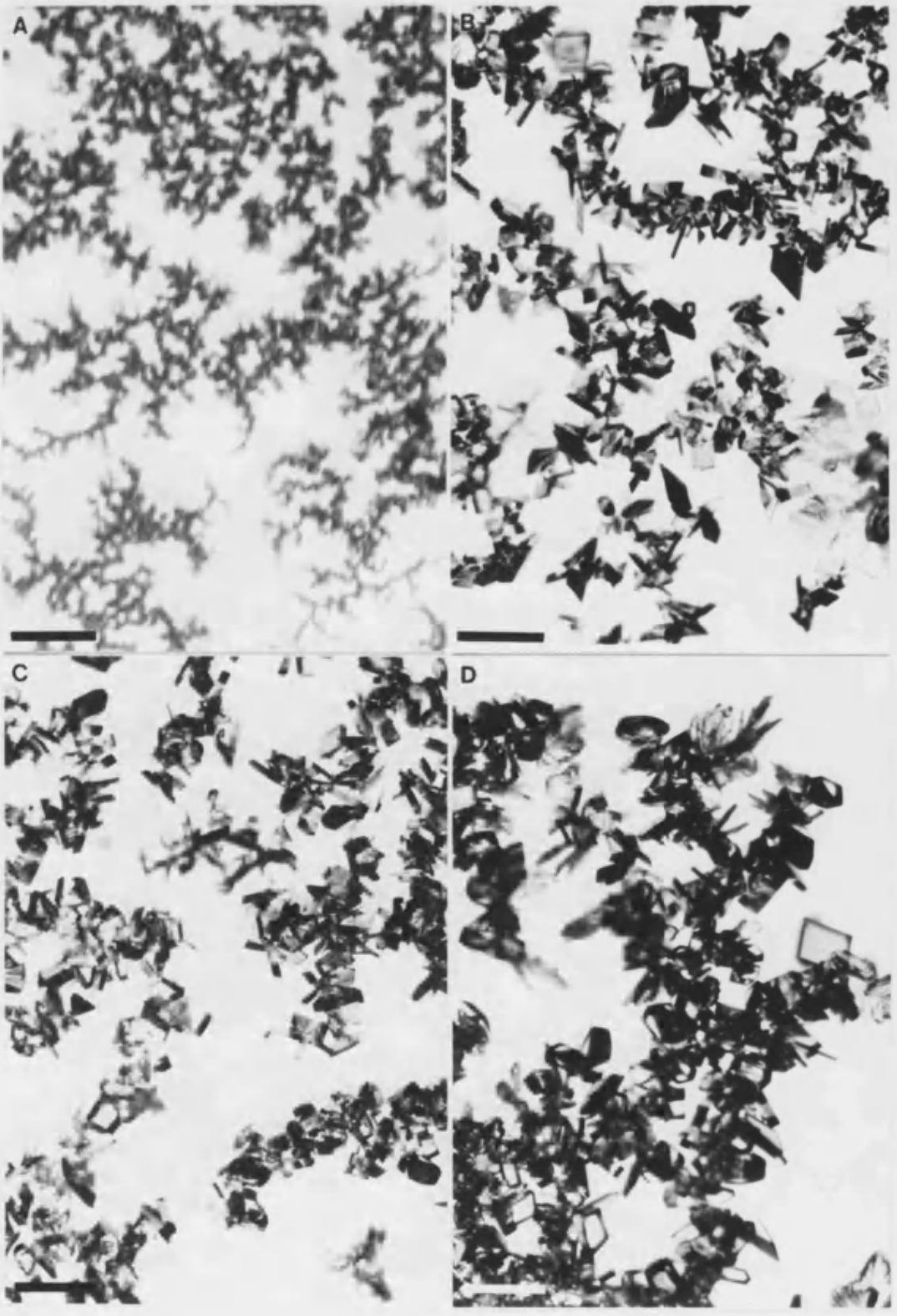

Fig. 5.1 *Optical micrographs of crystals grown at the surface of the crystallizing solution: (a and b) ordinary control, (c) MOPS buffer control and (d) NH_3HCO_3 buffer control. Scale bars: (a) 500 μm, others 100 μm.*

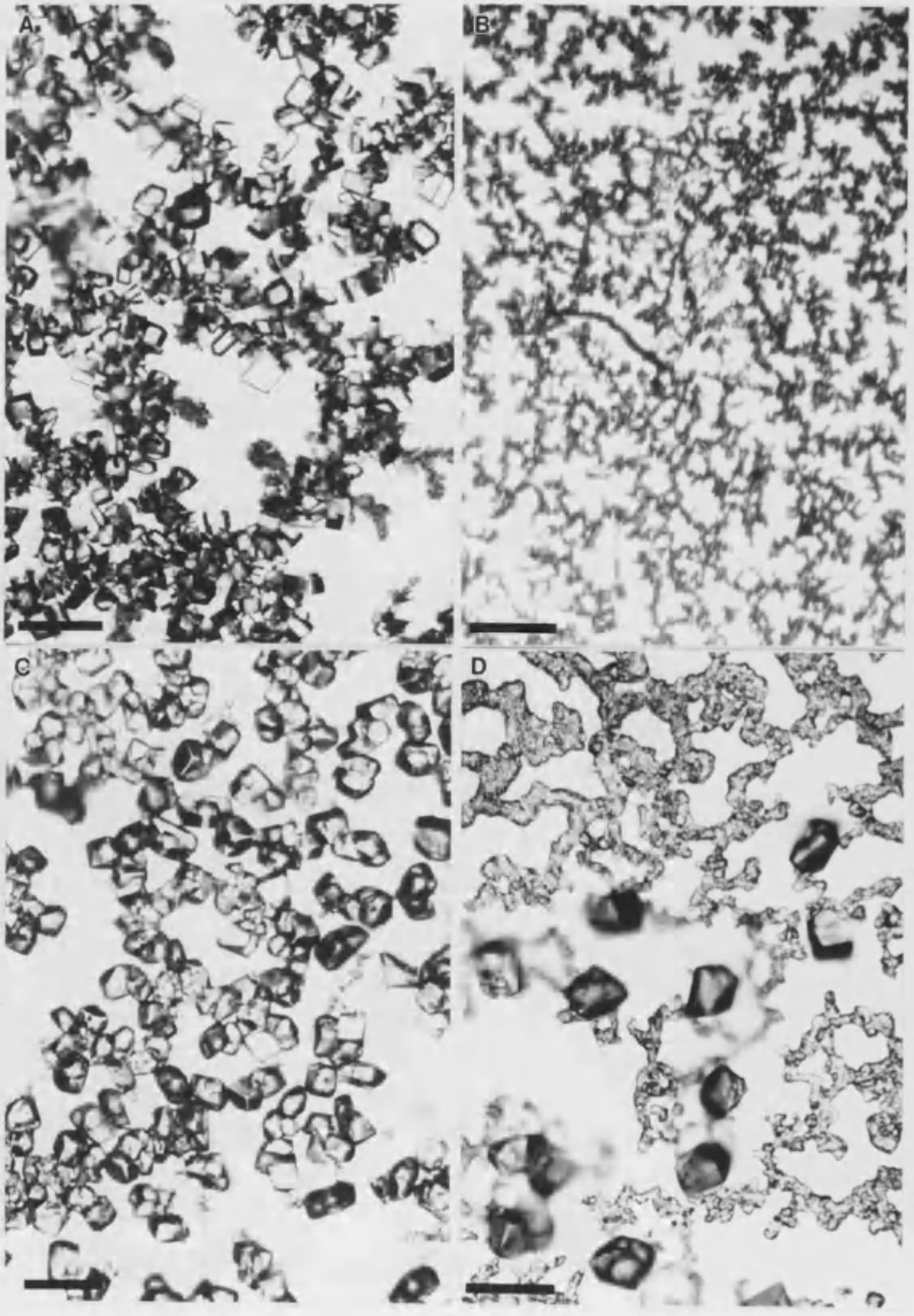

Fig. 5.2 *Optical micrographs showing the influence of coccolith polysacchardide on surface crystals: (a) 0.3 μgml^{-1} (b and c) 3 μgml^{-1} (d) 30 μgml^{-1}. Scale bars: (b) 500 μm, others 100 μm.*

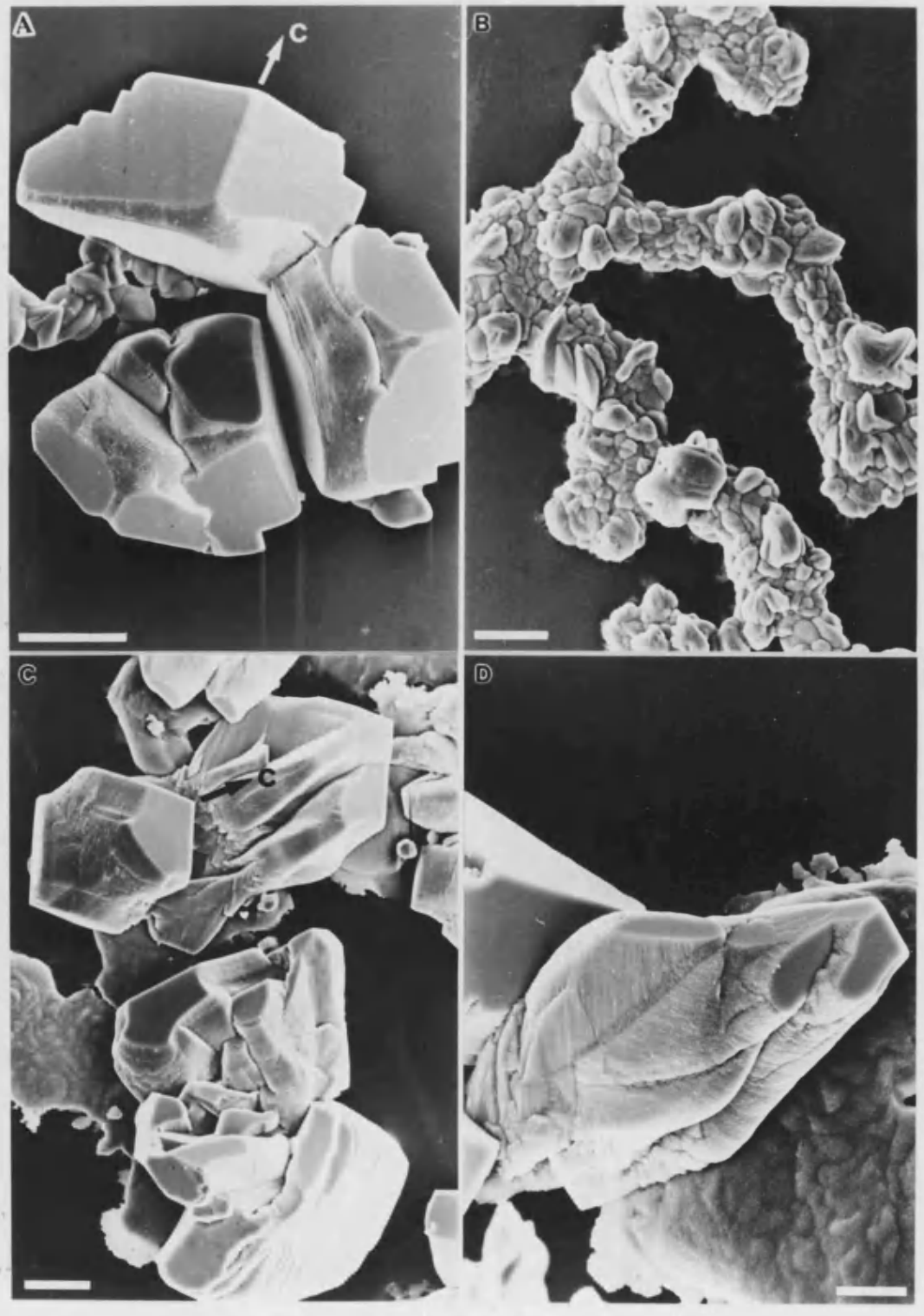

Fig. 5.3 *Scanning electron micrographs of surface crystals grown in the presence of coccolith polysaccharide: (a) 3 μgml^{-1} (b, c, d) 30 μgml^{-1}. Scale bars 20 μm.*

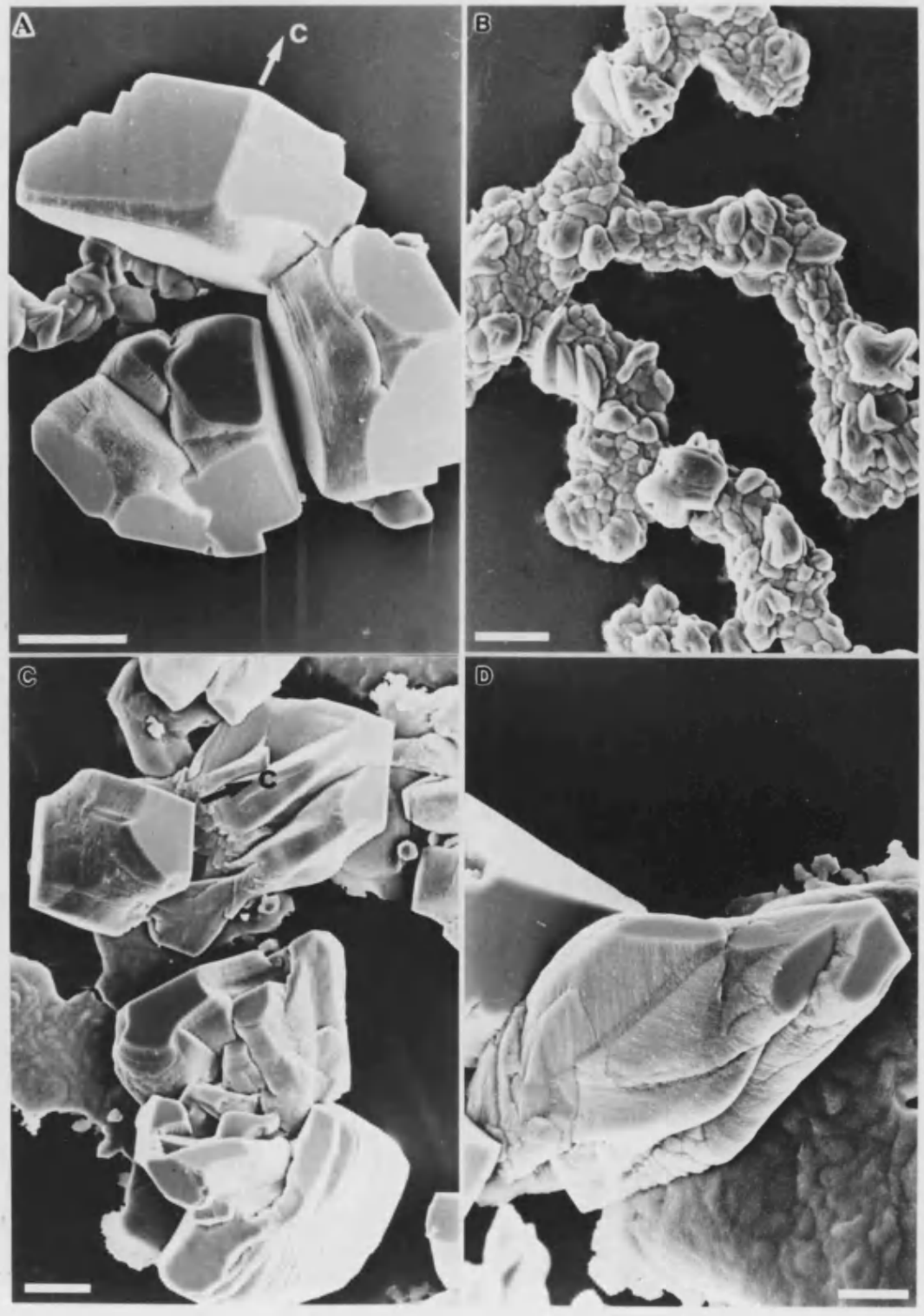

Fig. 5.3 *Scanning electron micrographs of surface crystals grown in the presence of coccolith polysaccharide: (a) 3 μgml^{-1} (b, c, d) 30 μgml^{-1}. Scale bars 20 μm.*

Polygalacturonic acid (PGU) and alginic acid (ALG) gave surprisingly contrasting results. PGU at 30 μgml^{-1} had almost no effect on crystallization at all (fig. 5.4a and fig. 5.5a). On the other hand, ALG was very similar in potency and aggregating power to PSL (fig. 5.4b). The main differences were that it caused comparatively less *c* axis elongation of the crystals but instead expressed distinctly foliated or laminated $\{1\bar{1}00\}$ first order prisms (fig. 5.5b, c, d). The $\{10\bar{1}4\}$ were severely pitted and grooved in directions that appeared to be parallel to the $\{1\bar{1}00\}$ faces. This suggested that growth was highly disrupted such that large numbers of defects were formed on the developing surfaces.

Anti-Freeze Glycopeptide (AFGP)

The Antarctic fish glycopeptide, at all the concentrations studied, had the extraordinary effect of strongly inhibiting calcite in favour of vaterite. The surfaces of these systems showed aggregated floret-shaped, vaterite crystals, 100-200 μm in size, with random crystallographic orientations (fig. 5.6). In the control, vaterite crystals were identical in all respects but were present in far fewer numbers. Duplicated experiments provided sufficient material for analysis. XRD confirmed that vaterite was the dominant phase (fig. 5.7c). Elemental analysis for C, H and N demonstrated increased levels of all three elements compared to the control indicating a significant affinity between AFGP and vaterite (table 5.2). The figures corresponded to a *ca.* 0.6 % uptake based on the nitrogen content.

An attempt was made to model the action of the glycopeptide by examining the influence of a synthetic polymer with a similar number of identical functional groups. AFGP is functionalized by hydroxyl groups present on the disaccharide side chains. Thus, a suitable material was polyvinyl alcohol (PVA). From a consideration of the molecular weight of the basic structural repeat unit (mw = 598) and of the each macromolecule fraction, the average number of OH's was calculated (120-360) for the mixture of additive material used. PVA (3 kDa) was chosen and tried in

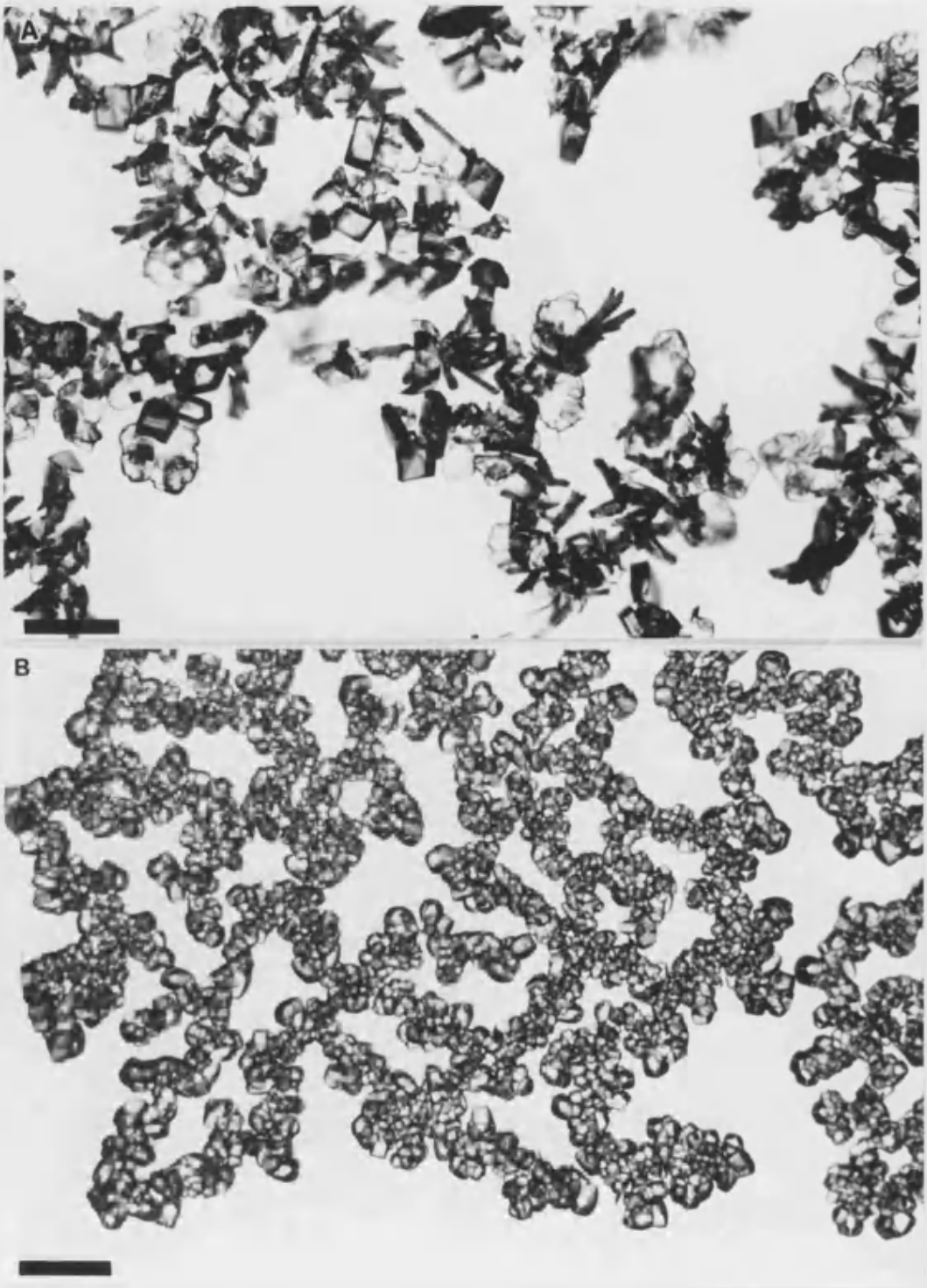

Fig. 5.4 *Optical micrographs of surface crystals for 30* $\mu g ml^{-1}$ *of (a) polygalacturonic acid and (b) alginic acid. Scale bars 100* μm.

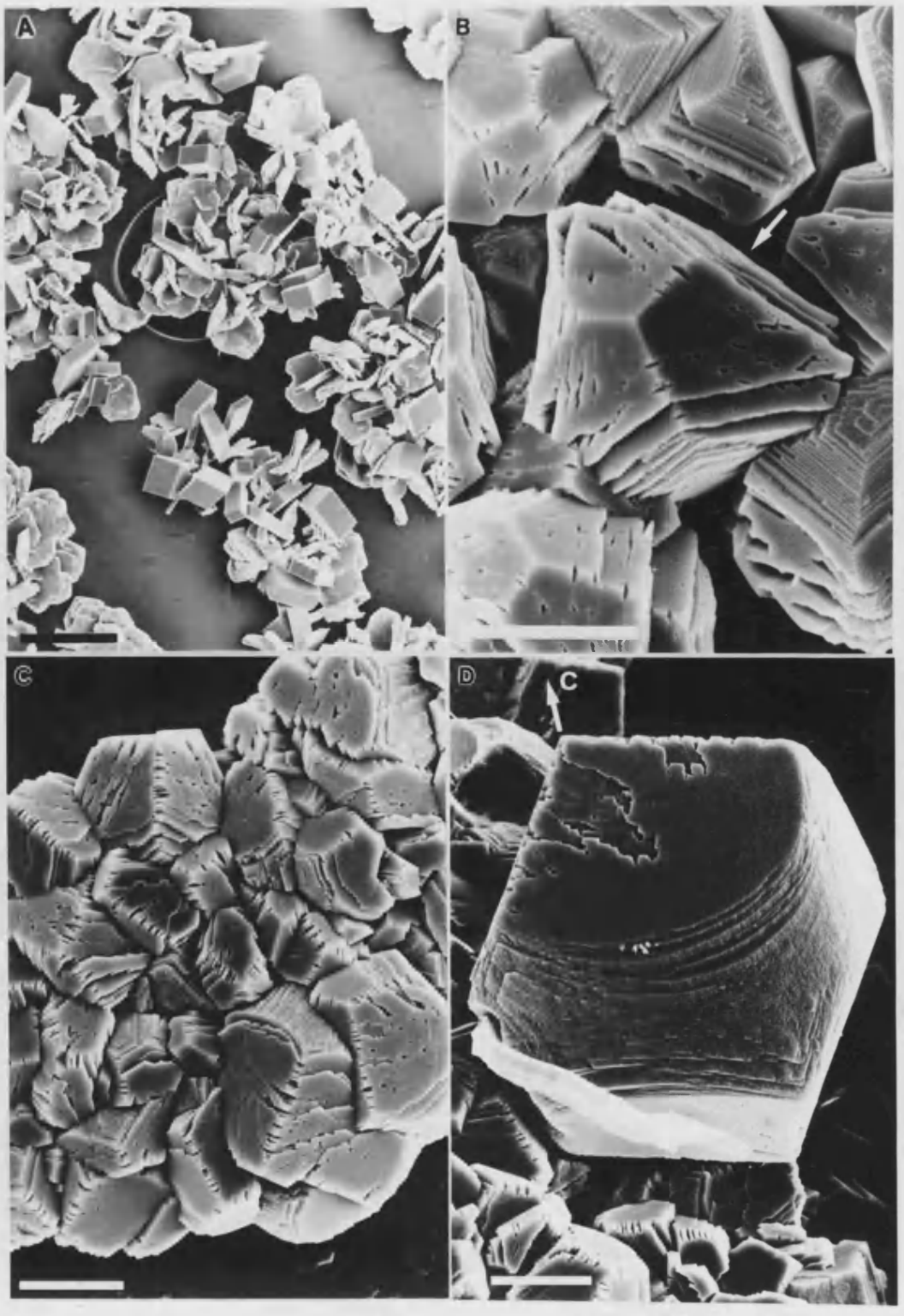

Fig. 5.5 *Scanning electron micrographs of surface crystals for (a) 30 μgml^{-1} polygalacturonic, (b) 3 μgml^{-1} and (c, d) 30 μgml^{-1} alginic acid. Scale bars (a) 100 μm, others 10 μm.*

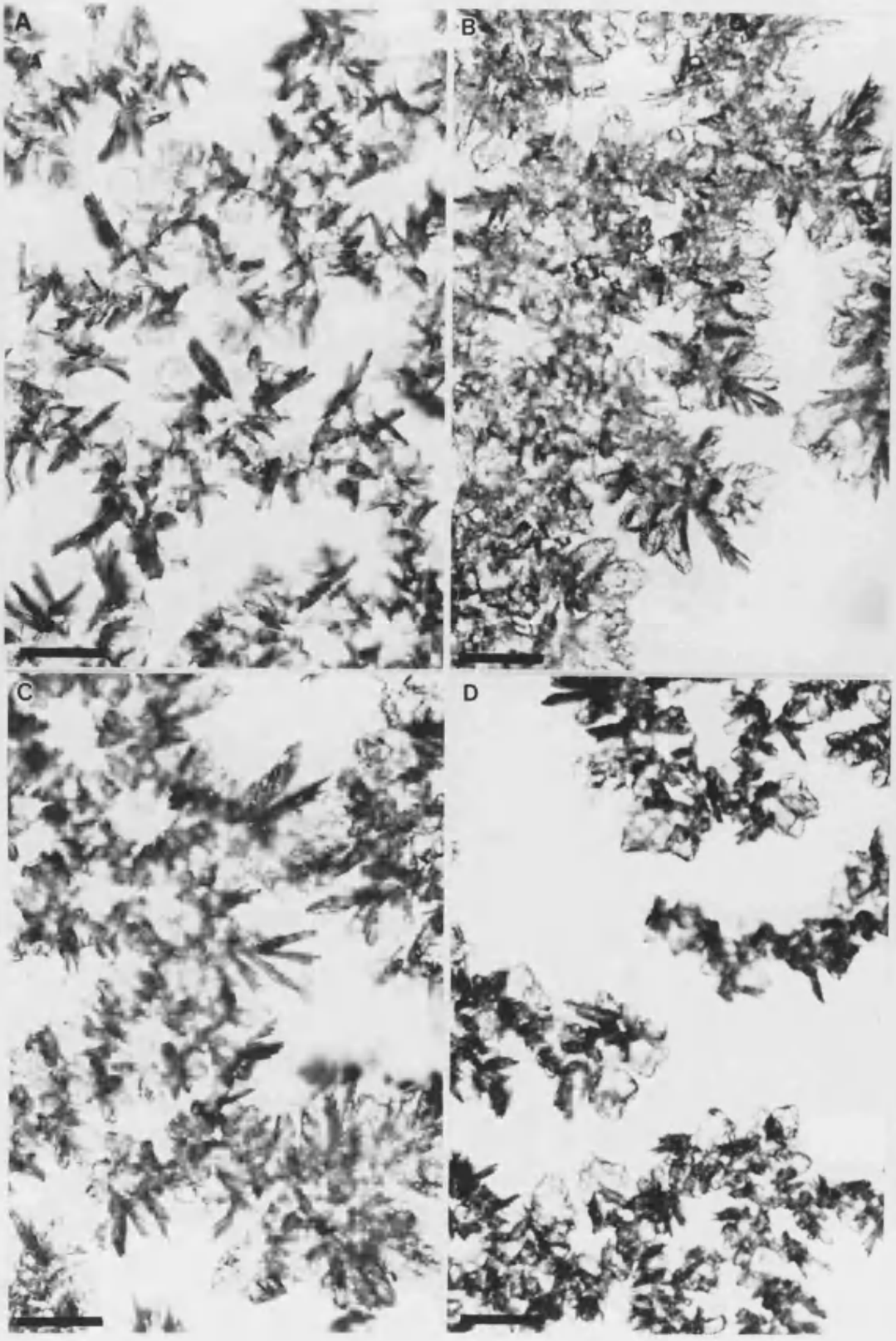

Fig. 5.6 *Optical micrographs demonstrating the effect of (a) 1600 μgml^{-1} and (b) 330 μgml^{-1} anti-freeze glycopeptide plus (c) 25 μgml^{-1} and (d) 250 μgml^{-1} polyvinyl alcohol. Scale bars 100 μm.*

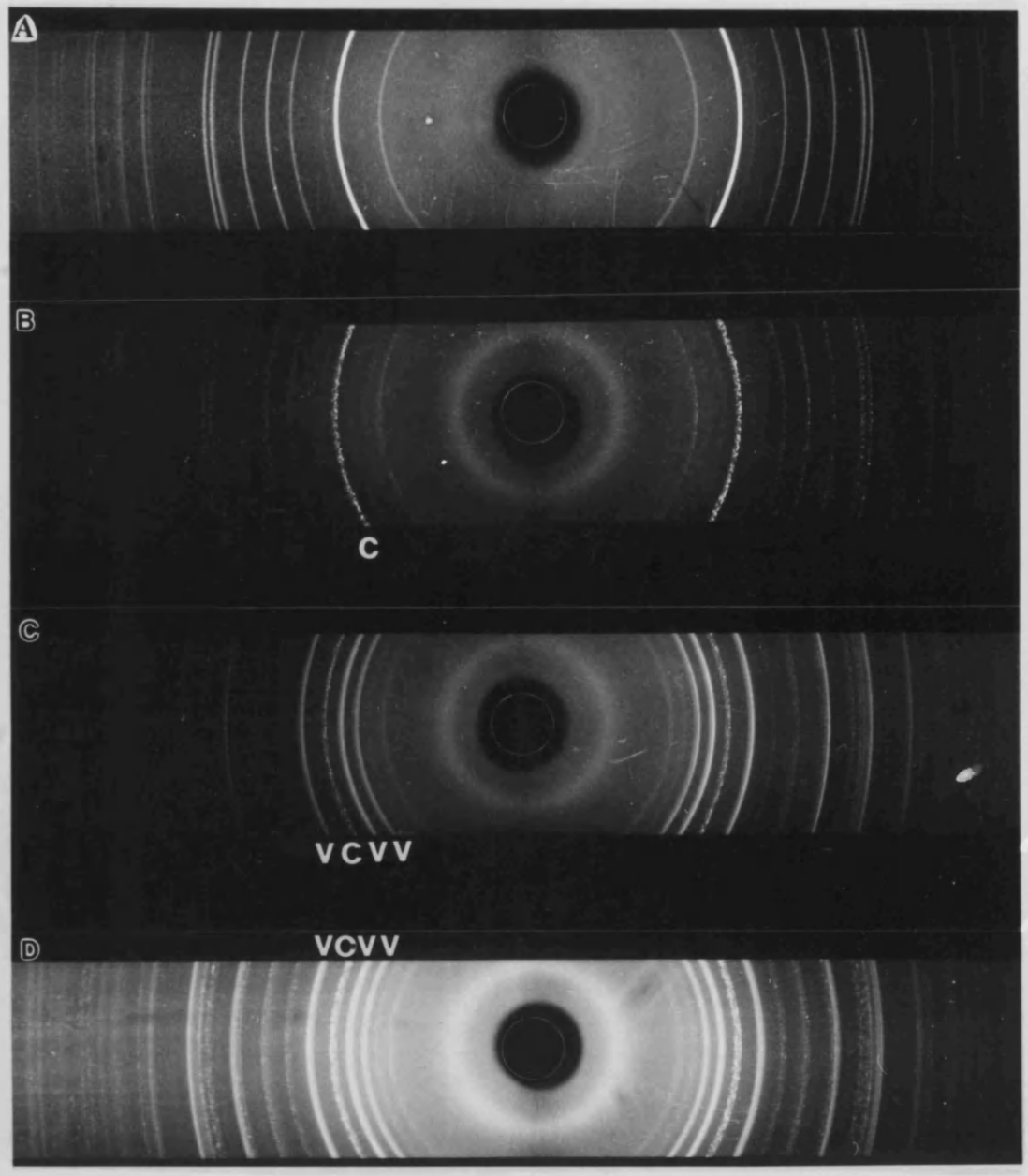

Fig. 5.7 *Powder XRD photographs of (a) BDH analar $CaCO_3$: pure calcite (b) ordinary control: calcite plus some vaterite (c) 330 $\mu g ml^{-1}$ anti-freeze glycopeptide: vaterite plus some calcite (d) 25 $\mu g ml^{-1}$ polyvinyl alcohol: vaterite plus some calcite.*

Sample	%C	%H	%N
control	11.98	0.00	0.01
AFGP-modified	12.13	0.13	0.07

Table 5.2 *Results of elemental analysis for C, H and N on vaterite crystals grown in the presence of anti-freeze glycopeptide (1600 μgml^{-1}).*

crystallization experiments. Interestingly, the polymer had an identical effect producing large amounts of vaterite at all concentrations (fig. 5.6 c, d; fig. 5.7d). This, therefore, strongly suggested that the hydroxyls were important in the interaction.

Carboxylate Derivative of Hyperbranched Polyphenylene (HBP)

At levels of 3.2 and 32 μgml^{-1}, the additive had no effect at all. Immediately upon addition of 320 μgml^{-1} of hyperbranched polyphenylene to the supersaturated solution, a precipitate formed. The same was observed if an equivalent addition was made to a 9 mM $CaCl_2$ solution at pH 6 suggesting the formation of a calcium complex. Despite this, the polymer had dramatic effects on crystallization at the air/water interface. Nucleation density was noticeably reduced (about half) compared to the control and larger (mean = 95 μm, σ = 38 μm *cf.* mean = 26 μm, σ = 11 μm) crystals had formed which were discretely nucleated with relatively little intergrowth (fig 5.8a, b). Regular and truncated plates of calcite were observed (fig. 5.8c) that were reminiscent of crystals grown under compressed stearic acid monolayers (Rajam *et al* 1991). Closer examination in the SEM, confirmed that the calcite showed many of the characteristic features of crystals altered by interactions with negatively charged stearate films. Although, the regular plates obtained with HBP (fig. 5.9a, c) were not as thin, they exhibited smooth $\{10\bar{1}4\}$ in combination with a roughened surface comprising three inclined faces meeting at a central

Fig. 5.8 *Optical micrographs of surface crystals grown in the presence of hyperbranched polyphenylene. Scale bars (a) 1 mm (b, c) 100 μm.*

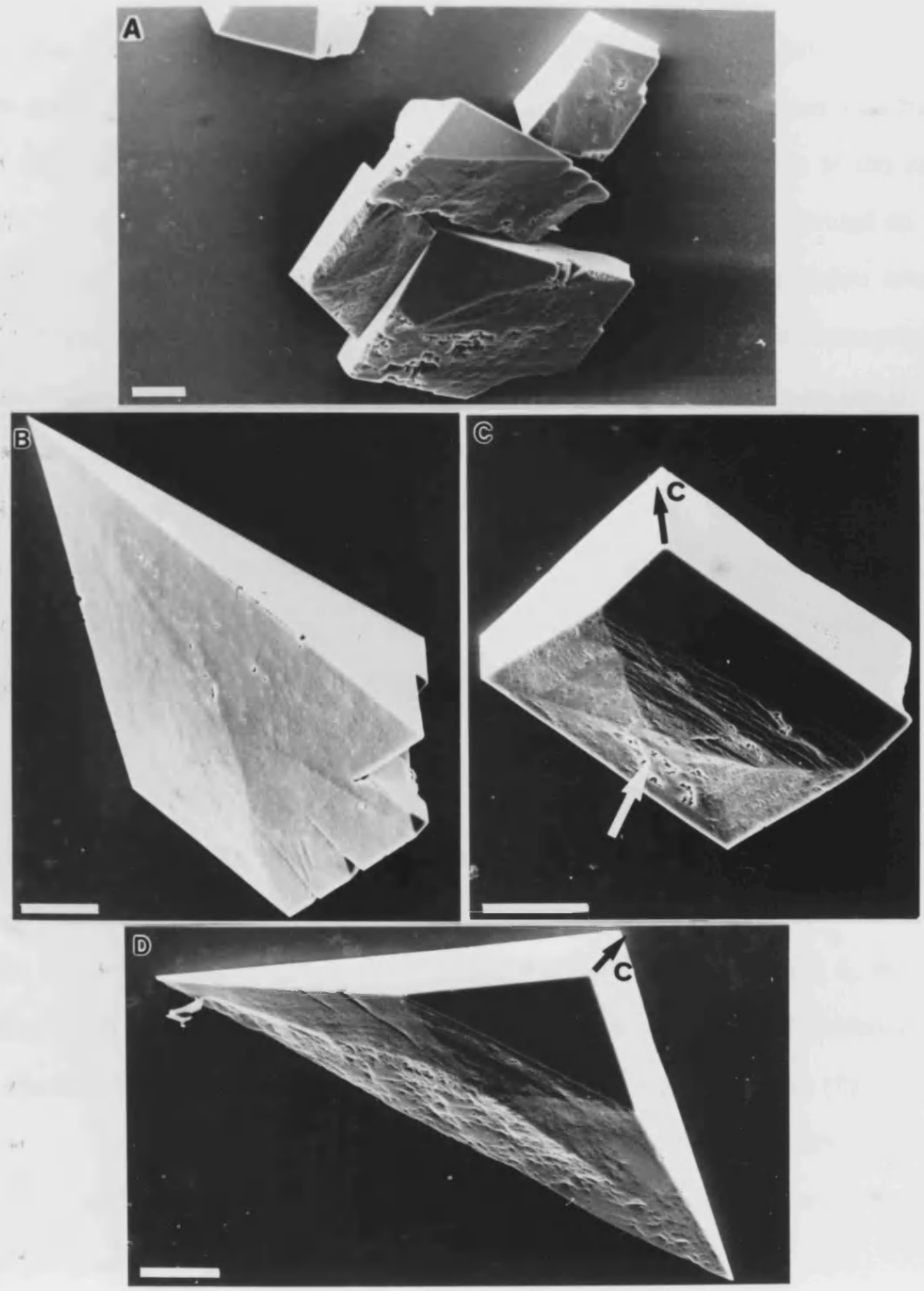

Fig. 5.9 *Scanning electron micrographs of hyperbranched polyphenylene-modified crystals. Scale bars 20 μm.*

elevation. These morphologies were termed type (I) calcite by Rajam *et al.* The main difference was that the roughened faces were not as well-developed with HBP. The truncated rhombs (fig. 5.9b, d) also resembled type (II) crystals in the cited work. Vaterite was evident as discs (arrows) which may have been oriented on the (0001) axis. In addition, some globular morphologies were present (open arrow) which may have been oriented type (II) vaterite (fig. 5.8b). No crystals were present at the bottom or sides of the container. Thus, the polymer appeared to be specific in its interaction by preferentially nucleating first order prismatic faces $\{1\bar{1}00\}$ at the air/water interface. It was possible that the impurities present in the polymer product were surface active. However, the reagents used in the synthesis (Kim and Webster 1990) were not amphiphilic nor were they carboxylated and thus it was unlikely that they were responsible for the specific changes noticed.

The surface activity of HBP was affirmed by fairly reproducible surface pressure/area isotherms (fig. 5.10a) typical of amphiphilic, molecules. Phase changes in the surface film, could be detected by discontinuities in the pressure/area curve (arrows). Thus, despite HBP being quite soluble in water at pH 6, positive adsorption at the air/water interface was significant. This was further demonstrated by diluting the sub-phase which caused the surface activity to diminish (fig. 5.10b). However, compressed films were not obtainable because the surfactant desorbed from the air/water interface when the barriers were left stationary hence limiting area per molecule data was not applicable.

Bovine and Monkey Osteocalcin (Gla)

Osteocalcin showed no evidence of any interaction below 0.96 μgml^{-1}. Above this level, however, it had quite a marked influence morphology. Crystals were noticeably rounded (fig. 5.11) with deep pits, crevasses and macrosteps (fig. 5.12) consistent with a considerable disturbance in the growth process. Despite this, many of the crystals retained their overall shape. However, a particular set of

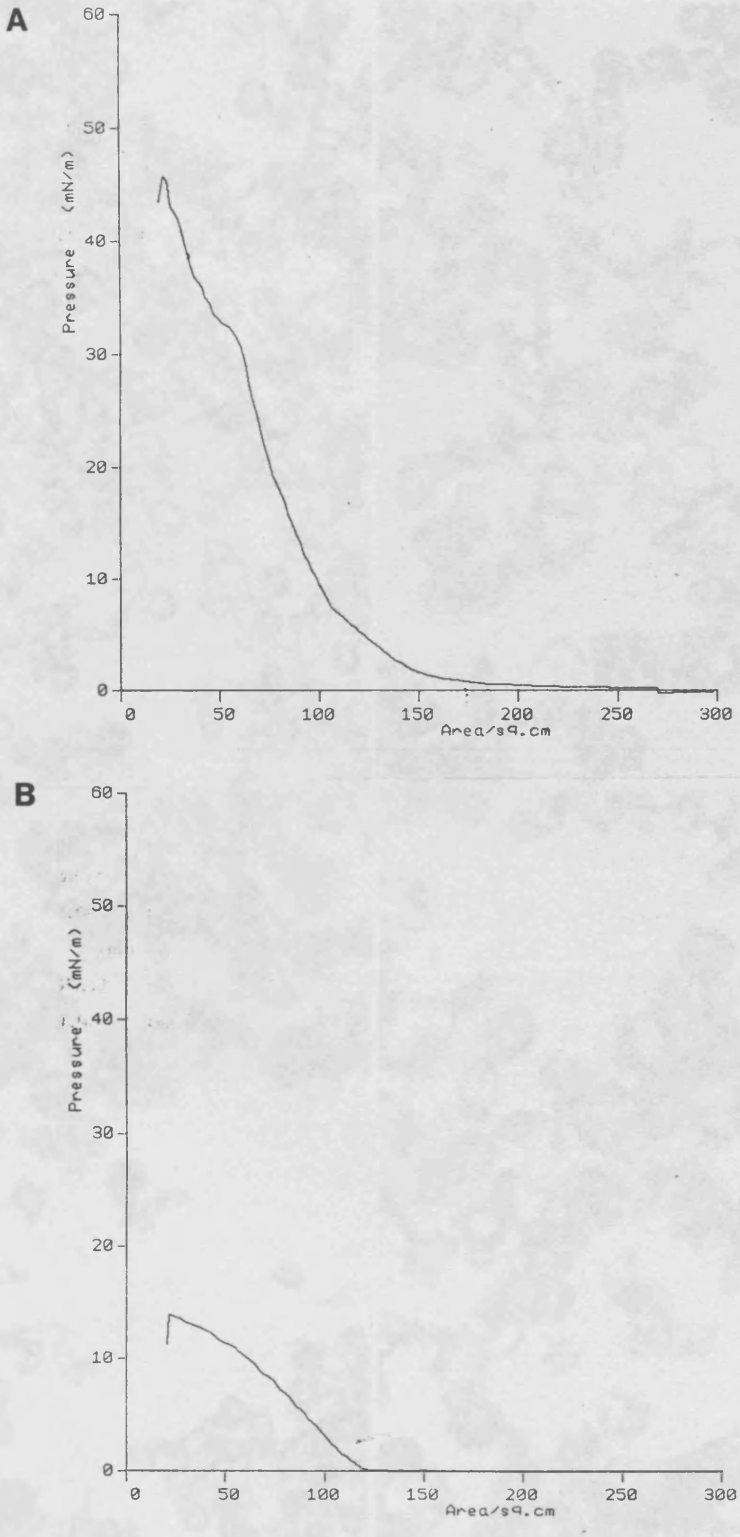

Fig. 5.10 *Surface pressure/area isotherms for hyperbranched polyphenylene present in the subphase (pH 6.2; 19.5 °C) at (a) 320 μgml^{-1} and (b) approximately 30 μgml^{-1}.*

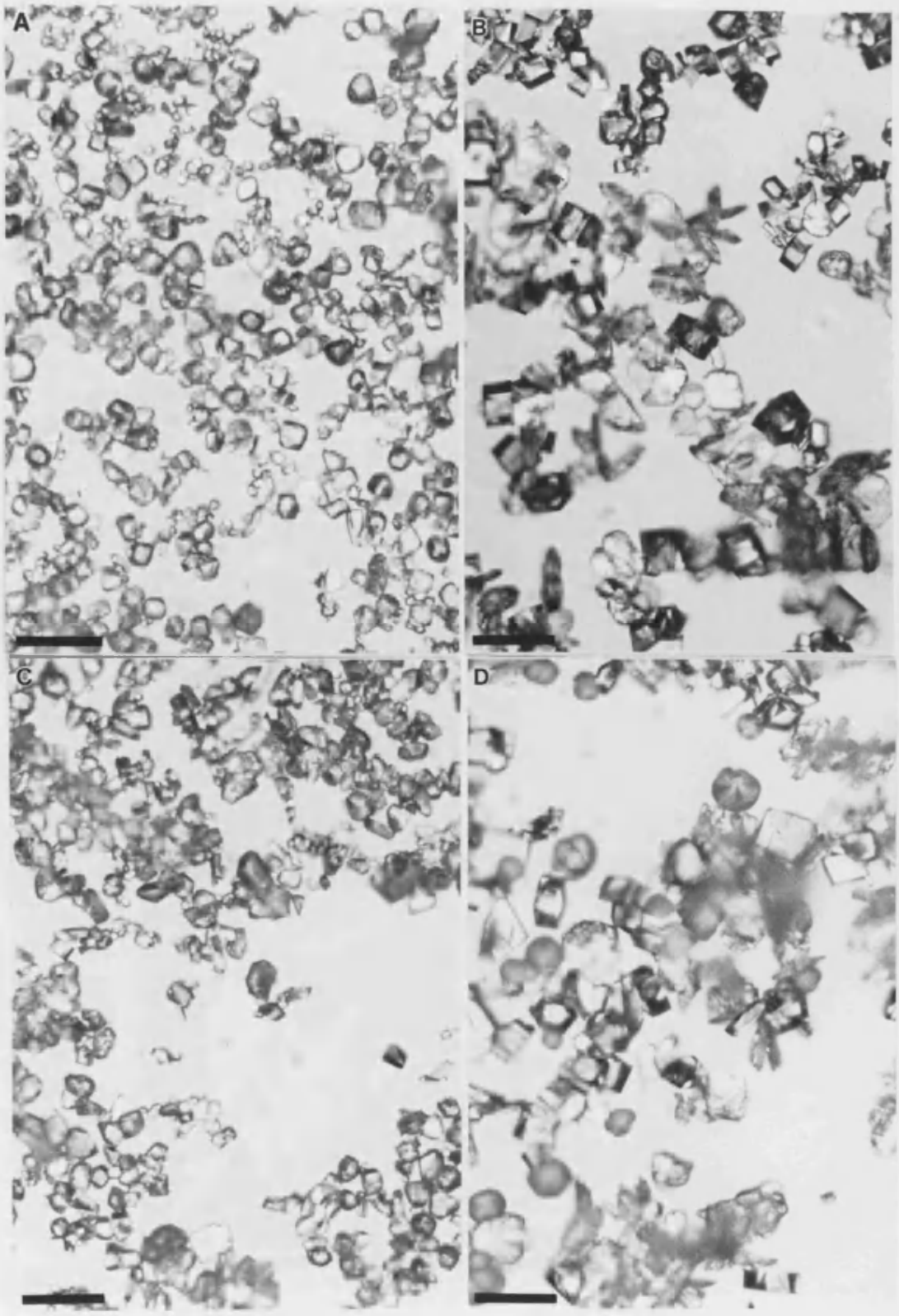

Fig. 5.11 *Optical micrographs showing the influence of (a) 3.0 μgml^{-1} and (b) 0.54 μgml^{-1} monkey osteocalcin plus (c) 3.0 μgml^{-1} and (d) 0.54 μgml^{-1} bovine osteocalcin on surface crystals. Scale bars 100 μm.*

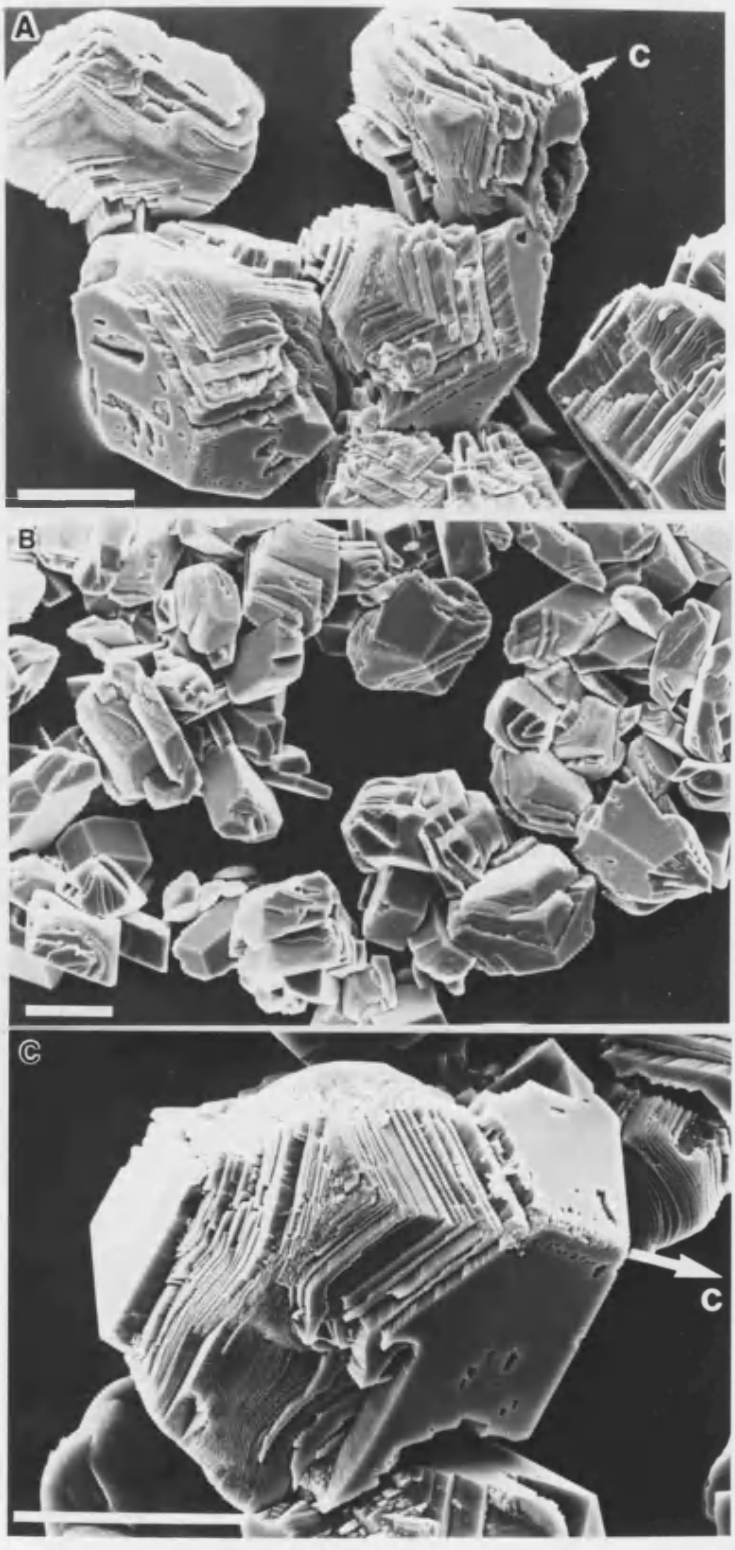

Fig. 5.12 *Scanning electron micrographs of osteocalcin (monkey)-modified surface crystals: (a) 3 μgml^{-1} (b) 1.9 μgml^{-1} and (c) 0.96 μgml^{-1}. Scale bars 20 μm.*

symmetry-equivalent faces could not be recognized and so the interactions appeared to be non-specific. Instead, the results indicated that the molecules had a high affinity for the crystals and were adsorbing on the growth steps and exposing cleavage planes. There was little discernable difference in the action of the homologous proteins from cow and monkey.

Proteoglycan Monomer

The proteoglycan stock solution (40 $mgml^{-1}$) was very viscous which inevitably caused errors in the aliquot volumes delivered. However, even the most concentrated solution had no effect on calcite morphologies eliminating vaterite instead (fig. 5.13a). SEM micrographs showed that calcite, at the bottom of the container vials, was coated in a thin film that was seen to be peeling off in places (fig. 5.13b, c). This was not the layer of gold, applied in sample preparation, because charging effects were not noticeable beneath the film. Also, it was not considered to be a drying artefact because the cover slips, on which the crystals were mounted, were thoroughly washed in distilled water and dried prior to gold coating. Insufficient proteoglycan was available to experiment with higher concentrations.

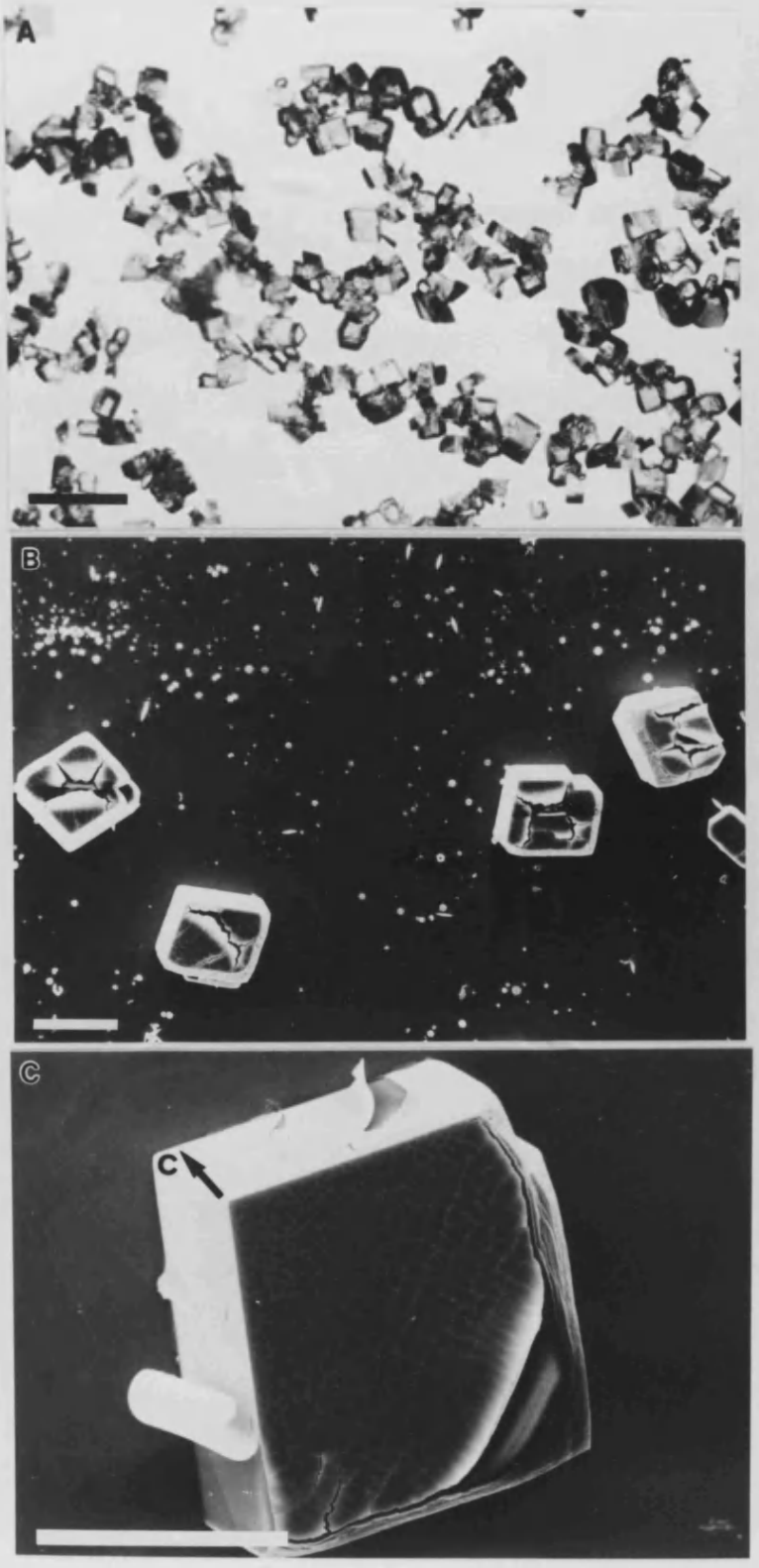

Fig. 5.13 *Micrographs showing crystals grown in the presence of proteoglycan monomer: (a) surface crystals; bar 100 μm (b and c) bottom calcite crystals; bars 20 μm.*

5.4 DISCUSSION

Morphology

The coccolith polysaccharide, alginic acid, hyperbranched polyphenylene and, to a lesser extent, the Gla proteins influenced the morphology of the calcite crystals. In the case of HBP and ALG, the interactions appeared to be quite specific for the first order prismatic faces $\{1\bar{1}00\}$. HBP was forming a fairly organized monolayer at the air/water interface and acting in the same way as stearic acid. Obviously, it is not as ordered as a compressed film which accounts for some of the differences. Nevertheless, the stearate experiments were essentially reproduced which is remarkable when one considers the dissimilarity between the two molecules. Because of the design of the hyperbranched polymer, it is severely restrained in conformation and thus will adopt a roughly spherical shape under most conditions. As such, it probably exists as a ball at the air/water interface.

Alginic acid is not a very well-characterized polysaccharide. It is known for its strong gel-forming abilities in the presence of calcium which stiffen the chains (Angyal 1973). Dilute solutions of the gelling material, agar, has also been observed to alter the morphology of calcite to spindle-shaped habits (E.J. Aso-Samper, personal communication). PSL seemed to have a pseudo-specific interaction. Specificity, in such interactions implies a high degree of order in the macromolecule consistent with some defined secondary structure. The prismatic faces expressed on the crystals can be used to infer bidentate binding of the anion groups eg carboxylates. However, based on the observations in chapter 4, the sulphates moieties can not be ruled out as possible ligands. Nevertheless, it is unlikely that sulphate is involved for PSL as they are believed to be hidden in the core of the molecule.

The apparently non-specific interaction of both the osteocalcin proteins was perhaps

surprising in view of the fact that they have well-ordered secondary structures in the presence of calcium. Moreover, the Gla residues furnish malonate moieties as functional anionic groups. One explanation maybe that at pH 6 the predominant α-helical structure, which brings the malonate moieties into register, may be unstable or may completely break down. Another possibility is that the charge density on the protein is too great and that this overrides the selectivity (Addadi *et al* 1990). The overall charge on fully ionized molecules is -9. Consideration of the primary sequence shows that the anionic residues are concentrated in one domain in the middle of the protein. It is therefore plausible that the subtle stereochemical interactions may be overwhelmed by stronger electrostatic attractions.

Stabilization of Polymorphs

Some of the macromolecules also appeared to be quite selective of the $CaCO_3$ polymorph formed. The most striking examples were the antifreeze glycopeptide and polyvinyl alcohol which stabilized vaterite. The results with the monofunctional model polymer, PVA, strongly suggested that the hydroxyl groups were responsible for this effect. In a patent, Merten and Bachman (1980) described a large variety of, so-called "hydrogen-bonding materials" (alcohols, sugars, amino acids etc) which were required to stabilize amorphous calcium carbonate. On the other hand, Lerner *et al* (1989) reported the use of ethanol/water mixtures to destabilize an amorphous phase (calcium phosphate; ACP) in favour of the thermodynamically stable polymorph (hydroxyapatite; HA). Thus, there is evidence to show that hydroxyl groups may be involved in the modification of kinetic processes in solution.

The formation of metastable phases can be considered a result of the direct inhibition of more stable polymorphs at the nucleation stage (Staab *et al*, Brooks *et al* 1950/51). This normally would require strong adsorption of the additive on the nucleus. The elemental analysis showed that the glycopeptide was associated with the vaterite crystals even after thorough washing in distilled water but was present in

only a small amount. Moreover, it has been demonstrated that the primary interaction between molecular additives and $CaCO_3$ crystal faces is electrostatic (chapter 4). Neutral hydroxyl-functionalized molecules would therefore not be expected to influence nucleation and growth to any degree. In fact, this is borne out by monolayer experiments using octadecanol which seems to have little effect on crystallization (Rajam *et al* 1991).

Another, more feasible, possibility might be related to the ability of hydroxyl groups to "make" or "break" the structure of water via hydrogen-bonding. As discussed by Lerner *et al* (1989), miscible alcohols weaken the hydration spheres surrounding dissolved ions in aqueous solution. This has the effect of aiding the dehydration process in crystal growth which, as mentioned before (chapter 3 and 4) is often the rate determining step. Enhanced rates of growth are thereby facilitated favouring kinetic or metastable products in accordance with Ostwald's Law. It is therefore proposed that AFGP and PVA directly interfere with the hydration atmospheres of lattice ions (calcium in particular) causing more rapid nucleation and thus large amounts of vaterite.

Other macromolecules such as PSL, ALG, Gla and the proteoglycan (PG) had the opposite effect on polymorphism tending to inhibit the metastable phases in favour of calcite. This was also noticed for crystallization from solutions of high ionic strength as in the case of sodium nitrate at a calcium/additive ratio of 0.01:1 (chapter 4). Thus, the polyelectrolytes studied in this chapter may be functioning in much the same way tending to screen ionic charges and so reducing the rate of nucleation.

Potency

In general, the macromolecules were very potent additives compared to the lower molecular weight compounds studied in the preceding chapter. This could be illustrated by osteocalcin which was the only monodisperse additive studied. About

3 μgml^{-1} of this protein was sufficient to cause a marked disruption in crystal growth. This corresponded to a Ca/additive molar ratio ≈ 20,000. Even if it is assumed that all 47-50 residues were Asp (in fact only about 5 are Asp, 5 Glu, 3 Gla, the majority are hydrophobic), this would correspond to a Ca/Asp ratio = 400:1 which is more than an order of magnitude more potent than the free amino acid (chapter 4).

Comparisons between macromolecules was problematic because of the polydispersity in molecular weights. However, it was evident that the most potent were Gla, ALG and PSL and the least were PG and PGU. The results with the polysaccharides were consistent with the inhibitory studies of Borman *et al* summarized in the introduction (5.1). Others investigations have noted that chondroitin sulphate (a major constituent of PG), despite being polyanionic and possessing many carboxylate groups, is a remarkably weak inhibitor of $CaCO_3$ (Simkiss 1964, Meyer 1984). PGU too is highly polyanionic although it differs from PG in that it has a much lower molecular weight and contains no sulphate. These results highlight the fact that possession of active functional groups (COO^- or OSO_3^-) and significant charge density are not the only factors contributing to the affinity of macromolecules for crystals. Additional factors may include conformation and mobility. Disordered and flexible secondary structures (eg random coils) will serve to dissipate charge density whereas α-helices or β-pleated sheets will have the opposite effect. Also, differences in the calcium binding abilities may explain disparate tendencies to affect crystallization.

Crystal Aggregation

The power to aggregate crystals appears to be connected with the presence of multifunctionality on the additive molecules. As was noticed in chapter 4 with difunctional anions eg methylene or ethylene diphosphonate. ALG, PSL, PG, Gla all possessed this ability which, as was explained in chapter 4, is probably because the

molecules can anchor to two or more nuclei simultaneously.

General Conclusions

One of the main objectives of this chapter was to ask whether other inhibitory macromolecules were specific or non-specific in their interactions with crystal faces. The coccolith polysaccharide has been proposed to be an inhibitor of crystal growth but it may also have a role in nucleation. The results in this chapter demonstrate that *in vitro* the molecule has a high affinity for calcite crystals, it excludes vaterite and can produce morphological changes that indicate a degree of specificity. However, the model polysaccharide, alginic acid, also showed these effects, and indeed seemed to be more specific, suggesting that the coccolith polysaccharide had no extra inherent capability to regulate crystal growth. Nevertheless, the results provide evidence that the macromolecule could be involved in morphological control during the biomineralization of coccoliths.

The bone Gla proteins studied appeared to be non-specific inhibitors of calcite in this crystallization system. However, this does not rule out the possibility that they could be more specific in the presence of their native mineral, hydroxyapatite. The proteoglycans too may have more of an effect with hydroxyapatite. The relatively acidic pH compared with physiological conditions may also have been a factor.

The anti-freeze glycoproteins, which normally are involved in the inhibition of ice crystals and thus are not directly relevant to $CaCO_3$ mineralization, served to highlight the fact that kinetic processes are important in these systems. The widespread presence of metastable $CaCO_3$ phases in biology, particularly aragonite and to a lesser extent vaterite, may be due to the cellular deployment of similar macromolecules that are rich in hydroxyl groups.

The hyperbranched carboxylate polymer was interesting because it illustrated the

tendency of soluble macromolecules to segregate at interfaces and thereby take part in specific regulation of crystallization. In this respect, it showed many of the features of self-assembly for the purpose carrying out particular functions. It is perhaps also feasible that organic matrix molecules could be synthesized, transported to a site and left to self-assemble at an interface in order to control mineral nucleation.

5.5 REFERENCES

Addadi, L., Weiner, S. (1985), *Interactions Between Acidic Proteins and Crystals: Stereochemical Requirements in Biomineralization,* Proc. Natl. Acad. Sci. USA, **82**, 4110-4114.

Addadi, L., Weiner, S. (1986), *Interactions Between Acidic Macromolecules and Structured Crystal Surfaces. Stereochemistry and Biomineralization*, Mol. Cryst. Liq. Cryst., **134**, 305-322.

Addadi, L., Moradian, J., Shay, E., Maroudas, N.G., Weiner, S. (1987), *A Chemical Model for the Cooperation of Sulfates and Carboxylates in Calcite Crystal Nucleation. Relevance to Biomineralization*, Proc. Natl. Acad. Sci. USA, **84**, 2732-2736.

Addadi, L., Moradian-Oldak, J., Weiner, S. (1990), *Macromolecule-Crystal Recognition in Biomineralization: Studies Using Synthetic Polycarboxylate Analogs*, in Surface Reactive Peptides and Polymers: Discovery and Commercialization, Sikes, C.S., Wheeler, A.P. (Eds.), pp 13-27, Washington: American Chemical Society.

Angyal, S.J. (1973), *Complex Formation between Sugars and Metal Ions*, Pure Appl. Chem., **35**, 131-145.

Berman, A., Addadi, L., Weiner, S. (1988), *Interactions of Sea Urchin Skeleton Macromolecules with Growing Calcite Crystals - A Study of Intracrystalline Proteins*, Nature, **331**, 546-548.

Borman, A.H., de Jong, E.W., Huizinga, M., Kok, D.J., Westbroek, P., Bosch, L. (1982), *The Role in $CaCO_3$ Crystallization of an Acid Ca^{2+}-Binding Polysaccharide Associated with Coccoliths of Emiliania huxleyi*, Eur. J. Biochem., **129**, 179-183.

Borman, A.H. (1986), *The Polysaccharide from Coccoliths of Emiliania huxleyi: Characterization and Biosynthesis*, PhD Thesis, University of Leiden, Netherlands.

Brooks, R., Clark, L.M., Thurston, E.F. (1950/51), *Calcium Carbonate and its Hydrates*, Phil. Trans. Roy. Soc. (London), **A243**, 145-167.

Carr, S.A., Hauschka, P.V., Biemann, K. (1981), *Gas Chromatographic Mass Spectrometric Sequence Determination of Osteocalcin, a γ-Carboxyglutamic Acid-containing Protein from Chicken Bone*, J. Biol. Chem., **256(19)**, 9944-9950.

Chen, C., Boskey, A.L., Rosenberg, L.C. (1984), *The Inhibitory Effect of Cartilage Proteoglycans on Hydroxyapatite Growth*, Calcif. Tissue Int., **36**, 285-290.

De Jong, E.W., Westbroek, P., Bosch, L., (1976), *Isolation and Characterization of a Ca^{2+}-Binding Polysaccharide Associated with Coccoliths of Emiliania huxleyi (Lohmann) Kamptner*, Eur. J. Biochem., **70**, 611-621.

DeVries, A.L. (1988), *The Role of Antifreeze Glycopeptides and Peptides in the Freezing Avoidance of Antarctic Fishes*, Comp. Biochem. Physiol., **90B(3)**, 611-621.

Hamilton, S.E., King, G., Tesch, D., Riddles, P.W., Keough, D.T., Jell, J., Zerner, B. (1982), *γ-Carboxyglutamic Acid in Invertebrates: Its Identification in Hermatypic Corals*, Biochem. Biophys. Res. Comm., **108(2)**, 610-613.

Hauschka, P.V. (1981), *Osteocalcin Structure: Ca^{2+}-Dependence of α-Helical Domains*, in "The Chemistry and Biology of Mineralized Connective Tissues", Veis, A. (Ed.), Amsterdam: Elsevier North Holland.

Kim, Y.H., Webster, O.W. (1990), *Water-Soluble Hyperbranched Polyphenylene: "A Unimolecular Micelle ?"*, J. Am. Chem. Soc. **112**, 4592-4593.

Lerner, E., Azoury, R., Sarig, S. (1989), *Rapid Precipitation of Apatite from Ethanol-Water Solution*, J. Cryst. Growth, **97**, 725-730.

Merten, H.L., Bachman, G.L. (1980), Monsanto Company, St Louis, USA, *Stabilized Amorphous Calcium Carbonate*, US Patent no. 4,237,147.

Meyer, H.J. (1984), *The Influence of Impurities on the Growth of Calcite*, **66**, 639-646.

Poser, J.W., Esch, F.S., Ling, N.C., Price, P.A. (1980), *Isolation and Sequence of the Vitamin K-Dependent Protein from Human Bone*, J. Biol. Chemistry, **255(18)**, 8685-8691.

Price, P.A., Otsuka, A.S., Poser, J.W., Kristaponis, J., Raman, N. (1976), *Characterization of a γ-Carboxyglutamic Acid-containing Protein from Bone*, Proc. Natl. Acad. Sci. USA, **73(5)**, 1447-1451.

Rajam, S. Heywood, B.R., Walker, J.B.A, Mann, S., Davey, R.J., Birchall, J.D., *Oriented Crystallization of $CaCO_3$ under Compressed Monolayers; Part 1*, J. Chem. Soc. Faraday Trans., **87(5)**, 727-734.

Raymond, J.A., Wilson, P., DeVries, A.L. (1989), *Inhibition of Growth of Nonbasal Planes in Ice by Fish Antifreezes*, Proc. Natl. Acad. Sci. USA, **86**, 881-885.

Sikes, C.S., Yeung, M.L., Wheeler, A.P. (1990), *Inhibition of Calcium Carbonate and Phosphate Crystallization by Peptides Enriched in Aspartic Acid and Phosphoserine*, in Surface Reactive Peptides and Polymers: Discovery and Commercialization, Sikes, C.S., Wheeler, A.P. (Eds.), pp 50-71, Washington: American Chemical Society.

Simkiss, K. (1964), *The Inhibitory Effects of Some Metabolites on the Precipitation of $CaCO_3$ from Artificial and Natural Seawater*, J. Consol. Internat. l'Explor. Mer., **29**, 6-18.

Staab, E., Addadi, L., Leiserowitz, L., Lahav, M. (1990), *Control of Polymorphism by 'Tailor-Made' Polymeric Crystallization Auxiliaries. Preferential Precipitation of a Metastable Polar Form for Second Harmonic Generation*, Adv. mater. **2(1)**, 40-43.

Wheeler, A.P., George, J.W., Evans, C.A. (1981), *Control of $CaCO_3$ Nucleation and Crystal Growth by Soluble Matrix of Oyster Shell*, Science, **212**, 1397-1398.

Wheeler, A.P., Sikes, C.S. (1988), *Control of $CaCO_3$ Crystallization by Polyanionic-Hydrophobic Polypeptides,* in Chemical Aspects of Regulation of Mineralization, pp 15-20, Mobile, Alabama: University of South Alabama Publications.

CHAPTER 6

Crystallographic Studies on the Immature Coccoliths of Emiliania huxleyi

6.1 INTRODUCTION

Coccoliths are units that comprise the exoskeleton of certain single-celled marine algae (Haptophyta), the so-called coccolithophores (fig. 6.1). These simple, microscopic organisms drift or float passively near the surface in the world's oceans. They are grouped together with the diatoms, dinoflagellates and microflagellates and collectively known as the phytoplankton. They are of great ecological importance being the primary producers of organic food in the marine environment and thus the first link in the food chain that supports many other forms of life. Furthermore, recent concerns over the "Greenhouse Effect" have focused on the role of all such phytoplankton in the global carbon cycle and hence the distribution of carbon dioxide in the atmosphere.

Description of the species E. huxleyi

One of the most important and best studied coccolithophores is the species *Emiliania huxleyi* (Lohmann 1902, Hay & Mohler 1967) previously known as *Coccolithus huxleyi* (Kamptner 1941). They are abundant in the Atlantic and Pacific oceans and can be easily cultured in a laboratory for use in systematic studies. At present, there are four common strains in culture which are actually two very similar pairs named L and 92, 92D and MCH. Each spherical cell is usually non-motile, about 5-10 μm in diameter and has a complete covering of coccolith plates termed the *test* or *coccosphere.* Non-calcifying cells are known and are of great physiological interest. The actual function of coccoliths themselves is uncertain although suggestions have included armoured protection, buoyancy control and light regulation (Young 1987).

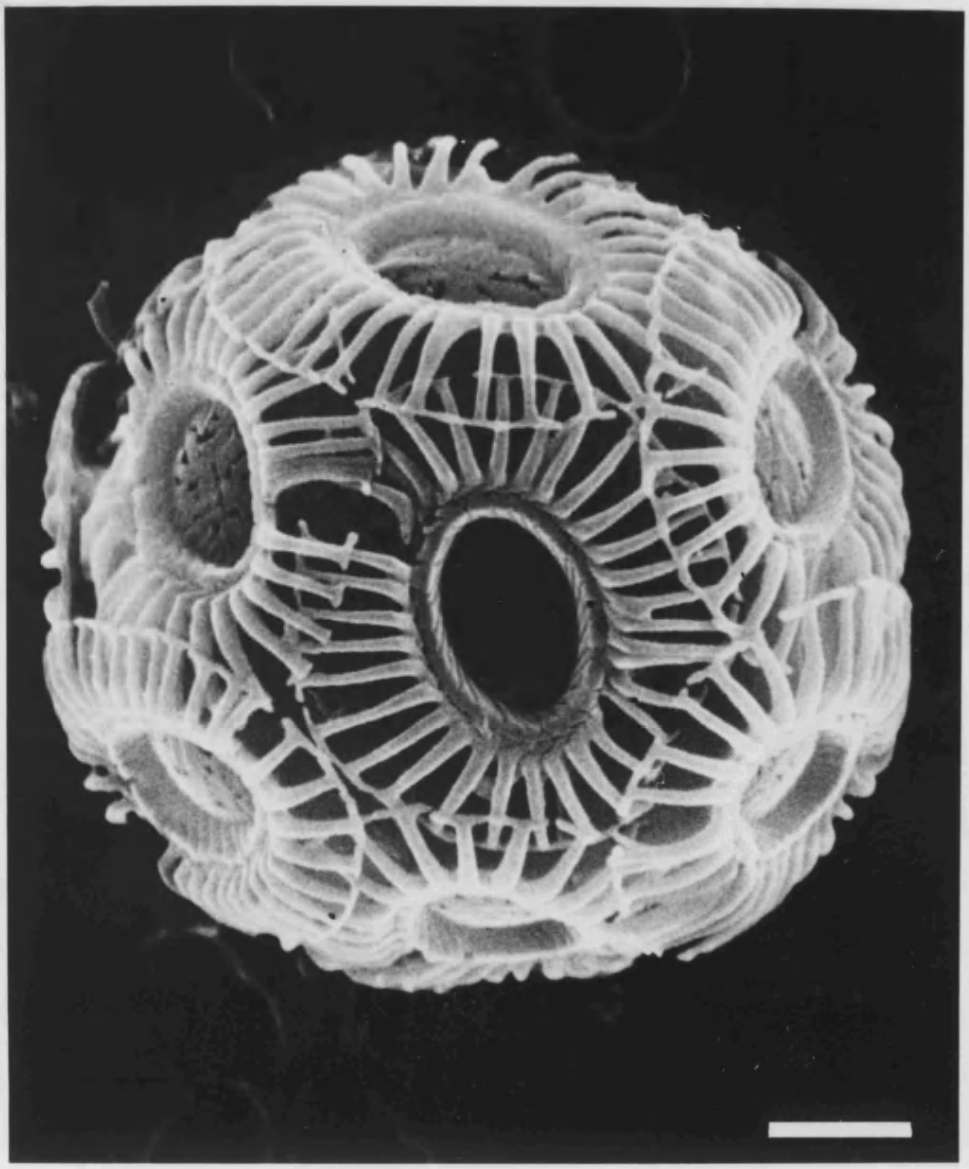

Fig. 6.1 *Scanning electron micrograph of a whole, coccolith-covered, cell of E. huxleyi. Scale bar 1 μm. Courtesy of Dr J. Young.*

Coccolith Formation in E. huxleyi

The biomineralization of coccoliths is a intriguing process in itself. Whole cell thin sectioning techniques have revealed that each coccolith is made, one at a time, in a specialised intracellular compartment (Wilbur and Watabe 1963, Klaveness 1972). Simple crystals form to begin with which then develop, in close association with the compartment, into the mature structure. The finished product (fig. 6.2) is then extruded to the outer cell surface and assembled, by an unknown mechanism, within the coccosphere which can be several layers thick in some strains. This manufacturing process occurs every 2 hours on average during the day but ceases in the dark which has prompted many to examine the apparent link between photosynthesis and calcification.

Cell Ultrastructure of E. huxleyi

The internal anatomy of the cell is representative of Haptophyta. Organelles include the nucleus, chloroplasts, mitochondria and the Golgi apparatus. The main body associated with intracellular coccoliths is the *reticular body* (RB) and is located closely apposed to the nucleus. Within the plasma membrane of the reticular body, there exists a completely detached linear vesicle or plate which forms prior to calcification. Crystal nuclei are first observed to deposit close to this plate. As the coccolith grows, it is surrounded by a membrane, the outline of which can be discerned after decalcification (Wilbur and Watabe 1963, Klaveness 1972). The membrane structure is termed the *coccolith vesicle* (CV) and the whole coccolith producing area the CV-RB complex. Any specific crystal nucleation template (*organic matrix*) would presumably exist at the base of the coccolith vesicle or in the adjacent, underlying region of reticular body.

Biochemical Investigations

The coccolith plates can be isolated from the cells by sonication and centrifugation. On dissolution in EDTA, two macromolecular fractions are obtained. The first is a

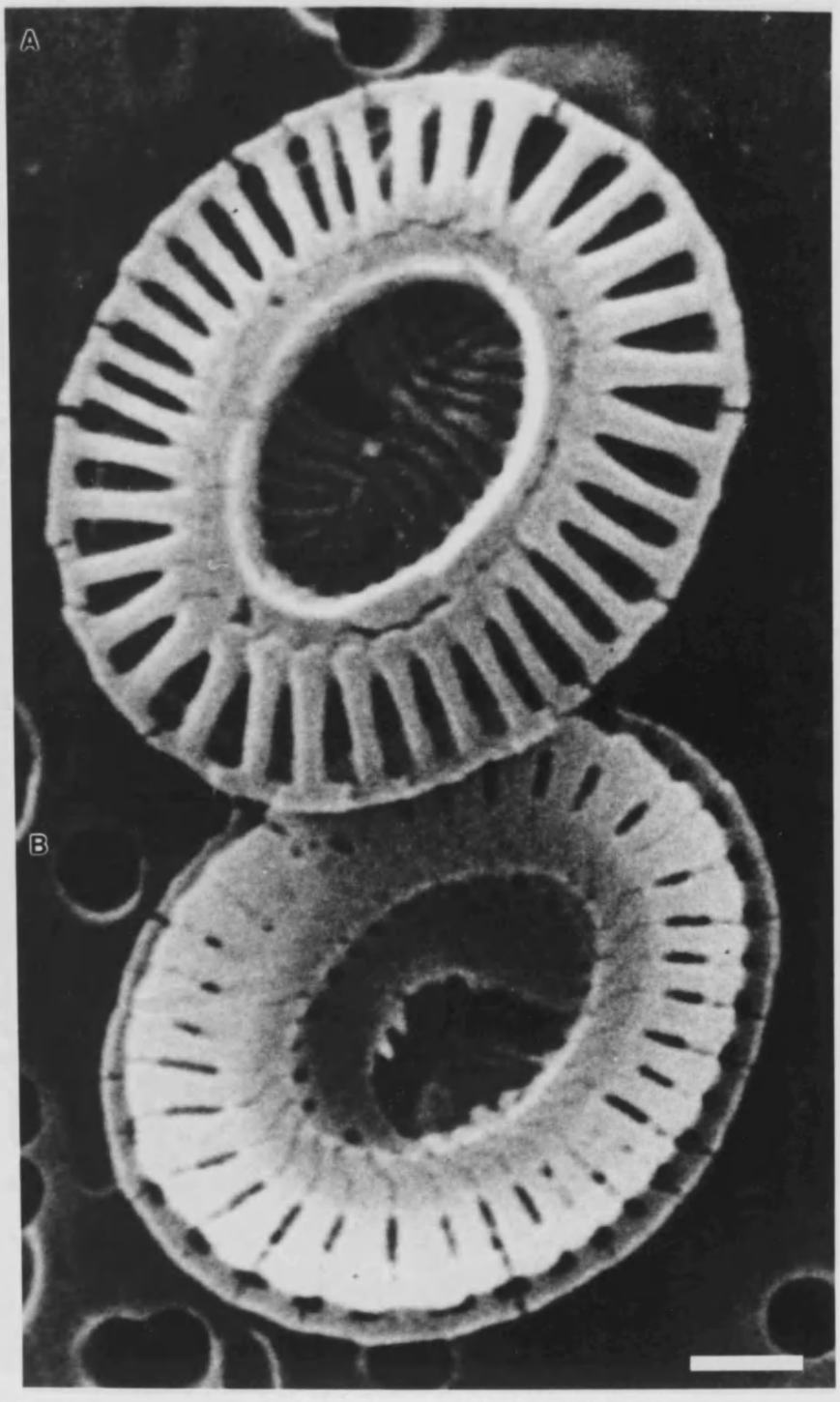

Fig. 6.2 *Scanning electron micrographs of individual coccoliths: (a) distal view and (b) proximal view. Scale bar 0.5 μm. Also courtesy of Dr J. Young.*

water insoluble substance which has been shown to be a glycoprotein. A water soluble fraction contains an complex acidic polysaccharide, the structure, of which, has been partially elucidated (de Jong *et al* 1976, Fitchinger-Schepman *et al* 1981, Borman *et al* 1982). Immunocytochemical stains, specific for the polysaccharide, have demonstrated its presence throughout the CV-RB complex and in the Golgi apparatus (Van Emburg *et al* 1989).

Coccolithogenesis

A recent hypothesis for coccolithogenesis has been put forward by Westbroek *et al* (1989) (fig. 6.3). They have postulated that the CV-RB complex is formed when vesicles, encapsulating polysaccharide, Ca^{2+} and CO_3^{2-}, pinch off from the Golgi body and diffuse to a site close to the nuclear membrane. Precipitation of $CaCO_3$ within the CV-RB complex is inhibited by the polysaccharide. Whilst anchored to the nuclear membrane, further vesicles are supplied from the Golgi body and the coccolith vesicle expands to the shape of the future coccolith. The organic matrix is established at this stage. A hollow space is then created along the periphery of this compartment and the polysaccharide withdrawn enabling the onset of crystallization. The organic matrix controls the initial crystallographic orientation and further growth occurs into the surrounding mould as new material is supplied from the reticular and Golgi bodies. The covering of polysaccharide on the inside of the cavity ensures termination of crystal growth.

Morphology and Crystallography of Coccoliths

The fine structure of coccoliths was first examined, when electron microscopes became generally available, in the early 1950's. Since then, the crystallographic structure of *E. huxleyi*, in particular, has been well studied (Watabe 1967, Parker *et al* 1983, Mann and Sparks 1988). Each coccolith scale is an elliptical array of about 30-35 interlocking, single-crystalline units of calcite arranged with their *c* axes approximately radially disposed (fig. 6.4 and 6.2). Morphologically, the units are

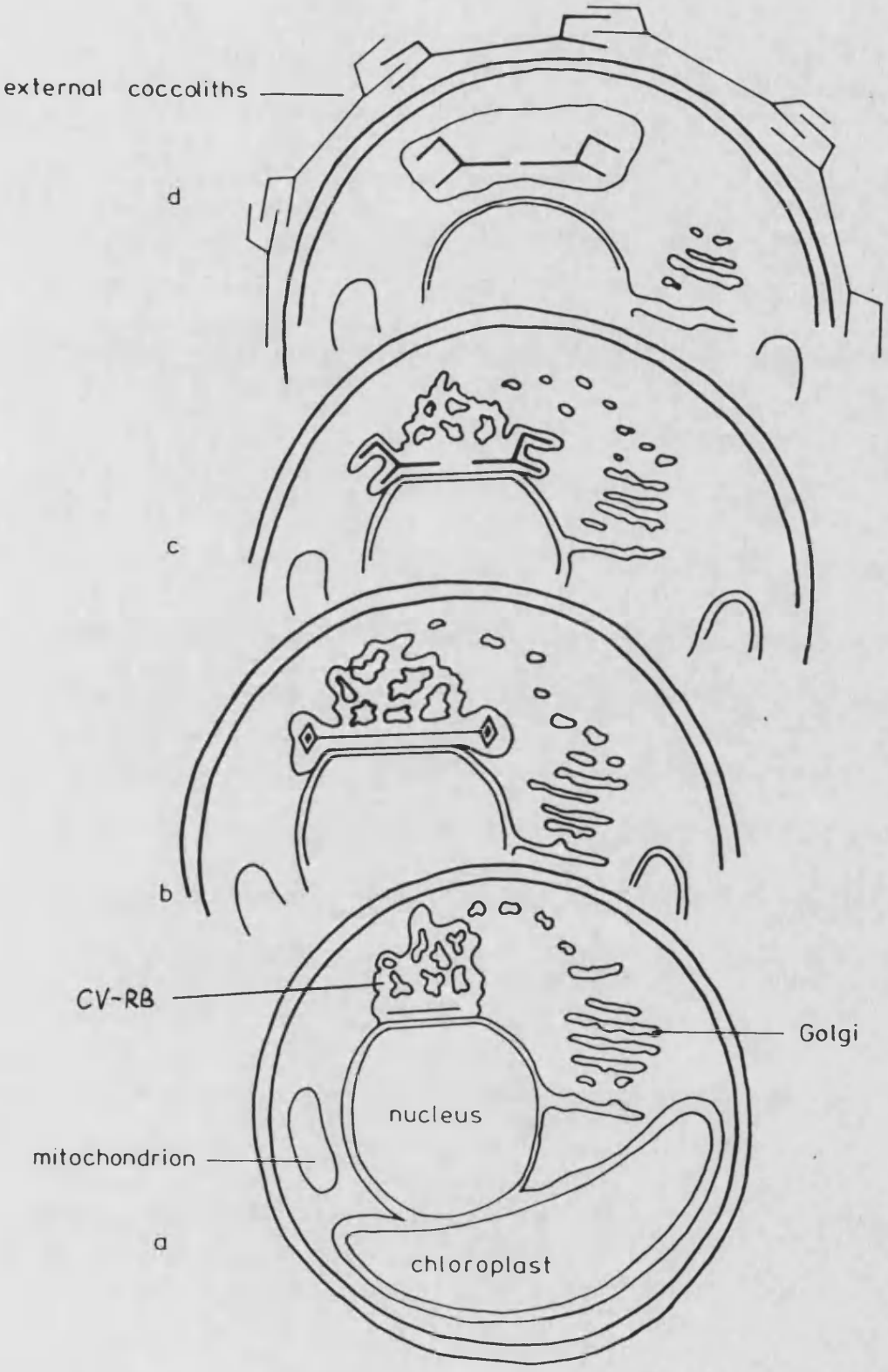

Fig. 6.3 *The Hypothesis for intracellular coccolith formation proposed by Westbroek et al (1989). See text for explanation. Redrawn from above reference.*

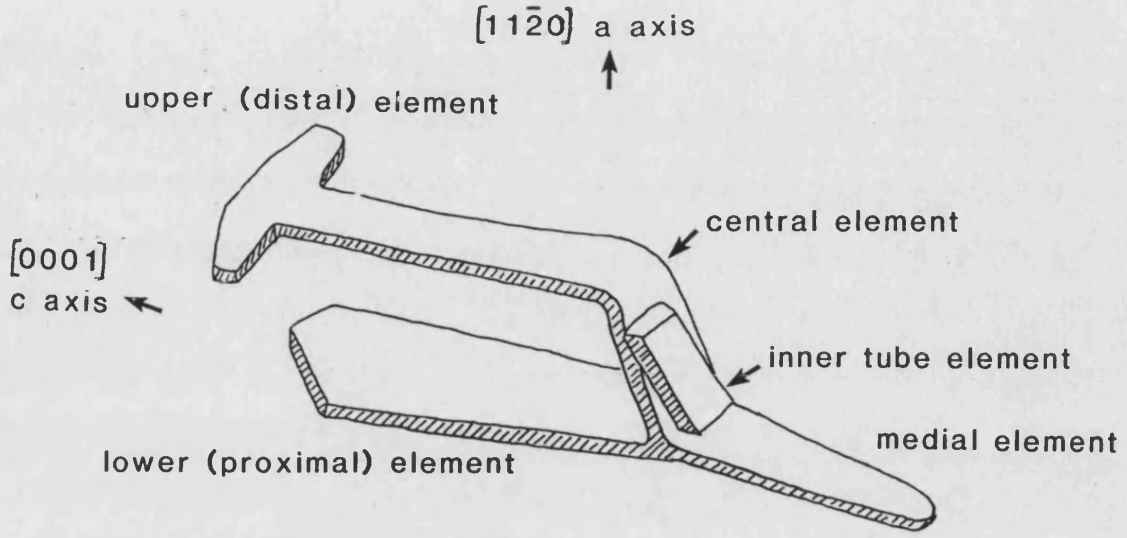

Fig. 6.4 Drawing of single-crystalline unit showing the various elements and crystallographic directions

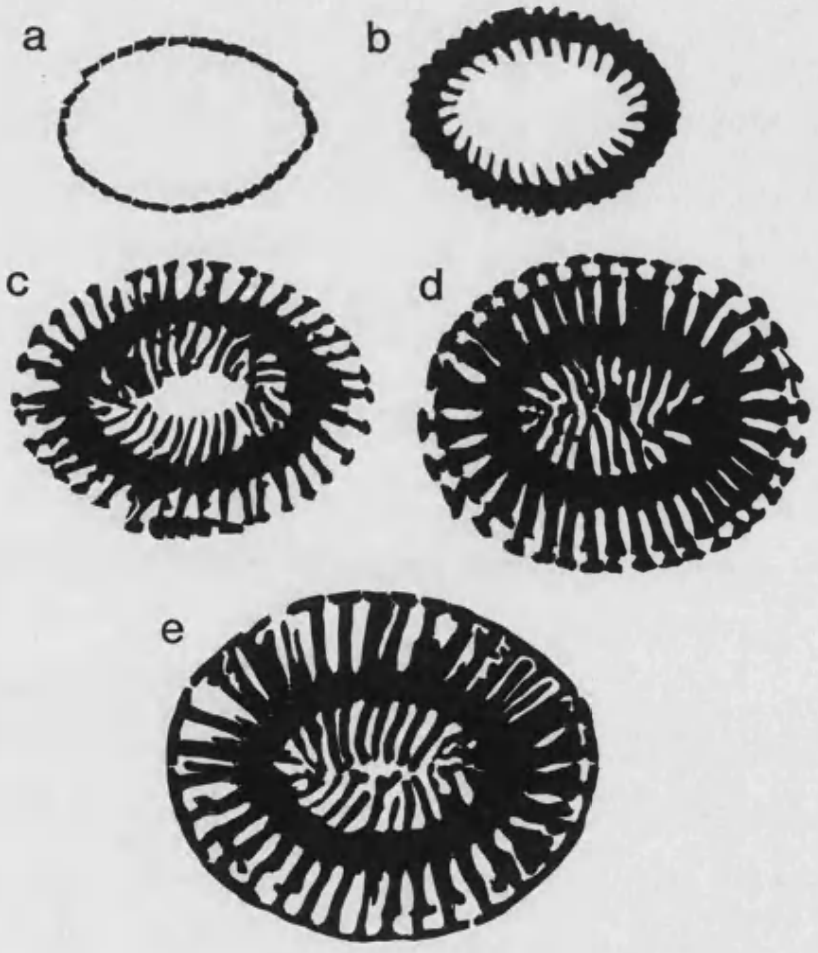

Fig. 6.5 Drawings depicting the ontogenetic development of an individual coccolith (Young (1989) unpublished data)

elaborate and non-crystallographic having five distinct elements. Precise intergrowth of all these units results in a robust structure having two, slightly curved, roughly parallel or concentric shields connected by a central wall. The overall design of the coccolith plate appears to be functional because the twin-shield shape facilitates interlinking to form a rigid shell and the curvature enables them to sit snuggly on the extracellular surface. The lower shield in direct contact with the cell is termed *proximal* and the other *distal* (fig. 6.2). In terms of general nomenclature, high radial symmetry is typical of the *heterococcoliths* and the possession of dual shields plus connecting tube classifies the *placoliths.*

One of the most fascinating features of these coccoliths is their morphological handedness or chirality. The lower proximal element, which is a thin prismatic (*a* face) plate, is truncated by distinctive $(10\bar{1}4)$ and $(\bar{1}018)$ rhombs. Viewed distally (ie from above the cell), the $(\bar{1}018)$ is always located on the left (Mann and Sparks 1988). This indicates a consistent selection of the *-a* face over the symmetry-related *+a* face surface during coccolith formation. Because the faces are structurally identical, some sort of chiral recognition process appears to be operation. The upper "hammer-shaped" elements also point in a similar direction thus the coccolith is right-handed (clockwise) in distal view and consequently left-handed in proximal view (fig. 6.1). In contrast, the inner tube cycle of elements have an opposite sense of imbrication and are thus left-handed in distal view.

Early Stages of Mineralization

Thin sections of cells in the process of forming intracellular coccoliths have shown that the earliest crystals are simple and most probably rhombohedral in morphology (Wilbur and Watabe 1963; p103, Van Emburg 1989; p29). When isolated from the cell, the so called *proto-coccolith ring* appears as a "necklace" of discrete, well-defined, euhedral nuclei in an elliptical array (Young 1989). Van Emburg (1989) was able to image the ring in its native intracellular environment.

Interestingly, it did not appear as a flat, planar ring but possessed a degree of curvature probably due to its location on the spherical nuclear envelope. Each component crystal in the ring develops into a mature segment. Ontogenetic growth sequences (ie of individual crystals) can be pieced together from TEM observations of many coccoliths at different stages of development (fig. 6.5) (Young, Van Emburg 1989).

Aim of this work

This study aimed to probe the structural nature of the proto-coccolith ring in greater detail. In particular, to clarify the initial crystallographic orientation and morphology of the proto-coccolith crystals and to gain improved understanding of the growth processes involved. Another objective was to re-examine the reported formation of vaterite and aragonite coccoliths of *E. huxleyi* grown in nitrate-depleted culture media (Wilbur and Watabe 1963) by attempting to reproduce the experiments.

6.2 MATERIALS AND METHODS

All coccolith material was obtained from Dr Jeremy Young of the Natural History Museum, London. Proto-coccoliths of *E. huxleyi* (strain L) were present in samples taken during the log phase of growth, cultured in high nutrient media. Samples were generally supplied as suspensions in weak NH_4HCO_3 solution.

Strain L was also used in experiments employing a comprehensive range of different nitrate and phosphate depleted media (conducted by Dr Jeremy Young). These coccoliths were similar to the strain (BT6) raised by Wilbur and Watabe (1963). Aqueous samples were freeze-dried and a few milligrams analysed by powder XRD using the Philips PW 1130 diffractometer (Cu K_α). A modern sediment ooze from the South Atlantic, collected by Challenger station 166, was also examined.

Specimens were prepared for transmission electron microscopy (TEM) by dropping mildly sonicated suspensions onto electron microscope grids and air-drying. Scanning electron microscopy (SEM) samples were prepared by lightly gold coating some of the TEM grids. SEM was carried out on a Hitachi S800 at the Natural History Museum (London). TEM, high resolution TEM (HRTEM), selected area electron diffraction (SAED) and energy dispersive X-ray analysis (EDXA) was conducted with the JEOL 2000FX. Electron illumination levels were kept as low as possible whilst working with the specimens to avoid beam damage. During the recording of lattice images (HRTEM), the correction for astigmatism and position of defocus was adjusted on an area of carbon close to the desired object. This object could then be manoeuvred into the field of view and the micrograph taken. Immediately after the exposure was completed, the object was again removed from the electron beam. Because of the diminutive size of the individual proto-coccolith crystals (≈ 0.15 μm) in comparison to the diameter of the image of the smallest field limiting aperture (0.45 μm), interference from neighbours was common and hence single crystal diffraction patterns were difficult to obtain. The situation could be improved by choosing individuals with a higher contrast (lower electron translucency) in bright field and positioning the aperture off the edge of these crystals. Patterns were indexed and interplanar/interzonal angles calculated as described in chapter 2.8 based on the simplest hexagonal unit cell of calcite (a = 4.99 Å, c = 17.0 Å).

6.3 RESULTS

Proto-coccolith Rings

A typical low magnification TEM micrograph of a sample is given in fig. 6.6. Whole coccoliths at various stages of development plus assorted fragments can clearly be seen. The proportion of proto-coccolith rings in any sample on the grid tended to be quite low. Thus, during the course of the study only 24 rings were studied in total. The majority of the rings were buckled or twisted to varying degrees

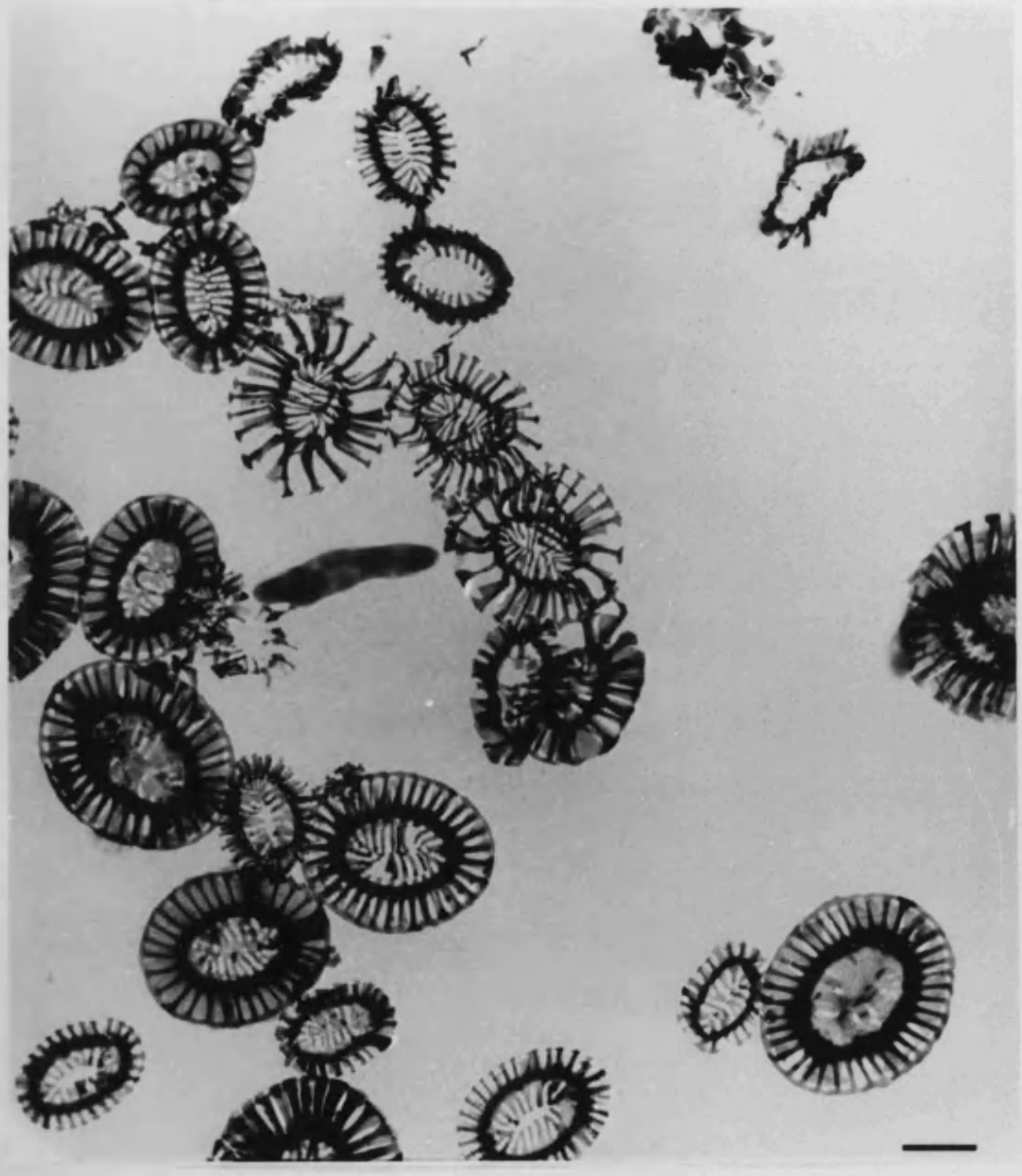

Fig. 6.6 *Low magnification transmission electron micrograph of a sample showing coccoliths at various stages of formation. Scale bar 1 μm.*

and were often broken. This probably reflected the relatively harsh preparation techniques employed or perhaps indicated something of the native intracellular orientation first observed by Van Emburg (1989). The well-organized, elliptical rings, composed of clearly separated crystals, were presumably held together by some kind of organic sheath that enveloped the structure. This skin is conceivably the coccolith vesicle reported by previous workers in whole cell thin sections.

Several close-ups of these rings are shown in fig. 6.7. The approximately elliptical dimensions were measured to be 1.0-2.0 μm (average 1.6 μm) major axis, 0.6-1.4 μm (average 1.0 μm) minor axis and the number of crystals per ring was 25-40 (average 31). EDXA of whole rings and ring sections detected Ca, C and O only (fig. 6.8a) thus indicating the presence of pure calcium carbonate. There was no evidence for other elements such as Mg or S. All electron diffraction data showed conclusively that the polymorph was calcite. Coccolith material composed of vaterite or aragonite crystals was not observed.

Proto-coccolith Crystals

Even though the high resolution TEM was capable of imaging particles less than 1 nm, R-unit nuclei no less than about 60 nm square were observed. This may have reflected a lack of durability in rings with crystals smaller than this size or perhaps the biological process was only able to eject proto-coccoliths above a certain size limit. In general, nuclei were between 80-130 nm in the radial or the circumferential dimension.

Lattice imaging revealed coherent fringes across the entire area of many individual proto-coccolith crystals confirming their single crystalline nature (fig. 6.9). $(01\bar{1}2)$, $(10\bar{1}4)$ and (0006) were commonly seen although multiple sets of fringes were rare. The crystals varied in electron translucency across their surfaces appearing darker in some areas (fig. 6.10) which was probably due to bending deformations and

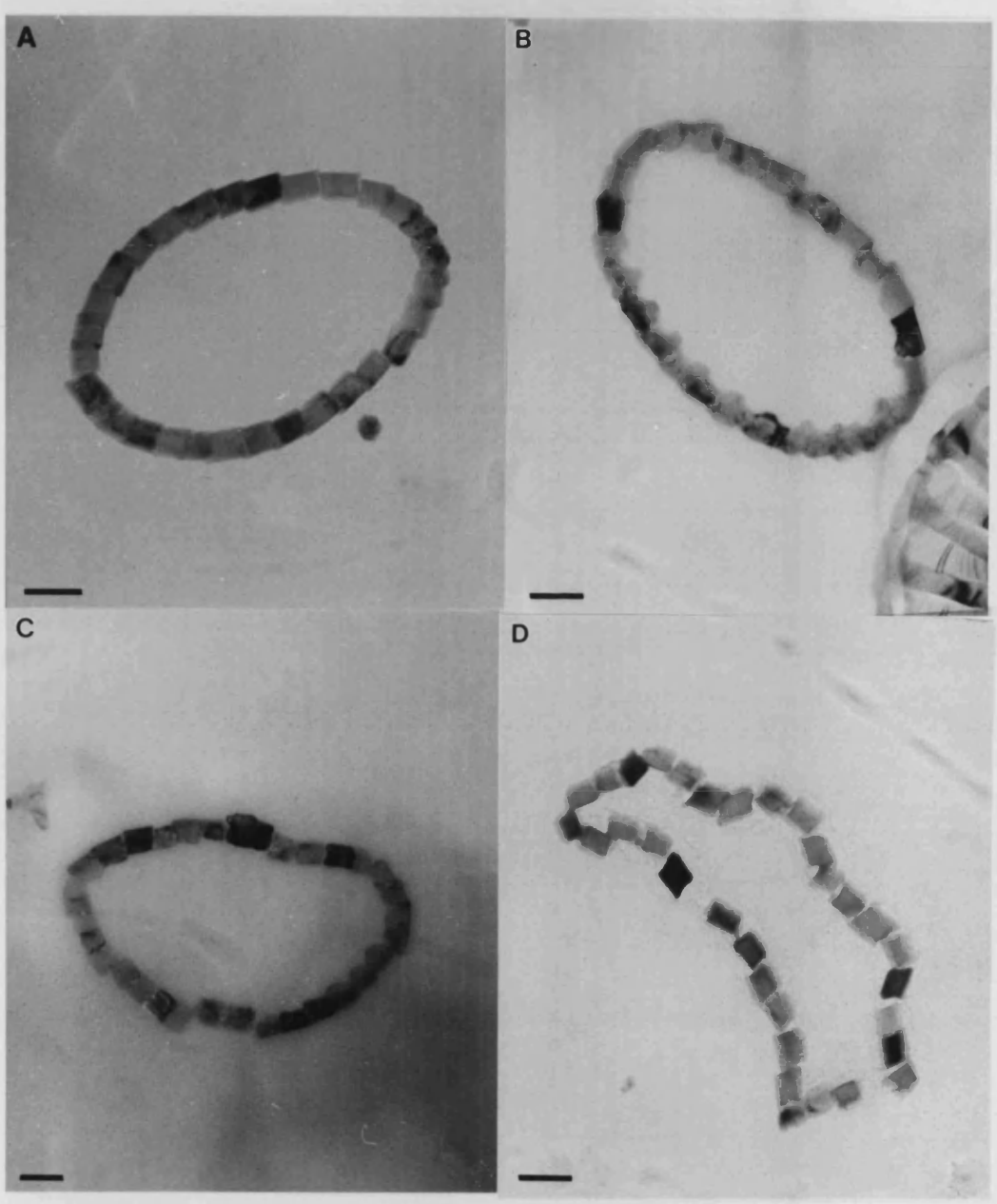

Fig. 6.7 *Transmission electron micrographs of proto-coccolith rings. Scale bars 200 nm.*

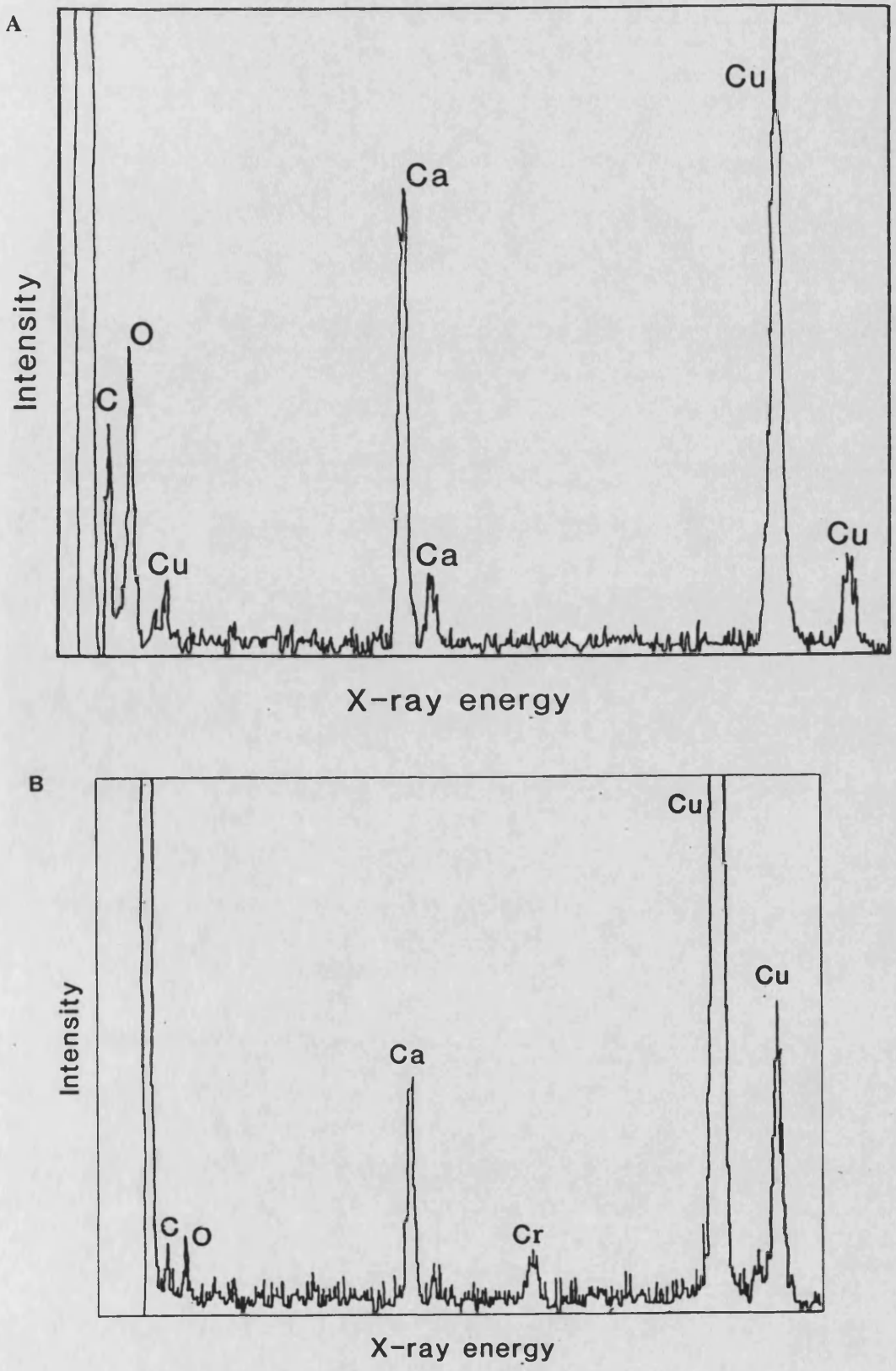

Fig. 6.8 *EDXA spectra taken from (a) whole proto-coccolith ring and (b) a flake of F. profunda. Cu peaks were from the sample holder.*

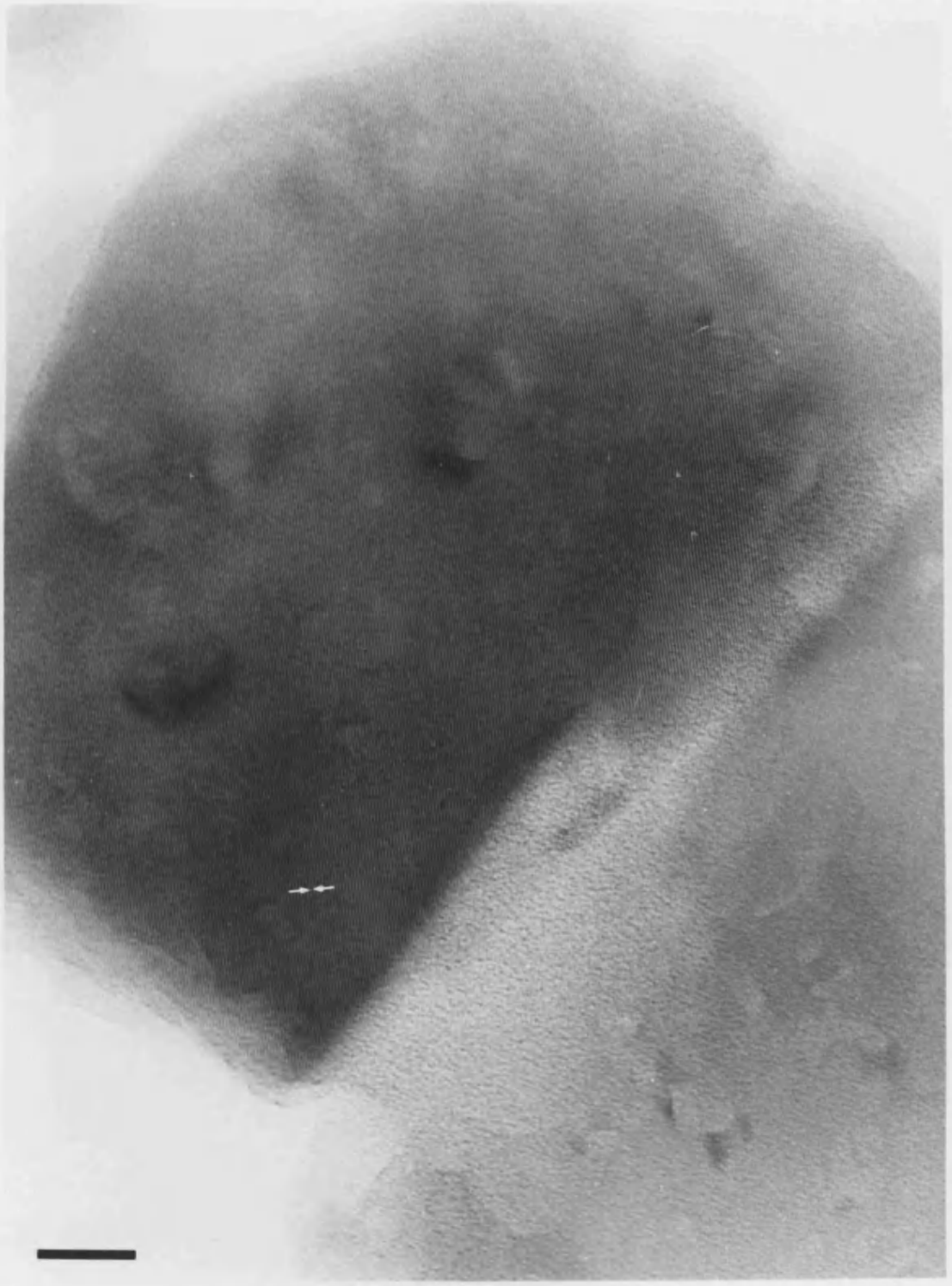

Fig. 6.9 *Lattice image of a single proto-coccolith crystal showing coherent* $(\bar{1}012)$ *fringes (3.8 Å). Scale bar 10 nm.*

Fig. 6.10 *Lattice image of another single proto-coccolith crystal also showing* $(\bar{1}012)$ *fringes (3.8 Å). Scale bar 10 nm.*

indicated their thin, plate-like nature. Some crystals had straight edges but many exhibited curved or roughened, non-crystallographic morphologies typical of membrane-bound $CaCO_3$ biominerals.

SAED was carried out in order to determine the crystallographic features of the crystals. Table 6.1 summarizes the observed orientations relative to the incident electron beam in the microscope. A variety of different zone axes were recorded. Closer inspection of the interzonal angles revealed two preferred orientations for the crystals namely <$\bar{1}$101> (plus <$\bar{4}$401>: 7 in total) and <$\bar{2}$110> (plus <$\bar{3}$211>, <$\bar{3}$122>, <$\bar{5}$231>: 8 in total). The <$\underline{\bar{1}\bar{0}}$.823> and <$\bar{8}$621> zones corresponded to directions in between the two principal orientations. Aspect ratio data (radial divided by the circumferential length), measured from each diffracting crystal, was a little uncertain because of the range of developing morphologies present. However, similar values for the <$\bar{2}$110> were evident indicating equant morphologies whereas the <$\bar{1}$101> and intermediate zones <$\underline{\bar{1}\bar{0}}$.823> and <$\bar{8}$621> corresponded to elongated crystals.

Using an inverse transformation matrix, it was possible to determine the planes or faces normal to these principal directions in calcite (see Appendix 3). The [$\bar{2}$110] vector is normal to the ($\bar{2}$110) (*a* face) whereas the [$\bar{1}$101] is perpendicular to a low angle, negative rhomb *e* (01$\bar{1}$8). It should be noted that, based on the diffraction data, the positive form (10$\bar{1}$8) could equally of been chosen. However, Dana (1932) refers exclusively to the (01$\bar{1}$8) in his extensive study of natural morphologies and so the negative form was assumed here. Thus, in conclusion, the electron diffraction study was able to infer the presence of well-developed *a* {$\bar{2}$110} and *e* {01$\bar{1}$8} faces on the crystals which caused them to rest on the grid with the observed orientations.

Recorded zone axis	<$\bar{1}$101>	<$\bar{3}$211>	<$\bar{2}$110>	<$\bar{8}$621>	<$\underline{1}\bar{0}$823>	<$\bar{4}$401>	<$\bar{5}$231>	<$\bar{3}$122>
Frequency	6	4	2	2	2	1	1	1
Aspect ratio	0.6-1.6	0.9-1.1	0.8-1.0	0.5-1.2	0.6	1.2	0.8	0.9

Interzonal Angles:
[$\bar{1}$101] ^ [$\bar{3}$211] = 46.5°
[$\bar{1}$101] ^ [$\bar{2}$110] = 60.0°
[$\bar{3}$211] ^ [$\bar{2}$110] = 13.5°
[$\bar{1}$101] ^ [$\underline{1}\bar{0}$823] = 30.7°
[$\bar{2}$110] ^ [$\underline{1}\bar{0}$823] = 30.4°
[$\bar{1}$101] ^ [$\bar{4}$401] = 10.6°
[$\bar{2}$110] ^ [$\bar{4}$401] = 60.0°
[$\bar{1}$101] ^ [$\bar{5}$231] = 62.8°
[$\bar{3}$122] ^ [$\bar{2}$110] = 10.8°
[$\underline{1}\bar{0}$823] ^ [$\bar{8}$621] = 7.0°

Table 6.1 *Results of electron diffraction on proto-coccolith crystals showing observed zone axes*

Fig. 6.11 shows TEM images of well-formed proto-coccolith ring sections plus associated diffraction patterns corresponding to the commonly observed [$1\bar{2}10$] (symmetry-equivalent to [$\bar{2}110$]) and [$\bar{1}101$] zones of calcite. The patterns can be superimposed on the dark middle crystals hence allowing the assignment of crystallographic directions and faces. In fig. 6.11a, the straight inner and outer edges correspond to {$10\bar{1}4$} and the *c* axis can be seen to emerge from two opposing obtuse vertices. Fig. 6.11b shows the *a* axis direction of a different crystal at a slightly later stage of development.

Ontogenetic Development of Proto-coccolith Crystals

The earliest observed nuclei were simple, semi-euhedral and slightly separated crystals of about 90-120 nm square (fig. 6.12a and 6.13a). They varied substantially in diffraction contrast which was due to the twisting of the ring out of the plane of the ellipse. A very notable feature of many units was their "Z" shape in projection

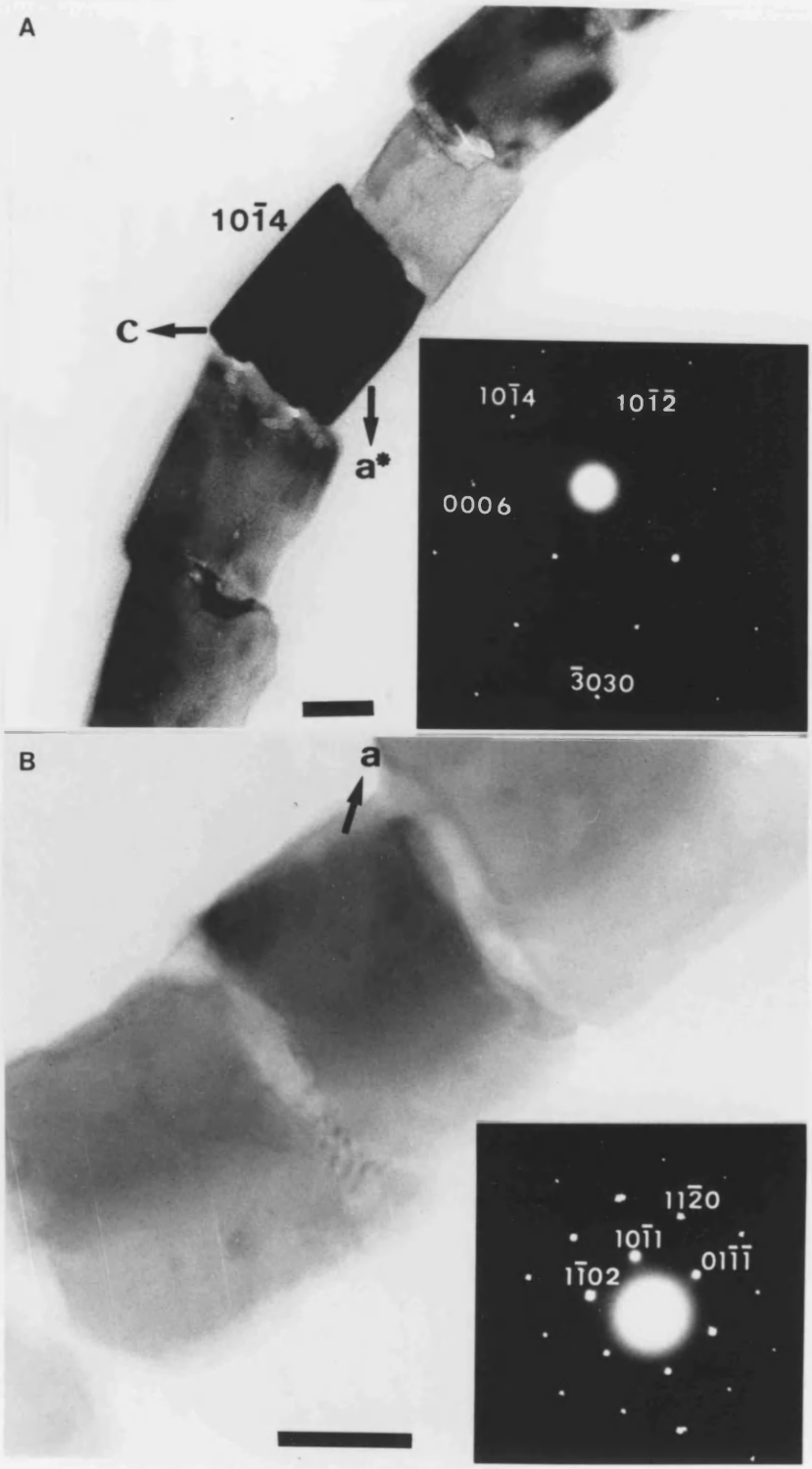

Fig. 6.11 *Transmission electron micrographs and associated selected area electron diffraction pattern for proto-coccolith crystals: (a) corresponding to the <1$\bar{2}$10> and (b) <$\bar{1}$101> zone of calcite. Scale bars 50 nm.*

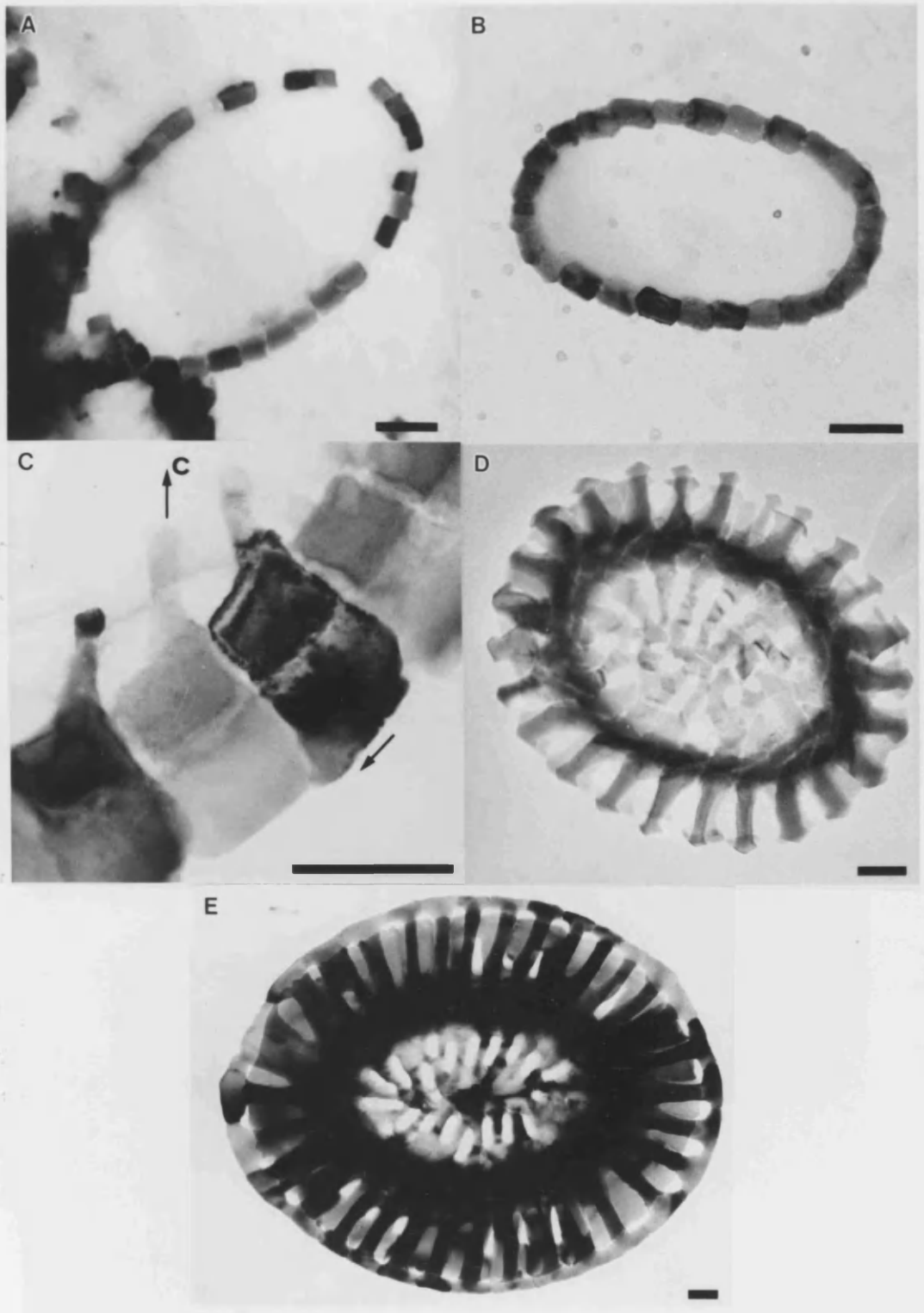

Fig. 6.12 *Transmission electron micrographs illustrating the ontogenetic development of an individual coccolith. Scale bars 200 μm.*

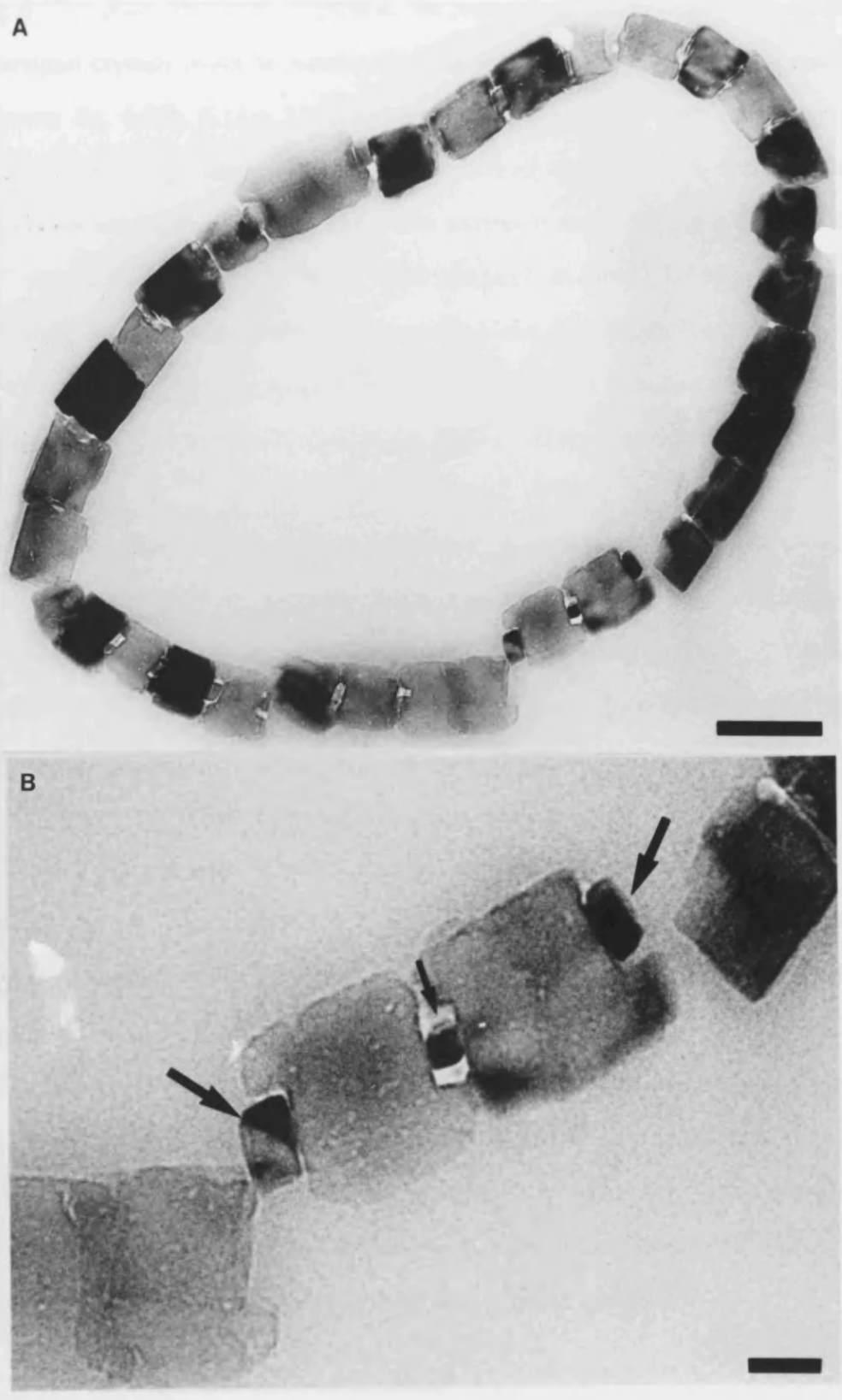

Fig. 6.13 *Transmission electron micrographs of proto-coccolith rings at an early stage showing both the R and the V unit nuclei. Scale bars: (a) 200 nm (b) 50 nm.*

(fig 6.13b). Also, on closer inspection, the presence of smaller (30-60 by 20-30 nm) interstitial crystals could be discerned which were located in between the main units (arrows: fig. 6.13b, 6.14a). Unfortunately, on most of these early rings, they were frequently missing leaving distinctive holes in their absence (fig. 6.14b). By analogy with other coccolith structures, they were termed *V-units* (Young *et al* 1991b). The "V" stands for vertical directed *c* axis, although it should be realized no direct structural evidence was found to support this claim (see discussion for explanation). The *c* axes of the main crystals point in a roughly radial direction and so are termed *R-units*. V-units were not observed in the SEM probably due their diminutive size.

The process appeared to continue with lateral expansion along the rim causing the units to become partially overlapped like a ring of dominoes (fig. 6.12b and top of fig. 6.15a). This had the effect of starting to obscure the smaller V-units which were rarely seen in proto-coccoliths of this type. The beginnings of the medial element were also evident at this stage. At first, a thin plate could be seen to extend out from the nucleus for approximately 100 nm (fig. 6.15b). A single corner of this plate then formed a "finger-like" protrusion (fig. 6.12c and 6.15d). Interestingly, these extensions were not directed radially, like the spokes of a wheel, but instead appeared to point at the focal positions of the ellipse. One half of the ring (divided by the major elliptical axis) was observed to be growing towards one focus while the units in the opposite half point at the other focus. This is clearly seen for the medial elements in fig. 6.5b and indeed for the outward-growing lower elements in fig. 6.2b. Useful diffraction patterns were hard to obtain from such crystals with outgrowths due to the substantial interference from neighbours. Nevertheless, the inward protrusions corresponded roughly to the [0001] direction.

The extension of the lower (proximal) element began with the outer edge of the "Z" growing along the rim to envelope the V-unit. Then as the growth front came up against the vicinal crystal, a curious splicing took place. This involved the outer

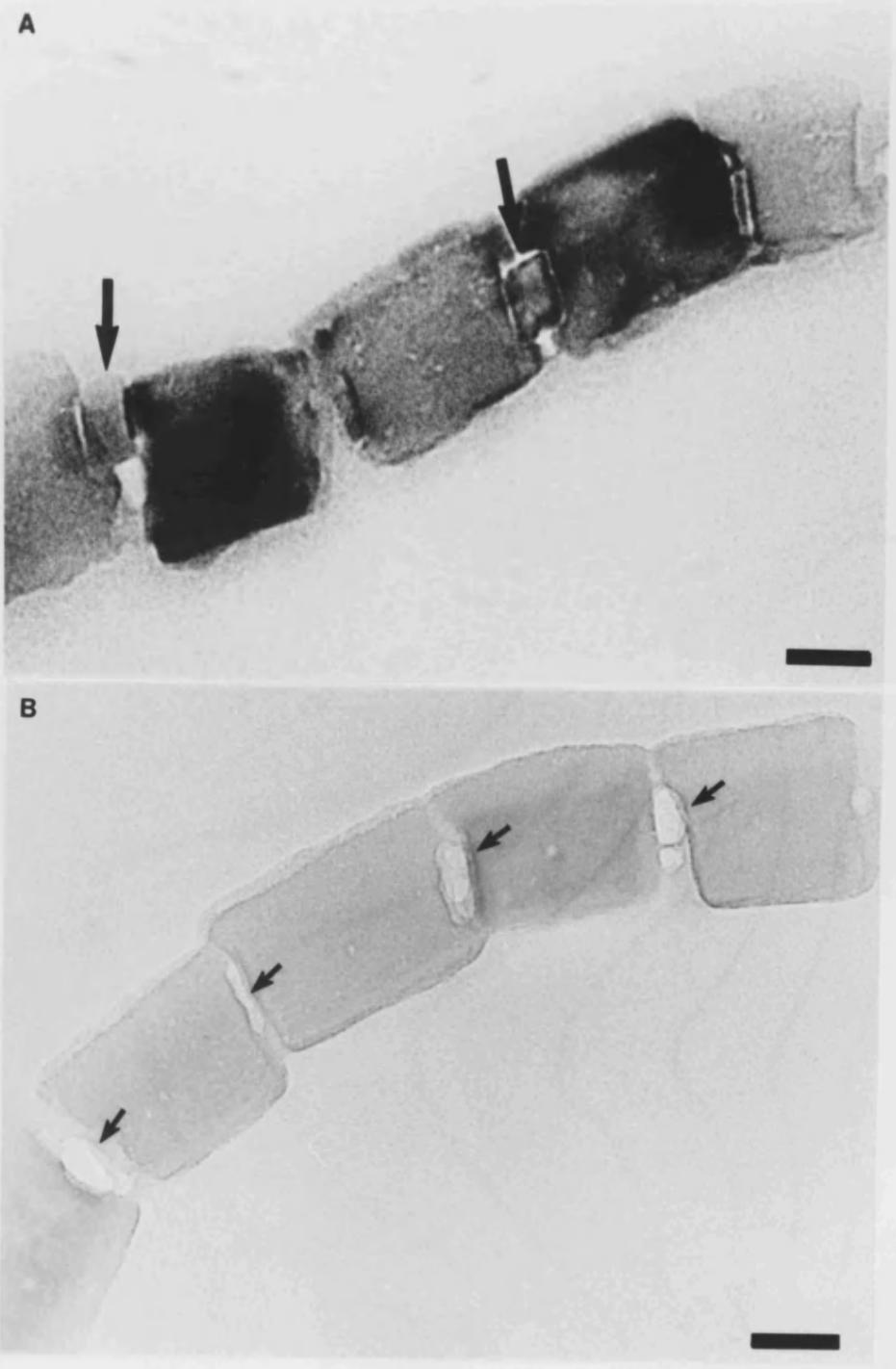

Fig. 6.14 *Transmission electron micrographs showing (a) the interstitial V units and (b) holes left in their absence. Scale bars 50 nm.*

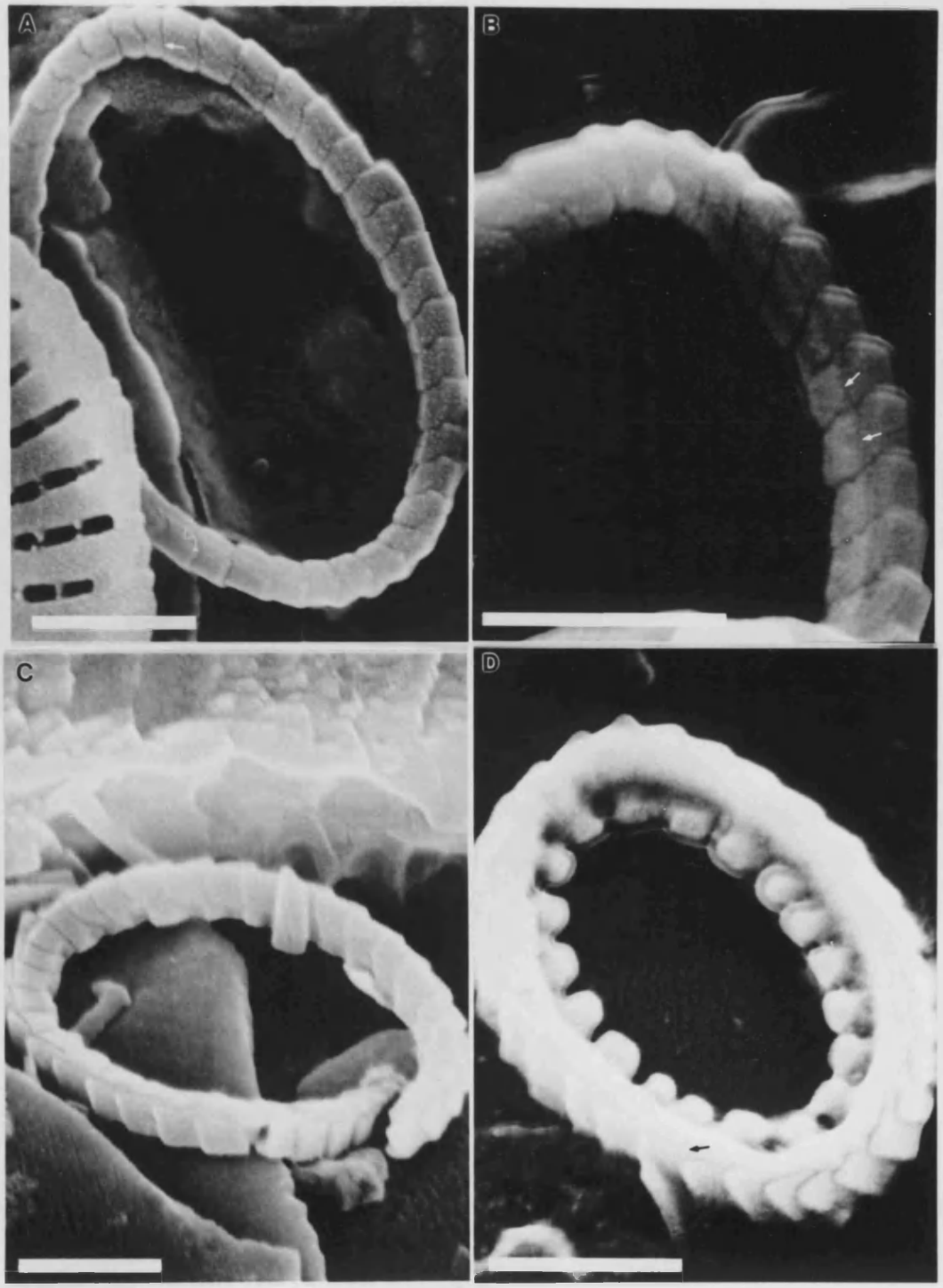

Fig. 6.15 *High resolution scanning electron micrographs of developing rings. Scale bars 0.5 μm.*

edge growing over and the inner edge growing under its neighbour (fig. 6.15c). The units then appeared to coalesce and the outer growth direction began the lower element proper (6.15d). The net effect of this overlapping and underweaving was to form an outer cycle of elements with clockwise or right-handedness in distal view and an inner cycle with anti-clockwise (left-handedness). This explained how the peculiar feature of opposite chirality, mentioned in the chapter introduction, originated.

Further accretion resulted in thickening the rim as the structure projected upwards and the lower element reached its full length (fig. 6.12d). The final stage involved the completion of the upper (distal) elements to form the characteristic "hammer" shape and the overall fusion of both shields (fig. 6.12e). A schematic summary of these observations is illustrated in fig. 6.16. It shows five growth stages which, in reality, are part of a continuous development. The crystals (three R-units and two V-units) are depicted as lying on the edge of a thin cylindrical ring which defines the nucleation belt.

South Atlantic Coccolith Ooze

A variety of taxa were present in the sample but the work focused on the important extant species *Florisphaera profunda* which was present in great abundance. These non-placolith, heterococcoliths are much bigger than *E. huxleyi* and are noted for their preference for deep waters. Each cell is covered with many large flakes each several microns square. The flakes were analysed by EDXA and found to be pure calcium carbonate (fig. 6.8b). SAED revealed them to be well-defined, single crystals of calcite with a similar morphology to the lower element of *E. huxleyi* (fig. 6.17). Another large, prominent species was *Hayaster perplexa* which again was composed of thin, *a* face flakes of calcite (fig. 6.18b). These were interleaved (in a similar way to the overlapping R-units in *E. huxleyi*) with their *c* axes directed radially to form a circular plate (fig. 6.18a).

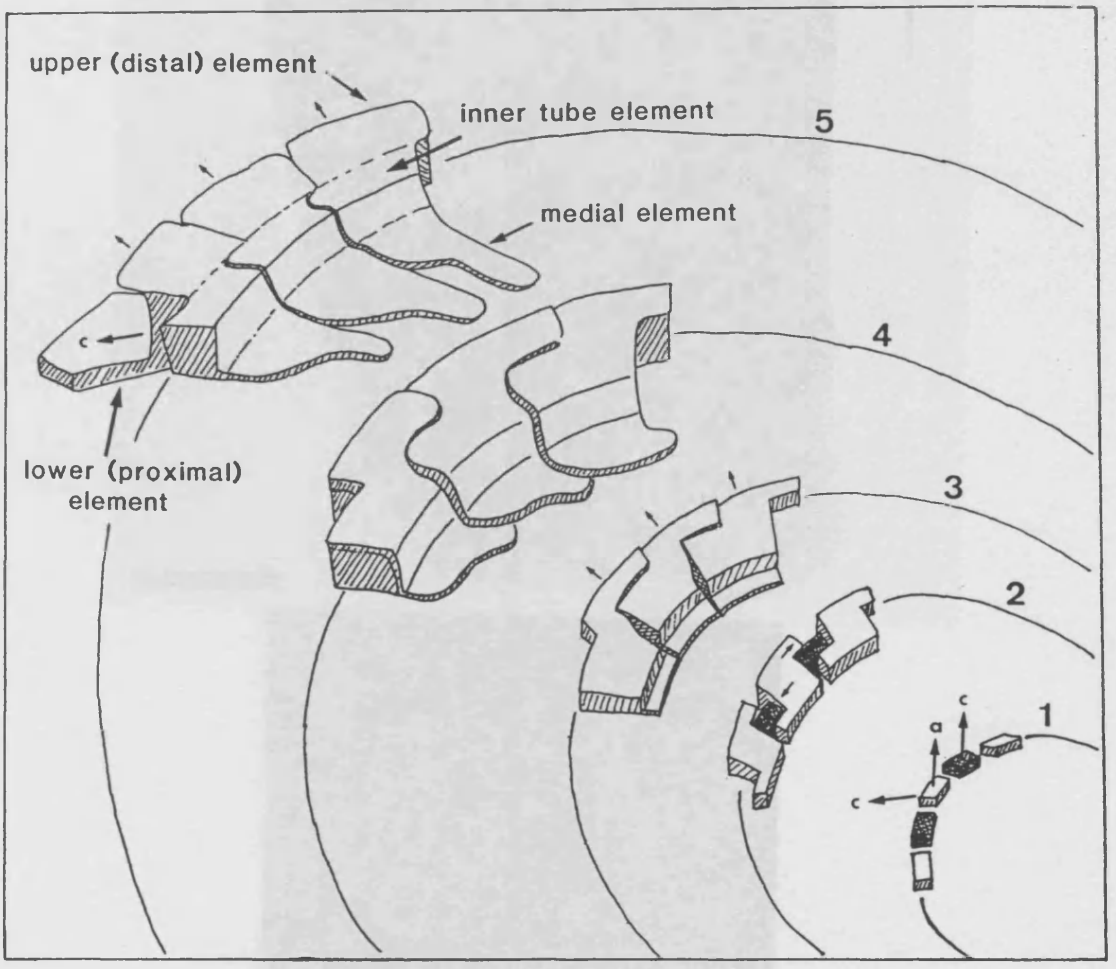

Fig. 6.16 *Schematic perspective drawing summarizing the observations on the ontogenetic development of proto-coccolith crystals. It shows five oriented nuclei (3R and 2V) with plate-like morphologies at the bottom right of the picture which grow in five stages (NB! actual growth is continuous) from right to left.*

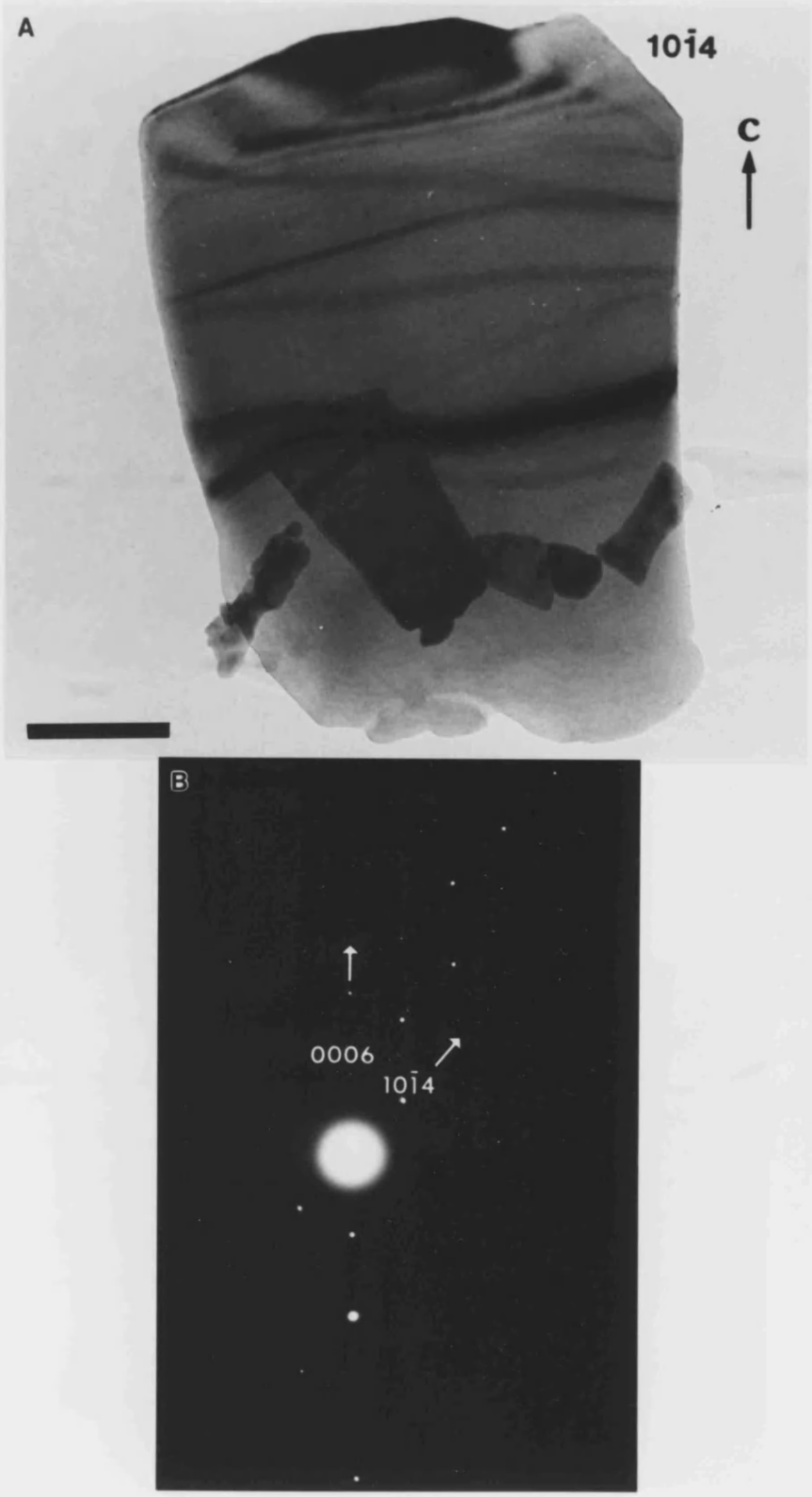

Fig. 6.17 *Transmission electron micrograph and associated selected area electron diffraction pattern (<1$\bar{2}$10> zone of calcite) of a single flake of F. profunda. Scale bar 0.5 μm.*

Fig. 6.18 *(a) Transmission electron micrograph of a whole coccolith of H. perplexa (b) TEM of a single radial unit and associated selected area electron diffraction pattern corresponding to the <$\bar{1}2\bar{1}0$> zone of calcite. Scale bars 0.5 μm.*

Coccoliths Grown in Nutrient-Depleted Conditions

The results of the XRD analysis are shown in table 6.2. The data shows conclusively that calcite is the only polymorph of calcium carbonate secreted by cells of *E. huxleyi*. The halite and unknown phase were attributed to salts present in the original culture medium that had not been removed during sample clean-up. The lines of the unknown were carefully compared with those of vaterite and aragonite but there was no match at all.

Medium	Nitrate (μm)	Phosphate (μm)	Phases Present in samples
Eppleys standard ratio High nutrient concentration	500	50	Pure calcite only
Eppleys standard ratio Low nutrient concentration	10	1	No sample dried down
Nitrate depleted	10	25	Halite (NaCl) + unknown not vaterite, aragonite or calcite
Extreme nitrate depleted	10	50	Pure calcite only
Phosphate depleted	500	6	Halite only
Extreme phosphate depleted	500	1	Halite (NaCl) + unknown not vaterite, aragonite or calcite

Table 6.2 *Results of powder XRD on coccoliths of E. huxleyi grown in depleted media*

6.4 DISCUSSION

Morphology and Orientation of Proto-coccolith Crystals

One of the major objectives of the work was to determine the orientation of the incipient nuclei with respect to the underlying organic matrix. Unfortunately, electron diffraction did not produce unequivocal results but instead drew attention to the three dimensional environment of the intracellular coccolith production site. Mature coccoliths are undoubtedly curved structures in their native surroundings due to their formation on the spherical surface of the nuclear envelope. Despite this, there seems to be a certain degree of inbuilt flexibility which allows coccoliths, removed from the cell, to fall flat on the TEM grid. Proto-coccolith rings were less prone to fall flat and consequently were found in a variety of orientations although the SAED data showed that two zones were preferred. The most likely candidate for the plane of nucleation was the *a* face $(\bar{2}110)$ of calcite. This is because it fits with the previous observations that the mature lower elements are elongated *a* face prisms (Mann and Sparks 1988). Furthermore, the expression of *a* faces as well as the radial disposition of *c* axes seemed to be a general feature of nucleation in heterococcoliths as was indicated by some of the non-placolith taxa studied in the South Atlantic ooze. On the other hand, there was evidence for a well-developed $(01\bar{1}8)$ face although crystals producing these diffraction patterns tended to be a little bigger and more elongated. Consequently, they were probably at a slightly later stage of growth and thus may be oriented as such due to a subsequent outgrowth.

TEM and SEM micrographs showed the morphology of the earliest nuclei to be plate or box-like and as such they are drawn in fig. 6.16. As was previously mentioned, SAED data inferred the presence of *r* $\{10\bar{1}4\}$, *a* $\{\bar{2}110\}$ and possibly *e* $\{01\bar{1}8\}$ faces. A strictly crystallographic habit bearing these forms is essentially an *a* face-modified, rhombohedron with truncations due to $\{01\bar{1}8\}$. An example, drawn by *MORPH*, is given in fig. 6.19. This morphology appears to be quite different in

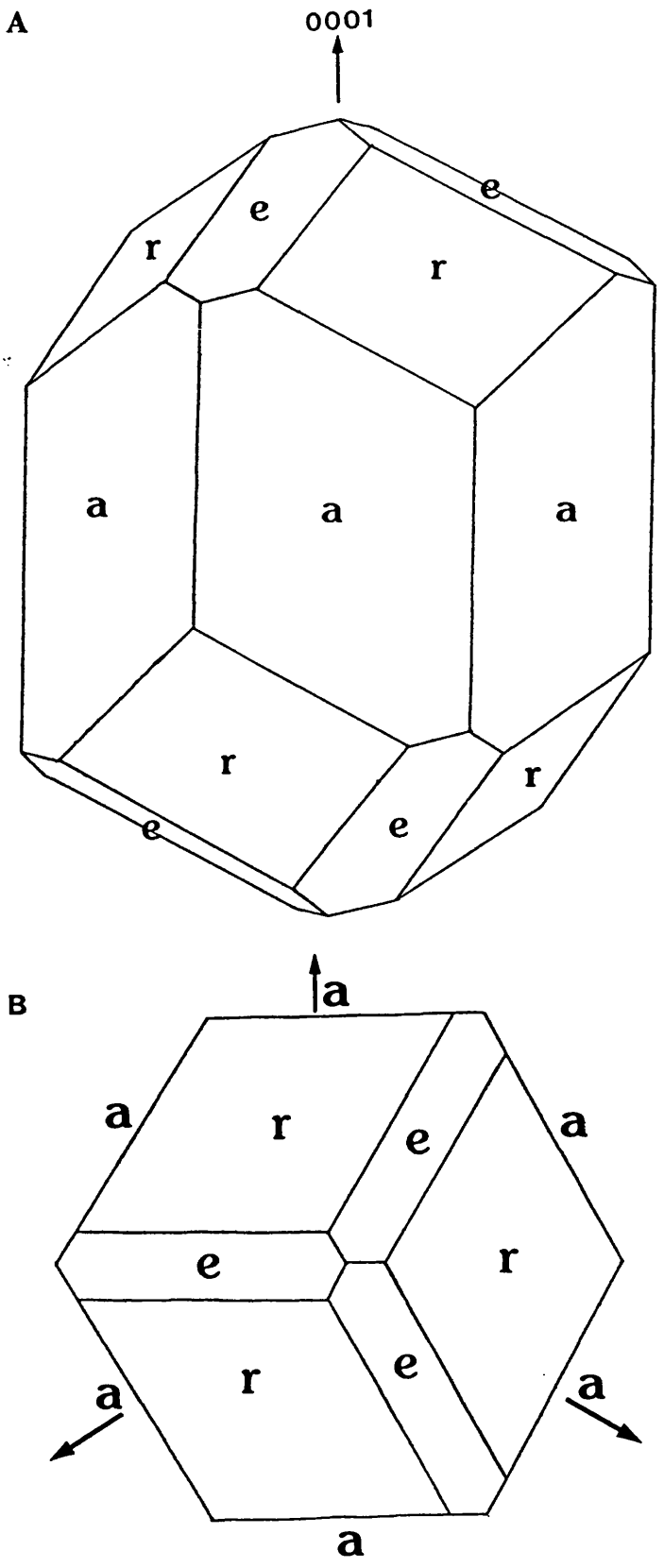

Fig. 6.19 *MORPH plot of a crystallographic habit of calcite exhibiting r {10$\bar{1}$4}, a {11$\bar{2}$0} and e {01$\bar{1}$8} forms: (a) projected onto the a plane and (b) projected onto the c plane.*

projection (fig. 6.19a) from those observed. Thus, the stringent biological control over morphology, evident in the sculpted, non-crystallographic shape of the mature segments, appears to be exerted even at the earliest stages of growth.

As far as is known, V-units have not previously been observed in coccoliths of *E. huxleyi*. They may of been missed before because they fall out easily or because they are only seen at the very earliest stages. It should be re-emphasized, however, that no direct evidence for their orientation was obtained. Their size, scarcity and fragile nature, made diffraction work (even micro-diffraction) and HRTEM analysis very difficult. Alternatively, evolutionary homology can be used to infer the likely crystal orientation.

Evolution of Coccolith Structures

Palaeontological studies on the fossil record have shown that extinct ancestors of *E. huxleyi* produced coccoliths with much simpler morphologies. Thus, it appears that the shape of coccoliths has become increasingly more complex during the evolution of the phylum. An interesting crystallographic feature of these early genera is the presence of two distinct crystal units in the rim cycles. Cross polarized light microscopy, has revealed that the units, which alternate around the ring, have different crystallographic orientations. One set of units have their *c* axes aligned radially (R) whereas the others are orientated vertically (V). *Toweius*, the last direct ancestral genus of *Emiliania*, has coccoliths composed of these two discrete units (fig. 6.20a). Up until now, *Emiliania* has appeared an exception being constructed of R-units only. The discovery of a relic or vestigial V-unit, however, has provided the missing link in this line of descent. Young (personal communication) has now proposed a plausible evolution of *Toweius* into *Emiliania* (fig. 6.20b). Moreover, this same pattern has also been observed an extinct, related genus *Watznaueria* (Young 1991). The alternating R and V-unit structure, in the light of this new evidence, appears to be a highly conservative feature of heterococcolith formation

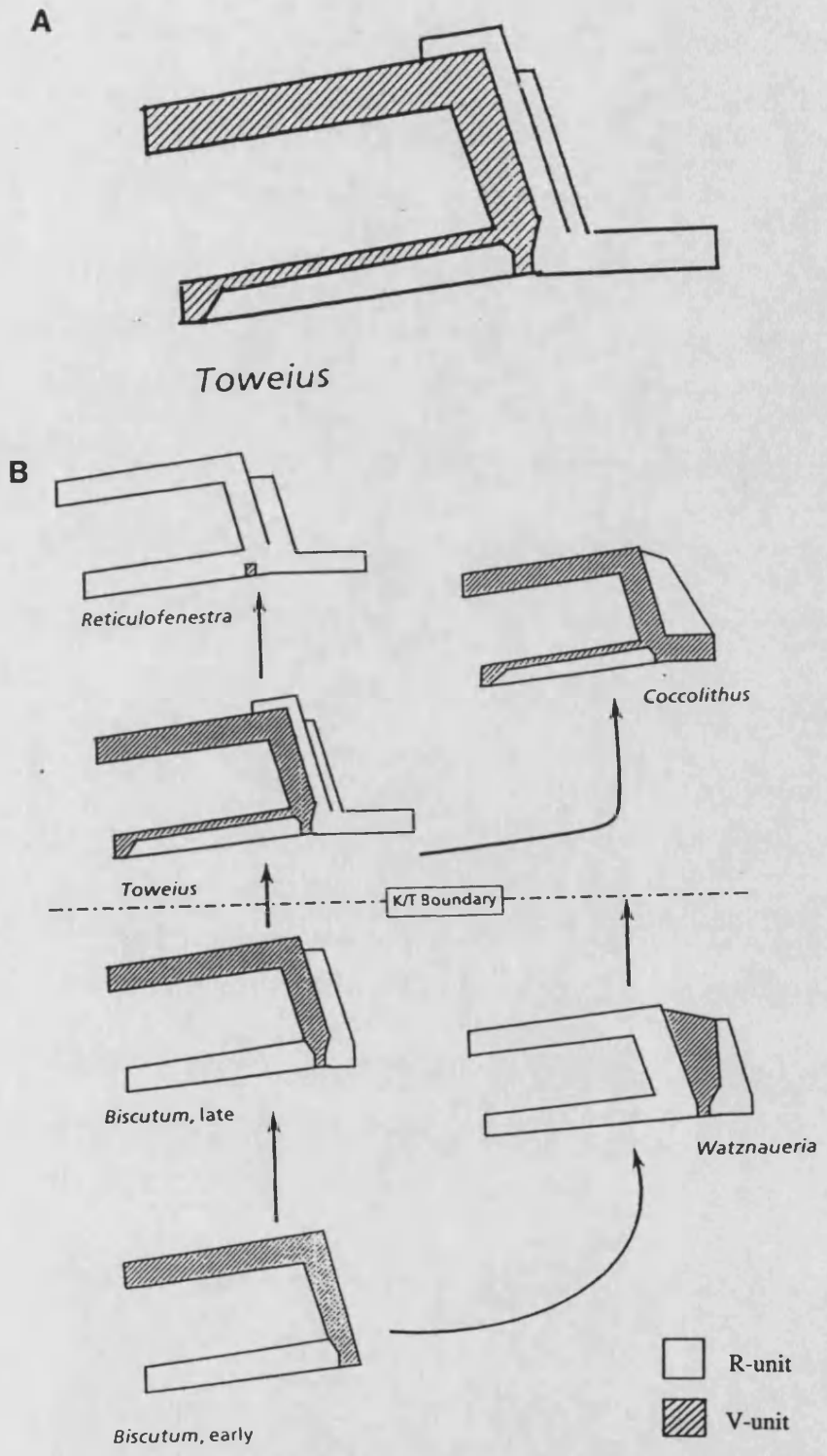

Fig. 6.20 *Schematic drawings of cross-sections through single crystal segments of coccoliths illustrating the position of the R and V-units (a) shows the structure of the extinct genus Toweius and (b) a possible evolutionary sequence from Biscutum to Reticulofenestra (E. huxleyi). Proposed and drawn by Dr J. Young.*

throughout a 230 million year history. It is therefore a potentially powerful basis for heterococcolith taxonomy with profound implications for academic and industrial geology.

It is tempting to speculate on the apparent evolutionary selection of R-units over V-units. One possibility might be based on the optical properties of calcite crystals. One of the proposed functions of coccoliths is to regulate the amount of light incident upon the photosynthetic cell. The concentration of light allows cells to live deeper in the photic zone near the ocean surface where nutrients are more abundant but light a limiting factor. Optically, coccoliths are essentially convexo-concave lens (fig. 6.21) and thus have the effect of converging parallel light rays incident upon them into the cell. Coccoliths constructed of largely R-units are highly birefringent compared to structures composed mainly of V (optically isotropic) units. Their selection would then be advantageous for the enhanced collection of light.

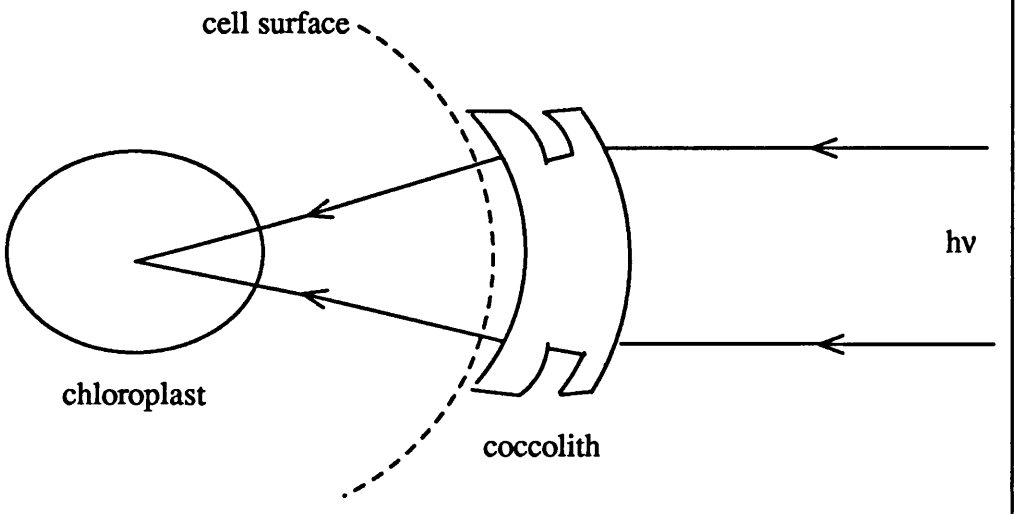

Fig. 6.21 *Schematic Diagram showing an extracellular coccolith acting as a converging lens aiding photosynthesis*

Overall nucleation plan in the cell

Biological regulation over $CaCO_3$ crystallization in *E. huxleyi* is clearly very sophisticated indeed. Perhaps, the most elaborate control is at the nucleation stage whereby the units are firmly anchored in a very specific crystallographic orientation. In mature coccoliths, the main (R) units are observed to be fixed crystallographically in two dimensions (ie in the *a* plane). Viewed distally, consecutive units are then rotated about the *a* axis (normal to the *a* plane) in a clockwise fashion such that the *c* axes are directed to the foci of the ellipse. The discovery of an -R-V-R-V- sequence of crystal units along the rim of the proto-coccolith ring, raises additional considerations that must now be accounted for in any general nucleation hypothesis.

Because of the crystallographically specific nature of the nucleation event, it seems plausible that some kind of molecular recognition between "template-type" organic molecules and the calcite lattice is taking place. The evidence presented in this chapter suggests that the nucleation of an R-unit occurs on the *a* plane. Matrix molecules specific for this face might therefore be located at the base of the coccolith vesicle. However, the V-unit, if truly oriented on a *c* face, requires the presence of (0001)-specific molecules at the base of the neighbouring nucleation space. An alternative and simpler explanation involves the use of a single folded ribbon of polymer as illustrated in fig. 6.22. For arguments sake, its surface would be specific for the *a* face of calcite only. The formation of R-units would then occur as already described via nucleation at the base of the ribbon. Subsequent growth could then follow unhindered in a radial fashion. As a consequence of the architecture of this type of folded ribbon wall, a crystal nucleating off *a* faces in the neighbouring cavity, would have its *c* axis directed vertically, thus developing into a V-unit. The surrounding wall would restrict growth in the radial direction. A second mirror image of this ribbon, placed opposite the first, would impede growth in opposite direction. It is envisaged that the folded ribbon would also form an elliptical cycle underlying the proto-coccolith ring. This proposal also fits with

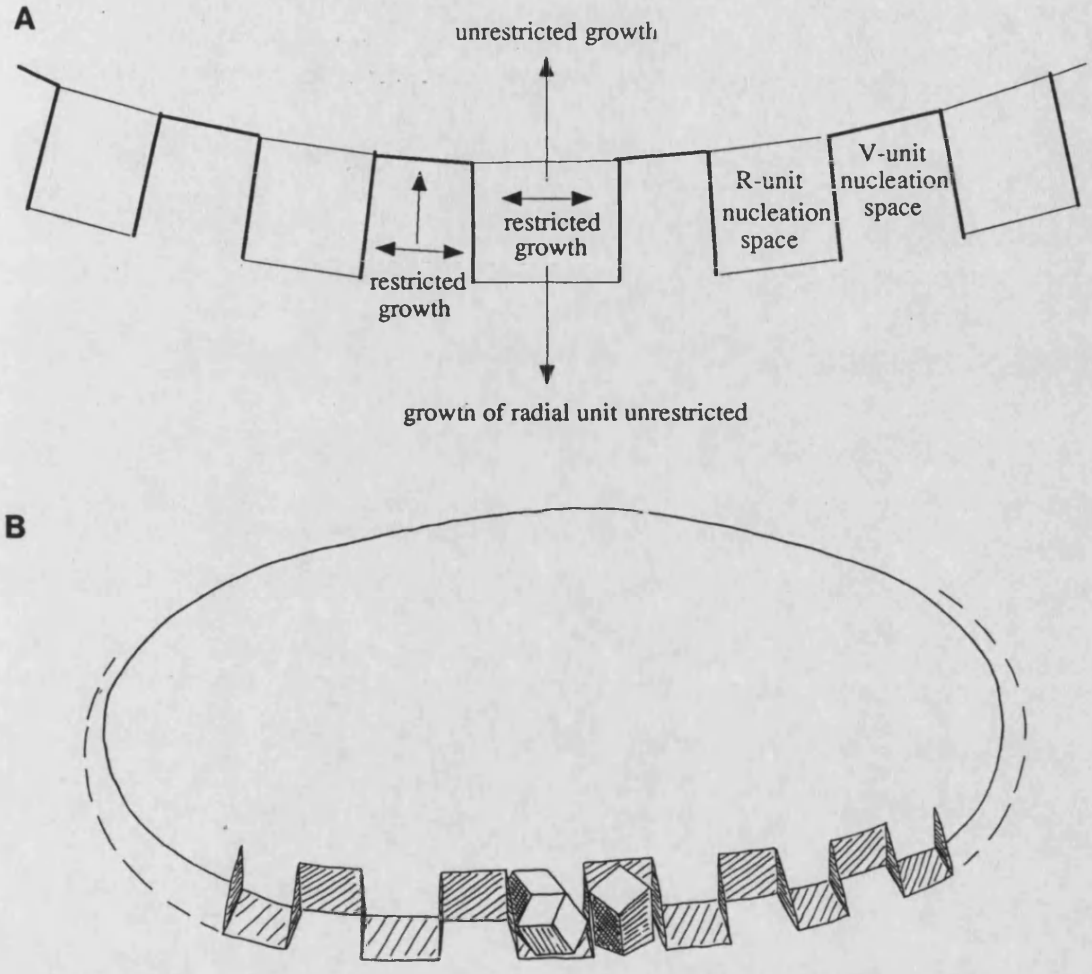

Fig. 6.22 *Schematic drawings of the proposed folded template (a) plan (distal) view and (b) perspective view showing R and V unit nuclei in vicinal spaces.*

observations that the R-unit spacing is constant even though the size of the ring plus the number of crystals varies considerably (Young 1989).

The type of molecules involved in the specific recognition of faces of calcium carbonate biominerals are usually acidic glycoproteins (Lowenstam and Weiner 1989). Coccoliths appear to be the only example of the use of acidic polysaccharides to regulate crystallization. However, it is feasible that the nucleation ribbon described above is constructed from organized assemblies of this polysaccharide. Experiments looking at the *in vitro* effects of this macromolecule on calcite crystal growth (chapter 5, p175) demonstrated its ability to select prismatic faces. This was encouraging although the recognition process was psuedo-specific and rather imprecise in contrast to the highly specific control *in vivo*. However, this does not rule out the possibility that the polysaccharide functions as a template. Future experiments are required to assess the effect of immobilized polysaccharide on nucleation. One other possibility is that the traces of protein found by the Dutch workers are derived from the centres involved in molecular recognition. The more abundant polysaccharide might then instead be linked to general growth inhibition in the coccolith vesicle.

Ontogenetic Development

The work on the ontogenetic development of proto-coccolith crystals extends that of Young (1989), Van Emburg (1989) and Westbroek *et al* (1989) as it shows some details of crystallographic directions involved. The results were consistent with the mechanism of growth by accretion from proto-coccolith crystals whose positions are fixed at the initial nucleation stage. Very little is known about the process by which calcite crystals are sculpted into the species-specific morphology of the mature segment. The CV-RB complex contains elaborate systems of vesicles coated with inhibitory polysaccharide which impose effective spatial constraints on developing crystals. In *E. huxleyi*, R-unit nuclei appear to be shaped via specific blocking of

growth directions. In this respect, the remarkable ability of the crystals to interleave with each other suggests that the containing vesicles themselves are also overlapped and entwined. It is therefore possible to speculate that these vesicle assemblies are laid down in a single, sweeping, elliptical movement stacking them, one at a time, alonside each other. A helical twist, (the pitch corresponding to the R-unit spacing) would then provide handedness.

Polymorphic Alterations in E. huxleyi

The biomineralization process in *E. huxleyi* appears to be unaffected by depletions of vital nutrients in the culture medium. The weight of the evidence suggests that the cell is only capable of forming coccoliths of calcite and not other polymorphs of calcium carbonate. Wilbur and Watabe (1963) presented results indicating that a strain, which normally deposits only calcitic coccoliths (BT6), formed significant quantities of vaterite and aragonite in nitrogen-depleted media (nitrate 400 μm, phosphate 72 μm). Furthermore, they found that another, normally non-calcifying strain in standard medium, also acquired the ability to produce aragonite and vaterite in nitrate-deficient conditions. Repeats of these experiments failed to substantiate the observations and therefore it is likely that the original data was anomalous.

This is consistent with the highly specific nature of the nucleation event. If molecular recognition processes are responsible for the alignment of each proto-coccolith crystal, then the organic molecules involved would be specific for faces of only one particular crystalline structure. Thus, the likelihood of the same molecules nucleating crystals of a different phase, without gross disruption of the coccolith shape and organization, is remote.

6.5 REFERENCES

Borman, A.H., (1982), *The role in $CaCO_3$ crystallization of an acid Ca^{2+}-binding polysaccharide associated with coccoliths of E. huxleyi,* Eur. J. Biochem., **129,** 179-183.

Dana, E.S. (1932), *A Textbook of Mineralogy*, 4th ed., Ford, W.E. (Ed.), New York: John Wiley and Sons.

De Jong, E.W., Bosch, L., Westbroek, P. (1976), *Isolation and Characterization of a Ca^{2+}-binding polysaccharide Associated with Coccoliths of Emiliania huxleyi (Lohmann) Kamptner*, Eur. J. Biochem., **70**, 611-621.

Fitchinger-schepmann, A.M.J., Kamerling, J.P., Versluis, C., Vliegenthart, F.G. (1981), *Structural Studies of the Methylated, Acidic Polysaccharide Associated with Coccoliths of Emiliania huxleyi (Lohman) Kamptner*, Carbohydrate Res., **93**, 105-123.

Hay, W.W., Mohler, H.P., Roth, P.H., Schmidt, R.R., Boudreaux, J.E. (1967), Trans. Gulf Cst. Ass. Geol. Socs., **17**, 428-480.

Klaveness, D. (1972), *Coccolithus huxleyi (Lohmann) Kamptner: I. Morphological Investigations on the Vegetative Cell and the Process of Coccolith Formation,* Protistologica, **8**, 335-346.

Lohmann, H. (1902), *Die Coccolithophoridae,* Arch. Protistenk., **1**, 89-165.

Mann, S., Sparks, N.H.C. (1988), *Single Crystalline Nature of Coccolith Elements of the Marine Alga Emiliania huxleyi as determined by Electron Diffraction and High Resolution Electron Microscopy*, Proc. R. Soc. (London), **B 234**, 441-453.

Parker, S.B., Skarnulis, A.J., Westbroek, P., Williams, R.J.P. (1983), *The Ultrastructure of Coccoliths from the Marine Alga Emiliania huxleyi (Lohmann) Hay and Mohler: an Ultra-High Resolution Electron Microscope Study*, Proc. R. Soc. (London), **B 219**, 111-117.

Van Emburg, P.R. (1989), *Coccolith Formation in Emiliania huxleyi*, Ph.D. thesis, University of Leiden, Netherlands.

Watabe, N. (1967), *Crystallographic Analysis of the Coccolith of Coccolithus huxleyi*, Calc. Tiss. Res., **1**, 114-121.

Westbroek, P., Young, J.R., Linschooten, K. (1989), *Coccolith Production (Biomineralization) in the Marine Alga Emiliania huxleyi*, J. Protozool., **36(4)**, 368-373.

Wilbur, K.M., Watabe, N. (1963), *Experimental Studies on Calcification in Molluscs and Alga Coccolithus huxleyi*, Annals, N.Y. Acad. Sci., **109(1)**, 82-112.

Young, J.R. (1987), *Possible Functional Interpretations of Coccolith Morphology*, Abh. Geol. B. A., Vienna, **39**, 305-313.

Young, J.R. (1989), *Observations on Heterococcolith Rim Structure and its Relationship to Developmental Processes*, in Nannofossils and their Applications, Crux, J.A, van Heck, S.E. (Eds.), British Micopalaeontol. Soc., Ser., 1-20.

Young, J.R. (1991), *An Ontogenetic Sequence of Coccoliths from the Late Jurassic Kimmeridge Clay of England*, Palaeontology, **34(4)**, 843-850.

Young, J.R., Didymus, J.M., Mann, S. (1991), *On the Reported Presence of Vaterite and Aragonite in Coccoliths of Emiliania huxleyi*, Botanica Marina, **34**, 589-591.

Young, J.R., Didymus, J.M., Bown, P.R., Prins, B., Mann, S. (1992), *The V/R Model: Crystal Assembly and Phylogenetic Evolution in Heterococcoliths*, Nature, in press.

CHAPTER 7 SUMMARY AND FUTURE WORK

This thesis has described a study of molecular recognition processes between soluble organic molecules and crystal surfaces of the mineral calcite. In this way, some of the complex processes in biomineralization have been modelled. Changes in crystal morphology were used to infer certain kinds of information about the interactions occurring at this inorganic/organic interface.

To begin with, the development and characterization of a suitable crystallization system was described in detail. The main body of the work was reported in chapter 4 and concentrated on simple, low molecular weight molecules as models to elucidate some fundamental interactions. The importance of electrostatic charge density on the molecules was stressed and how its dissipation or concentration affected potency. Furthermore, the stereochemistry of these additives was found to play an important role in selecting certain faces and not others.

The subsequent chapter then focused on some actual biogenic macromolecules in addition to several synthetic polymers. These were found to interact in a similar fashion to the low molecular weight analogues but with enhanced potency. To a large extent, the functionalization of the molecules determined the effects on crystallization. Carboxylated and sulphated macromolecules were the most potent and specific whereas those containing hydroxyls had little influence on calcite but instead affected crystallization kinetics. Other factors such as conformation and charge density were discussed. Also, more evidence was obtained for the involvement of a polysaccharide implicated in coccolith formation. Aspects of this biological system were studied in detail in chapter 6 which focused on the early stages of coccolith formation. A new crystal unit, visible only at the earliest stages, was discovered which appeared to have profound implications for the phylogenetic evolution of the genera. The initial orientation of the nuclei and the subsequent

growth stages were clarified. A previous claim that coccoliths could be deposited in other polymorphic forms of $CaCO_3$ was shown to be spurious.

The work presented in this thesis has shown that molecular recognition is a powerful and wide-ranging concept which can be used to explain many phenomena in both synthetic and biological crystallization systems. It has also highlighted some of the unique insights that model studies can provide in biomineralization which is a complex and challenging field of inquiry. Obviously, the ultimate goal is to understand the interactions between macromolecules and crystals *in vivo*. In order for this to come about, we need to pool information from studies in three main areas. Firstly, investigations on manipulative biological systems, like the coccoliths for example, are essential. Secondly, comprehensive biochemical characterization of the proteins and polysaccharides involved is required; primary and secondary structures are still not available for the majority of macromolecules. Lastly, carefully designed model systems can then be used to focus on the detailed nature of processes occurring at the inorganic/organic interface.

Some of the results and findings may also have important implications for controlled crystal growth in industry and technology. The size and morphology of particles dictate many properties in manufacturing processes such as dissolution/reaction rates, flow and packing characteristics. Also, there is often the requirement for systems in which the crystals are either dispersed or aggregated, inhibited or promoted. The work in this thesis has shown that all these features can be influenced by additives to varying extents.

Recommendations for Future Work

Morphological studies of additives are already being successfully applied to a range of other mineral systems (haematite, N.J. Reeves, personal communication; barium sulphate, J.D. Hopwood, personal communication and Davey *et al* (1991);

hydroxyapatite, J. Moore, personal communication). However, we still know relatively little about some of the mechanisms by which additives affect crystal growth and the physical nature of the crystal solution interface. Thus, future work might concentrate in these areas.

Adsorption studies of additives on large, geological single crystals with well-defined faces could provide information concerning any preferential surface coverage or might be used to demonstrate binding strengths. Morphologies exhibiting combinations of faces such as $\{10\bar{1}4\}$, $\{1\bar{1}00\}$, $\{40\bar{4}1\}$, $\{11\bar{2}0\}$, {0001} would allow direct comparisons. Additives such as aspartate, malonate or phosphate could be investigated quantitatively using FTIR, XPS, or SIMS. Adsorption isotherm data would also be very useful enabling calculation of affinities of adsorbates for adsorbent (Hay and Moreno 1979). Although this work so far has not produced sound evidence for occlusion of molecules inside crystals, there are enough studies in the literature to warrant continuing these investigations (Ichikuni 1983, Ishikawa and Ichikuni 1981, Berman *et al* 1988). Simple leaching experiments on phosphate or sulphate-modified calcite or the use of fluoro-probes might provide some answers. Alternatively, synchotron XRD analysis of mosaic spread and coherence length could be attempted.

There is also more potential for analytical methods in studying adsorbed compounds: ^{31}P NMR of phosphate, phosphoester groups in presence/absence of calcium and/or crystals (Lee *et al* 1977); ESR of vanadyl ions, in place of Ca, to probe interactions with carboxylates and phosphoester groups (Peckauskas *et al* 1976); calorimetric studies of the thermodynamics of adsorption in an attempt to ascertain whether binding is exothermic or entropically-driven. It may be possible to observe differences between potent and non-potent molecules.

With the recent advance of atomic force microscopy (AFM), additives could

conceivably be studied on the surface of large, geological single crystals. This might enable an assessment of the molecular orientation and binding modes ie unidentate or chelate. Computer simulation of adsorbed organic molecules might provide information on feasible conformations. Energy minimization calculations could be carried out for simple molecules such as malonate or aspartate over a simulated crystal surface.

There are a great number of other biogenic macromolecules which could be screened for specific interactions with their corresponding mineral phase *in vitro*. In the $CaCO_3$ system, phosphates were effective habit modifiers and so proteins functionalized by these anions would be interesting. For example, phosphorylated mollusc shell matrices, dentin phosphophoryns and egg yolk phosvitin. Other potentially important materials which are not readily available include the reported coccolith glycoprotein and the Gla-containing proteins from $CaCO_3$ corals. Osteocalcin and the proteoglycan should also be tried with hydroxyapatite. Experiments assessing the influence of immobilized macromolecules (particularly the coccolith polysaccharide and model glycans) on the nucleation of $CaCO_3$ would also be interesting. This might be done by anchoring to agarose beads or might involve a macromolecule-vesicle complex eg liposomes/monolayers/lipid tubules. Proteins such as serum albumin could be used as controls.

The remarkable effects of the anti-freeze glycoproteins and other hydroxyl-containing molecules should be further investigated. Kinetic studies of nucleation in more suitable crystallization systems such as metastable solution mixtures would be worthwhile. A reduced anti-freeze glycoprotein, with no hydroxyls, is available and would provide useful comparisons.

With regards to the continuing investigation of E. huxleyi, further lattice imaging work is needed to determine the orientation of the proposed V-unit nuclei. The V/R

model of crystal nucleation also needs further corroboration via the structural analysis of other placolith genera. Larger coccolith species would be advantageous in SEM observations. Perhaps one other unresolved question concerns the crystallographic features of the medial proximal element. Electron diffraction data from these often rather inaccessible regions of the coccolith plates would be beneficial.

References

Berman, A., Addadi, L., Weiner, S. (1988), *Interactions of Sea Urchin Skeleton Macromolecules with Growing Calcite Crystals - A Study of Intracrystalline Proteins*, Nature, **331**, 546-548.

Davey, R.J., Black, S.N., Bromley, L.A., Cottier, D., Dobbs, B., Rout, J.E. (1991), *Molecular Design Based on Recognition at Inorganic Surfaces*, Nature, **353**, 549-550.

Hay, D.I., Moreno, E.C. (1979), *Differential Adsorption and Chemical Affinities of Proteins for Apatitic Surfaces*, J. Dent. Res., **58(B)**, 930-940.

Ichikuni, M. (1983), *Anionic Substitution in Calcium Carbonate*, in Significance of Trace Elements in Solving Petrogenetic Problems and Controversies, Augustithis, S.S. (Ed.), pp 83-94.

Ishikawa, M., Ichikuni, M. (1981), *Coprecipitation of Phosphate with Calcite,* Geochem. Journal, **15**, 283-288.

Lee, S.L., Veis, A., Glonek, T. (1977), Biochemistry, 16, 2971-2979.

Peckauskas, R.A., Termine, J.D., Pullman, I., (1976), Biopolymers, 15, 569-581.

APPENDIX 1

Operational Procedures in Transmission Electron Microscopy

Routine operation of the transmission electron microscope (fig. A1.1) required a number of procedures to be carried out prior to use (Wischnitzer 1981). Firstly, the cold trap or anti-contamination device (ACD) had to be filled with liquid nitrogen. This device prevented dust, vapours and gases contaminating the apertures and lenses and so leading to a loss of resolution. The next requirement was the alignment of all the various lenses and apertures in the column so as to be optically centred relative to each other. This was necessary in order to minimize the effects of circuit instability which cause aberrations due to electrons that are not coincident with the optical axes of the lenses. Lastly, it was important that residual astigmatism was eliminated from the lenses. Alignment and the correction for lens asymmetry were carried out in the following sequence:

(a) Adjusting the heating current in the filament (electron source) such that the electron gun was operating at its optimum level (saturation point). This enables the illumination to be sufficiently bright to view objects at the highest magnification whilst not overworking the filament and so reducing its life. When undersaturated, the filament can be aligned with respect to the gun axis using the gun tilt control.

(b) Positioning the electron source on the condenser lens axis to ensure an even illumination of the specimen as the intensity of the beam is varied ie via focusing or defocusing of the condenser lens.

(c) Checking the astigmatic condition of the condenser lens to produce a symmetrical beam as it is focused or defocused.

(d) Centring the condenser aperture to prevent illumination sweep.

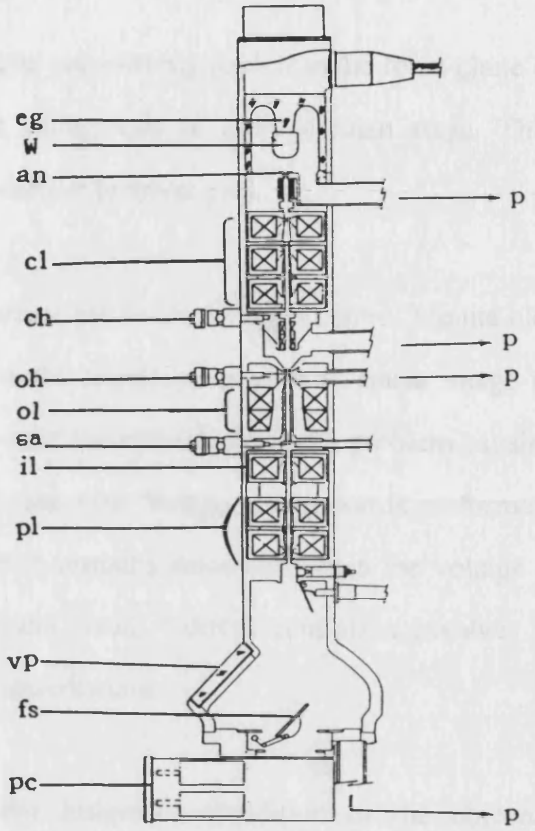

eg	electron gun	*sa*	selected area aperture holder
W	Wehnelt cylinder	*p*	to pumping system
an	anode	*il*	intermediate lens
cl	condenser lens (triple)	*pl*	projector lens
ch	condenser aperture holder	*vp*	viewing port
oh	objective aperture holder	*fs*	fluorescent screen
ol	objective lens	*pc*	photographic chamber port

Fig. A1.1 *Diagram of a transmission electron microscope*

(e) Alignment of the projector lenses and objective aperture by positioning the caustic spot and the shadow of the aperture at the centre of the fluorescent screen.

(f) Establishing specimen eucentricity such that the focal plane of the objective lens is coincident with the tilting axis of the specimen stage. This is done after the insertion of sample or carbon-formvar grid.

(g) Determining the current centre and voltage centre. Minute electrical disturbances in the lens current and the accelerating voltage cause image movement which is relatively insignificant near the optical axis but a problem causing loss of resolution at larger distances from the axis. Voltage centration is performed by finding a point in a focused image which remains stationary when the voltage is varied (wobbled) whilst keeping the current fixed. Current centration involves varying the current whilst keeping the voltage constant.

(h) Lastly, checking the astigmatic condition of the objective lens. This was ascertained by viewing the carbon grains deposited on the formvar support at a magnification of 400-500K and corrected using the astigmators where appropriate.

The accuracy of alignment could be assessed by the value of the objective lens current (200 KeV: 7.08 mA; 120 KeV: 5.22 mA).

References

Wischnitzer, S. (1981), *Introduction to Electron Microscopy*, 3rd ed., pp 81-95, New York: Pergamon Press.

APPENDIX 2

Interplanar Spacing of (hkl) in Hexagonal System

$$\frac{1}{d^2} = \frac{4}{3}\left(\frac{h^2 + hk + k^2}{a^2}\right) + \frac{l^2}{c^2}$$

for calcite: $a^2 = 24.9\ \text{Å}^2$, $c^2 = 291\ \text{Å}^2$

Interplanar angle between $(h_1k_1.l_1)$ and $(h_2k_2.l_2)$ in Hexagonal System

$$\text{Cos}\,\theta = \frac{h_1h_2 + k_1k_2 + 0.5\,(h_1k_2 + h_2k_1) + 0.0646\,(l_1l_2)}{\sqrt{(h_1^2 + k_1^2 + h_1k_1 + 0.0646\,l_1^2)\,(h_2^2 + k_2^2 + h_2k_2 + 0.0646\,l_2^2)}}$$

$$0.0646 = \frac{3a^2}{4c^2} \quad \text{for calcite}$$

APPENDIX 3

Computer Software and Methods

Below is a typical output dataset obtained from the Inorganic Crystal Structure Database (ICSD) part of the Cambridge Crystallographic Database located at Daresbury, UK.

```
REFERENCE STRUCTURE = 21552   A,B,C =   4.990   4.990  17.061
  ALPHA,BETA,GAMMA =  90.000  90.000 120.000    SPGR =167 R3-CH
  3   0 CODEN=  100676 SYMOPS=50411
 40     RFAC= 2.2 ERRFLAG=0 (C-C)ESD=0
  1 CA1      0.00000   0.00000   0.00000
  2 C1       0.00000   0.00000   0.25000
  3 O1       0.25680   0.00000   0.25000
```

This information was then combined with the full set of symmetry operations for the space group $R\bar{3}c$ as published in the International Tables for Crystallography (1983) and converted into a coded input dataset suitable for the unit cell plotting program, *PLUTO*. The example is shown below:-

```
TITLE CALCITE (HEXAGONAL)
CELL  4.990  4.990  17.061  90  90  120
C *** Multiplicity = 36; Wyckoff = f; Site symm = 1 ***
SYMM  X, Y, Z
SYMM  -Y, X-Y, Z
SYMM  -X+Y, -X, Z
SYMM  Y, X, -Z+1/2
SYMM  X-Y, -Y, -Z+1/2
SYMM  -X, -X+Y, -Z+1/2
SYMM  -X, -Y, -Z
SYMM  Y, -X+Y, -Z
SYMM  X-Y, X, -Z
SYMM  -Y, -X, Z+1/2
SYMM  -X+Y, Y, Z+1/2
SYMM  X, X-Y, Z+1/2
C******* Asymmetric unit **********
CA1     0.00000   0.00000   0.00000
C1      0.00000   0.00000   0.25000
O1      0.25680   0.00000   0.25000
C*********************************
OPT SOLID PACK CELLPLOT
VIEW Z0 ZROT 90
RANGE 0 1 0 1 0 1
RADII ATOMS CA 0.45 C 0.25 O 0.3
SEGMENTS ON
SEGMENTS 20
END
```

Cells projections could be chosen by the use of the command VIEW, VIEW LINE or VIEW MATRIX inserted near the end of the input datacard. Thus, projections of planes or faces could be visualized by specifying the normal vector. This could be calculated by matrix methods (McKie and McKie 1986).

Metric Tensors and Reciprocal Metric Tensors

Direction [uvw] normal to a face (hkl) is given as follows:-

$$\begin{bmatrix} U \\ V \\ W \end{bmatrix} = \begin{pmatrix} H \\ K \\ L \end{pmatrix} \begin{pmatrix} T_C^{-1} \end{pmatrix}$$

where T_c^{-1}, the reciprocal metric tensor for calcite is

$$T_C^{-1} = \begin{pmatrix} 0.0535 & 0.0267 & 0 \\ 0.0267 & 0.0535 & 0 \\ 0 & 0 & 0.00343 \end{pmatrix}$$

conversely, the (hkl) perpendicular to a zone axis [uvw] is :-

$$\begin{bmatrix} U \\ V \\ W \end{bmatrix} \begin{pmatrix} T_C \end{pmatrix} = \begin{pmatrix} H \\ K \\ L \end{pmatrix}$$

where T_c, the metric tensor (inverse of above matrix) is :-

$$T_C = \begin{pmatrix} 24.9 & -12.4 & 0 \\ -12.4 & 24.9 & 0 \\ 0 & 0 & 291 \end{pmatrix}$$

Crystal morphology plots could be made using the program *MORPH*, a typical input dataset of which is shown below:-

```
C*************** Input Dataset for MORPH *************
C*********** Space Group and Crystal System *********
R-3crhom
C*****************  Lattice Vectors *****************
           0.1448293188   0.0836172462   0.3408324621
          -0.1448293188   0.0836172462   0.3408324621
           0.0000000000  -0.1672344924   0.3408324621
C***** hkl's and relative surface energy values *****
2 1 1 0.60
2 -1 -1 0.50
1 0 -1 0.50
```

Faces could be specified by inserting the corresponding Miller indices, based on a rhombohedral cell (a = 6.36 Å, α = 46.1°). The larger the relative surface energy values chosen, the smaller the surface area of the face drawn in the plot.

References

International Tables for Crystallography (1983), Vol. A, Space Group Symmetry, Hahn, T. (ed.), Dordrecht (Holland): D. Reidel Publishing Co.

McKie, D., McKie, C. (1986), *Essentials of Crystallography*, Oxford: Blackwell Scientific Publications.